Marilena Cozzolino · Elisa Di Giovanni
Paolo Mauriello · Salvatore Piro
Daniela Zamuner

Geophysical Methods for Cultural Heritage Management

Springer Geophysics

The Springer Geophysics series seeks to publish a broad portfolio of scientific books, aiming at researchers, students, and everyone interested in geophysics. The series includes peer-reviewed monographs, edited volumes, textbooks, and conference proceedings. It covers the entire research area including, but not limited to, applied geophysics, computational geophysics, electrical and electromagnetic geophysics, geodesy, geodynamics, geomagnetism, gravity, lithosphere research, paleomagnetism, planetology, tectonophysics, thermal geophysics, and seismology.

More information about this series at http://www.springer.com/series/10173

Marilena Cozzolino · Elisa Di Giovanni
Paolo Mauriello · Salvatore Piro
Daniela Zamuner

Geophysical Methods for Cultural Heritage Management

Springer

Marilena Cozzolino
University of Molise
Campobasso
Italy

Elisa Di Giovanni
ITABC (CNR)
Monterotondo
Italy

Paolo Mauriello
University of Molise
Campobasso
Italy

Salvatore Piro
ITABC (CNR)
Monterotondo
Italy

Daniela Zamuner
ITABC (CNR)
Monterotondo
Italy

Contents

Chapter 1
Management of Cultural Heritage: Contribution of Applied Geophysics

Abstract The book is based on three different concepts: Management and Cultural Heritage, and to then move toward a particular research field, that is Applied Geophysics, and the contribution that it can make. In order to get a successful management, it is necessary to achieve some requirements that include identification, protection, preservation, enhancement, fruition and transmission of Cultural Heritage to future generations. The contribution of geophysical methodologies flows into these requirements through its scope and application. The Cultural Heritage represents the fundamental recognition of the value of a territory as a symbol and an emblem of history and culture, a memory that preserves and records the changing through the time of men and landscapes, a dynamic and evolutionary proof, a sign in space and time of tangible and intangible, material and no-material actions. Cultural Heritage is a wide concept and it has changed through the time, integrating and expanding the typology of heritage included. Having at one time referred exclusively to the monumental remains of cultures, cultural heritage as a concept has gradually come to include new categories. At present, the two largest agencies engaged in the conservation and protection of the world cultural heritage, UNESCO and ICOMOS divide the Cultural Heritage into two large groups: tangible and intangible, inextricably bound up with each other. This heritage is manifested through tangible forms such as artefacts, buildings or landscapes and also through intangible forms including voices, values, traditions, oral history. This book is meant as a tool for capacity-building creation for the best cultural heritage management. The geophysical methodologies, in fact, are applications for the knowledge, conservation and enhancement of a part of the tangible heritage, especially to the archaeological and built heritage. The aim is to improve and implement knowledge, skills and competences in this scientific field and improve its decision-making and management processes through experiences developed in different approaches and in different contexts. Among the objectives set, there is the application of these methodologies in solving management issues, through a multidisciplinary approach in order to have a better knowledge and resolution of these issues.

1.1   Introduction

This volume is based on three demanding concepts: Management and Cultural Heritage, and to then move toward a particular research field, that is Applied Geophysics, and the contribution that it can make.

Why do I talk about demanding concepts? Because in order to get a successful management, it is necessary to achieve some requirements that include identification, protection, preservation, enhancement, fruition and transmission of Cultural Heritage to future generations.

Because the contribution of geophysical methodologies flows into these requirements through its scope and application. Because Cultural Heritage represents the fundamental recognition of the value of a territory as a symbol and an emblem of history and culture, a memory that preserves and records the changing through the time of men and landscapes, a dynamic and evolutionary proof, a sign in space and time of tangible and intangible, material and no-material actions.[1]

Our past comes back to life through management and through that complex system of correlated and sequential processes and actions that allow it. The importance of planning and designing cultural heritage through an optimum management is also demonstrated by what it is referred in the European Union guidelines. The call is to develop innovative ideas based on scientific interdisciplinarity, on the use and development of new technologies, on the enhancement of knowledge and skills, on technology transfer, underlining the economic, social and employment aspect of the territory.

But what is Cultural Heritage? Cultural Heritage is a wide concept and it has changed through the time, integrating and expanding the typology of heritage included. Having at one time referred exclusively to the monumental remains of cultures, cultural heritage as a concept has gradually come to include new categories. At present, the two largest agencies engaged in the conservation and protection of the world cultural heritage, UNESCO and ICOMOS divide the Cultural Heritage into two large groups: tangible and intangible, inextricably bound up with each other. This heritage is manifested through tangible forms such as artefacts, buildings or landscapes and also through intangible forms including voices, values, traditions, oral history.

The tangible Cultural Heritage encompasses several main categories of heritage: movable (paintings, sculptures, coins, manuscripts), immovable (monuments, archaeological sites, and so on), underwater (shipwrecks, underwater ruins and cities). The International Convention for the Safeguarding of the Intangible Cultural Heritage, 2003, sets down a number of domains in which such heritage may be identified: oral traditions, languages, performing arts, social practices, rituals, knowledge and practices concerning nature and the universe, traditional

---

[1]*ICOMOS, International Cultural Tourism Charter. Principles And Guidelines For Managing Tourism At Places Of Cultural And Heritage Significance*. ICOMOS International Cultural Tourism Committee 2002.

craftsmanship including techniques and skills involving the associated cultural spaces, which communities, groups but also single individuals acknowledge as part of their cultural heritage. Finally there is the Natural heritage: natural sites with cultural aspects such as cultural landscapes, physical, biological or geological formations and Heritage in the event of armed conflict.[2]

It is clear that for a better management on such an important and diverse Heritage it is important to set some priorities. The phases of the Heritage Cycle, described by Simon Thurley, begins with understanding the culture; only then may we begin to value it. From there, we can learn to care for a culture and eventually enjoy it and so the circle goes. In order to ensure this cycle, it is necessary to respond to some requirements, as establishing a common approach to the definition, evaluation and improvement of management systems. This has made possible to promote the exchange of best practices, to encourage the development of improved approaches, to provide orientations and practical tools that can be finalized to precise objectives, to raise awareness of different issues and to promote a common policy of action.

The 2018 will be the first European year of cultural heritage[3] and it confirms the importance of this cultural asset and the necessity of doing research and experimentation with new languages and technologies to improve its management.

That is why, this volume is meant as a tool for capacity-building creation for the best cultural heritage management. The geophysical methodologies, in fact, are applications for the knowledge, conservation and enhancement of a part of the tangible heritage, especially to the archaeological and built heritage. The aim is to improve and implement knowledge, skills and competences in this scientific field and improve its decision-making and management processes through experiences developed in different approaches and in different contexts. Among the objectives set, there is the application of these methodologies in solving management issues, through a multidisciplinary approach in order to have a better knowledge and resolution of these issues.

The geophysical issues related to cultural heritage have been critically discussed through the single case studies in order to highlight the various possible applications, which have been divided into main groups: Monuments, Historical Buildings, Urban Centers, Archaeological Parks, Preventive Archeology, Ancient viability.

Particular attention has been given to the integration of geophysical methodologies with the most modern data collection and management and three-dimensional modeling: Integration of 3D metric survey and geophysical prospections and Geographical Information Systems implemented with geophysical prospections.

The first chapters of the book, dedicated to methodologies, analyze the physical principles that are at the basis of their application, in order to use later the information provided by them in the surveys. It is not easy to define the most appropriate

---

[2]http://www.unesco.org.

[3]http://www.consilium.europa.eu.

methodology for any cultural heritage problem, as often different methodologies can come to the same end, and not always applying a methodology rather than another is determined. Beyond the differences in the operating principles, in the instruments used for measurements, in the type of responses provided, and in the applicability fields of the various geophysical survey techniques, the common goal is to provide as many elements as possible to assess consistently the issue, object of the research.

The deductive approach of the second part of the book, dedicated to many case studies, has been a well-thought-out and strongly desired choice for two fundamental reasons. The first is to give a much more applicative role to the full content, providing all the useful information to interpret not only the methodological choice but also the results achieved. This in order to evaluate, for each case, the cognitive contribution made. The second motivation lies in the attempt of representing a kind of coded protocol of intervention applicable and expandable in other research contexts that plan in detail how to use and apply each method, data processing and correlation between different anomalies, geophysical data inversion and results presentation.

So, the contribution that can be derived from the systematic use of geophysical surveys in the archaeological research is very important, not only to identify buried ruins, otherwise identifiable only through invasive surveys, but also for the extensive mapping of the territory that allows to have a wider vision of the anthropic activity in the subsoil in order to understand the ancient landscape and the settlement dynamics, thus it represents a great tool to monitor through images the territory.

In the built heritage, the results of geophysical surveys provide good elements to encourage and promote the regular planning in diagnostic, consolidation and restoration works. The great potentiality of these methodologies lies in the non-invasiveness during the data acquisition phase, which, above all when surveys are conducted on perishable or high-quality surfaces, is really a discriminating factor.

In the book, close attention has been paid to the visualization and modeling techniques used in a case study from geophysical data. The graphical representation used to describe geophysical data has been thought to enhance the different perceptions between the interpretation of the data and the data itself, in order to better explain the anomalies described.

From the case studies, it is possible to highlight how geophysical methodologies can and must be focused on appropriate and necessary interventions. These interventions are designed, created and built expressly for the research and the context. Only in this way, the scientific contribution obtained can be turned toward the creation of a common approach to improve the management of cultural heritage.

Chapter 2
Geophysical Methods

Abstract Geophysical methods can measure various physical properties of the subsurface soils and rocks. Such properties are not only shaped by geophysical processes but they can also reflect alterations caused by humans. Prospecting methods were originally designed to measure geophysical features at the scale of several metres or kilometres, while archaeological features are of interest at the scale of centimetres or a few metres, at most. Thus, some methods are readily adapted to archaeological sites, while others are of marginal or negligible value. Geophysical methods provide raw data which must then be processed and evaluated. The first step is to present the data in a form which can be understand by archaeologists, either by constructing a model of the physical phenomena thought to be responsible and changing this until the measured data are accounted for within a minimum error, or by using information which provide some degree of separation of the components of the measurements which are due to archaeological sources from those of natural or modern origin. Usually, the geophysical methods are classified into two main groups of *passive* and *active* methods. Within the first group, the amplitude of nearly steady magnetic, gravitational and electrical perturbation fields, generated by buried features, are measured at the sensing device. In the second group, artificial seismic, electrical and electromagnetic (inductive and impulsive) signals are emitted by the device, which then senses the return signals, more or less altered by the typical responses of the subsurface features.

2.1 The Geophysical Prospections: Passive and Active Methods

Geophysical methods can measure various physical properties of the subsurface soils and rocks. Such properties are not only shaped by geophysical processes but they can also reflect alterations caused by humans. Prospecting methods were originally designed to measure geophysical features at the scale of several metres or kilometres, while archaeological features are of interest at the scale of centimetres or a few metres, at most. Thus, some methods are readily adapted to archaeological sites, while others are of marginal or negligible value.

Geophysical methods provide raw data which must then be processed and evaluated. The first step is to present the data in a form which can be understand by archaeologists, either by constructing a model of the physical phenomena thought to be responsible and changing this until the measured data are accounted for within a minimum error, or by using information which provide some degree of separation of the components of the measurements which are due to archaeological sources from those of natural or modern origin.

Usually, the geophysical methods are classified into two main groups of *passive* and *active* methods. Within the first group, the amplitude of nearly steady magnetic, gravitational and electrical perturbation fields, generated by buried features, are measured at the sensing device. In the second group, artificial seismic, electrical and electromagnetic (inductive and impulsive) signals are emitted by the device, which then senses the return signals, more or less altered by the typical responses of the subsurface features (Aitken 1974; Weymouth 1986a; Wynn 1986; Scollar et al. 1990; Cammarano et al. 1997; Campana and Piro 2009).

2.1.1   Passive Methods

In this category, traditionally, the method of major consequence to archaeology is the magnetic prospecting (Aitken 1974; Weymouth 1986b; Gibson 1986; Campana and Piro 2009). By this method, high sensitivity instruments are utilized for the measurement of the total magnetic field of the earth (Scollar et al. 1990; Becker 1995, 2009; Becker et al. 2005; Neubauer et al. 1997a, 2005; Hesse et al. 1997; Tsokas et al. 1997a; Herbich 2005; Fassbinder et al. 2005; Kuzma et al. 2005; Aminpour 2005; Benech 2007). Ferrous metallic objects or inhomogeneities in the magnetic properties of soils will cause variations in the measured field.

It can be mentioned in passing that another passive method, namely the gravitational surveying, is often utilized by geophysicists in archaeology. The method depends on the density difference between feature and its surrounding matrix. It is not sufficiently sensitive, however, for typical archaeological purposes (Linington 1966; Di Filippo et al. 2005a, b). It is however very useful for large-scale site reconnaissance.

Finally, the Self-Potential (SP) method has proven to be the least expensive geophysical method available for archaeological purposes. The equipment consists of only a digital voltmeter, some wire, and several low noise unpolarizable electrodes (Black and Corwin 1984; Corwin and Hoover 1979; Cammarano et al. 1997). Wynn and Sherwood (1984) reported that the SP method often shows anomalies over archaeological targets in areas where one or more other geophysical methods fail to indicate anything unusual.

2.1.2   Active Methods

This category includes several methods of great value in archaeological prospections:

(a) <u>Seismic methods</u> These involve introducing a pulse of sound into the earth and measuring the time of return of the pulse reflected by discontinuities in mass density and elastic properties of the soil. Geophysicists have used the refraction seismic method in archaeology with relatively little success (Aitken 1974; Carabelli 1966; Carson 1962). The refraction method works best in mapping undisturbed layers having velocities increasing with depth. The method, however, becomes much less useful and interpretation becomes very qualitative and difficult when there are velocity inversions, which are representative of human cultural disturbance, or highly three-dimensional target bodies, such as burial sites or stone walls and foundations. The reflection seismic method is also often used mainly to detect cavities in an otherwise homogeneous rock mass or in ancient stone structures (Stright 1986; Tsokas et al. 1995a).

(b) <u>Electromagnetic methods</u> The next group, which we consider, can be lumped under the very general term of non-contacting electromagnetic methods (often called also EM or induction methods). In all of these methods a transmitter coil sends a primary signal into the ground causing a secondary signal to be emitted. The secondary signal is then picked up by a receiver coil. Objects and soils that conduct electrical currents or become magnetized alter the nature of the secondary signal (Scollar 1962; Foster 1968; Tite and Mullins 1970; Tabbagh 1974, 1986; Bevan 1983; Frohlich and Lancaster 1986; Dalan 1991; Hesse 1991, 1992; Hesse and Doger 1993; Tsokas et al. 1994; Bozzo et al. 1991, 1994; Sarris et al. 1998).

(c) <u>Galvanic methods</u> They are the ones that have been and still are adopted fairly widely in archaeological prospection. Galvanic or soil-conduction electrical methods have been used since 1950s (Aitken et al. 1958). The best known technique is the resistivity profiling for which typically a Wenner or pole-pole or dipole-dipole array is employed. Resistivity methods are mainly helpful in detecting gross porosity changes caused by buried stone structures. Many authors, such as Aitken (1974), Hesse (1966), Bernabini et al. (1985, 1988), Weymouth (1986b), Hesse et al. (1986), Clark (1986, 1990), Brizzolari et al. (1992c), Carabelli (1967), Noel and Xu (1991), Lapenna et al. (1992), Bozzo et al. (1995), Orlando et al. (1987), Patella (1978), Tsokas et al. (1994), Cammarano et al. (1998), Dabas et al. (2000), Piro et al. (2001b, 2015), Cardarelli et al. (2006b, 2007), have used these methods for archaeological prospecting. All the galvanic techniques measure the electrical resistivity of soils and rocks, and hence they respond to any local variation of this parameter produced by human activities. It is a rather slow but inexpensive method. Recent developments with conductivity-meters permit a more expensive but faster approach to similar information.

The development of the technology associated with automatically multiplexed electrode arrangements and automatic measuring systems facilitate the acquisition of a large number of measurements in a limited time. Further, the advent of fast computers allowed the development of automated resistivity inversion schemes, which aim to construct an estimate of a subsurface resistivity distribution that is consistent with the experimental data (Papadopoulos et al. 2006).

Several two dimensional smoothness constrained inversion algorithms for ERT (Electrical Resistivity Tomography) data have been presented in literature (Sasaki 1992; Xu and Noel 1993; Loke and Barker 1995; Tsourlous 1995; Cardarelli and Fishanger 2006a).

(d) Ground Penetrating Radar The Ground Penetrating Radar (GPR) offers a high resolution sounding capability with detection of features of the order of a few tens of millimetres thickness at ranges of several metres. The range decreases to a few metres in conductive materials such as clays, silts and soils with saline or contaminated pore water (Davis and Annan 1989).

Radar signals are transmitted into the ground and then reflected by discontinuities in the electric properties of soils. The reflection times of the signals provide depth information (Moffatt 1974; Morey 1974; Ulriksen 1982; Bevan 1983; Vaughan 1986; Finzi Piro 1991, 2000; Brizzolari et al. 1992d; Malagodi et al. 1996; Conyers and Goodman 1997; Goodman and Nishimura 1993; Nishimura and Goodman 2000; Goodman et al. 2004a, b, 2007; Neubauer et al. 2002; Piro et al. 2001c, 2003; Goodman and Piro 2013). The GPR method can be of fairly rapid field use but neither the equipment nor the interpretation of radargrams are simple tools.

The resolution of the system will improve at higher frequencies if the ratio of the bandwidth to the centre frequency remains the same. This is one reason ground-penetrating radar systems are made to operate at a number of different frequencies. There must be a compromise between range and resolution for GPR systems. The attenuation decreases as the frequency decreases in wet geological materials. The resolution is increased as the bandwidth is increased and this usually requires that the centre frequency of the radar be increased (Davis and Annan 1989).

The principal weakness of GPR is that it cannot normally penetrate below a clayey horizon. Often the use of incorrect antennas means that important features are obscured or missed entirely. This happens because of poor resolution of or excessive signal attenuation by the feature of interest. Efforts are now being made to convert move out correction and signal processing seismic techniques to radar data.

In the last ten years advances in GPR data visualization and processing have significantly increased the utility of this geophysical remote sensing tool, particularly for the field of archaeological prospection (Goodman and Piro 2013).

Chapter 3
Geophysical Methods for Cultural Heritage

Abstract The Electrical Resistivity Tomography (ERT) has been used by many geophysics for archaeological investigations since the 1960s. The electrical resistivity parameter, on which the method is based, has such a large variability to allow the great majority of the structures and bodies of archaeological and architectural interest to be readily distinguished, in principle, from the hosting material. In general, the rock resistivity depends on many factors, as water content in fissures and fractures, porosity, degree of saturation and nature of pore electrolytes. In dry state, most rocks are non-conducting, i.e. they have extremely high resistivities, which decrease rapidly with existence of fluids, usually containing various ions to form the electrolytic solution. In archaeological prospecting, the presence of a high resistivity anomaly is usually an indicator of some resistive structure, such as the presence of accumulated tiles, a stone wall, building foundation or a cavity respect to the less resistive hosting soil. Instead, the presence of a moist ditch filling in a resistive rock background is characterised by a low conductive anomaly. In the study of historical buildings, where for capillary ascent of humidity and ingression of more or less aggressive waters, internal alteration nucleuses, typically characterised by very low resistivities, become the sources of degradation and even dis-aggregation of structure. To investigate the resistivity distribution along a profile, an apparent resistivity dataset is collected by means of a device composed of a pair of energizing electrodes that sends the current into the ground and a pair of potentiometric electrodes that measures the potential difference generated by the current input. Nowadays, sophisticated low-cost multi-electrode instruments are available, which store a considerable sequence of data in a detailed way. A numerical inversion is used to convert measured apparent resistivity distributed along a pseudosection to electrical resistivity values displayed as a function of depth below surface. The geoelectric resistivity tomography (ERT) approach comes from taking many apparent resistivity determinations at as many locations as possible and involves the joint inversion of many independent tests, using an algorithm to discern subtle details from differences, which would otherwise not be seen in any one test.

3.1   Geoelectrical Method

3.1.1   Introduction

Geoelectrics is one of the most reliable prospecting tools in the field of Cultural Heritage, thanks to the technological and methodological developments in recent years, which have made it a fast target-oriented method. The electrical resistivity parameter, on which the method is based, has such a large variability to allow the great majority of the structures and bodies of archaeological and architectural interest to be readily distinguished, in principle, from the hosting material. In general, the rock resistivity depends on many factors, as water content in fissures and fractures, porosity, degree of saturation and nature of pore electrolytes. In dry state, most rocks are non-conducting, i.e. they have extremely high resistivities, which decrease rapidly with existence of fluids, usually containing various ions to form the electrolytic solution.

In archaeological prospecting, the presence of a high resistivity anomaly is usually an indicator of some resistive structure, such as the presence of accumulated tiles, a stone wall, building foundation or a cavity respect to the less resistive hosting soil. Instead, the presence of a moist ditch filling in a resistive rock background is characterized by a low conductive anomaly. In the study of historical buildings, where for capillaric ascent of humidity and ingression of more or less aggressive waters, internal alteration nucleuses, typically characterized by very low resistivities, become the sources of degradation and even dis-aggregation of structure (Cammarano et al. 1997).

3.1.2   Basic Theory

The solution for the electrical potential arising from an electrical current flowing into the ground from a point source of current (a grounded electrode) is the starting theoretical point for the resistivity prospecting method. In practice, there is always a device of four electrodes used to measure the ground resistivity: two are used for injecting a current of intensity I and two for detecting a voltage (potential difference) ΔU. Inhomogeneities, like electrically better or worse conducting bodies, are inferred from the fact that they deflect the current and distort the normal behaviour. The complete theory of the resistivity method is extensively discussed in geophysical textbooks such as Dobrin and Savit (1988), Telford et al. (1990), Parasnis (1997) and Reynolds (1997). The fundamental assumption is that a stationary and continuous electric current flows in a homogenous and isotropic conductive medium. This hypothesis implies that the electrical current density vector is

$$\nabla \cdot J = 0 \qquad (3.1)$$

where J is the current density. Equation (3.1) states that continuous current flow in regions of finite conductivity does not allow the accumulation of free charge, unless there is a source or sink inside. Using Ohm's Law

$$E = \rho J \tag{3.2}$$

where E is the electric field and ρ is the resistivity, from Eq. (3.1) we obtain

$$\nabla \cdot \frac{E}{\rho} = \frac{\nabla \cdot E}{\rho} + E \cdot \nabla \frac{1}{\rho} = 0 \tag{3.3}$$

Equation (3.3) leads to Poisson's differential equation

$$\frac{\nabla \cdot \nabla U}{\rho} + \nabla U \cdot \nabla \frac{1}{\rho} = 0 \tag{3.4}$$

where U is the electric potential. Taking into account the Faraday's Law

$$\nabla \times E = -\frac{\partial B}{\partial t} \tag{3.5}$$

where B is the magnetic induction, since $\nabla \times E = 0$ for $B = 0$, the electric field E can thus be regarded as the gradient of a scalar potential

$$E = -\nabla U \tag{3.6}$$

This formula is of practical importance for the determination of the resistivity. In practice, the potential difference ΔU can be measured for an array of known geometry and a known injection current. For a homogeneous isotropic subsurface, the resistivity is equal to the bulk resistivity of the halfspace and hence constant for any injection current and electrode geometry:

$$\rho = k \frac{\Delta U}{I} \tag{3.7}$$

where I is the current flowing between two energizing electrodes and k is the geometrical factor depending on the disposition of the C_1 and C_2 energizing electrodes and the P_1 and P_2 receiving electrodes:

$$k = \frac{2\pi}{\left[\frac{1}{r_{C_1 P_1}} + \frac{1}{r_{C_2 P_1}} - \frac{1}{r_{C_1 P_2}} - \frac{1}{r_{C_2 P_2}}\right]} \tag{3.8}$$

However, as the resistivity is an intrinsic property of a homogeneous material and the subsoil is generally a complex distribution of different materials with different resistivities, the key concept of apparent resistivity, ρ_a, is defined. In simple terms,

ρ_a is a volumetric average of a heterogeneous half-space, except that the averaging is not done arithmetically but by a complex weighting function dependent on the 4-electrode device. As long as the electrode arrangement is varied, the ratio in Eq. (3.8) will generally change. This results in a different value of the calculated resistivity for each measurement.

Several electrode arrangements are used in geoelectrical prospecting (Table 3.1).

The *Wenner array* (Griffiths and Turnbull 1985; Griffiths et al. 1990) provides the alignment of the four electrodes on a straight line with a constant distance and therefore the terms of Eq. (3.8) for the calculation of apparent resistivity assume

Table 3.1 Common array types used in geoelectrical prospecting

Array	Scheme	Geometric factor
Wenner alfa		$k_{w\alpha} = 2\pi a$
Wenner beta		$k_{w\beta} = 6\pi a$
Wenner gamma		$k_{w\gamma} = 3\pi a$
Schlumberger		$k_S = \frac{\pi}{2l}\frac{\left(L^2-x^2\right)^2}{\left(L^2+x^2\right)}$
Dipole-dipole radial		$k_{DDrad} = (\pi r^3/aL\cos\alpha)$
Dipole-dipole azimuthal		$k_{DDaz} = (2\pi r^3/aL\,sen\alpha)$
Dipole-dipole equatorial		$k_{DDeq} = (2\pi r^3/aL)$
Dipole-dipole axial		$k_{DDas} = (\pi r^3/aL)$ or $k_{DDas} = \pi n(n+1)(n+2)a$
Pole-dipole		$k_{PD} = 2\pi\frac{a(a+b)}{b}$
Moving gradient		$k_{Gm} = \frac{\pi\left(L^2-x^2\right)^2}{2s\left(L^2+x^2\right)^2}$

the same value denoted by a. Varying the position of the electrodes is possible to obtain three combinations which are indicated with alpha, beta and gamma (Carpenter and Habberjam 1956). The geometric factor is given by

$$k_{w\alpha} = 2\pi a, \tag{3.9}$$

$$k_{w\beta} = 6\pi a, \tag{3.10}$$

$$k_{w\gamma} = 3\pi a. \tag{3.11}$$

The Wenner configuration does not produce very satisfactory performances for the detection of archaeological and geological structures at great depths. For example a laminar structure, with high resistivity and positioned at a modest depth at the centre of the alpha array, causes little disturbance to the current distribution while, if it is positioned between the second receiver and energizer electrodes, causes an improved disturbance increasing the potential difference (Clark 1990).

If the structure is conductive, it causes a distortion of the lines of current greater than the non-conductive structure. If we consider that the potential difference, which is measured across the receivers electrodes, is inversely proportional to the coefficient of the device geometry, the Wenner array has among all, the strongest signal strength.

The geometric coefficient in all the variants of the Wenner device, depends on a. The disadvantage, however, is that this configuration has low horizontal coverage with increasing electrode spacing and has a lower number of measures, for the same length of the profile, widening the dipoles.

In *Schlumberger array,* the distance between the energizing electrodes is greater than that between the receiving electrodes (Pazdirek and Blaha 1996). This configuration is used primarily for vertical electrical soundings, but may also be used in the acquisition of profiles. Often the configuration is symmetrical. The geometric factor is defined as follow:

$$k_S = \frac{\pi}{2l} \frac{(L^2 - x^2)^2}{(L^2 + x^2)}. \tag{3.12}$$

Even in this case, as in the Wenner device, there is a good signal/noise ratio, but the disadvantage arises from the need to use very long cables to connect current electrodes, which complicates the operations of data acquisition. In addition, due to the small distance between the receiving electrodes, this array is very suitable for the definition of small structures.

In the *Dipole-Dipole array*, the energizing electrodes are very distant compared to the receiving electrodes. Various types of arrangements, depending on the alignment that exists between the two pairs of electrodes, are considered (Table 3.1):

(1) radial arrangement: the receiving electrodes are placed respect r (distance of the centre of receiving dipole from the midpoint of energizing dipole);

$$k_{DDrad} = \left(\pi r^3 / aL \cos \alpha\right). \tag{3.13}$$

(2) azimuthal arrangement: the receiving electrodes are perpendicular to r;

$$k_{DDaz} = \left(2\pi r^3 / aLsen\alpha\right). \tag{3.14}$$

(3) equatorial arrangement: the receiving electrodes are perpendicular to the axis of the energizing dipole;

$$k_{DDeq} = \left(2\pi r^3 / aL\right) \tag{3.15}$$

(4) axial or polar arrangement: receiving electrodes are aligned with the energizing electrodes. With this arrangement $L = a$ and na is the distance between the internal electrodes (one receiving electrode and one measuring electrode).

$$k_{DDas} = \left(\pi r^3 / aL\right) \tag{3.16}$$

or

$$k_{DDas} = \pi n(n+1)(n+2)a. \tag{3.17}$$

The axial configuration is the most used in archaeological applications since it is very sensitive to lateral variations of resistivity (Loke 2004) and it does not require very long cables. It has the disadvantage of acquiring measurements with increasing noise when the n factor increases (n is the distance between energizing and receiver electrodes). In this case, as can be deduced from the relationship that expresses the geometric coefficient, the potential difference is inversely proportional to the cube of the n factor. Given the high proximity of the current electrodes, a limited penetration of current is obtained and, for this reason, it is particularly suitable for investigating buried shallow bodies.

The *Pole-Dipole array* is an asymmetrical arrangement in which an electrode is placed at a great distance compared to the other ones. The signal/noise ratio is lower than the Wenner array, but better than the dipole-dipole axial configuration, in fact, the potential drop decreases with the square of n. As a disadvantage, in addition to having a long cable between the energizing electrodes, the device is asymmetric and

in some cases the results obtained using this configuration are affected by this asymmetry. In order to eliminate these distortions, it is appropriate to repeat the measurements using a mirror arrangement of the electrodes (Loke 2004) by doubling, in this case, the acquisition time.

$$k_{PD} = 2\pi \frac{a(a+b)}{b} \tag{3.18}$$

where a is the distance C_1P_1 and b is the distance C_1P_2.

In the *Moving Gradient array*, the energizing electrodes are positioned at the ends of the profile and are kept fixed while the receiving electrodes, whose spacing is constant, move from one side to another side of the line. The advantage of such configuration with respect to the dipole-dipole device is to provide measures with a lower noise.

$$k_{Gm} = \frac{\pi(L^2 - x^2)^2}{2s(L^2 + x^2)^2}. \tag{3.19}$$

The choice of a configuration with respect to another one is of fundamental importance and must be made considering the type of target that is requested to be detected, the depth of investigation that is intended to achieve, the sensitivity of the instrumentation that is implemented, the level of background noise, the perceptibility of changes in the lateral and vertical resistivity of the device type, the available space along the profile and the signal power of current injection. Generally, for investigations that are designed to determine the presence of archaeological structures, the dipole-dipole axial array produces better results. In fact, it is particularly sensitive to lateral variations in resistivity and, during the field operations, the configuration is simpler to implement as it has the characteristic of maintaining a constant distance between the electrodes belonging to the same pair and does not require very long cables.

3.1.3 Instrumentation

Actually different commercial companies offer systems for resistivity imaging surveys such as Abem Instruments (Sweden), Advanced Geophysical Instruments (USA), Campus Geophysical Instruments (UK), Geofyzika (Czech Republic), GF Instruments (Czech Republic), Geometrics (USA), Geolog (Germany), IDS Scintrex (Canada), Iris Instruments (France), K.D. Jones Instrument Corporation (USA), OYO (Japan), Pasi Geophysics (Italy), MAE srl (Italy), ZZgeo (Australia).

The instrument type can be broadly divided into static and dynamic systems. Most instruments are of the static type involving, during the survey, many

electrodes planted into the ground and connected to a multi-electrode cable in order to get a wide data coverage. Instead, dynamic systems use a small number of probes and change the position of the whole system to obtain an extensive analysis (Loke 2004).

Different mobile systems (as Geometrics Ohm-Mapper system and the Corim System) have been recently developed using capacitive coupling to induce the flow of current in the ground (Gerard and Tabbagh 1991; Shima et al. 1996; Panissod et al. 1998). This system has some limitations such as a more limited depth of penetration due to the limited amount of current that can be induced into the ground compared to direct contact systems and the problem that it can be only used in areas that are paved, such as roads and city areas (Loke 2004).

The last generation of instrument is represented by the ARP© (Automatic Resistivity Profiler) system developed by the group co-ordinated by Michel Dabas at the University of Paris and experimented with by surveyors from the University of Siena in a variety of contexts. The ARP© system was first designed for agricultural applications in 2001 (GEOCARTA company, spin-off from CNRS, France). It was not before 2004 that the system was released for archaeological surveying, due to the necessary increase in terms of positional accuracy and measurement accuracy (Dabas 2009). The ARP system is a V-shaped multipole system with one transmitting dipole and three receiving dipoles, the length of which increases with their distance from the transmitter. Rolling electrodes are towed by an all-terrain vehicle even in very harsh environments. This method reduces the effect of the superficial geophysical noise on larger receiver dipoles, it uses three investigation depths without switching and the size of the arrays remains limited to a value equivalent to that of the investigation depth Panissod et al. (1998); Dabas (2009).

3.1.4   Field Work

The property of subsurface may be explored by moving the electrode array of fixed size, with a constant electrode separation, on a single line. In order to have an optimal response during the survey, the choice of the electrode spacing is fundamental for determining shape, size and depth of the features: the increasing of electrode separation will increase depth penetration with a loss of resolution and a reduction of signal size; instead a smaller electrode spacing becomes more critical and the surveyed subsurface is slower. The electrode spacing of one meter is a good compromise in archaeological prospections taking into account the dimensions and depth of structures (generally they are buried few meters under the soil) and the time available for the survey.

For example, in the axial dipole-dipole array the succession of measures provides that energizing electrodes are kept fixed while receiving electrodes are moved

by a distance n, $2n$, $3n$, and so on until the end of the line (n corresponds to the inter electrode distance). It then proceeds by moving the energizing electrodes of a position by repeating the measurements varying the distance in the same way. The process stops when the four electrodes are placed at the end of the profile. The increase of the distance between the two pairs of electrodes is realized in order to affect increasing portions of subsoil to the current flow, thereby determining values of apparent resistivity that will be referred to gradually increasing depth. If the target to be detected is stretched, such as a foundation or a road, the better profile is obtained perpendicularly to it, as far as we can predict this situation. Conversely, if it is irregular, a large number of parallel profiles forming a grid pattern is realized in order to test the extension and the size of the buried body: a 3D data matrix of the volume below the surface under investigation is obtained, from which horizontal sections at various depths are extracted after appropriate mathematical processes. The sections display the various underground structural features on a map that allow getting to the better archaeological interpretation.

3.1.5 Processing and Representation

To represent the data from a 2-D imaging survey, the pseudosection contouring method is normally used. Using the dipole-dipole array, the plotting convention is to attribute the values of apparent resistivity at the intersection point of two 45° lines descending from the current dipole and from the voltage dipole. The resulting maps of apparent resistivity are contoured at constant (usually logarithmic) inter-vals. The contoured sections are called pseudosections because they look somewhat like resistivity cross-sections of the ground, but actually, they are simply a graphical representation of the apparent resistivity dataset. The vertical scale is not depth but some function of the array spacing. For simplest geological models, the relative pseudosections do have an intuitive relationship to the actual section but mostly they do not. For a layered earth, the contour lines are horizontal and rise and fall in value in the same sense as the actual resistivity, but for the case of even a single vertical contact between dissimilar resistivities the pseudosection is a complex map with no direct relationship to the actual model. Similar procedures exist for other array types as well.

It must be remarked that any of the apparent resistivity representations, as described above, has only a rough relationship with the real resistivity pattern, whose modelling is the ultimate purpose of the survey. In fact, shape and amplitude of the anomalies, which strictly represent shifts among different apparent resistiv-ities, depend not only on the unknown true resistivity pattern and data density, but also on contamination due to even small inhomogeneities close to electrodes. In order to remove corrupting effects and model the survey targets as accurately as possible, a numerical inversion is needed to convert apparent into real resistivities.

The electrical resistivity tomography (ERT) approach comes from taking many apparent resistivity determinations at as many locations as possible and involves the joint inversion of many independent tests, using an algorithm to discern subtle details from differences that would otherwise not be seen in any one test. The inversion of an apparent resistivity dataset collected by the profiling field technique gives rise to a two-dimensional (2D) ERT. If one assembles a set of parallel profiles the inversion of the whole apparent resistivity dataset provides a three-dimensional (3D) ERT. In archaeological prospections, this operation can be useful to individuate anomalies that shows lateral and vertical variations by drawing sequences of pseudosections and/or horizontal slices at increasing pseudodepths.

Until the availability of computers, the interpretation was based on the adjustment procedures curves. Since the direct problem for stratified media was solved by the theory of linear filters (Gosh 1971a, b), many papers have appeared dealing with the automatic and numerical interpretation (Inman 1975; Koefoed 1979; Pous et al. 1987; Zohdy 1989). In recent years, there has been an increase in the use of two-dimensional and three-dimensional algorithms.

Menke (1989) says that the inverse problem is simply the set of methods used to extract useful information from our environment from physical measurements or data. In geophysical inversion, we seek to find a model that gives a response that is similar to the actual measured values. The model is an idealized mathematical representation of a section of the earth. The model has a set of model parameters that are the physical quantities we want to estimate from the observed data. The model response is the synthetic data that can be calculated from the mathematical relationships defining the model for a given set of model parameters. All inversion methods essentially try to determine a model for the subsurface whose response agrees with the measured data subject to certain restrictions (Loke 2004).

Resistivity inversion is a typical nonlinear, ill-posed, and underdetermined problem, Sasaki (2006), Ha et al. (2006), Pidlisecky et al. (2007), Marescot (2008).

The mathematical link between the model parameters and the model response for the 2-D and 3-D resistivity models is provided by the finite-difference (Dey and Morrison 1979) or finite-element methods (Silvester and Ferrari 1990).

One of the most accepted geophysical inversion procedure is the Gauss-Newton least-squared inversion (Lines and Treitel 1984) thanks to its range of applications and its robustness. An evolution of this technique is the Occam's inversion that demands smoothness of the model as a general constraint (Constable et al. 1987; de Groot-Hedlin and Costable 1990).

Furthermore, mainly in 3D cases, the number of the model parameters to be inverted is so high that the large computer time required to solve the problem makes the approach almost unpractical in routine applications. An efficient way of dealing with 2D and 3D inversion derives from a linearised form of the nonlinear problem. One-step and iterative linear methods have been proposed (Barker 1992; Loke and Barker 1996; Narayan et al. 1994; Chunduru 1996). In particular, Loke and Barker (1996) have developed a fast and versatile implementation of the smoothness-

constrained least-squares inversion in which a quasi-Newton methods is used to solve the Jacobian matrix of partial derivative during each iteration. The main advantage of such methods is that they can greatly reduce the computer time needed to generate an approximate model.

Smith and Vozoff (1984), Li and Oldenburg (1994), Dabas et al. (1994), Ellis and Oldenburg (1994), Tsourlos (1995) and Zhang et al. (1995) have also described other algorithms for resistivity inversion.

Such deterministic methods have strong limitations that depend on the physical principles on which they are based and are absolutely unbeatable. The fundamental aspect of the problem is that, in these reversal procedures, is awarded a purely deterministic process of interpretation whose main consequence is the non-uniqueness of the results: more models can generate the same set of data inside the experimental error, although small, connected to the measurement. This means that a starting model chosen a priori as input to the process binds the problem: if one changes the starting model, the result changes. Another problem concerns how to make the inversion, which is done by performing the inversion of the Jacobian matrix of the system: the inversion is an extremely unstable process that is possible only by introducing the so-called damping factors, which are filters and constraints of the algorithm. If these are changed, the result of the inversion is changed again.

Besides the well-known inversion procedures, there are other techniques that aim to obtain approximate representations of the subsoil in shorter times compared to those required by the "classical" iterative methods. These methodologies give approximated images of the resistivity patterns in the subsoil, in which zones of high or low resistivity are approximately represented. However, the resulting resistivity values are generally very different from the real ones and the resistivity gradient is generally much lower than the corresponding gradient obtained by the inverted models, Martorana and Capizzi (2014).

A filtered back-projection resistivity technique (BPRT) was described in more recent years. The procedure is based on a convolution of the experimental data with a filter function calculated on the basis of the sensitivity factors of each voxel on the various resistivity data, Cosentino et al. (1995, 1997, 1998). The calculation of the influence factors in a discrete set of representative points (centers of the voxels, to be utilized for the back-projection) is based on the integral of the influence density function on the volume of each voxel. In a recent paper, Martorana and Capizzi (2014) described an implementation of this technique considering a two-step approach. Initially a damped least squares solution is obtained after a full matrix inversion of the linearized geoelectrical problem. Furthermore, because of the results, a subsequent filtering algorithm is applied to the Jacobian matrix, aiming at reducing smoothness, and the linearized damped least square inversion is repeated to get the result. The technique was used to process 2D apparent resistivity datasets, in order to obtain a fast and contrasted resistivity image, useful for a rapid data check in field or as a starting model to constrain the inversion procedure.

A probability tomography method (RAOP) has been developed in more recent years as a simple and fast anomaly source imaging tool Mauriello et al. (1998, 1999a, b). The purpose of the technique is the design of an occurrence probability space of elementary anomaly sources, located anywhere inside an explored underground volume. In geoelectrics, the decomposition is made within a regular resistivity lattice, using the Frechet derivatives of the electric potential weighted by resistivity difference coefficients. The main features of the method are: unnecessity of a priori information; full, unconstrained adaptability to any kind of dataset, drastic reduction of computing time of even two orders of magnitude with respect to standard deterministic inversion tools, independence from data acquisition techniques and spatial regularity, capability to resolve complex continuous resistivity variation. Many field cases were dealt with using this approach (e.g. Cammarano et al. 2000; Compare et al. 2009a, b) and in all cases, the procedure proved to be a reliable tool for the most probable locations of the sources of the measured apparent resistivity anomalies to be highlighted at the appropriate depths. No information can, however, be deducted as it regards the estimation of the real resistivities to associate with these bodies. In order to approach also this last objective, the probability-based ERT inversion (PERTI) has been proposed by Mauriello and Patella (2009). The purpose was to combine the high geometrical resolution power of the probability tomography imaging with the need of reconstructing the most probable real resistivity pattern Cozzolino et al. (2012, 2013).

Figure 3.1a shows a 2D model composed by three infinitely long horizontal prisms with rectangular cross-section and resistivity 500, 10 and 30 Ω m, respectively, placed inside a uniform half-space with resistivity 100 Ω m Mauriello and Patella (2009). The section is assumed to be investigated using a dipole-dipole array along a profile long 36 m with an electrode distance of 1 m. The three prisms are 3 m wide and 1.3 m high, with the top surfaces placed at 1.5 m of depth. The pseudosection, contaminated by a 5% random noise, is plotted in Fig. 3.1b. In order to accommodate the wide resistivity range detected inside the ground and to better show order of magnitude changes, a common logarithmic scale has been used for visualization of apparent resistivity sections and the real resistivity maps (for the use of logarithmic scales in geoelectrics, see, e.g. Chambers et al. 2006). It is worth recalling that the anomaly dragging with the shape of inverted V, is a phantom effect, typical of the dipole–dipole array. It is, essentially, a contamination of the whole section due to the presence of a strong resistivity inhomogeneity close to the current or potential dipole. Figure 3.1c, d show the resistivity sections obtained by the RAOP, Mauriello and Patella (1999a, b) and ERTLAB softwares [Multi-Phase Technologies (www.mpt3d.com) and Geostudi Astier (www.geoastier.com)].

To conclude this section, we report the responses from a prospection realized inside the partially ruined monumental complex of Bedestan (Cyprus), with the aim to detect buried traces of a Byzantine basilica of the sixth century, Cozzolino et al. (2013). The survey has been conducted on the floor of the monument, using a dipole–dipole electrode array along two perpendicular sets of profiles (Fig. 3.2a).
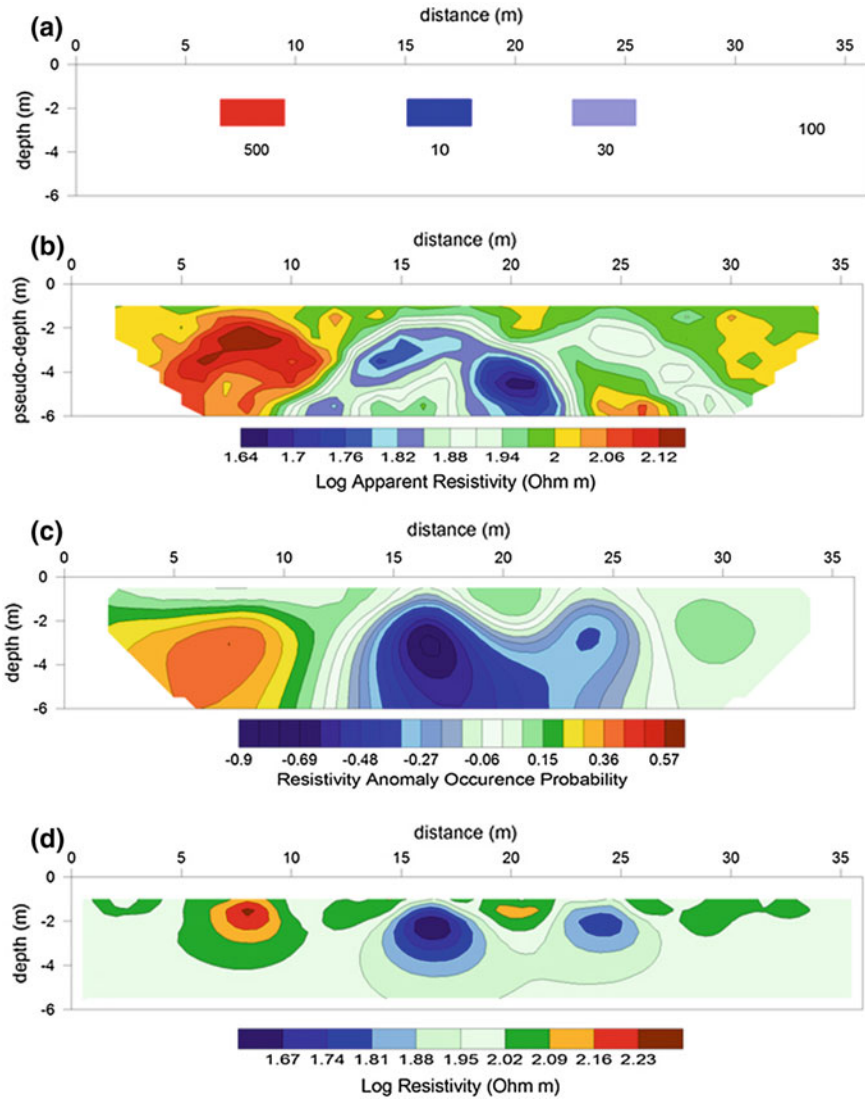
Fig. 3.1 2D three-prism model (**a**), the simulated pseudosection (**b**), the model reconstruction by the RAOP (**c**) and ERTLAB software (**d**)

Figure 3.2b shows a sequence of horizontal slices, depicting the contoured apparent resistivity values at increasing pseudodepths. A variation of the apparent resistivity from 10 Ω m to about 400 Ω m can readily be observed, with a concentration of apparent resistivity highs below the front half of the Bedestan complex, which are well distinguished from an area of almost uniform low apparent resistivity values in the rear half of the complex. The comparison between PERTI, Mauriello and

Fig. 3.2 The ERT survey planning inside the Bedestan monument. Full and dashed lines over the sketched topographic map of the complex indicate longitudinal and transversal ERT profile sets, respectively (**a**). Contoured appa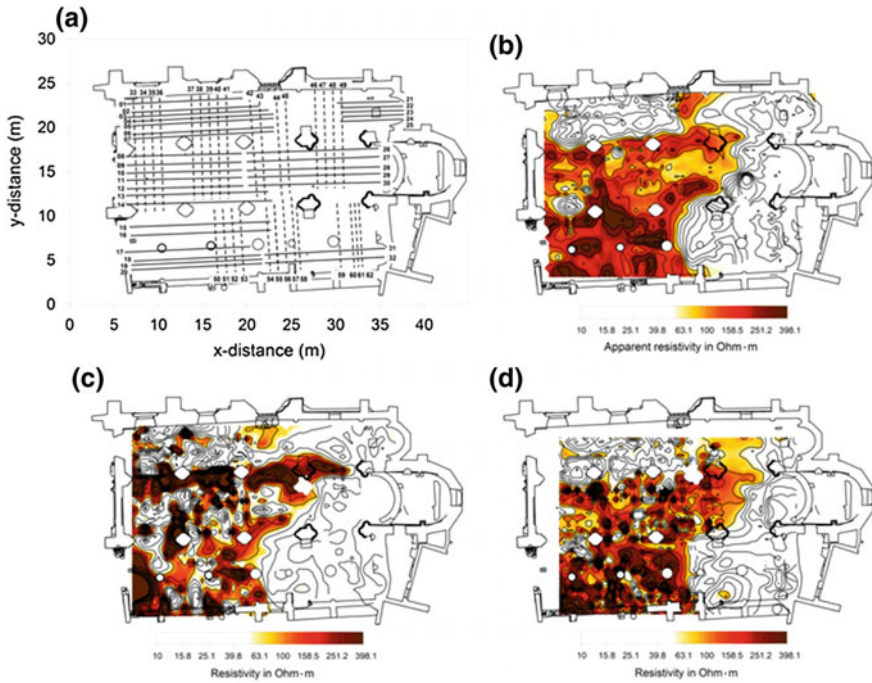rent resistivity maps on horizontal slices at 1 m in depth (**b**). Modelled real resistivity map constructed by the PERTI method (**c**) and by the ERTLab method (**d**)

Patella (2009) and ERTLab (Fig. 3.2c, d) shows a general agreement, as regards the features of the main resistive structures that demonstrate in plan the shape of a church characterised by a central nave with an apse and two side aisles.

3.2 The Ground Penetrating Radar (GPR) Method

Abstract The Ground Penetrating Radar is an electromagnetic impulsive method much suited for shallow depth investigations, as it can supply subsurface profiles grouped in vertical radar sections. The transmitter-receiver antenna is pulled along the surface of a site, signals are sent with a highly directive radiation pattern into the ground and echoes are returned from targets in the ground within a few meters. The emitted radar signal is a pulse of electromagnetic radiation with nominal frequency value in the range 15–2500 MHz (1 MHz = 10^6 Hz). The velocity of an electromagnetic wave in air is 30 cm/ns (1 ns = 10^{-9} s). In soils the velocity is less, as typical values are in the range 5–15 cm/ns. According to the media impedance and

to their heterogeneity, the radar pulse can be reflected towards the surface or else it can be attenuated and diffused, hence quickly totally dissipated. When reflected echoes emerge, the received signal can be correlated with the transmitted one and the delay of arrivals, i.e. the travel time in the ground, is a function of velocity. The vertical scale in radargrams is proportional to the two-way travel time (twt): it can be transformed in a depth scale if the wave propagation velocity is known. In general, it can be stated that the wave propagation velocity is affected by the dielectric constant and by the magnetic susceptibility of the media. The electric conductivity contributes to the wave attenuation and to its reflection. Another important attribute of radar is the resolving power, or the ability to locate small objects. The wavelength affects the ability of the Georadar to identify thin layers or isolated features. Resolution is more than l/2 and the depth of horizontal interfaces can be determined to about l/10. In order to get a better resolution, a higher frequency antenna could be used, but this would increase attenuation, while low frequency antennas have a coarser resolution but their penetration depth is remarkably better. Strong attenuations occur in electrically conductive media. If the conductivity is low, but the number of electrical interfaces is high, multiple reflections could reduce penetration depth, while poor conductivity combined with a small number of reflecting interfaces will cause the wave to be attenuated as a function of the distance between the antenna and the reflecting interface. The strength of reflections of radar pulses depends primarily on the magnitude of change in the dielectric coefficient or conductivity at a discontinuity, and not on the bulk magnetic susceptibility or on the resistivity contrast. The dielectric constant is a measure of how easily charges polarize or separate in a target excited by electromagnetic radiation. Metals have essentially an infinite dielectric coefficient and thus produce very strong reflections. A pit with a well-defined boundary will produce a better reflection. Walls and foundations are also good reflectors. Typical archaeological applications are the search for graves, buildings and the identification of anthropic soil transformations. The increasing necessity for detailed three-dimensional resolution of the shallow depth structures makes the 3D GPR acquisition one of the most important remote sensing tools. One of the most useful representation of the GPR data sets collected along closely spaced parallel profiles is to display the data in horizontal maps of recorded reflection amplitudes measured across the survey grid. These maps, referred to as amplitude time slices, allow easy visualization of the location, depth, size and shape of radar anomalies buried in the ground. The maps can be created at various reflection time levels within a data set to show radar structures at a specified time (depth) across a surveyed site. Mapping the energy in the reflected radar returns across a survey grid can help to create useful information that can sometimes mirror the general archaeological site plan result obtained from invasive excavation. In areas where the stratigraphy is complex and buried features are difficult to discern, amplitude time slice analysis is one of the most efficient post processes which can be applied to the raw data to extract the 3-D shapes of buried remains.

3.2.1 Introduction

Generally the term Ground Penetrating Radar (GPR) has been applied to all methods of geophysical prospection utilizing electromagnetic radiation in a range from 15 MHz to 12.4 GHz to image buried structures. This encompasses a wide range of applications and the term is used to describe the more common available GPR systems suitable for archaeological prospections (Conyers and Goodman 1997; Reynolds 1997; Daniels 2004; Goodman and Piro 2013).

GPR can often be more costly than conventional methods of area geophysical survey (e.g. magnetic and earth resistance techniques), but does present some unique capabilities to provide estimates of the depth to target features and, under suitable conditions, present three-dimensional models of buried remains. GPR can also be the only practical method to apply on particular sites, or within historical and modern buildings, where the presence of hard surfaces and ground ferrous disturbances precludes the use of other geophysical techniques as magnetic and earth resistance.

A wide range of site conditions may be considered for GPR survey, including concrete, tarmac and even fresh water, although the technique is limited by the attenuation of the electromagnetic signal in conductive media. In practice, this will largely be determined by the concentration of clay and the moisture content of the soil at the site. Highly conductive media, such as metal objects or salt water will prove largely opaque to the GPR signal. Strong reflectors in the near surface will also reduce the energy transmitted to immediately underlying targets and this may include the local water table (or other near surface interface).

For normal ground-coupled antenna, good physical contact with the site surface is necessary to ensure adequate coupling of the radar energy with the soil. As far as possible, vegetation and any other surface obstructions should be removed from the site prior to the survey.

High-frequency air-launched horn antennas are designed to be operated from above the ground surface for civil engineering applications, but do not have sufficient depth penetration for archaeological prospections.

Many site-condition variables must be considered when using GPR but in general it will respond to a wide range of archaeological features and is often successful over sites where earth resistance survey has proved fruitful (as presence of masonry walls, void spaces, etc.). GPR is sensitive to the interface between differing materials and some target features produce highly distinctive GPR anomalies.

Precise depth estimation from GPR survey is often difficult to achieve, yet is a critical process for the successful presentation of the results. Unprocessed GPR data, expressed in terms of the time delay of returned reflections, can always be recalibrated in the light of additional information to present a more accurate physical depth estimate for other unexcavated targets.

While the use of GPR for detailed large area surveys (more than 1 ha) has in the last few years increased, it is often applied as a complementary technique, following

the acquisition made employing magnetic or earth resistance methods, to locate archaeological structures identified over a more limited area of the site.

Care must be taken into account to ensure that GPR survey is appropriate to a site, particularly if it is the only technique to be applied. The proximity to sources of radio-frequency interference that may affect the data quality should be considered.

The increasing necessity for detailed three-dimensional resolution of the shallow depth structures makes the 3D GPR acquisition one of the most important remote sensing tools. The advantages of 3D surveying are documented for the case of mapping geological features (Grasmueck 1996; Sigurdsson et al. 1998); as well as archaeological investigations, where the higher horizontal and vertical resolution is required (Conyers et al. 1997; Leckbush 2000; Malagodi et al. 1996). High-resolution acquisition techniques, using a sub-meter profile spacing interval have been successfully applied in locating subsurface archaeological structures (Goodman et al. 1995; Malagodi et al. 1996; Pipan et al. 1996–1999–2001; Basile et al. 2000), and also to image large scale archaeological features (Nishimura et al. 2000; Neubauer et al. 2002; Piro et al. 2001, 2003).

3.2.2   Basic Theory

The Ground Penetrating Radar is an electromagnetic impulsive method much suited for shallow depth investigations, as it can supply subsurface profiles grouped in vertical radar sections. The transmitter-receiver antenna is pulled along the surface of a site, signals are sent with a highly directive radiation pattern into the ground and echoes are returned from targets in the ground within a few meters (Fig. 3.3a).

The emitted radar signal is a pulse of electromagnetic radiation with nominal frequency value in the range 15–2500 MHz (1 MHz = 10^6 Hz). The velocity of an electromagnetic wave in air is 30 cm/ns (1 ns = 10^{-9} s). In soils the velocity is less, as typical values are in the range 5–15 cm/ns.

GPR systems employ e.m. (electromagnetic) source, generated by a transmitter antenna on the ground surface and record the amplitude and time-delay of secondary reflections from buried structures.

According to the media impedance and to their heterogeneity, the radar pulse can be reflected towards the surface or else it can be attenuated and diffused, hence quickly totally dissipated. When reflected echoes emerge, the received signal can be correlated with the transmitted one and the delay of arrivals, i.e. the travel time in the ground, is a function of velocity (Fig. 3.3b). The secondary reflections are produced when the GPR pulse is incident upon any media with contrasting conductivity σ or permittivity ε_r or both to the medium above. The magnetic susceptibility μ of the sub-surface will also influence the propagation of a radar wave, but for most practical considerations it may be ignored.
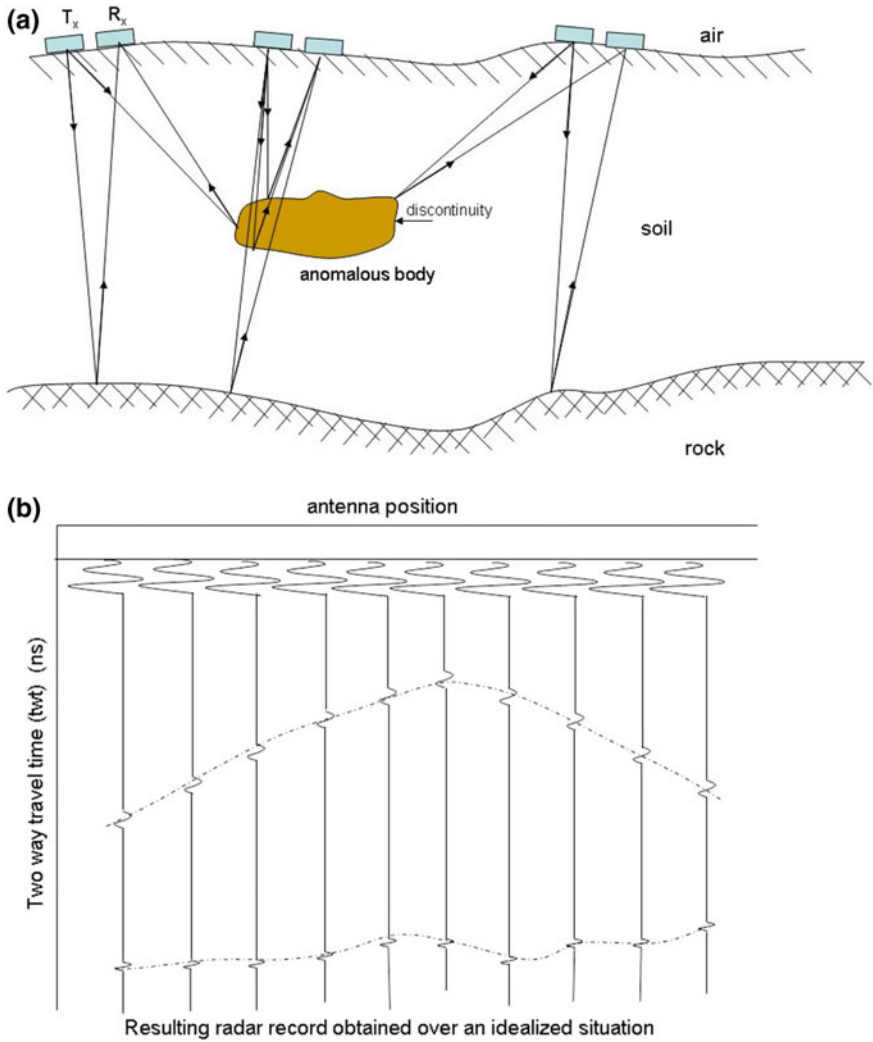
Fig. 3.3 a Schematic view of the physical mechanism of the GPR source/target coupling effect.
b Example of GPR profile

The vertical scale in radargrams is proportional to the two-way travel time (twt):
it can be transformed in a depth scale if the wave propagation velocity is known.

In general, it can be stated that the wave propagation velocity is affected by the
dielectric constant ε_r and by the magnetic susceptibility μ of the media. The electric
conductivity σ contributes to the wave attenuation and to its reflection.

The propagation of electromagnetic waves is described by the wave equations:

$$\nabla^2 E = \gamma^2 E \tag{3.20}$$

$$\nabla^2 H = \gamma^2 H \tag{3.21}$$

where $\gamma^2 = i\omega\mu(\sigma + i\omega\varepsilon)$, $i = \sqrt{-1}$, $\omega = 2\pi f$ in rad/s, f is the frequency in Hz, σ is the conductivity in mho/m, $\mu = \mu_0\mu_r$ is the magnetic susceptibility and $\varepsilon = \varepsilon_0\varepsilon_r$ is the electric permittivity.

The propagation factor or wave number $\gamma = \alpha + j\beta$ is that square root of γ^2 whose real and imaginary parts are positive. The attenuation factor **α** and the space shift constant **β** are:

$$\alpha = \omega\left\{\frac{\mu\varepsilon}{2}\left[1+\left(\frac{\sigma}{\omega\varepsilon}\right)^2\right]^{1/2} - 1\right\}^{1/2} \tag{3.22}$$

and

$$\beta = \omega\left\{\frac{\mu\varepsilon}{2}\left[1+\left(\frac{\sigma}{\omega\varepsilon}\right)^2\right]^{1/2} + 1\right\}^{1/2} \tag{3.23}$$

respectively. Moreover, the wave length **λ** and phase velocity **v** are respectively defined as

$$\lambda = \frac{2\pi}{\beta} \tag{3.24}$$

and

$$v = \mathrm{lf} = \frac{\omega}{\beta} \tag{3.25}$$

The electromagnetic field E_0 originating at z = 0, t = 0, at a distance z and time t will be described by E(z,t) as follows

$$\mathbf{E}(z,t) = \mathbf{E}_0 e^{-\alpha z} \cdot e^{i(\omega t - \beta z)} \tag{3.26}$$

The first exponential function is the attenuation term and the second is the propagation term. From the first exponential function it is seen that the attenuation is 1/e at a distance z = 1/a, which is also called the *skin depth d.*

The intrinsic impedance Z is the relation between the electric field and the magnetic field, i.e.

$$Z = \frac{\mathbf{E}}{\mathbf{H}} \tag{3.27}$$

Z is a complex quantity which is calculated according to

$$Z = \sqrt{\frac{i\omega\mu}{\sigma + i\omega\varepsilon}} \tag{3.28}$$

The following simple formulas can be used in practical field measurements

$$v = \frac{c}{\sqrt{\varepsilon_r}} \tag{3.29}$$

which is the wave propagation velocity, where c is the velocity of the light in free space (0.3 m/ns),

$$s = \frac{vt}{2} \tag{3.30}$$

which is the reflector depth, where t is the travel time t (ns),

$$K = \frac{\sqrt{\varepsilon_{r_1}} - \sqrt{\varepsilon_{r_2}}}{\sqrt{\varepsilon_{r_1}} + \sqrt{\varepsilon_{r_2}}} \tag{3.31}$$

which is the reflection coefficient (R = 1 − K is the penetration coefficient), and

$$A = 12.863 \times 10^{-8} f \sqrt{\varepsilon_r} \left[\left(tg^2\delta + 1 \right)^{1/2} - 1 \right]^{1/2} \tag{3.32}$$

which is the attenuation in the medium.

A limiting factor for the GPR survey is the attenuation, or signal power loss, Fig. 3.4.

This is expressed in decibels/meter (dB/m), the number of decibels being 10 times the logarithm of the ratio of the signal power to the initial power. Considering antenna efficiencies and reflection losses, a typical system can operate with a 50 dB loss (Weymouth 1986b).

Another important attribute of radar is the resolving power, or the ability to locate small structures. The wavelength affects the ability of GPR to identify thin layers or isolated features. Resolution is more than l/2 and the depth of horizontal interfaces can be determined to about l/10 (Weymouth 1986b). In order to get a better resolution, a higher frequency antenna could be used, but this would increase

Fig. 3.4 Values of velocity (**a–b**) and attenuation (**b–c**) for different frequencies of an electromagnetic wave and for different conductivities (after Davis and Annan 1989)

(a)

VELOCITY (m/ns)

CONDUCTIVITY (mS/m)

$c/\sqrt{K}$

1 000
100
10
1

WATER RELAXATION EFFECT
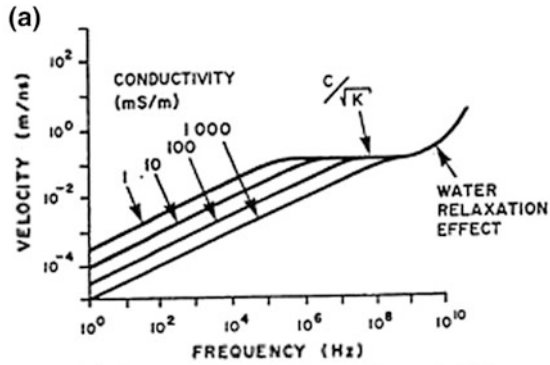
FREQUENCY (Hz)

The relation between velocity and frequency at different conductivities.

(b)

-Typical dielectric constant, electrical conductivity, velocity and attenuation observed in common geological materials at 100 MHz

Material	K	σ (mS/m)	V (m/ns)	α (dB/m)
Air	1	0	0.30	0
Distilled water	80	0.01	0.033	2×10^{-3}
Fresh water	80	0.5	0.033	0.1
Sea water	80	3×10^4	0.01	10^3
Dry sand	3–5	0.01	0.15	0.01
Saturated sand	20–30	0.1–1.0	0.06	0.03–0.3
Limestone	4–8	0.5–2	0.12	0.4–1
Shales	5–15	1–100	0.09	1–100
Silts	5–30	1–100	0.07	1–100
Clays	5–40	2–1000	0.06	1–300
Granite	4–6	0.01–1	0.13	0.01–1
Dry salt	5–6	0.01–1	0.13	0.01–1
Ice	3–4	0.01	0.16	0.01

(c)

ATTENUATION (dB/m)

WATER RELAXATION EFFECT

1000
100
10
1

CONDUCTIVITY (mS/m)
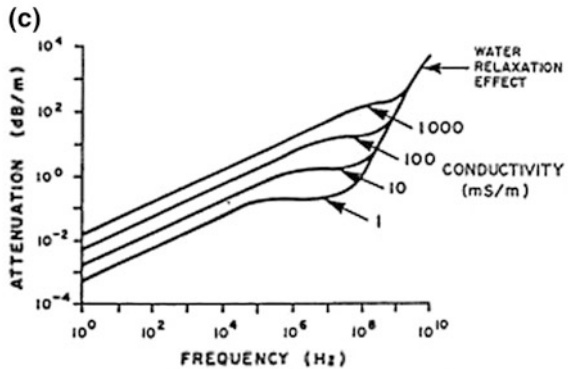
FREQUENCY (Hz)

- The relation between attenuation and frequency at different conductivities.

attenuation, while low frequency antennas have a coarser resolution but their penetration depth is remarkably better.

Strong attenuations occur in electrically conductive media. If the conductivity is low, but the number of electrical interfaces is high, multiple reflections could reduce

penetration depth, while poor conductivity combined with a small number of reflecting interfaces will cause the wave to be attenuated as a function of the distance between the antenna and the reflecting interface (Finzi and Piro 1991, 2000).

The strength of reflections of radar pulses depends primarily on the magnitude of change in the dielectric coefficient or conductivity at a discontinuity, and not on the bulk magnetic susceptibility or on the resistivity contrast. The dielectric constant is a measure of how easily charges polarize or separate in a target excited by electromagnetic radiation.

Metals have essentially an infinite dielectric coefficient and thus produce very strong reflections. A pit with a well-defined boundary will produce a better reflection. Walls and foundations are also good reflectors. Typical archaeological applications are the search for graves, buildings and the identification of anthropic soil transformations.

The maximum depth of penetration for a GPR is governed by a combination of signal scattering and attenuation within the subsurface, through the dissipation of radio-frequency energy as eddy currents within conductive media.

The resulting time-amplitude data is displayed as a two-dimensional profile with X-axis indicating the horizontal location of the antenna on the ground surface and the Y-axis representing the increasing time-delay (depth) from the initial pulse.

3.2.3 Instrumentation

GPR system is based on antenna unit housing the transmitter and receiver, an electronic control unit with a data console and a power supply. Different configurations of these systems are offered by the major manufactures and each may have advantages in particular survey conditions.

The GPR impulse covers a comparatively broad band of frequencies, usually defined by a nominal centre frequency. Because of the increased attenuation of higher frequencies, low-centre-frequency antennas will provide a greater depth of penetration. However, the longer wavelengths produced by low-centre-frequency antenna will reduce the vertical and lateral resolution of buried targets and only physically large structures will be detected at depth.

The majority of commercial GPR systems allow operation with a number of interchangeable antenna units with different centre frequencies to suit the soil conditions, depth of penetration and resolution required. For near-surface archaeological surveys a bistatic antenna unit, consisting of a separate transmitter and receiver dipole bow-tie will be used. Most mid-to-high-centre-frequency antennas will also be shielded to minimize unwanted reflections.

More specialized antenna units designed for specific requirements such as rapid acquisition of densely sampled data-sets are the multiple parallel antenna arrays.

The central units provide the driving signal to the antenna and sample the received response at a sufficiently high frequency. Modern systems digitize the receiver data directly, enabling detailed post-acquisition processing.

Increasingly GPR systems offer multi-channel operation where two or more sets of antennas can be recorded in a near-simultaneous manner. This might allow a site to be covered with a range of centre frequencies, imaging both near-surface and deeper-lying targets, or a parallel array of antenna units can be used for the rapid acquisition of densely sampled data.

More recently integrated GPR systems have been designed for single user operation with all of the components mounted on a compact wheeled cart.

3.2.4   Field Work

This section presents only the use of impulse GPR system operating in a common offset antenna configuration. Preliminary field tests are necessary to confirm that the equipment is functioning properly, and that instrument parameters are correctly set. Antennas of differing centre frequencies should be tested to determine an appropriate balance between resolution and depth penetration. The acquisition may have to be conducted with more than one frequency of antenna, either because of rapidly changing site conditions or the need to resolve targets of differing physical size and depth of burial.

The requirement for the survey grid is similar to other geophysical techniques but acquisition on standing buildings may impose special requirements for recording the position of the antenna over the face of a wall or ceiling. Survey profiles should, where possible, be positioned parallel to any surface irregularities to maintain good antenna coupling with the ground surface.

Strong radar reflectors present at the surface of the site may produce spurious reflections in the data caused by uncoupled energy leaking from the transmitter. This may occur over sites with uneven terrain where the antennas do not make good physical contact with the ground surface.

There are three main modes of GPR data acquisition:

1. Scanning—GPR systems provide a real-time visual display of the recorded data and may be used to locate known or suspected features, perhaps during the invasive works in the field. Cart-based systems may be reversed along the profiles while scrolling the data backwards to identify the location of an anomaly.
2. Individual recorded profiles—single profiles may be recorded over the suspected location of known features or to investigate anomalies identified by other geophysical techniques.

3. Detailed area survey—Area survey over a regular grid of closely spaced traverses is strongly recommended for detailed GPR investigations. Ideally, to avoid spatial aliasing, traverse spacing should be less than the approximate footprint of the radar energy at the required depth of investigation. Under typical conditions for a 400 MHz centre-frequency antenna any traverse spacing above 0.25 m will be spatially aliased. However, as such densely sampled surveys are difficult to achieve over large areas unless a multi-channel system is available, a profile separation of 0.5 m is suggested where spatial aliasing will not be detrimental to the interpretation of the target features. The non-symmetric radiation pattern from a GPR antenna causes the orientation of the targets—with respect to the direction of the profile—to influence the anomaly produced. Repeat survey over orthogonal profiles, or very closely spaced parallel traverses (0.1 m) will improve the definition of features running closely parallel to the original orientation of the data profiles.

   Profiles collected over a regular grid may be acquired in either a parallel or zigzag direction, providing sufficient care is taken with the positioning of the antenna to avoid any offset between alternate lines.

The number of scans (traces) to be recorded along each profile, the time window through which reflections are measured for each trace and the number of times each trace is repeated at a particular sample point (stacking), should be set to appropriate values to image the targets under investigation. Because of the low S/N (signal-to-noise ratio) of the GPR signal, oversampling is recommended. For a typical archaeological survey, with a mid-centre-frequency antenna (400 MHz), traces should be recorded at least every 0.05 m along a profile. Establishing the correct time window through field trials is more important as this will determine the maximum depth to which the GPR system will record data.

Any time to depth estimate should be supported with details of how the sub-surface velocity was determined and applied to the data, taking into account any significant alteration of soil type across the site. This may be achieved through either calibration between a recorded reflection and a known-depth target, analysis of the shapes of diffraction hyperbolas, common mid-point (CMP) measurements made in the field.

3.2.5 Processing and Representation

The resulting high-density data are best presented as a series of time-slices where each successive time slice represents the horizontal variation of reflector strength (energy) across the survey area for a given two way travel time (twt or depth estimate). Visualizing the GPR results in this format may greatly assist the interpretation of complex data-sets. Additional modes of display and data analysis, including examination of the individual profiles, are also recommended. The use of

3D representations of the strongest reflectors, may enhance the visualization of data-sets or anomalies (Goodman and Piro 2013).

One of the most useful representation of the GPR data sets collected along closely spaced parallel profiles is to display the data in horizontal maps of recorded reflection amplitudes measured across the survey grid. These maps, referred to as amplitude time slices, allow easy visualization of the location, depth, size and shape of radar anomalies buried in the ground. The maps can be created at various reflection time levels within a data set to show radar structures at a specified time (depth) across a surveyed site. Mapping the energy in the reflected radar returns across a survey grid can help to create useful information that can sometimes mirror the general archaeological site plan result obtained from invasive excavation.

The raw reflection data acquired by GPR is nothing more than a collection of many individual traces along 2-D transepts within a grid. Each of those reflection traces contains a series of waves that vary in amplitude depending on the amount and intensity of energy reflection that occurred at buried interfaces. When these traces are plotted sequentially in standard 2-D profiles, the specific amplitudes within individual traces that contain important reflection information are usually difficult to visualize and interpret. In areas where the stratigraphy is complex and buried features are difficult to discern, amplitude time slice analysis is one of the most efficient post processes which can be applied to the raw data to extract the 3-D shapes of buried remains (Malagodi et al. 1996; Conyers and Goodman 1997; Goodman et al. 1993, 2004a, b; Goodman and Piro 2013; Piro et al. 2000, 2001).

Due to velocity changes across the area and with depth, a slice map made across a constant level time window, will not represent a level slice in terms of depth in the ground. Horizontal time slices must therefore be considered only approximate depth slices. Without very detailed velocity control throughout a grid, it is impossible to construct perfectly horizontal depth slices (Leckbusch 2000).

To compute horizontal time slices, the employed software compares amplitude variations within traces that were recorded within a defined time window. When this is done, both positive and negative amplitudes of reflections are compared to the norm of all amplitudes within that window. No differentiation is made between positive or negative amplitudes in this analysis, only the magnitude of amplitude deviation from the norm. Low-amplitude variations within any one slice denote little sub-surface reflection, and therefore indicate the presence of fairly homogeneous material. High amplitudes indicate significant subsurface discontinuities and in many cases detect the presence of buried features. Finally data are interpolated and gridded on a regular mesh (Fig. 3.5).

A high-to-low amplitude scale is normally presented as part of the legend of each map, but without specific units because, in GPR, reflected wave amplitudes are usually arbitrary.
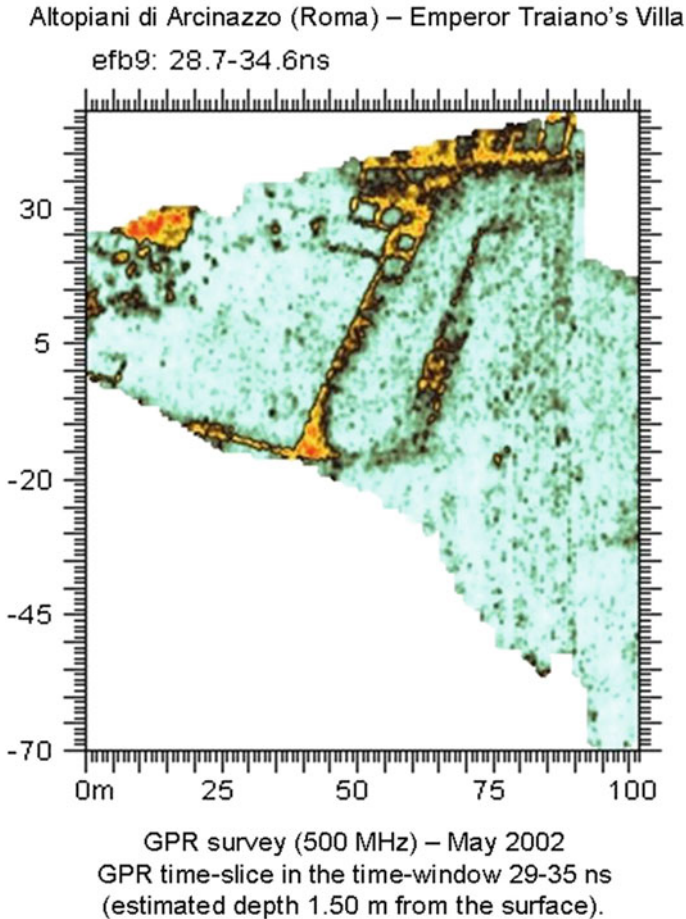
Fig. 3.5 Traiano's Villa, GPR time slice in the time window 29–35 ns (twt). The map shows clear anomalies due to the presence of walls and rooms

3.3 Magnetic Surveying

Abstract The magnetic methods were first applied in the 1950s and have since then become the backbone in archaeological prospecting. Now, they are used even more frequently than the other prospecting methods. Typically, soils that have had campfires over them show increased magnetic susceptibility, resulting from the consequent reducing environment. This condition causes the formation of magnetite even when moderate amounts of iron are present. Magnetometers can easily detect variations of less than 0.1% magnetite content in soil. The magnetic surveying is a passive technique, relying, for the source of its signal, on the presence of the earth's magnetic field. In magnetic surveying, the field strength is measured with a

magnetometer placed a few tens of centimetres above the ground level. Measurements can be taken either along profiles or on a mesh of points. Above a flat, homogeneous medium the magnetic field would result quite uniform. However, the presence of local concentrations of soils, rocks and iron objects, magnetized by the earth's main field, slightly alter the magnetic field all nearby. These anomalies may be observed in the measured values. The aim is to interpret such kind of anomalies in terms of possible archaeological resources. The degree of soil magnetization is a function of the external field strength and of a property of soils known as magnetic susceptibility. The sources of susceptibility are iron compounds in soils, principally hematite, magnetite and maghemite. All soils have magnetic susceptibility to some degree, but what is fundamental in generating anomalies is the susceptibility contrast of a structure with respect to the surrounding matrix. Natural and anthropogenic causes can generate this contrast. Anthropic features with significant contrasts include pits with organic content, ditches filled with top soil, intrusive structures such as walls and foundations, fire hearths, burned houses and bricks. In archaeological prospectings, three types of instruments are currently used, namely the fluxgate gradiometer, the alkali metal (cesium or potassium) optical pumping magnetometer and the proton free precession magnetometer. Under ideal conditions, if the magnetic field were measured on a row of points above a flat, uniform earth, all the values would be the same. If the uniform earth contained even one small, isolated feature having a magnetic susceptibility greater than that of the surrounding rock, the feature would be more magnetized than the surrounding soil and would set up its own local magnetic field. This extra induced field is known as a dipole field. This local dipole field then adds vectorially to the field of the earth to produce an anomaly. Anomalies exist in archaeological sites as a consequence of the contrast in magnetic properties between the archaeological features of interest and the surrounding medium, both of which are usually composed of material of natural origin such as rocks or soil or even empty space. This magnetic contrast is a function of both the concentration and the thermal and mechanical history of magnetite in either the archaeological target or its hosting material. The anomalies observed in archaeological sites are in most situations very complex as a consequence of several factors. The sources of the anomalies are relatively shallow and therefore very close to the magnetometer, which of course automatically tends to emphasize the highly complex nature of the near field of any magnetic object. The various sources of magnetic anomalies from soils, near surface rocks and the clutter of ancient and/or modern human habitations, including the many objects of real interest, are usually very strong. However, the measures collected in archaeological contexts are often masked by noise. For such main reason, it is advisable during the survey to employ portable gradiometers. The gradiometer automatically removes the regional field and thus it notably increases the resolution of the local anomalies. A composite source can be therefore portrayed as a more resolved anomaly, since different edges of the source can this way be separated into two or more discrete anomalies.

3.3.1 Introduction

The magnetic methods were first applied in the 1950s (Aitken et al. 1958) and have since then become the backbone in archaeological prospecting. Now, they are used even more frequently than other geophysical methods. Typically, soils that have had campfires over them show increased magnetic susceptibility, resulting from the consequent reducing environment. This condition causes the formation of magnetite even when moderate amounts of iron are present. Magnetometers can easily detect variations of less than 0.1% magnetite content in soil.

Magnetometer survey offers the most rapid ground coverage of the various survey techniques and responds to a wide variety of anomalies caused by past human activity. It should thus be the first technique considered for detailed survey of an area and other, techniques should usually follow afterwards, targeting in depth areas of interest identified by the wider magnetometer survey.

It can identify thermoremanently magnetized features such as kilns and furnaces as well as in-filled ditches and pits and areas of industrial activity (both recent and ancient). Unless composed of materials that contrast magnetically with the surrounding soil (brick carrying a thermoremanent magnetization), magnetometers do not detect wall footings directly and in this case it is complemented by GPR or earth resistance surveys.

3.3.2 Basic Theory

Under ideal conditions, if the magnetic field were measured on a row of points above a flat, uniform earth, all the values would be the same. If the uniform earth contained even one small, isolated feature having a magnetic susceptibility greater than that of the surrounding rock, the feature would be more magnetized than the surrounding soil and would set up its own local magnetic field. This extra induced field, which is similar to that of the earth, but at a notably smaller scale, is known as a dipole field. This local dipole field then adds vectorially to the field of the earth to produce an anomaly. Figure 3.6 shows a profile produced by the earth's main field combined with an anomalous magnetic field due to a local feature (Piro 2009).

The magnetic surveying is a passive technique, relying, for the source of its signal, on the presence of the earth's magnetic field. The appropriate unit by which to measure the field strength is the nanoTesla (nT) and picoTesla (pT), (Parasnis 1986; Breiner 1973; Becker 1995). In magnetic surveying, the field strength is measured with a magnetometer placed a few tens of centimetres above the ground level. Measurements can be taken either along profiles or on a mesh of points. Above a flat, homogeneous medium the magnetic field would result quite uniform. However, the presence of local concentrations of soils, rocks and iron objects, magnetized by the earth's main field, slightly alter the magnetic field all nearby. These anomalies may be observed in the measured values. The aim is to interpret
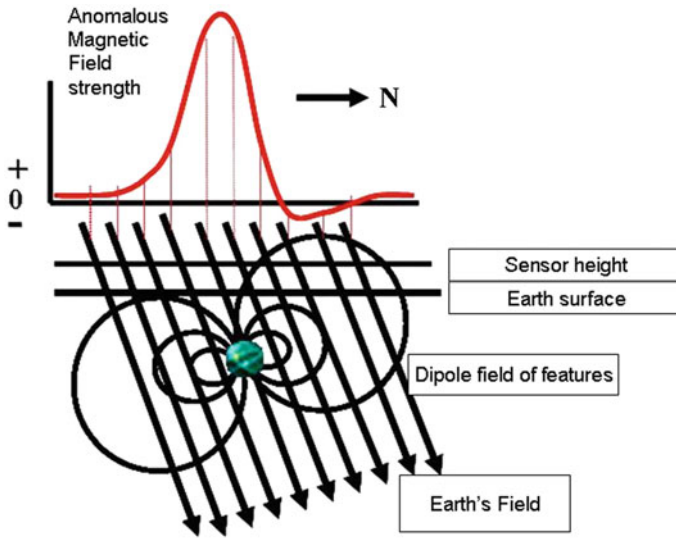
Fig. 3.6 Diagram of a south-north magnetic profile produced by the earth's main field combined with an anomalous magnetic field due to a local feature (after Weymouth, redrawing 1986b)

such kind of anomalies in terms of possible archaeological resources (Aitken 1974; Breiner 1973; Huggins 1984; Weymouth 1986a, b; Brizzolari et al. 1992–1993; Scollar et al. 1990; Eder-Hinterleitner et al. 1996; Neubauer et al. 1997a, b; Piro et al. 1998, 2000, 2007; Becker and Fassbinder 2001; Ciminale and Loddo 2001; Godio and Piro 2005).

The degree of soil magnetization is a function of the external field strength and of a property of soils known as magnetic susceptibility. The sources of suscepti-bility are iron compounds in soils, principally hematite, magnetite and maghemite.

If some demagnetized object is placed in a magnetic field, it can become magnetized. In absence of external field, if the object presents magnetism, this magnetization is called remanent. If this magnetism is a consequence of heating, we have thermoremanent magnetization. All soils have magnetic susceptibility to some degree, but what is fundamental in generating anomalies is the susceptibility con-trast of a structure with respect to the surrounding matrix. Natural and anthro-pogenic causes can generate this contrast. Anthropic features with significant contrasts include pits with organic content, ditches filled with top soil, intrusive structures such as walls and foundations, fire hearths, burned houses and bricks.

In the case of fire hearths, burned houses, and bricks, an additional contribution arises from the thermoremanent magnetism that they retain. Although the ther-moremanent magnetism of individual bricks will probably be randomized in moving from kiln to construction, they can also have a strong induced magnetism.

Anomalies exist in archaeological sites as a consequence of the contrast in magnetic properties between the archaeological features of interest and the

surrounding medium, both of which are usually composed of material of natural origin such as rocks or soil or even empty space. This magnetic contrast is a function of both the concentration and the thermal and mechanical history of magnetite in either the archaeological target or its hosting material.

The remanent magnetization of archaeological objects is particularly significant not only because of its high relative intensity, but also because it is intimately associated with many objects of ancient habitations, as bricks, tiles, pottery, kilns, hearths and similar features (see Fig. 3.7).

This remanent magnetization, which as above said is a thermoremanent one, is created when the magnetite-bearing clay is heated to a relatively high temperature and then cooled in presence of the earth's magnetic field.

To estimate the expected maximum effect due to an archaeological object, we can consider the anomaly due to a single cube of rock representing a buried body, which is given by

$$T = \left(\Delta\chi F d^3\right)/r^3 \qquad (3.33)$$

where T is the anomaly amplitude in nT, $\Delta\chi$ is the susceptibility contrast per unit volume, F is the earth's field intensity also in nT, d is the dimension of one side of the cube in whatever distance unit and r is the distance between the magnetometer and the center of the cube in the same units as d.

The anomalies observed in archaeological sites are in most situations very complex as a consequence of several factors. The sources of the anomalies are relatively shallow and therefore very close to the magnetometer, which of course automatically tends to emphasize the highly complex nature of the near field of any magnetic object.

The various sources of magnetic anomalies from soils, near surface rocks and the clutter of ancient and/or modern human habitations, including the many objects of real interest, are usually very strong. However, the measures collected in archaeological contexts are often masked by noise. For such main reason, it is advisable during the survey to employ portable gradiometers. This instrument is a differential magnetometer in which the spacing between the two sensors is fixed and small with respect to the distance to the sources, whose magnetic gradient effects are to be measured. The difference in intensity divided by the distance between the two sensors is then the gradient attributed to the midpoint of the two sensors spacing (Breiner 1973). The most significant constraint included in the above definition is hence the requirement that the spacing s between the sensors must be small with respect to the distance r to the source of the anomaly. For example, if one considers a dipole, one sensor at r would measure an anomaly T. A second sensor at $2r$ would only measure 1/8 T. The second sensor is essentially not sensing the anomaly at all and may as well be at infinity.
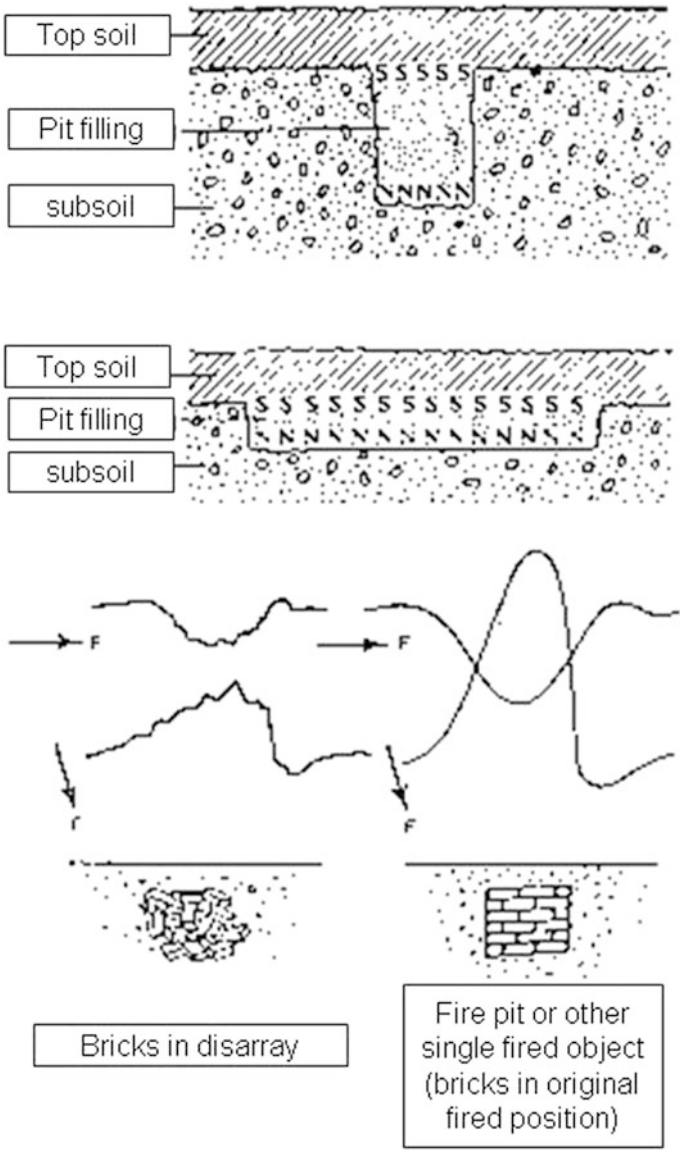
Fig. 3.7 Examples of magnetic anomalies due to the presence of a pit (**a**) and bricks (**b**) (after Breiner 1973)

Therefore, the magnetic field gradient can be expressed as:

$$\frac{dT}{dr} = \lim_{\Delta r \to 0} \frac{T_{r+\Delta r} - T_r}{\Delta r} \approx \frac{\Delta T}{\Delta r} \tag{3.34}$$

where ΔT is the total field differential between the two sensors positions, spaced Δr apart, and dT/dr is the derivative or gradient of T in the direction of r.

The gradiometer automatically removes the regional field and thus it notably increases the resolution of the local anomalies. A composite source can be therefore portrayed as a more resolved anomaly, since different edges of the source can this way be separated into two or more discrete anomalies.

3.3.3   Instrumentation

In archaeological prospections, three types of instruments are currently used, namely the fluxgate gradiometer, the alkali metal (cesium or potassium) optical pumping magnetometer and the proton free precession magnetometer.

The most frequently magnetometer used for routine survey in archaeological prospection is the fluxgate gradiometer. This instrument combines sensitivity of the order of 0.1 nT (nanoTesla) with lightweight design and rapid measurement rates, and several commercial systems are now available. However alkali-vapour magnetometers are now becoming popular having long been routinely used in Europe (Becker 1995; Becker and Fassbinder 2001, 2005; Fassbinder et al. 2005; Linford et al. 2007). These instruments may also be named optically-pumped magnetometers (caesium, potassium, rubidium). They offer sensitivities of the order of 0.05–0.01 nT and can make measurements at similar rates to fluxgate systems.

The main practical difference between the two types of instrument is that an alkali-vapour magnetometer measures the total absolute magnitude of the local magnetic field, while a fluxgate gradiometer measures the relative difference between the magnitude of the vertical component of the local field measured by two sensors positioned one above the other (separated typically by a distance of 0.5 or 1 m). When required, it is possible to configure an alkali-vapour magnetometer as a gradiometer by differencing the measurements made by two separate, appropriately mounted, sensors. In general alkali-vapour instruments are more sensitive (Becker 1995) but it is usually necessary to mount them on some form of mobile system or cart to take full advantage of their enhanced sensitivity (Becker 1995, 2009).

A number of manufactures have adapted their systems to allow multiple sensors to be mounted horizontally in parallel. This enables two or more traverses of data to be collected simultaneously, increasing the speed at which surveys may be carried out (Geoscan Research, Bartington, Forrester).

3.3.4   Field Work

Before starting a survey, the magnetometer must be correctly configured for use. Most magnetometers require some warm-up period before they settle into stable operation. This is typically of the order of few minutes for alkali-vapour instruments but fluxgate gradiometers, being more sensitive to differences in temperature, typically require about fifteen-twenty minutes to adapt to site conditions. Most fluxgate gradiometers must then be balanced (aligning the two fluxgate sensors along the vertical axis) and zeroed (calibration of the measurement scale for the local condition). This procedure should usually be done over an area of uniform magnetic field preferably using the same location throughout the survey. Particular care must be taken in the selection of this location when calibrating dual or multi-sensor instruments as a proportionally larger area free of local magnetic field perturbations is required.

It is very important that the operator holding the sensor staff should be magnetically "clean". All ferrous metal should be removed from the body and the operator checked by taking repeated readings with the operator in different positions with respect to the sensor. Even such small items as ventilation eyelets on hats can cause trouble. Keeping the operator and sensor oriented the same way for all readings can eliminate so-called heading errors which cause a shift in readings.

Repeatability, or the measurement noise, should be determined by repeating a row of points and examining the variation in the diurnally corrected values. It is advisable to repeat this procedure when the person holding the sensor, or when equipment, is changed.

The best conditions for a survey are fairly uniform, fine-grained soil with at least a moderate magnetic susceptibility and potential for enhancement. This last requirement can be checked by measuring the magnetic susceptibility of soil samples taken from various levels at the site. Unfavorable conditions include sandy soil of low susceptibility, significant surface irregularities, a quantity of igneous boulders, and a near surface undulating bedrock. The last three items contribute unwanted, stationary noise.

Another source of unwanted noise is modern, surface iron debris. Sometimes this material can be identified and removed using a metal detector. On a prehistoric site, a modest amount of iron debris can be tolerated because such items produce characteristic anomalies easily identified as such. On an historic site, modern iron can be confused with iron of archaeological interest. However if the historic iron is fairly deep, it can be distinguished from surface iron.

An aspect of magnetic surveying not encountered with the other methods is that the signal—that is the magnetic field of the earth—varies in time. This variation has several components, the basic one being the diurnal variation. During the day the strength of the field, at any one location, in the mid-northern or mid-southern latitudes, decreases in the morning and rises again at the end of the day. The total shift can be several tens of nanoTesla. Superimposed on this change are higher

frequency excursions, the number and size depending on the geomagnetic activity of the earth, which in turn is related to sunspot activity.

The existence of the diurnal variation shapes the choice available for mode of operation. One of this is to use a gradiometer in which two sensors are placed one above the other and separated by 50 cm to 1 m. the difference between the two readings is recorded. This measures the vertical gradient or change of the field. The gradiometer automatically cancels the diurnal variations. It also tends to remove longer-range trends since sources close to the gradiometer will more strongly influence both sensors to the same extent. This system is not as sensitive to deeper sources that may be of interest, and the equipment can be more cumbersome in operation.

Field conditions may suggest the type and configuration of magnetometer that it is most practical to employ. Gradiometers discriminate more strongly than total-field systems in favour of anomalies in close proximity to the sensors (Breiner 1999). This property can limit the maximum depth at which features can be detected and total field systems are perhaps more suited when remains are expected to be deeply buried. However, gradiometers can survey in closer proximity to modern ferrous objects such as wire fences or pylons. Indeed, this configuration is often the only way to carry out a magnetometer survey near a busy road as it reduces the effect of transient magnetic anomalies caused by passing vehicles, which cannot be readily filtered out by post-processing. Most archaeological features will produce weak magnetic anomalies, so magnetometers with several range settings should be set at their most sensitive and certainly ought to be configured to measure differences of the order of 0.1–0.3 nT. However, in some instances reduced sensitivity may be necessary to avoid saturating the sensors when mapping very high magnitude anomalies.

Given the relative rapidity of modern magnetometers, the preference should be for a detailed magnetometer survey of the entire area subject to evaluation. The area to be surveyed is typically divided into a series of regular square or rectangular blocks or sub-grids and each is then methodically surveyed by conducting a series of equally spaced parallel traverses across it with the magnetometer. Measurements are recorded at regular, closely spaced, intervals along each traverse. This is usually achieved by setting the instrument to take readings at fixed time intervals, or by recording fiducial markers at regular distances so that variations in space can be subsequently corrected during the processing. However some recent magnetometer systems can integrate directly with a GPS system to log the position of each measurement directly and obviate the need for a pre-established survey grid.

An important aspect of the field procedure is the grid layout. As in the case of resistivity surveying, if more than a few parallel profiles are going to be run, the grid layout must be efficiently organized. It is convenient to break the area down into squares or blocks of 10, 20, 30 or 40 grid units on a side. The distance between readings should not be larger than about half the size of anticipated anomalies. Pits and hearths within a meter of the surface call for a grid unit of 1 m or even 50 cm.

House foundations and cellars can be surveyed with a large unit. For a broader sweep to look for possible areas of interest, a 2-m grid unit can be used followed up with a finer grid over selected areas.

Using the difference mode and surveying on a fairly flat, clear site, a block of 400 points at a 1-m interval can be surveyed in about 15–20 min. Including setup and relocating time and allowing for different types of terrain, three to six blocks (1200–2400 points) can be done in 40 min, using two people on the moving the tapes or lines and one person at the gradiometer recording the data.

The choice of sensor height is influenced by the rapid decrease in signal strength with distance from the source. If the sensor is too low, the soil surface irregularities will have too strong an influence. If the sensor is too high, weaker, subsurface features will be lost. For feature of the order of a meter in size, such as pits and hearths, and lying within a meter of the surface, a reasonable range of sensor heights is from 40 to 60 cm. Since commercial magnetometer sensors are constructed to be held on a staff 1 or more meters above the surface, it is necessary to modify magnetometers so that there is a 40–60 cm section below the sensor, as well as a section of the staff, to be used as a handle, above the sensor.

For detailed area to survey the maximum separation between measurements along a traverse should be no more than 0.25 m. Clark (1986) considers the sample resolution necessary to discriminate between near surface magnetic objects and more deeply buried archaeological features and concludes that a sample separation of 0.25 m enables full characterization of anomalies with minimal distortion to their shape.

Modern magnetometers can sample rapidly, have data loggers with large internal memory capacities and can quickly transfer stored data to a computer. Hence sample density along traverses has relatively little impact on the time taken to survey an area. The same is not true of the separation between traverses where the time taken is inversely proportional to the traverse separation. Closer traverse separation increases the number of times the magnetometer must be traversed across the area to achieve the necessary coverage. Practically some compromise is necessary and, for evaluation surveys, where the primary goal is to establish the presence or absence of archaeological remains, the maximum acceptable separation between traverses is 1 m. Clark (1990) notes that dense measurement along traverses is usually effective for characterizing the nature of features so that it is then often sufficient only to establish their extent in the cross-traverse direction.

Where it is necessary for the survey to identify smaller discrete features a closer traverse separation should be used and 0.5 m is recommended.

Boundaries such as hedges and fences will often constrain the orientation of the survey grid. However where possible it is preferable for traverses to be walked at right angles to the direction of recent ploughing to minimize any adverse effects of the latter on subsequent plots. Where the alignment of anticipated linear archaeological features can be predicted in advance, it is again preferable to avoid orienting traverses in this direction.

Linear anomalies parallel to magnetometer traverses can be inadvertently removed by processing to counter the directional sensitivity of the instrument. At all latitudes the greatest peak-to-peak magnetic anomaly is obtained in the north-south direction (Breiner 1999). So when employing a sampling interval along the traverses narrower than the separation between them and if there are no other constraints on traverse orientation, a north-south orientation will achieve optimal benefit from the anisotropic sample density.

Fluxgate magnetometers can exhibit excessive sensitivity to motion-induced errors when oriented in a particular direction to the Earth's magnetic field, the direction being specific to each instrument. Taking into account traverse direction, care must be adopted to avoid surveying with the magnetometer while oriented in this adverse direction, changing the way the instrument is carried if necessary. A similar consideration applies with respect to alkali-vapour sensors, which are insensitive to magnetic fields directions aligned too closely to a particular direction dictated by the sensor's geometry known as the tumble angle. Attention must be taken to ensure sensors are aligned appropriately for the local magnetic field direction.

Instrument traverses may be recorded in either "zig-zag" or "parallel" modes (Gaffney and Gater 2003). While the zig-zag mode enables the most rapid ground coverage, there can be a tendency for the response of alternate traverses to be offset with respect to one another. This can occur when the magnetometer is not held in the correct relative position or because of an incorrect walking space relative to an odometer rate.

The effect is often most pronounced when traverses run up and down slopes and results in linear anomalies at right angles to the traverse direction being "staggered" and producing a herring-bone pattern. The worst effects of this problem can be eliminated by post-processing, but are often difficult to remove completely. Hence for portions of survey over particularly difficult terrain, parallel traverses should be considered and in all cases attention should be taken to eliminate the effect as far as possible by correct data collection procedures.

Continuous reading magnetometers can also be employed for scanning. The instrument is carried along traverses spaced and oriented according to local requirements without logging the signal. Its output is observed by the operator and anomalies marked, then further investigated by more intensive scanning or by detailed recorded survey and/or augering. However the method depends for much of its success on the experience of the operator, and even the most skilled surveyors are unlikely to be able to detect, by scanning alone, dispersed or weakly magnetized features, which may nonetheless be of considerable significance.

While most magnetometers now boast nonvolatile storage capacities capable of storing more than a day's worth of surveying, it is advisable to transfer data frequently to a notebook to avoid excessive data loss in the event of an instrument malfunction.
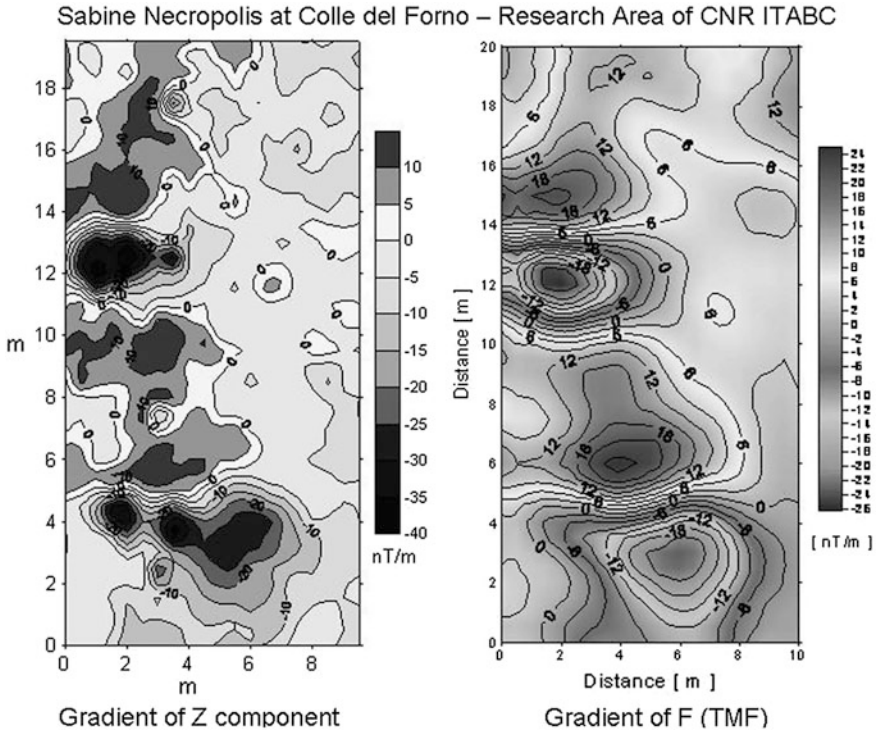
Fig. 3.8 Sabine Necropolis at Colle del Forno. Contour map of the gradient of Z component (of TMF–total magnetic field) for the test_area

As in all geophysical surveying methods, the site to be surveyed should be evaluated for suitability and potential for the method to be used. In the case of magnetics, the weather conditions do not affect the results except in the case of extreme heat or cold, which puts the equipment under stress. What is important is the magnetic nature of the soil and the anthropogenic features.

In Fig. 3.8 and 3.9 examples of contour maps of the gradient of the vertical component Z of the total magnetic field are shown.

In Fig. 3.10a, b, the results after the application of numerical technique to enhance the S/N ratio and to obtain the inversion are shown.
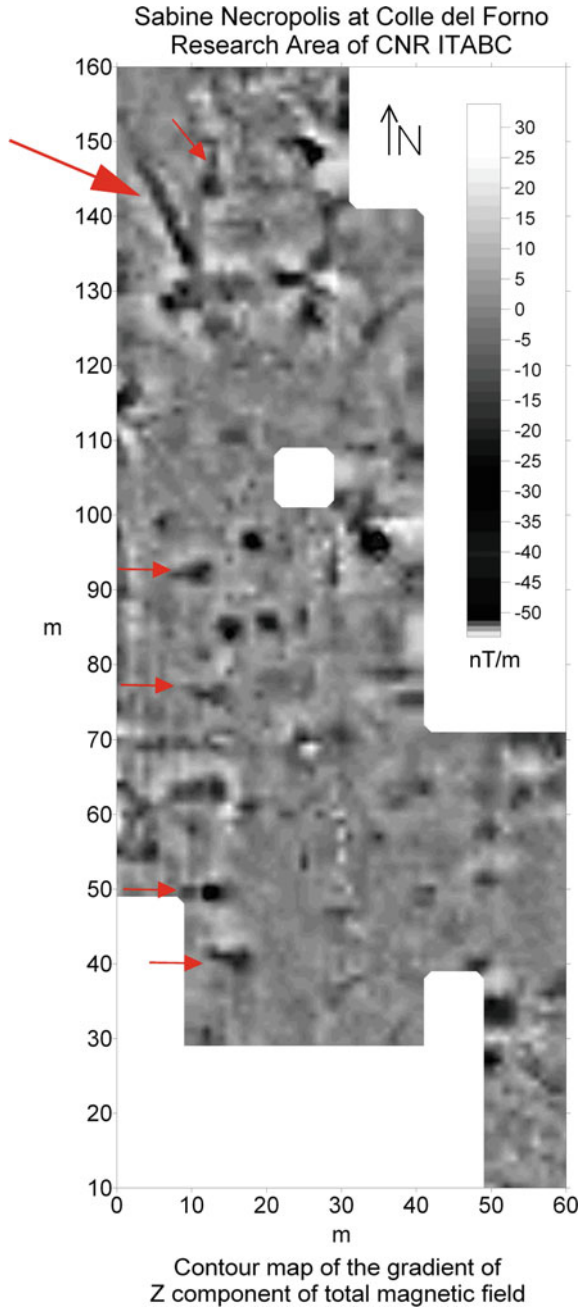
Fig. 3.9 Sabine Necropolis at Colle del Forno. Contour map of the gradient of Z component (of TMF) for the total investigated surface
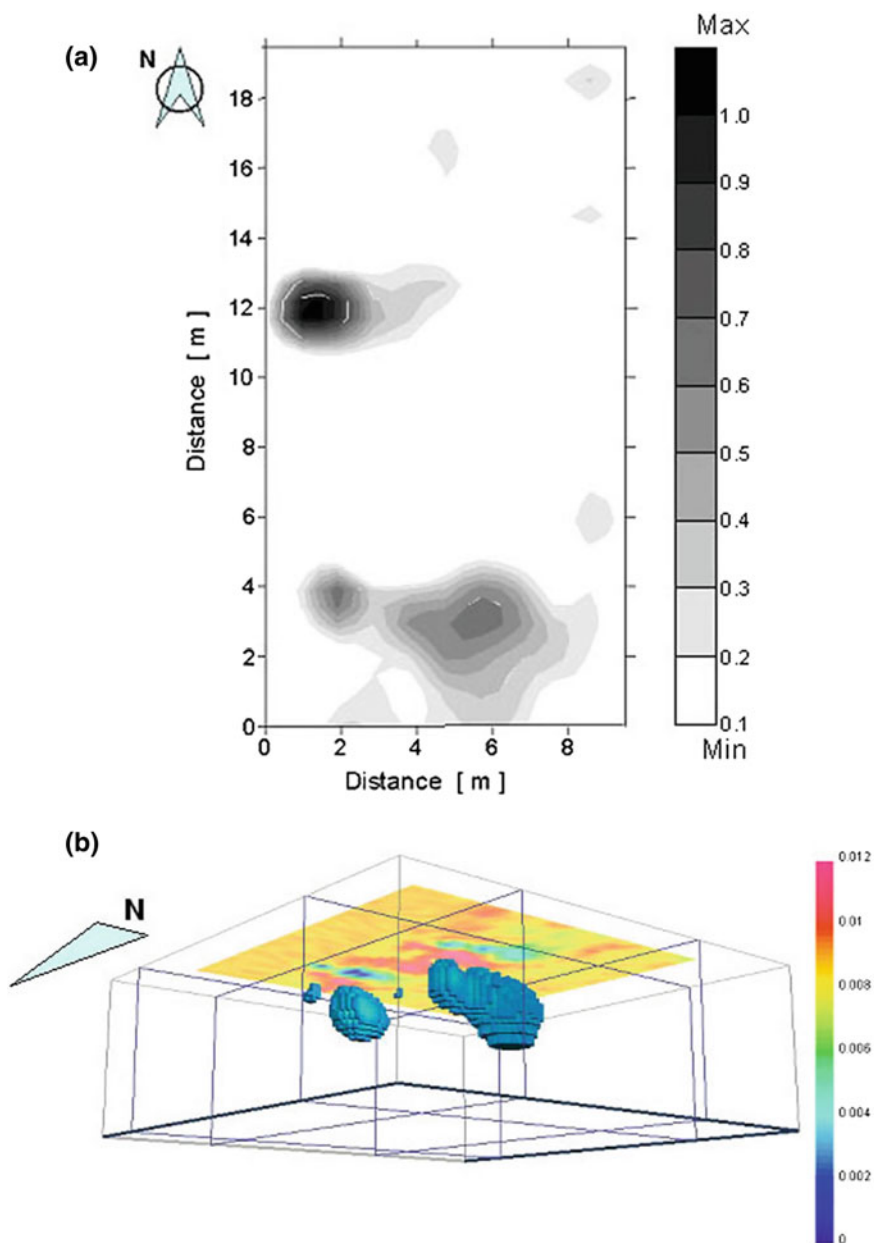
Fig. 3.10 a Sabine Necropolis at Colle del Forno. Results of the cross-correlation analysis of the vertical gradient of the Z component for test_area. **b** Rendering of the results of 3D inversion; the main structures, for area1 and 2, are well pointed out

3.4 Electromagnetic Method

Abstract Electromagnetic methods provide an excellent way to obtain information about electrical ground conductivities, based on the electromagnetism induced principles (EMI). The investigation depth of an electromagnetic field depends upon its frequency and the electrical conductivity of the ground. Electromagnetic techniques rely on two major instrumental systems and equipment, used especially in archeological field, that characterize the survey method and their application. They can be classified as frequency domain electromagnetic method (FDEM) and time domain electromagnetic method (TDEM) systems. In the FDEM one or more frequencies are used; in TDEM the measurements are seen as a function of time. The main advantage of EM methods is that they do not require direct contact with the ground like other geophysical methods. Therefore, measurements can be carried out in a faster way even in environments with a not really well defined and bumpy morphology. EM methods make it possible to clearly highlight discontinuities—surfaces and structures—with a strong vertical development, buried archaeological structures characterised by good electrical conductivity or magnetic susceptibility (metals, brick structures, structures filled with water with a high saline content, etc.). Surveys with regular grid allow to obtain an accurate analysis of the ground as well as to identify the trends of the structural elements it contains by moving along equidistant lines with variable interspace depending on the desired level of resolution and detail. Furthermore, the interpolation of the sampled and measured values allows to obtain and represent data through in phase and quadrature, susceptibility and conductivity horizontal maps related to each frequency.

3.4.1 Introduction

The electromagnetic methods are used in many types of environmental and geological applications, especially in archaeological investigations for the location of buried structures or highly conductive metal elements (Clark 1986, 1990; Bevan 2013; Kvamme 2000; Musset et al. 2000). The rapid improvement in microelectronics has allowed a more widespread use of this methodology, both in the frequency domain and in the time domain. So, it is possible to get a more detailed and resolved information for this research environment. The use of this methodology in the Cultural Heritage is linked to the possibility to represent the electric geometry of any buried man-made ambient, by mapping variations in the electrical conductivity.

3.4.2 Basic Theory

The electromagnetic methods allow the study of the electrical properties subsoil by analyzing the soil's reaction to the propagation of electromagnetic fields (Reynolds 1997; Dobrin et al. 1988; Frischknecht et al. 1991; Nabighian 1991; Parasnis 1997; Mc Neill 1980a, b; Spies et al.1991; Tite et al. 1969, 1970). The mode operation of the various electromagnetic methods are all based on Maxwell equations that regulate the electromagnetic phenomena (Ward et al. 1988).

The first law asserts that the electric field flux, through any closed surface, is proportional to the charge enclosed by it; the second one asserts that the magnetic induction flux, through any closed surface, is equal to zero. This is equivalent to say that magnetic field-lines are closed and there are no sources from which they can flow (magnetic monopoles) as it happens for the field lines of an electric field, which flow from the positive charges to the negative ones.

The third law asserts that the electric circuitry is equal to the time rate of charge of the magnetic flux, connected to the calculation path of the circuitry.

The last one asserts that the magnetic circuitry is equal to the time rate of charge of an electric field in dielectrics (displacement current) plus the charges flowing in the conductors (conduction current).

The phenomenon of the production and propagation of electromagnetic waves in space is based on the laws cited above. If a time-varying electric field is generated in a given point, in space a time-varying electric field, as a consequence, a time-varying electromagnetic field is created close to it. With this result, we can say that the electromagnetic field propagates in space. According to Maxwell, the speed of propagation of an electromagnetic wave through space is given by the following formula:

$$v = \frac{c}{\sqrt{\varepsilon r}}$$

where $c = 3 \times 10^{10}$ m/s is the speed of the light in vacuum and ε, the relative dielectric constant. An electromagnetic wave can be produced by an oscillator circuit in which an alternating current flows and whose intensity varies with a sinusoidal law. The frequency of the circuit is given by the following formula:

$$\upsilon = \frac{1}{\sqrt{LC}}$$

The current that flows through the circuit is an oscillating current, that is damped due to *Joule* effect, according to which a part of the electromagnetic energy of the circuit is continuously transformed into heat. It is also due to the emission of electromagnetic waves, which carry energy through space continuously.

To eliminate such damping and get a sinewave current, the oscillator circuit is placed into a more complex system, where a triode draws energy from anode battery and transfers it to the oscillator circuit, in order to compensate the energy loss.
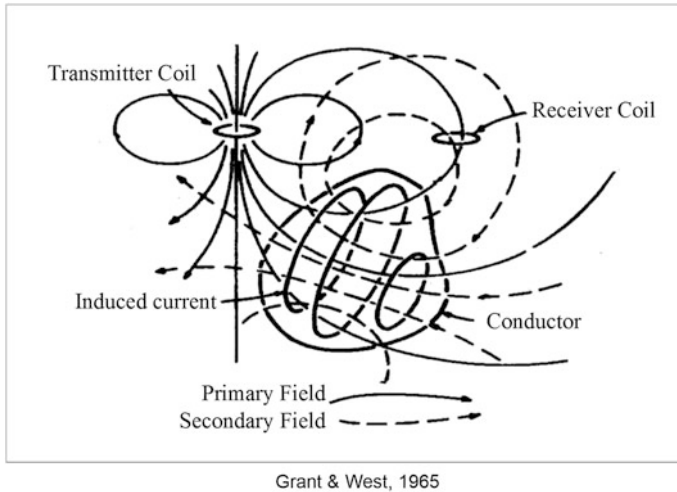
Grant & West, 1965

Fig. 3.11 Schematization of induction system

It is possible to say, therefore, that for the Maxwell's law, a variable Em source can generate an induced electromotive force (that is able to oppose the force that has generated it) which can produce secondary currents in conductive material, affected by a time-varying EM field. These secondary currents produce secondary time-varying EM fields. The EM signal, that the instrument collects through the receiver, is the vector sum of the primary time-varying EM field and of the secondary induced one, that oscillates with the same frequency as the primary (Fig. 3.11).

The resulting field will be assimilated to the primary one and it will provide data to carry out and define conductivity.

The EM response obtained depends on v (vibration frequency of primary field) on $1/\rho$ (apparent conductivity of the investigated soil) and on mechanical alignment between transmitter and receiver. The return signal increases in intensity when it affects higher conductive soils. The depth investigation decreases as the primary field frequency increases. This is due to the "skin effect" that takes place in conductors when they are affected by high-frequency EM signals.

The EM method used in the case studies, discussed in the second part of this book, is based on the electromagnetism induced principles (EMI).

The EM studies the soil response to an electromagnetic stress and it is based on the study of the propagation, in the subsoil, of a primary magnetic field (p.m.f.) generated from an alternating current circulating through a transmitter coil or a metallic antenna[1] (Telford et al. 1976; Bigman 2012).

---

[1]Telford W.M., Geldart L.P., Sheriff R.E., Keys D.A., 1976. Applied Geophysics. Cambridge University Press, New York, U.S.A., 860 pp.

Once emitted, the p.m.f propagates across above and below the ground. The p.m.f. component that penetrates into the subsoil, whose flow varies in time, can encounter buried electrical conductors.

In this case, eddy loops of electrical current (eddy currents) are induced within conductors through charge carriers. The eddy currents are proportional to the apparent electrical conductivity, measured in mS/m. The eddy currents, generated in the ground, induce a secondary electromagnetic field (s.e.f.), directly proportional to the induced currents that generated it. The s.e.f. and its geometrical components are function of the conductivity of the investigated geological and archaeological structures. On the surface the s.e.f. combines with the primary and, travelling directly over the soil, arrives at the receiver coil, generating a resulting magnetic field which is called elliptically polarized. This resulting magnetic field is identified by alternating currents that induce the flux in a receiver coil. The differences between emitted and received magnetic fields reveal the presence of conductors in the soil and provide us with information on their geometry and their electrical properties. In particular, the s.e.f. has a frequency equal to the primary field whereas the direction, amplitude and phase are different (Conyers et al. 2008).

The geometric components of secondary magnetic field are called in-phase and quadrature components.

The in-phase component is proportional to the intensity of the s.e.f., the quadrature component is proportional to phase displacement between the emitted and received electromagnetic waves, and it is also an indicator of the conductivity of the soil investigated. It is proportional to the flattening of the polarization ellipse and then to the relation between semi major and minor axis.

The apparent conductivity for the quadrature component is given by the following formula:

$$\sigma_a = \frac{4}{\omega\mu_0 s^2}\left(\frac{H_S}{H_P}\right)$$

where

σ_a is the apparent conductivity;

ω is the angular frequency of the sinewaves transmitted;

μ_0 is the permeability of vacuum;
s is the gap between central coil points;

H_S is the secondary magnetic field to the receiver coil;

H_P is the primary magnetic field to the receiver coil.

When an electric current flows across a wire or a coil, this creates a magnetic field around the wire, but it does not reproduce itself everywhere and at any time but it goes quickly away. If there is an alternating current, the alternations of the magnetic field will propagate as a series of sinewaves. The wave length λ is related to frequency *f* by the relation:

$$v = f\lambda$$

where *v* is the propagation speed.

In the ground, the waves are diffused more slowly so the surges are closest. Propagating, the waves become weaker or subside, because their energy is distributed and can be absorbed. For this reason, in an electromagnetic system, the transmitter coil should not be located too far away from the receiver. When an electromagnetic wave travels through a conductor, it is progressively absorbed as much as higher conductivity is.

For the rocks that have an X conductivity value, the amplitude decreases of the same value for each wave length travelled, with an exponential decrease. As the amplitude never does, you cannot give a simple attenuation length. Instead, it is possible to use the penetration depth, that is the distance at which the amplitude decreases to *1/e* (*e = 2.718…*).

The penetration depth of the primary electromagnetic field is the depth at which the field can still be observed. It depends on the frequency and the conductivity of the medium in which it is propagated. In particular, during propagation, its amplitude decreases exponentially with the depth.

The penetration depths are low for both high frequencies and low resistivity (high conductivity). For this reason, low frequencies are necessary to reach deep target but, if coverage soil is very conductive, it may be impossible to make an electromagnetic survey below it. On the other hand, it is very useful to search conductors under a high resistivity coverage soil (Mc Neill 1980a, b).

3.4.3   Instrumentation

Actually, different commercial companies offer systems for electromagnetic surveys such as Geonics (Canada, http://www.geonics.com), Terraplus (Canada, http://www.terraplus.ca), GSSI (New Hampshire, http://www.geophysical.com), Dualem (Canada, http://www.dualem.com), Frontier Geosciencies Inc. (Canada, http://www.frontiergeo.com), GF Instruments (Czech Republic, http://www.gfinstruments.cz), Geomodel (http://www.geomodel.com).

The electromagnetic methods can be divided into FDEM (frequency-domain electromagnetic method) and TDEM (time domain electromagnetic method). In FDEM the current transmitted varies sinusoidally on time at a certain frequency while in the TDEM the current transmitted, still periodic, is a symmetric square wave.

This important difference characterizes the survey method, the equipment involved and especially its application and environments (Beaussillon et al. 1996; Viberg 2012; Scollar 1962; Reynolds 1997).

The FDEM instruments are formed by a transmitter and a receiver. The sinusoidal alternating current in the transmitter coil generates an alternating magnetic field in the ground. If the soil is made of homogeneous material and a little conductor, the field that propagates through the air is equal to the one that propagates in the ground: you will see only a slight reduction of amplitude. Whereas if there is a conductor in the ground, the magnetic component incidence of electromagnetic field induces alternating currents in it, the so called eddy currents. The potential difference measured by the receiver is the sum of the potential differences of an electromagnetic field created by the eddy currents flux. This is caused by the varying induced EM field in the ground and the main magnetic field generated by the coil transmitter that travelled to the receiver through the air. The result, therefore, will be the combined effect of primary and secondary fields, and the latter will differ in amplitude and phase from the primary one. The differences between the resultant field and the primary one reveal the presence of a conductor and give us information about its geometry and electrical characteristics (Witten et al. 2003; Dalan 1995).

The equipment is made of a transmitter coil, generally a multi-frequency one, which generally acts as a vertical dipole, horizontal loop, and a receiver coil that measure the components in phase and quadrature of the vertical magnetic field, at diverse frequencies. The quadrature component is proportional to the difference in-phase between the wave emitted by the transmitter and the one received. It proofs also the conductivity of the subsoil between the two coils. The in-phase component is proportional to the intensity of the EM field induced by the electromagnetic wave transmitted by the instrument. This component is, therefore, function of the existence of metal objects and materials with high concentrations of metal ions.

The depth exploration is function both of the gap between the coils and the frequencies used. This instrument, in general, provides values of apparent conductivity and magnetic susceptibility. In fact, this instruments have a different depth survey depending on whether you use the loops horizontally or vertically. In the first case, VDM (vertical dipole mode), as the magnetic dipole, equal to the transmitter coil, is vertical, the depth investigation doubles. In the second, HDM (horizontal dipole mode) two different conductivity values are obtained, with different depths (Tabbagh 1984 a-b-c, 1985, 1986a-b, 1994; Tabbagh et al.1993).

In TDEM equipment, a transmitter coil is energized with a square wave. The different dimension of a coil influences the depth investigation. In the transmitter coil, during the "one time" a static magnetic field stabilizes on the ground. When the current extinguishes in the electromagnetic primary field, it extinguishes, the induced electromagnetic field in the ground induces concentric currents flux, eddy currents, in either the ground or hidden conductors nearby. These currents decay overtime, producing a surface magnetic field decay. Therefore, it is easy to identify the superficial conductors or measure the soil conductivity.

Compared to the instruments that operate in frequency domain, these that operate in time domain have three main differences. The first is that the transmitter coil must be bigger (at least 5*5 *m*), but this makes the method impractical. The second is that being the measurement made when the transmitter is off line, it is not necessary to maintain the exact position and alignment between the coils. For this reason, this methodology is versatile even with uneven soils. At the end when the transmitter is "off time", that is, when there is not a primary electromagnetic field, there are no particular problems to determine the zero level of the signal received.

Electromagnetic time domain systems are commonly used with the "central loop sounding" mode. In this system, the transmitter coil is placed in the center of the transmitter circle whose dimension may change from 25 to 200 m. When the transmitter stops the signal, blocking rapidly the primary magnetic field, eddy currents are instantly generated the eddy currents in the proximity of the transmitter. In this way, the magnetic field keeps the same value it had before the signal interruption, everywhere in the soil. Those circles of every horizontal concentric current are spread overtime, in great depth. The decay is measured depending on time of the magnetic field in the center circle, by using the same method when measuring soil resistivity as a depth function. The measurements of transient anomalies of magnetic field can easily start a few microseconds after the interruption of the transmission. This, translated in terms of frequency domain, means that the soil reaction has been measured at frequencies in the order of *kHz* hundreds, in top soil layers.

The electromagnetic methods used in the archaeological investigations are often in frequency domain (Dalan 1989a, b, c; 1991, 1993a, b; 1995; Aubry et al. 2001; Cornelison 1997). The equipment used is composed by: portable systems, battery powered with a multi frequency electromagnetic induction system and with transmitter and receiver sensors placed at fixed distances. In the 1950s and 1960s, the electromagnetic equipment was complex, awkward and with long time for the acquisition data. Today, the time requirement for the survey of a hectare of land requires only a few hours.

3.4.4 Field Work

In order to have an optimal response during the survey is necessary that the data are collected in a regular grid with equally spaced profiles. The spacing between them is variable, depends on the level resolution and details to achieve. The survey planning is adapted to the morphology of the ground and the profiles are positioned orthogonal to the supposed target to be tracked in order to visualize anomalies in each profiles and follow the alignments and geometries that will be formed.

The FDEM system ensures a good performance when there are moderately and highly conductive soils; it is less performing with highly resistive soils. The radiating diffusion of this system, linked to the depth investigation, ensures an excellent lateral resolution. One drawback of the system is, that measuring the in-phase component, the space between the coils and their alignment (when you are in the

presence of the equipment in which the transmitter and receiver coils are separated) must be carefully checked, which is not always easy when there are uneven and not regular soils. Moreover as the signal records also the primary EM field, that is greater than that induced, only a small part of the signal is useful to the investigation. These measures are susceptible to conductors placed below conductive layers and in general are not affected by changes in top soil conductive layer. Despite these small drawbacks, the system is useful for fast measurement and it is used in archaeological and environmental fields (Auken et al. 2006).

A TDEM survey is completely comparable to a vertical electrical survey (S.E.V.) in direct current. Therefore, the interpretation of TDEM survey is comparable to vertical electrical survey. This system is limited, however, in the calculation of resistivity and the depth of a half-intermediate layer. It can be very useful as a supplement to other investigation methods.

It is clear that the different distances between the loops, as well as the different frequencies, condition the investigation depth in both methodologies. In the first, FDEM, this happens because field lines of secondary magnetic field excite the receiver coil, placed at different distances. It is generated by loop of induced currents at different depths. On the other hand, in TDEM, this happens because of the skin effect (Benech et al. 1999).

In archeology, being required the survey depth by a few meters, the coils can be kept close to each other at distances of the one meter.

To resolve this problem, many recent electromagnetic equipment can be used to reach distance at three different frequencies, in order to obtain apparent conductivity values that are related to different survey depths. It is possible to obtain vertical electrical survey simply by varying the distance between the coils (geometrical survey) or frequency (parametric survey).

For a good investigation with these instruments, we can remember that they are influenced by the presence of power line, metal enclosures, metal objects on the surface, pipes, wire nets placed in 5 m area, which alter the survey results.

In order to reach a good result by this application, dry soils are needed; in presence of clay soil the exploration depth is reduced of *30/40%*. It is also possible to use these instruments on tarmac (blacktop) and beton, without a power line.

3.4.5 Processing and Representation

The in-phase component compared to the primary field, measured in parts-per-thousand (ppt), is generally indicative of the presence of conductive and susceptible metallic structures that greatly amplify the ground response. In case of low induction number, the relationship between the quadrature component of the secondary magnetic field and of the primary magnetic field can be considered directly proportional to the apparent electrical conductivity.

The study of the distribution of the quadrature component with depth at the first penetration meters from the ground is usually used to identify the areas with higher
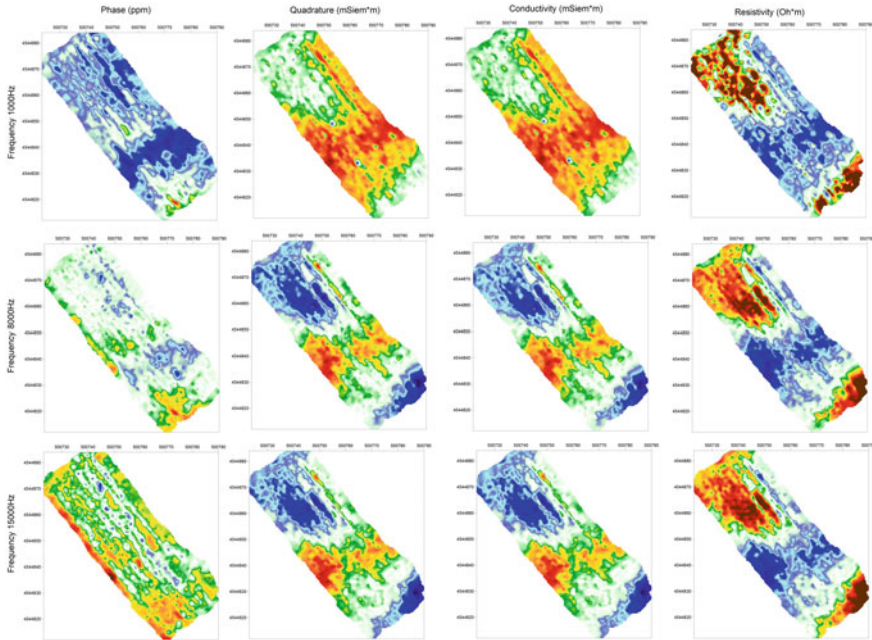
Fig. 3.12 Horizontal maps in phase and quadrature, conductivity and resistivity related to each frequency

or lower resistivity or electrical conductivity; this allows identifying the presence of conductor and/or resistant bodies. The use of the magnetic susceptibility parameter (particularly suitable for metal search) allows further discrimination.

Obviously if the subsurface layer is not electrical homogeneous, the electrical conductivity given by the formula is "apparent" as well as the apparent resistivity of the geoelectrical method. In order to get distribution and values, it is necessary to proceed with an inversion algorithm, that differs from the inversion of the geo-electrical method only in the way in which the apparent conductivity is simulated.

Apparent conductivity values can be transformed through the application of a further mathematical algorithm to resistivity values and processed by using the same procedure of the geoelectrical methodology (Spies et al. 1986).

Through the interpolation of the values obtained for each single point, it is possible to represent the data through in phase and quadrature, susceptibility and conductivity horizontal maps related to each frequency (Fig. 3.12).

The inversion of an apparent resistivity collected dataset gives rise to a two-dimensional (2D) ERT. In order to identify anomalies with lateral and vertical variation is necessary to apply to the dataset the inversion algorithm that provides a three-dimensional (3D) ERT (Bongiovanni et al. 2008; Haber et al. 2004; Osella et al., 2005; Xiong 1992; Xiong et al. 1995; Zhdanov 2010).

References

Aitken M.J., Webster G., Rees A., 1958, Magnetic Prospecting, Antiquity, 32, pp. 270–271.

Aitken, M.J., 1974. Physics and archaeology, 2nd edition. Oxford: Claredon Press, 286 pp.

Alaia, R., Patella, D., and Mauriello, P., 2008. Application of the geoelectrical 3D probability tomography in a test-site of the archaeological park of Pompei (Naples, Italy), *Journal of Geophysics and Engineering*, 5, 67–76, https://doi.org/10.1088/1742-2132/5/1/007.

Aubry L., Benech C., Marmet E., Hesse A., 2001, *Recent achievements and trends of research for geophysical prospection of archaeological sites,* in Journal of Radioanalytical and Nuclear Chemistry, Vol. 247, No. 3, pp. 621– 628.

Auken EL, Pellerin L, Christensen NB, Sorensen K., 2006, *A survey of current trends in near-surface electrical and electromagnetic methods*, in Geophysics 71(5), pp. 249–260.

Barker, R., 1992. A simple algorithm for electrical imaging of the subsurface, *First Break*, vol. 10, no. 2, pp. 53–62.

Basile, V., Carrozzo, M.T., Negri, S., Nuzzo, L., Quarta, T. And Villani, A.V. 2000. A ground-penetrating radar survey for archaeological investigations in an urban area (Lecce, Italy). Journal of Applied Geophysics, 44: 15–32.

Beaussillon R., Benech C., A. Tabbagh A., 1996, *A two frequency slingram apparatus for archaeological and pedological application*, in 2nd Environmental and Engineering Geophysical Society Meeting, Nantes, 2–5 September 1996, p. 15.

Becker H., 1995. From nanotesla to picotesla. A new window for magnetic prospecting in archaeology. Archaeological Prospection 2:217–228.

Becker H. And Fassbinder J.W.M., 2001. Magnetic prospecting in archaeological sites. ICOMOS ed: Paris.

Becker H., 2009. Caesium magnetometry for landscape-archaeology. In *Seeing the Unseen– Geophysics and Landscape Archaeology*, Ed. Campana S. and Piro S., CRC Press Taylor & Francis Group, pp 129–165.

Becker H., Criminale M., Gallo D., 2005. Aerial photography and high-resolution magnetic surveys at the Celone River Valley (Southern Italy). Proceedings of 6th International Archaeological Prospection Conference, Ed. Piro S. (ISBN88–902028), Roma, pp. 21-24.

Benech C. and Marmet E., 1999, *Optimum Depth of Investigation and Conductivity Response Rejection of the Different Electromagnetic Devices Measuring Apparent Magnetic Susceptibility*, in Archaeological prospection, Volume 6, Issue 1, pag. 31–45.

Benech C., 2007. New approach to the study of city planning and domestic dwellings in the ancient near East. Archaeological Prospection 14: 87-103.

Berdichevsky, M.N. & Zhdanov, M.S., 1984. Advanced theory of deep geomagnetic sounding. Amsterdam, Elsevier, 408 pp.

Bernabini, M., Brizzolari, E., Monna, D., Padula, G., Piro, S. & Versino, L., 1985. Individuazione di cavità sepolte mediante prospezione geoelettrica. Esempio di applicazione: ricerca di tombe nella necropoli di Colle del Forno nei pressi di Montelibretti (Roma). Bollettino del Servizio Geologico d'Italia, CIII, 67-79.

Bernabini, M., Brizzolari, E. & Piro, S., 1988. Improvement of signal-to-noise ratio in resistivity profiles. Geophysical Prospecting, 36, 559-570.

Bevan BW, 1983, *Electromagnetics for mapping buried earth features, in Journal of Field Archaeology* 10, Issue 1, pp. 47–54.

Bevan B.W., 2013, Electromagnetics for mapping buried earth features, in Journal of Field Archaeology, 10, Issue 1, pp. 47–54.

Bigman D.P., 2012, *The use of Electromagnetic induction in locating graves and mapping cemeteries: an example from native North America*, in Archaeological prospection, Volume 19, pag. 31–39.

Black, W.E. & Corwin, R.F., 1984. Application of self-potential measurements to the delineation of ground-water seepage in earth fill embankments. 54th Annual International Meeting, SEG, Expanded abstracts, 162-164.

Bongiovanni M.D., Bonomo N., de la Vega M., Osella A., 2008. Rapid evaluation of multifrequency EMI data to characterize buried structures at a historical Jesuit Mission in Argentina, in *Journal of Applied Geophysics* 64, pp. 37–46.

Bozzo E., Merlanti F., Ranieri G., Sambuelli L., Finzi E., 1991. EM-VLF soundings on the eastern hill of the archaeological site of Selinunte. Bollettino di Geofisica Teorica ed Applicata 34: 132-140.

Bozzo E., Merlandi F., 1992. Magnetic and geoelectrical measurements on the eastern hill of the archaeological site of Selinunte. Bollettino di Geofisica Teorica ed Applicata 34: 145–156.

Bozzo E., Lombardo S., Merlanti F., Pavan M., 1994. Geoelectric and electromagnetic measurements within an organised archaeological framework: the Marzabotto example. Annali di Geofisica 37 (suppl. 5): 1199-1213.

Bozzo E., Lombardo S., Merlanti F., 1995. Geophysical surveys at the Poliochni archaeological site (Lemnos Island, Greece): preliminary results. Archaeological Prospection 2: 1-13.

Breiner, S., (1973 and 1999): Applications manual for portable magnetometers. Geometrics, Sunnyvale U.S.A., 57 pp.

Brizzolati E., Ermolli F., Orlando L., Piro S., Versino L., 1992a. Integrated geophysical methods in archaeological surveys. Journal of Applied Geophysics 29:47-55.

Brizzolari E., Piro S., Versino L., 1992b. Monograph on the Geophysical Exploration of the Selinunte Archaeological Park. Foreword. Bollettino di Geofisica Teorica ed Applicata, 34.

Brizzolari, E., Cardarelli, E., Feroci, M., Piro, S. & Versino, L., 1992c. Vertical electric soundings and inductive electromagnetism used to investigate the calcarenitic layer in the Selinunte Archaeological Park. Bollettino di Geofisica Teorica ed Applicata, 34: 109-119.

Brizzolari, E., Orlando, L., Piro, S. & Versino, L., (1992d): Ground Probing Radar in the Selinunte Archaeological Park. Bollettino di Geofisica Teorica ed Applicata, 34: 181–192.

Brizzolari, E., Cardarelli, E., Feroci, M., Piro, S. & Versino, L., 1992e. Magnetic survey in the Selinunte Archaeological Park. Bollettino di Geofisica Teorica ed Applicata, 34: 157–168.

Brizzolari, E., Cardarelli, E., Piro, S. & Versino, L., 1993. Detection of subsurface magnetic anomalies of archaeological interest: computation of tridimensional magnetic anomalies and interpretation using bidimensional cross-correlation. In "Geophysical Exploration of Archaeological Sites, Series Theory and practice of Applied Geophysics", Vol. 7, Ed. A. Vogel. Wiesbaden: Vieweg Publishing, 3–16.

Caldwell G.T. and Bibby M. H., 1998, *The instantaneous apparent resistivity tensor: a visualization scheme for LOTEM electric field measurements,* in Geophysics J. Int, 135, pp. 817–834.

Cammarano, F., Mauriello, P., Patella, D., Piro, S., 1997, Integrated geophysical methods for archaeological prospecting. In: *Volcanism and Archaeology of the Mediterranean Area*, M. Cortini and B. De Vivo (Ed.), Research Signpost, Trivandrum, India.

Cammarano F., Mauriello P., Patella D., Piro S., Rosso F., Versino L., 1998. Integration of high resolution geophysical methods. Detection of shallow depth bodies of archaeological interest. Annali di Geofisica, Vol. 41, n.3, 359-368.

Cammarano, F., Di Fiore, B., Patella, D., and Mauriello, P., 2000, Examples of application of electrical tomographies and radar profiling to Cultural Heritage, *Annals of Geophysics*, 43, 309–24, http://www.annalsofgeophysics.eu.

Campana S., Piro S., 2009. Seeing the Unseen. Geophysics and Landscape Archaeology. Campana & Piro Editors. CRC Press, Taylor & Francis Group. Oxon UK, ISBN 978-0-415-44721-8.

Carabelli, E. 1966. A new tool for archaeological prospecting: the sonic spectroscope for the detection of cavities. Prospezioni Archeologiche, 1, 25-35.

Carabelli, E. 1967. Ricerca sperimentale dei dispositivi più adatti alla prospezione elettrica di cavità sotterranee. Prospezioni Archeologiche, 2, 9-21.

Cardarelli E., Di Filippo G., Tuccinardi E. 2006b. Electrical resistivity tomography to detect buried cavities in Rome: a case study. Near Surface Geophysics Vol. 4, pp. 387-392.

Cardarelli E., Fischanger F., 2006a. 2D data modeling by electrical resistivity tomography for complex surface geology. Geophysical Prospecting Vol. 54 pp.121-133

Cardarelli E., Fischanger F., Piro S., 2008. Integrated geophysical survey to detect buried structures for archaeological prospecting. A casehistory at Sabine Necropolis (Rome, Italy). Near Surface Geophysics journal (EAGE), Vol. 6, n. 1, 15-20.

Carpenter, E.W. and Habberjam, G.M., 1956. A tri-potential method of resistivity prospecting. *Geophysical Prospecting, 29*, 128–143.

Chambers, J. E., Kuras, O., Meldrum, P. I., Ogilvy, R. D., and Hollands, J., 2006, Case history—electrical resistivity tomography applied to geologic, hydrogeologic, and engineering investigations at a former waste-disposal site, *Geophysics*, **71**, B231–9.

Chunduru, R. K., Sen, M. K. and Stoffa, P. L., 1996. "2-D resistivity inversion using spline arameterization and simulated annealing," Geophysics, vol. 61, no. 1, pp. 151–161.

Ciminale M., Loddo M., 2001.Aspects of magnetic data processing. Archaeological prospection, 8: n.4, 239–246.

Clark, A.J., 1986. Archaeological geophysics in Britain. Geophysics, 51, 1404–1413.

Clark A.J., 1990. Seeing beneath the soil: prospecting methods in archaeology. London: Batsford.

Compare, V., Cozzolino, M., Mauriello, P., Patella, D., 2009a. Resistivity probability tomography at the Castle of Zena (Italy). *Journal of Image and Video Processing, Eurasip*, vol. ID 693274, ISSN: 1687-5176, https://doi.org/10.1155/2009/693274.

Compare, V., Cozzolino, M., Mauriello, P., Patella, D., 2009b. 3D Resistivity probability tomography at the prehistoric site of Grotta Reali (Molise, Italy). *Archaeological Prospection*, vol. 16, n.1; p. 53–63, ISSN: 1099-0763, https://doi.org/10.1002/arp.347.

Constable, S. C., Parker, R. L. and Constable, C. G., 1987. Occam's Inversion: a practical algorithm for generating smooth models from EM sounding data. *Geophysics, 52, 289–300*.

Conyers LB, Ernewein EG, Grealy M, Lowe KM., 2008, *Electromagnetic conductivity mapping for site prediction in meandering river floodplains,* in Archaeological Prospection 15, pp. 81–91.

Conyers L.B., Goodman D., 1997. Ground Penetrating Radar. An introduction for archaeologists. AltaMira Press, Walnut Creek, California, (ISBN 0-7619-8927-7).

Cornelison, J.E., Jr., 1997, *An Archeological and Electromagnetic Survey of Moores Creek National Battlefield (31PD273), Pender County, North Carolina*. SEAC Technical Reports 6, Southeast Archeological Center, National Park Service, Tallahassee, Florida.

Corwin, R.F. & Hoover, D.B. 1979. The self-potential method in geothermal exploration. Geophysics, 44, 226-245.

Cosentino, P., Luzio, D., Martorana, R. and Terranova, L., 1995. Tomographic techniques for pseudo-section representation, in *Proceedings of the 1st Meeting of Environmental and Engineering Geophysical Society*, pp. 485–488, Turin, Italy.

Cosentino, P., Luzio, D. and Martorana, R., 1998. Tomographic resistivity 3D mapping: filter coefficients and depth correction, in *Proceedings of the 4th Meeting of Environmental and Engineering Geophysical Society*, pp. 279–282, European Section, Barcelona, Spain.

Cosentino, P. and Luzio, D., 1997. Tomographic pseudo-inversion of resistivity profiles, *Annali di Geofisica*, vol. 40, no. 5, pp. 1127–1144.

Cozzolino, M., Di Giovanni, E., Mauriello, P., Vanni Desideri A. and Patella, D., 2012. Resistivity tomography in the Park of Pratolino at Vaglia (Florence, Italy). *Archaeological Prospection*. (http://www.interscience.wiley.com), https://doi.org/10.1002/arp.1432.

Cozzolino, M., Mauriello and Patella, D., 2013. Resistivity Tomography Imaging of the substratum of the Bedestan Monumental Complex at Nicosia, Cyprus. Archaeometry. (http://www.interscience.wiley.com), https://doi.org/10.1111/arp.12018.

Dabas, M., 2009. Theory and practice of the new fast electrical imaging system ARP. In Campana, S., Piro, S., (dir.). *Seeing the Unseen*, Taylor and Francis Group, London, 105–126.

Dabas M., Hesse A., Tabbagh A., 2000. Experimental resistivity survey at the Roman Town of Wroxeter. *Archaeological Prospection* 7: 107-118.

Dabas, M., Tabbagh, A., and Tabbagh, J., 1994. 3-D inversion in subsurface electrical surveying – I. Theory: Geophysics. J. Int., 119, 975–990.

Dalan, R.A., 1989a, *Geophysical Investigations of the Prehistoric Cahokia Palisade Sequence*. Illinois Cultural Resources Study No. 8. Illinois Historic Preservation Agency, Springfield.

Dalan, R.A., 1989b, *Electromagnetic Reconnaissance of the Central Palisade at the Cahokia Mounds State Historic Site*, The Wisconsin Archeologist,70(3):309–332.

Dalan, R.A.,1989c, *Defining Archaeological Features with Electromagnetic Surveys at the Cahokia Mounds State Historic Site*, 59th Annual Internat. Mtg., Soc. Expl. Geophys., Expanded Abstracts 89:285.

Dalan, R.A.,1991, *Defining Archaeological Features with Electromagnetic Surveys at the Cahokia Mounds State Historic Site*, Geophysics 56(8):1280–1287.

Dalan, R.A., 1993a, *Issues of Scale in Archaeological Research*, Effect of Scale on Archaeological and Geoscientific Perspectives, J. K. Stein and A. R. Linse, eds., pp. 67–78. Special Paper 283. Geological Society of America, Boulder, Colorado.

Dalan, R.A., 1993b, *Landscape Modification at the Cahokia Mounds Site: Geophysical Evidence of Cultural Change.* Unpublished PhD. Dissertation, University of Minnesota, Minneapolis.

Dalan, R.A., 1995, *Geophysical Surveys for Archaeological Research: Electromagnetic Surveys,* Ms. on file, Interagency Archeological Services, National Park Service, Denver.

Daniels D., 2004. Ground Penetrating Radar. London: IEE.

Davis, J.L. & Annan, A.P. 1989. Ground-penetrating radar for high-resolution mapping of soil and rock stratigraphy. Geophysical Prospecting, 37, 531–551.

deGroot-Hedlin, C. and Constable, S., 1990. Occam's inversion to generate smooth, two-dimensional models form magnetotelluric data.*Geophysics, 55, 1613–1624*.

Deignan, T. and W. Brennan, 1992, *EM Data Acquired at Brown Sheep Camp.* Ms. on file, Interagency Archeological Services, National Park Service, Denver.

Dey, A. and Morrison, H.F. 1979. Resistivity modelling for arbitrarily shaped two-dimensional structures, *Geophysical Prospecting*, **27**, 106–136.

Di Filippo M., Di Nezza M., Marchetti M., Urbini S., Toro A., Toro B., 2005a. Geophysical research on Via Appia: the so-called "Monte di Terra" funeral monument. Proceedings of 6th International Archaeological Prospection Conference, Ed. Piro S. (ISBN88-902028), Roma, pp. 292-294.

Di Filippo M., Di Nezza M., Piro S., Santoro S., Toro B., 2005b. Integrated geophysical and archaeological investigations in the "Domus del Centenario", Pompei IX, 8 (Italy). Proceedings of 6th International Archaeological Prospection Conference Ed. Piro S. (ISBN88-902028), Roma, pp. 295-299.

Dobrin M.B. and Savit C. H., 1988. Introduction to Geophysical Prospecting: McGraw-Hill.

Dolphin, L.T., R.L. Bollen, and G.N. Oetzel, 1974, *An Underground Electromagnetic Sounder Experiment*, Geophysics 39(1):49–55.

Eder-Hinterleitner A., Neubauer W., Melichar P., 1996. Restoring magnetic anomalies. Archaeological prospection, 3: 185–197.

Ellis, R. G. and Oldenburg, D. W., 1994. The pole-pole 3-D DC resistivity inverse problem: A conjugate-gradient approach. In *Geophys. J. Internat., 119, 187–194*.

Farquharson, C.G., Oldenburgh, D.W., Routh, P.S., 2003, *Simultaneous 1D inversion of loop–loop electromagnetic data for magnetic susceptibility and electrical conductivity*, Geophysics 68 (6), 1857–1869.

Fassbinder J.W.E And Reindel M., 2005. Magnetometer prospection as research for pre-Spanish cultures at Nasca and Palpa, Perù. Proceedings of 6th International Archaeological Prospection Conference, Ed. Piro S. (ISBN88–902028), Roma, pp. 6-10.

Finzi, E. & Piro, S., 1991. Metodo per impulsi elettromagnetici. Georadar. Atti del Seminario "Geofisica per l'Archeologia", Quaderni ITABC, 1, 53–70.

Finzi E., Piro S., 2000. Radar (GPR) methods for historical and archaeological surveys. In "Non-destructive techniques applied to landscape archaeology", The Archaeology of Mediterranean Landscape, Vol. 4, pp. 125–135.

Frischknecht, F. C., V. F. Labson, B. R. Spies, and W. L. Anderson, 1991, Profiling Methods Using Small Sources, in Electromagnetic Methods in Applied Geophysics, Vol. 2., M. N. Nabighiam, ed., pp. 15–270. Society of Exploration Geophysicists, Tulsa, Oklahoma.

Frohlich, B. & Lancaster, W.J. 1986. Electromagnetic surveying in current Middle Eastern archaeology: Application and evaluation. Geophysics, 51, 1414–1425.

Gaffney, C. and Gater, J. 2003 Revealing the Buried Past: geophysics for archaeologists. Tempus, Stroud.

Gaffney V., Patterson H., Piro S., Goodman D., Nishimura Y., 2004. Multimethodological approach to study and characterise Forum Novum (Vescovio, Central Italy). Archaeological Prospection, Vol. 11, pp. 201–212.

Gerard, R. and Tabbagh, A., 1991. A mobile four electrodes array and its application to electrical survey of planetary grounds at shallow depths. J. Geophys. Res., 96 (B-3), 4117–4123.

Gibson, T.H. 1986. Magnetic prospection on prehistoric sites in western Canada. Geophysics, 51, 553–560.

Godio A., S. Piro, 2005. Integrated data processing for archaeological magnetic surveys. THE LEADING EDGE (SEG), Vol. 24, N. 11, 1138–1144.

Goodman, D. & Nishimura, Y. 1993. A Ground-radar view of Japanese burial mounds. Antiquity, 67, 349–354.

Goodman D., Piro S., 2013. GPR Remote sensing in Archaeology. Springer (Ed), ISBN 978–3-642-31856-6, ISBN 978-3-642-31857-3 (eBook), https://doi.org/10.1007/978-3-642-31857-3. Springer, Berlin, (Germany).

Goodman D., Piro S., Nishimura Y., Patterson H., Gaffney V., 2004a. Discovery of a 1st century Roman Amphitheater and Town by GPR. Journal of Environmental and Engineering Geophysics, Vol. 9, issue 1, pp. 35–41.

Goodman D., Schneider K., Barner M., Bergstrom V., Piro S., Nishimura Y., 2004b. Implementation of GPS navigation and 3D volume imaging of ground penetrating radar for identification of subsurface archaeology. Proceedings of the Symposium on the Application of Geophysics to Engineering and Environmental Problems, pp. 806–813. Environmental and Engineering Geophysical Society, Colorado Springs, Colorado.

Goodman D., Schneider K., Piro S., Nishimura Y. Pantel A.G., 2007. Ground Penetrating Radar Advances in Subsurfaces Imaging for Archaeology. In "Remote Sensing in Archaeology", Ed. J. Wiseman and F. El-Baz. Chapter 15, pp. 367–386.

Gosh, D.P.,1971a. Inverse filter coefficients for the computattion of apparent resistività standard curves for horizzontally stratified earth. Geophysical Prospecting, 19: 769–775.

Gosh, D.P. 1971b. The application of linear filter theory to direct interpretation of geoelectrical resistività sounding measurements. Geophysical Prospecting, 19: 192–217.

Grasmueck, M. 1996. 3-D ground penetrating radar applied to fracture imaging in gneiss. Geophysics, 61 (4): 1050–1064.

Griffiths, D.H. and Turnbull, J., 1985. A multi-electrode array for resistivity surveying. First Break 3 (No. 7), 16–20.

Griffiths D.H., Turnbull J. and Olayinka A.I. 1990, Two-dimensional resistivity mapping with a computer- controlled array. First Break 8, 121–129.

Ha, T., Pyun, S. and Shin, C., 2006. Efficient electric resistivity inversion using adjoint state of mixed finite-element method for Poisson's equation, Journal of Computational Physics, vol. 214, no. 1, pp. 171–186.

Haber, E., Ascher, U.M., Oldenburg, D.W., 2004, Inversion of 3D electromagnetic data in frequency and time domain using an inexact all-at-once approach, Geophysics 69 (5), 1216–1228.

Herbich T., 2005. Geophysical surveying in Egypt: recent results. Proceedings of 6th International Archaeological Prospection Conference, Ed. Piro S. (ISBN88–902028), Roma, pp. 421-426.

Hesse A., 1966. Prospections Geophysiques a faible profondeur. Applications a l'Archeologie. Dunod, paris.

Hesse A., Jolivet A., Tabbagh A., 1986. New prospects in shallow depth electrical surveying for archaeological and pedological applications. Geophysics 541(3): 585-594.

Hesse A., 1991. Les methods de prospection electromagnetique appliqués aux sites arcaeologiques. Atti del Seminario Geofisica perl' Archeologia. Quaderno n. 1 ITABC-CNR, 41-52.

Hesse A., 1992. A comprehensive archaeological and geophysical survey of a Knidian pottery workshop of amphorae in Resadiye, Datca Peninsula, Turkey. Proceedings of 28th International Symposium on Archaeometry (Archaeometry '92), Los Angeles, California, USA.

Hesse A., Doger E., 1993. Atelier d'amphores Rhodiennes et constructions en Pierre à Hisaronu (Turquie): un cas original de prospection electro-magnetique. Revue d'Archeometrie 17: 5-10.

Hesse A., Barba L., Link K., Oritz A., 1997. A magnetic and electrical study of archaeological structures at Loma Alta, Michoacan, Mexico. Archaeological Prospection 4: 53–67.

Howell, M., 1968a, *An Electro-magnetic Technique for the Location of Anomalous Soil Features*, Bulletin of the Bristol Archaeological Research Group 3(2):32–34.

Howell, M., 1968b, *The Soil Conductivity Anomaly Detector (SCM)*, Archaeological Prospection. *Prospezioni Archeologiche* 3:101–104.

Huang, H., Won, I., 2000. *Conductivity and susceptibility mapping using broadband electromagnetic sensors*, Journal of Environmental and Engineering Geophysics 5 (4), 31–41.

Huang H., and Won I. J., 2004, *Electromagnetic detection of buried metallic objects using quad–quad conductivity*, Geophysics, Vol. 69, No.6, pp. 1387–1393.

Huggins, R. 1984. Some design considerations for undertaking a magnetic survey for archaeological sources. Proceedings of the Society of Exploration Geophysicists Annual Meeting, Atlanta, Georgia, 209–212.

Ingeman-Nielsen T. and Baumgartner F., 2006, *Numerical modelling of complex resistivity effects on a homogenous half-space at low frequencies*, in Geophysical Prospecting, 2006, 54, pp. 261–271.

Inman, J.R., 1975. Resistivity inversion with ridge regression. Geophysics, 40: 798–817.

Koefoed, O., 1979. Geosounging principles, Resistivity sounding measurements. Amsterdam, Elsevier Scienntific.

Kozhevnikov, N. O. and S. P. Nikiforov,1995, *Magnetic Viscosity of Fired Clays and Possibility of it Use for Archaeological Prospection*, Science & Site: Evaluation and Conservation, J. Beavis and K. Barker, eds., pp. 163–169. Occasional Paper 1. School of Conservation Sciences, Bournemouth University, Poole, England.

Kuzma L. And Tirpak J., 2005. Proceedings of 6th International Archaeological Prospection Conference, Ed. Piro S. (ISBN88-902028), Roma, pp. 13-16.

Kvamme, K.L., 2000, *Current Practices in Archaeogeophysics: Magnetics, Resistivity, Conductivity, and Ground-Penetrating Radar,* Earth Sciences an Archaeology, P. Goldberg, V. Holliday, and R. Ferring, eds., Plenum Press, New York.

Lapenna, V., Mastrantuono, M., Patella, D. & Di Bello, G. 1992. Magnetic and geoelectric prospecting in the archaeological area of Selinunte (Sicily, Italy). Bollettino di Geofisica Teorica ed Applicata, XXXIV, 133–143.

Leckebusch, J. 2000. Two- and Three-dimensional Ground-penetrating Radar Survey across a medieval chair: a case study in Archaeology. Archaeological Prospection, 7 (4): 189–200.

Li, Y. G. and Oldenburg, D. W., 1994. Inversion of 3-D dc resistivity data using an approximate inverse mapping, Geophysics, J. Int., 116, 527–537.

Lines, L. R. and Treitel, S., Tutorial. A review of least-squares inversion and its application to geophysical. *Geophysical Prospecting 32, 159–186,* 1984.

Linford N., Linford P., Martin L., Payne A., 2007. Recent results from the English Heritage caesium magnetometer system in comparison to recent fluxgate gradiometers. Archaeological Prospection, Vol. 14, 151–166.

Linington, R.E. 1966. Test use of a gravimeter on Etruscan chamber tombs at Cerveteri. Prospezioni Archeologiche, 1, 37-41.

Loke, M.H., 2004. Tutorial: 2-D and 3-D electrical imaging surveys. http://www.geoelectrical.com.

Loke, M. H. and Barker, R. D., 1996. Rapid least-squares inversion of apparent resistivity pseudosections by a quasi-Newton method,*Geophysical Prospecting*, vol. 44, no. 1, pp. 131–152.

Malagodi, S., Orlando, L., Piro, S. & Rosso, F. 1996. Location of archaeological structures using GPR method. 3-D data acquisition and radar signal processing. Archaeological Prospection, 3: 13–23.

Marescot, L., Lopes, S. P., Rigobert, S. and Green, A. G., 2008. Nonlinear inversion of geoelectric data acquired across 3D objects using a finite-element approach, *Geophysics*, vol. 73, no. 3, pp. F121–F133.

Mauriello, P., and Patella, D., 1999a. Imaging 3D structures by resistivity probability tomography, in *Proceedings of the 61st EAGE Conference and Technical Exhibition*, Helsinki, Finland.

Mauriello, P., and Patella, D., 1999b. Resistivity anomaly imaging by probability tomography," *Geophysical Prospecting*, vol. 47, no. 3, pp. 411–429.

Mauriello, P., Monna, D. and Patella, D., 1998. 3D geoelectrical tomography and archaeological applications, *Geophysical Prospecting*, vol. 46, no. 5, pp. 543–570.

Mauriello, P., and Patella, D., 2009. A data-adaptive probability-based fast ERT inversion method, Progress In Electromagnetics Research, 97, 275–90, https://doi.org/10.2528/pier09092307.

Mc Neill, J. D., 1980a, *Electrical Conductivity of Soils and Rocks.* Technical Note TN-5. Geonics Limited, Mississauga, Ontario, Canada.

Mc Neill, J. D., 1980b, *Electromagnetic Terrain Conductivity Measurement at Low Induction Numbers.* Technical Note TN-6. Geonics Limited, Mississauga, Ontario, Canada.

Menke, W, 1989. Geophysical data analysis: Discrete Inverse Theory, 2° ed. San Diego, Academic Press, 1989.

Moffatt, D.L., 1974. Subsurface video pulse radar. Proceedings of an Engineering Foundation Conference on Subsurface Exploration for Underground Excavation and Heavy Construction, New England College. American Society of Civil Engineers, New York.

Morey, R.M., 1974. Continuous subsurface profiling by impulse radar. Proceedings of Engineering Foundation Conference on Subsurface Exploration for Underground Excavation and Heavy Construction, New England College. American Society of Civil Engineers, New Yor, 213-232.

Musset Alan E. and Khan Aftab M., 2000, Looking into the earth, An introduction to geological geophysics, Cambridge University Press.

Nabighian, M. N., 1991, *Electromagnetics Methods in Applied Geophysics.* Vol. I, Theory 523 pp., Vol. II, Applications, 972 pp. Society of Exploration Geophysicists, Tulsa.

Narayan, S., Dusseault, M. B. and Nobes, D. C., 1994. Inversion techniques applied to resistivity inverse problems, *Inverse Problems*, vol. 10, no. 3, pp. 669–686.

Neubauer W., Eder-Hinterleitner A., 1997a. Resistivity and Magnetics of the Roman Town Carnuntum, Austria. An example of combined interpretation of prospection data. Archaeological Prospection 4: 179–189.

Neubauer W., Eder-Hinterleitner A., 1997b. 3D-interpretation of post-processed archaeological magnetic prospection data. Archaeological Prospection 4: 191–205.

Neubauer W., Eder-Hinterleitner A., Seren S., Melichar P., 2002. Georadar in the Roman Civil town Carnuntum, Austria. An approach for archaeological interpretation of GPR data. Archaeological Prospection, 9: 135–156.

Neubauer W., Locker K., Eder-Hinterleitner A., Melichar P., 2005. Geophysical prospection of middle neolithic circular ring ditch systems in lower Austria. Proceedings of 6th International Archaeological Prospection Conference, Ed. Piro S. (ISBN88-902028), Roma, pp. 43-47.

Nishimura, Y. And Goodman, D. 2000. Ground-penetrating radar survey at Wroxeter. *Archaeological Prospection*, 7 (2): 101–105.

Orlando, L., Piro, S. & Versino, L., 1987. Location of subsurface geoelectric anomalies for archaeological work: a comparison between experimental arrays and interpretation using numerical methods. *Geoexploration*, 24, 227-237.

Osella A, de la Vega M, Lascano E, 2005, 3D electrical imaging of an archaeological site using electrical and electromagnetic methods, in *Geophysics* 70(4), pp. 101–107.

Panissod, C., Dabas, M., Hesse, A., Jolivet, A., Tabbagh, J. and Tabbagh, A., 1998. Recent developments in shallow depth electrical and electrostatic prospecting using mobile arrays. *Geophysics*, 65, 1542–1550.

Papadopoulos N.G., Tsourlos P., Tsokas G.N., Sarris A., 2006. Two-dimensional and Three-dimensional resistivity imaging in archaeological site investigation. *Archaeological Prospection* 13: 163-181.

Parasnis. D. S., 1986. Principles of applied geophysics. London: Chapman and Hall, 402 pp.

Parasnis D.S., 1997, Principles of Applied geophysic: Chapman & Hall, London, 5th edition.

Parchas, A. and Tabbagh, A., 1978, *Simultaneous measurement of electrical conductivity and magnetic susceptibility of the ground in the EM prospecting*, in Archaeophysika 10, pp. 682–691.

Pazdirek, O. and Blaha, V., 1996. Examples of resistivity imaging using ME-100 resistivity field acquisition system. EAGE 58th Conference and Technical Exhibition Extended Abstracts, Amsterdam.

Pellerin L., 2002, *Applications of Electrical and Electromagnetic Methods for Environmental and Geotechnical Investigations,* in Surveys in Geophysics, 23, pp. 101–132.

Pidlisecky, A., Haber, E. and Knight, R., 2007. RESINVM3D: a 3D resistivity inversion package, *Geophysics*, vol. 72, no. 2, pp. H1–H10.

Pipan, M., Finetti, I. And Ferigo, F. 1996. Multi-fold GPR techniques with applications to high-resolution studies: two case histories. European Journal of Environmental and Engineering Geophysics, 1: 83–103.

Pipan, M., Baradello, L., Forte, E., Prizzon, A. And Finetti, I. 1999. 2-D and 3-D processing and interpretation of multi-fold ground penetrating radar data: a case history from an archaeological site. Journal of Applied geophysics, 41: 271–292.

Pipan, M., Baradello, L., Forte, E. And Finetti, I. 2001. Ground Penetrating radar study of Iron Age tombs in South Eastern Kazakhstan. Archaeological Prospection, 8 (3): 141–155.

Piro S., Samir A., Versino L., 1998. Position and spatial orientation of magnetic bodies from archaeological magnetic surveys. Annali di Geofisica 41(3): 343–358.

Piro S., Cammarano F., Mauriello P., 2000. Quantitative integration of geophysical methods for archaeological prospection. Archaeological Prospection, Vol. 7, n.4, pp 203–213.

Piro S., Sambuelli L., Godio A., Taormina R., 2007. Beyond image analysis in processing archaeomagnetic geophysical data: examples on chamber tombs with dromos. *Near Surface Geophysics Journal (EAGE)*, Vol. 5, n.6, 405–414.

Piro S., 2009. Introduction to geophysics for archaeology. In "Seeing the Unseen. Geophysics and Landscape Archaeology". Campana & Piro Editors. CRC Press, Taylor & Francis Group. Oxon UK, (ISBN 978-0-415-44721-8), pp. 27-64.

Piro S., Goodman D., Nishimura D., 2001a. The location of Emperor Traiano's Villa (Altopiani di Arcinazzo–Roma) using high-resolution GPR surveys. Bollettino di Geofisica Teorica ed Applicata Vol. 43, n.1–2, pp. 143–155.

Piro S., Tsourlos P., Tsokas G.N., 2001b. Cavity detection employing advanced geophysical techniques: a case study. European Journal of Environmental and Engineering Geophysics Vol. 6, pp. 3-31.

Pous, J., Marcuello, A. And Queralt, P., Resistivity inversion with a priori information. *Geophysical Prospecting,* 35: 590–603, 1987.

Pous, J., Marcuello, A. And Queralt, P., 1987. Resistivity inversion with a priori information. *Geophysical Prospecting*, 35: 590–603.

Powers C.J., Singha Kamini, and Peter Haeni F., 1999, *Integration of Surface Geophysical Methods for Fracture Detection in Bedrock at Mirror Lake*, New Hampshire, Presented at the USGS Toxic Substances Hydrology Program Meeting, March 8–12, '99, Charleston, SC.

Pracser E., Adam A., Szarka L., Muller I., Turberg P., 2000, *Slingram measurements in the Mecsek Mountains. Hungary,* Acta Geodaetica et Geophysica Hungarica, Vol. 35 (4), pp. 397–414.

Pérez-Flores,M. A., Méndez-Delgado, S., Gómez-Treviño, E., 2001. Imaging low frequency and dc electromagnetic fields using a simple linear approximation. Geophysics 66 (4), 1067– 1081.

Reynolds J. M., 1997, An Introduction to Applied and Environmental Geophysics: John Wiley & Sons.

Saey T., De Smedt P., Meerschman E., Monirul M., Meeuws F., Van De Vijver E., Lehouck A., And Van Meirvenne M., 2012. Electrical Conductivity Depth Modelling witha Multireceiver EMI Sensor for Prospecting Archaeological Features, in *Archaeol. Prospect*. 19, pp. 21–30.

Sasaki, Y., 2006. 3-D resistivity inversion using a subspace method, *Geophysical Exploration*, vol. 59, no. 5, pp. 425–430.

Scollar, I.,1962, *Electromagnetic Prospecting Methods in Archaeology*, Archaeometry 5: 146–153.

Scollar I., Tabbagh A., Hesse A., Herzog I., 1990. Archaeological prospecting and Remote Sensing. Cambridge University Press: Cambridge.

Shamper C. and Rejjba F., 2011, *1D inversion of multi-component and multi-frequency low-induction number EM Device (PROMIS) for near surface exploration,* in PIERS online, vol.7, No. 2, pp. 126–130.

Sheng Y., 1986, *A single apparent resistivity expression for long-offset transient electromagnetics*, Geophysics, 51, pp. 1291–1297.

Shima, H., Sakashita, S. and Kobayashi, T., 1996. Developments of non-contact data acquisition techniques in electrical and electromagnetic explorations. Journal of Applied Geophysics, 35, 167–173.

Sigurdsson, T. And Overgaard, T. 1998. Application of GPR for 3-D visualization of geological and structural variation in a limestone formation. Journal of Applied Geophysics, 40: 29–36.

Silvester, P.P. and Ferrari, R.L., 1990. Finite elements for electrical engineers (2nd. ed.). Cambridge University Press.

Smith, N. C. and Vozoff, K., 1984. Two-dimentional dc resistivity inversion for dipole-dipole data, IEEE Trans, Geosciences, Remote Sensing, 22, 21–28.

Spies B.R. e Eggers D.E., 1986, *The use and misure of apparent resistivity in electromagnetic method,* Geophysics, 51, 1462–1471.

Spies B.R. e Frischknecht F.C, 1991, *Electromagnetic sounding in electromagnetic methods* in Applied geophysics, vol. 2, Applications, ed. Nabigian, M.N., Society of exploration Geophysicists, Tulsa.

Stright, M.J., 1986. Evaluation of archaeological site potential on the outer continental shelf using high-resolution seismic data. Geophysics, 51, 605-622.

Tabbagh, A., 1974. Méthodes de prospection électromagnétique applicables aux problèmes archélogiques. Archaeophysika, 5, 350-437.

Tabbagh, A.,1984a, On the Comparison between Magnetic and Electromagnetic Prospection Method for Magnetic Features Detection, Archaeometry 26(2):171–182.

Tabbagh, A.,1984b, Interest in the Slingram EM Method for Archaeological Prospecting. *54th Annual Internat. Mtg., Soc. Expl. Geophys*., Expanded Abstracts 84:206–208.

Tabbagh, A.,1985, The Response of a Three Dimensional Magnetic and Conductive Body in Shallow Depth Electromagnetic Prospecting, in Geophysical Journal of the Royal Astronomical Society 81:215–230.

Tabbagh, A.,1986a, What is the Best Coil Orientation in the Slingram Electromagnetic Prospecting Method?, Archaeometry 28(2):185–196.

Tabbagh, A., 1986b, Applications and Advantages of the Slingram Electromagnetic Method for Archaeological Prospecting, Geophysics 51(3):576–584.

Tabbagh, A., A. Hesse, and R. Grard,1993, Determination of Electrical Properties of the Ground at Shallow Depth with an Electrostatic Quadripole: Filed Trails on Archaeological Sites, Geophysical Prospecting 41:579–597.

Tabbagh, A.,1994, Simultaneous Measurements of Electrical Conductivity and Dielectric Permittivity of Soils Using a Slingram Electromagnetic Device in Medium Frequency Range, Archaeometry 36(1):159–170.

Telford W.M., Geldart L.P., Sheriff R.E., Keys D.A., 1976. Applied Geophysics. Cambridge University Press, New York, U.S.A., 860 pp.

Telford W. M., Geldart L.P. and Sheriff R.E., 1990, Applied Geophysics: Cambridge University Press, 2nd edition.

Tite, M. S. and C. Mullins, 1969, *Electromagnetic Prospecting: A Preliminary Investigation*, Prospezioni Archeologiche 4:95–102.

Tite, M. S. and C. Mullins, 1970, *Electromagnetic Prospecting on Archaeological Sites Using a Soil Conductivity Meter,* in Archaeometry 12(1):97–104.

Tsokas G.N., Giannopoulos A., Tsourlos P. Vargemezis G., Tealby J.M. Sarris A., Papazachos C. B., Savopoulou T., 1994. A large scale geophysical survey in the archaeological site of Europos (northern Greece). Journal of Applied Geophysics 32: 85–98.

Tsokas G.N., Papazachos C.B., Vafidis A., Loukoyiannakis M.Z., Vargemezis G., Tzimeas K., 1995. The detection of monumental tombs buried in tumuli by seismic refraction. Geophysics, 60(6), 1735-1742.

Tsokas G.N., Sarris A., Pappa M., Bessios M., Papazachos C.B., Tsourlos P., Giannopoulos A., 1997b. A large scale magnetic survey in Makrygialos (Pieria), Greece. Archaeological Prospection 4: 123–137.

Tsourlos, P., 1995. Modelling, interpretation and inversion of multielectrode resistivity survey data, PhD. Thesys, University of York.

Ulriksen, C.P.F., 1982. Application of the impulse radar to civil engineering. PhD Dissertation, Lund University of Technology, Lund, Sweden, 179 pp.

Van der Kruk J., Meekes J.A.C., Van den Berg P.M and Fokkema J.T., 2000, *An apparent resistivity concept for low-frequency electromagnetic sounding techniques*, in *Geophysical Prospecting*, 2000, 48, pp. 1033–1052.

Viberg A., Remnant echoes of the past, 2012, Archaeological geophysical prospection in Sweden, Doctoral Thesis in Archaeological Science 2012 Stockholm University, pp. 36–42.

Von Der Osten Wondelburg H., 2005, *Application of Ground Penetrating Radar, magnetic and Electric Mapping, and Electromagnetic induction Methods in archaeological investigation,* in Near Surface Geophysics, edited by Dwain K. Butler, pp. 621–626. Society of exploration Geophysicists, Tulsa, Oklahoma.

Ward, S. H., and G. W. Hohmann, 1988, *Electromagnetic theory for geophysical applications*, *in* M. N. Nabighian, Ed., Electromagnetic methods in applied geophysics: Society of Exploration Geophysicists, 130–311.

Westerberg K., 1965, *The Beam-Slingram: a new portable EM-instrument for ore prospecting,* in Geoexploration, Volume 3, Issue 3, pp. 149–154.

Weymouth, J.W. 1986 a: Archaeological site surveying program at the University of Nebraska. Geophysics, 51, 538–552.

Weymouth, J.W. 1986 b: Geophysical methods of archaeological site surveying. In "Advances in Archaeological Method and Theory", Vol.9, 311–395.

Witten AJ, Calvert G, Witten B, Levy T, 2003, *Magnetic and electromagnetic induction studies at archaeological sites in southwestern Jordan,* in Journal of Environmental and Engineering Geophysics 8, pp. 209–215.

Won and Elena I. Novikova, 2000, *Electromagnetic response of an earth having a continuous conductivity variation in depth,* Journal of Environmental and engineering geophysics, vol.5, issue 3, pp. 37/44.

Xiong Z., 1992, Electromagnetic modeling of three dimensional structures by the method of system iteration using integral equations,*Geophysics* 57, pp. 1556–1561.

Xiong Z., Tripp A., 1995, A block iterative algorithm for 3D electromagnetic modeling using integral equations with symmetrized substructures, in*Geophysics* 60, pp. 291–295.

Zhang, Z., Liu, Q., 2001. Two nonlinear inverse methods for electromagnetic induction measurements, *IEEE Geoscience and Remote Sensing* 39 (6), 1331–1339.

Zhang, J., Manckie, R. L. And Madden, T. R., 3_D resistivity forward modelling and inversion using conjugate gradients, Geophysics, 60, 1313–1325, 1995.

Zhdanov M., 2010, *Electromagnetic geophysics: Notes from the past and the road ahead*, in Geophysics, vol. 75, NO.5, pp. 75A49–75A66.

Zohdy, A.A.R., A new method for the automatic interpretation of Schlumberger and Wenner sounding curves, Geophysics, 54 (2), 245–253, 1989.

Chapter 4
Case Histories: Application of Geophysical Prospection to Cultural Heritage

Abstract The second part of this book is focused on the application of the different geophysical methodologies - Geoelectrical, Ground Penetrating Radar and Electromagnetic - to Cultural Heritage, both in Italian and foreign sites. In order to highlight the various possible applications, the case studies, related to the most frequent diagnostic surveys, have been divided into main topic: Monuments, Historical Buildings, Urban Centres, Archaeological Parks, Preventive Archeology and Ancient viability.

In this chapter the case histories are presented as following: for "Monuments" the ERT surveys at the Royal Residence of San Leucio (Caserta, Italy) and GPR investigation at the Royal Palace of Naples (Italy); for "Historical Buildings" the ERT survey at the Castle of Zena (Carpeneto Piacentino, Piacenza, Italy) and the Castle of Shawbak (Jordan) and GPR investigation at the S. Giovanni in Laterano Basilica (Rome, Italy), Cathedral of Termoli (Campobasso, Italy) and Capua's Castle (Campobasso, Italy); for "Urban Centres" the ERT and GPR surveys in the historical centre of Nicosia (Cyprus), the ERT surveys in the historical centre of Alife (Caserta, Italy) and High Resolution GPR Surveys at Palatino Hill (Rome, Italy) and in the Medieval Town of Prato (Florence, Italy); for "Archaeological Park", the ERT surveys in the Park of Pratolino (Vaglia, Florence, Italy), in the Cuma Site (Naples, Italy) and at Norba (Latina, Italy) and the Extensive Ground Remote Sensing Investigations in Aquinum Roman Site (Castrocielo, Frosinone, Italy); for "Preventive Archeology" the GPR surveys in the Territory of Ancient Tarquinia (Viterbo, Italy) and the ERT surveys in the territory of Petroio (Florence, Italy); for "Ancient viability" the Remote sensing, EMI and ERT surveys for studying the road network of Egnazia site (Fasano, Brindisi, Italy).

Two case studies, the Treasury Tomb in the Archaeological Park of Petra, Jordan and the Abbey of Santa Maria a Mare, San Nicola Island, Tremiti (Foggia, Italy), concern the important and innovative research issue related to integration of 3D metric survey and geophysical prospection. Finally, the case study of Molise Region (Italy) provide a scientific contribution to the integration of geophysical prospections with the most modern data collection (Geographical Information System).

Each case study is composed by an introduction that describes the historical-archaeological context; the survey planning that explains both the methodological

approach and the data acquisition and the last subsection with the discussion of data processing and results. Detailed figures complete the respective text sections.

4.1 Monuments

4.1.1 ERT surveys at the Royal Residence of San Leucio (Caserta, Italy)

The King Ferdinando IV Borbone' Royal Recidence of San Leucio (Fig. 4.1), located in the territory of Caserta (Italy), was the headquarters of one of the most prestigious real industries specialized in silk production. The building was built in the second half of the sixteenth century, probably by the lord of Caserta Andrea Matteo Acquaviva (1572–1634), and, during the first half of the eighteenth century, it was in conditions of neglect. With the first maintenance, conducted in the seventies of the eighteenth century, the building was used as accommodation for the keepers of the forest and the gamekeeper. In 1776, the large ballroom was transformed into a parish church dedicated to San Ferdinando Re and later the Bourbon Ferdinand IV commissioned the expansion of whole building, intended to accommodate a silk factory, to the architect Francesco Collecini (1723–1804), a

Fig. 4.1 King Ferdinando IV Borbone' Royal Recidence of San Leucio (Caserta, Italy)

Fig. 4.2   Maria Carolina Asburgo' exotic bathroom (Caserta, Italy)

student and former aide of Luigi Vanvitelli. The old Casino becomes the central body of a large rectangular building with an interior courtyard, which includes, in addition to the Royal Apartments, housing for teachers and factory directors, a normal school and, on the upstream side, a regular room for mill, a winder, a spinning wheel and other local manufacturing accessories.

The industrial site itself became a symbol of royal power.[1] Many of the artists already engaged in the decoration of the apartments of the Royal Palace of Caserta also worked in San Leucio as the case of Fedele Fischetti (1732–1792), author of the frescoes in the large dining room and Carlo Brunelli (XVIII century), author of the paintings of the parish church of San Ferdinando Re.

In this building Maria Carolina Asburgo, wife of the king, wanted for herself the construction of an exotic bathroom with an elliptic shape, built inside the floor of a whole room (Fig. 4.2). Philiph Hackert realized same frescos, following the encaustic technique, which represent female dancing figures (Martucci et al. 1993; Cundari 2005), on the walls of the chamber.

In a project of general restoration of the bathroom, the Electrical Resistivity Tomography was carried out using a set of vertical and horizontal axial dipole-dipole profiles (Fig. 4.3), directly effected on the wall of the fresco in order

---

[1]http://reggiaofcaserta.altervista.org/it/parco/san-leucio-belvedere-seta/.

Fig. 4.3 Vertical and horizontal axial dipole-dipole profiles carried out on the fresco

to understand the reason of an excessive moisture that was damaging it. The work was made in collaboration the Bugli Carlo & C. S.A.S. Company (Restoration and Conservation of Artistic Heritage).

4.1.1.1 Survey Planning

A Cartesian reference system has been defined with the (x, y)-plane coinciding with the wall of the fresco, the origin placed at the left side, on the top, of the surface (Fig. 4.4), and the x, y and z-axis positive rightwards, upwards and inwards, respectively. The geoelectrical survey was carried out along 21 profiles, disposed as follows (Fig. 4.4):

– 17 vertical and parallel profiles (101,…, 117) were realized on the wall, from left to right and with a varying distance between them. The origin of the lines was put on the top of the fresco and surveys were distanced of 0.5 m from the top and the bottom boundary of the wall. Along each profile, 13 electrodes with dipolar spread of 0.25 m were fixed, getting a total length of 3 m.

– 4 horizontal and parallel profiles (201, …, 204) were effected from the top to the bottom of the fresco and the origin was located at a distance of 0.25 m from the left side (except for the profile 204 for which the distance was put at 0.89 m). Along each profile, 43 electrodes with dipolar spread of 0.25 m were fixed, getting a total length of 10.5 m (profile 204 was long 9.75 m).
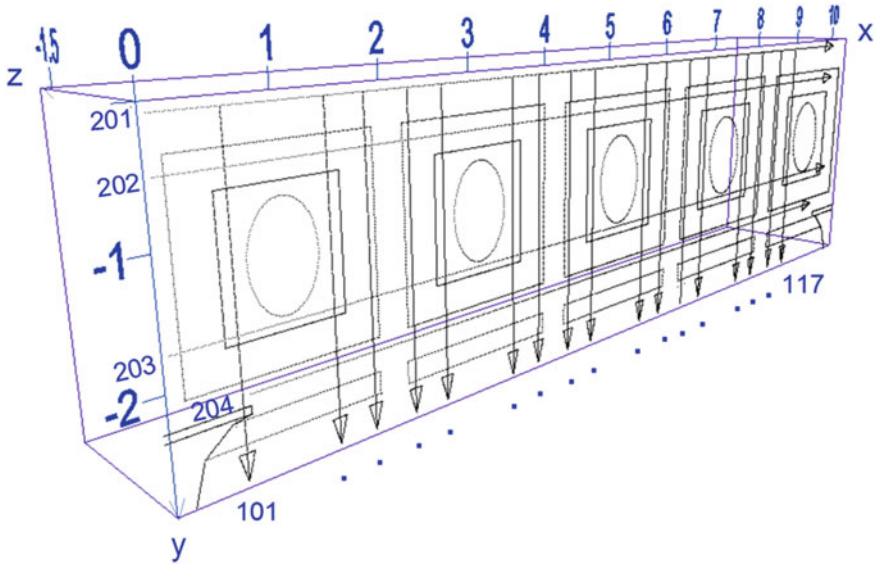
Fig. 4.4 The geoelectrical profiles about the fresco of Maria Carolina Asburgo. 201,…, 204: horizontal profiles. 101,…, 117: vertical profiles

In every case, small steel nail electrodes were used, in order to avoid damages to the painting. The purpose of the geoelectrical profiles was a large-scale reconnaissance of the resistivity inside the wall.

4.1.1.2   Data Processing and Results

Figures 4.5, 4.6 and 4.7 show a perspective view of the tomospace obtained through the application of the 3D probability-based ERT imaging applied to the *{ρa}* datasets using different drawing styles. The sequences have the purpose to put in evidence the tridimensional distribution of zones in which there is more concentration of moisture. As low resistivity values represent conductive materials, such as the presence of water, the color scale adopted in those visualizations was realized in order to empathize only values minor to 2.25 Ω m (the average resistivity).

Figure 4.5 shows vertical sections at increasing offset from the origin of the z-axis. The superficial section, realized at 0.25 m inside the wall (Fig. 4.5a), presents the most intense concentration of conductive anomalies focused in the central part of the fresco. At rising depth, the average resistivity increase.

In Fig. 4.6 the location and the form of the anomaly sources is displayed by a sequence of horizontal tomography sections at increasing depth from the origin of the x-axis. The succession put in evidence that the position of the conductive
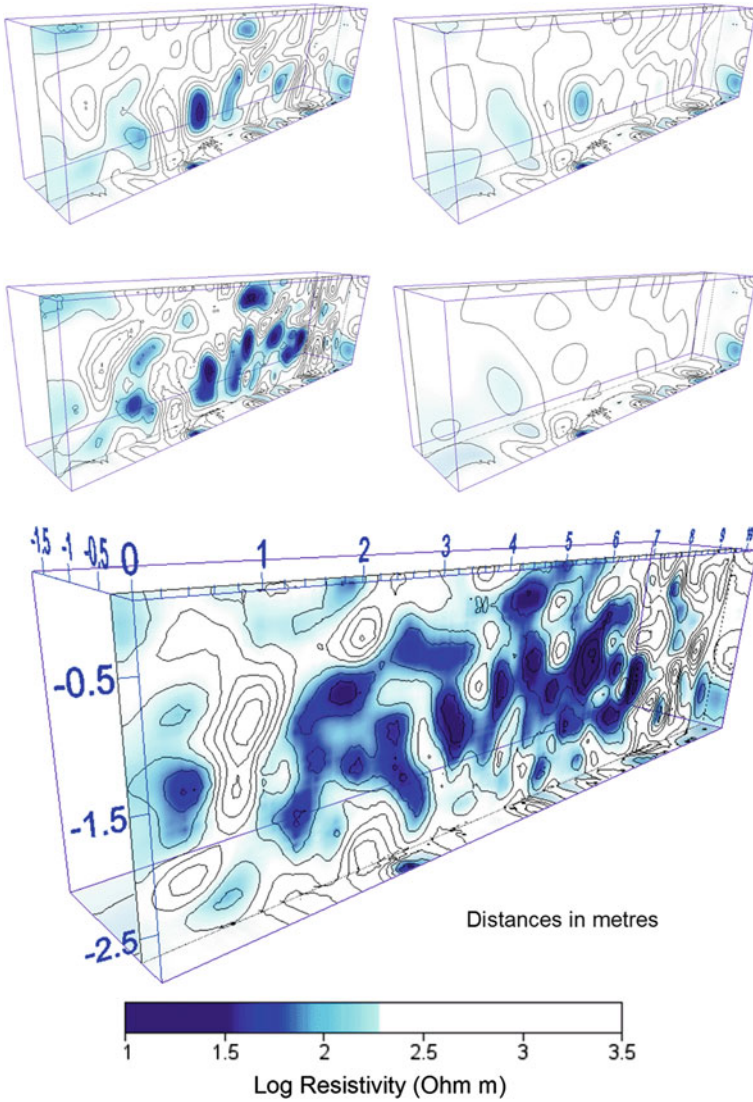
Fig. 4.5 Geoelectric tomography with a sequential view of the vertical sections at increasing offset from the origin of the z axis

nucleus is above all placed between 1 and 7.5 m on the x-axis and interest all the wall.

The same situation can be appreciated in Fig. 4.7 where vertical sections, at increasing depth from the origin of the y-axis, are displayed.

The probable shape of this wet nucleus can be better analyzed looking at Figs. 4.8 and 4.9, where perspective views under two different angles are displayed.
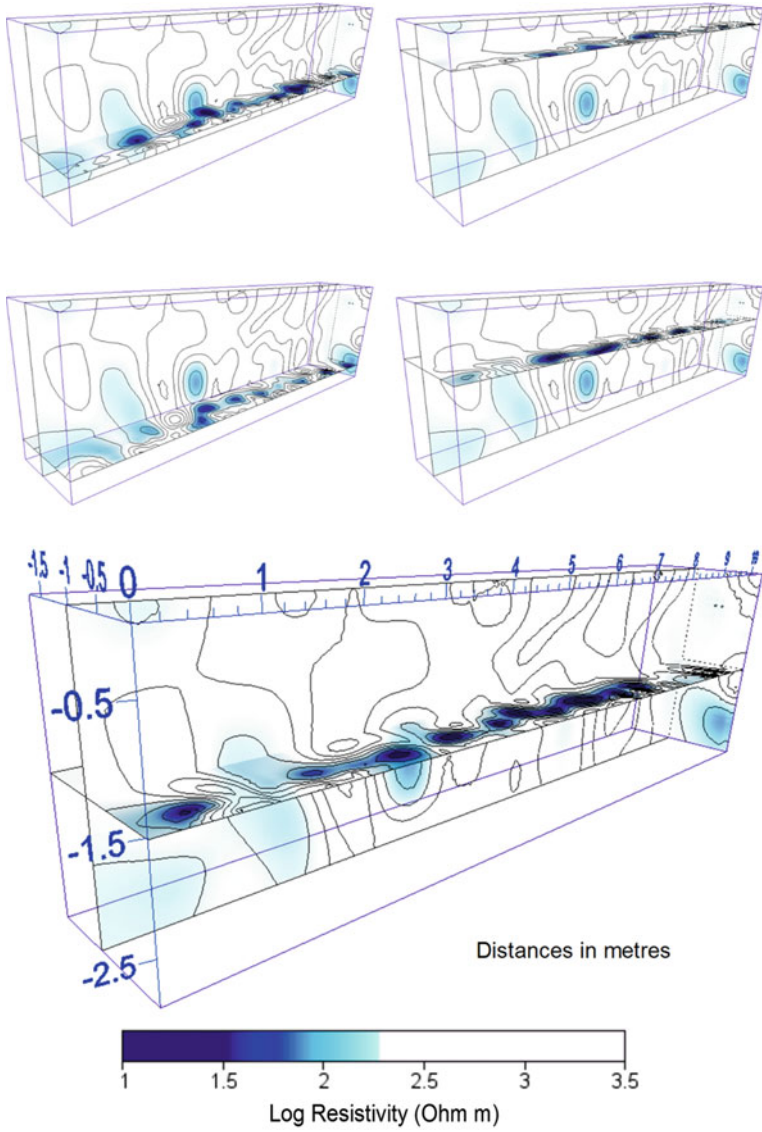
Fig. 4.6 Geoelectric tomography with a sequential view of the horizontal sections at increasing offset from the origin of the x axis
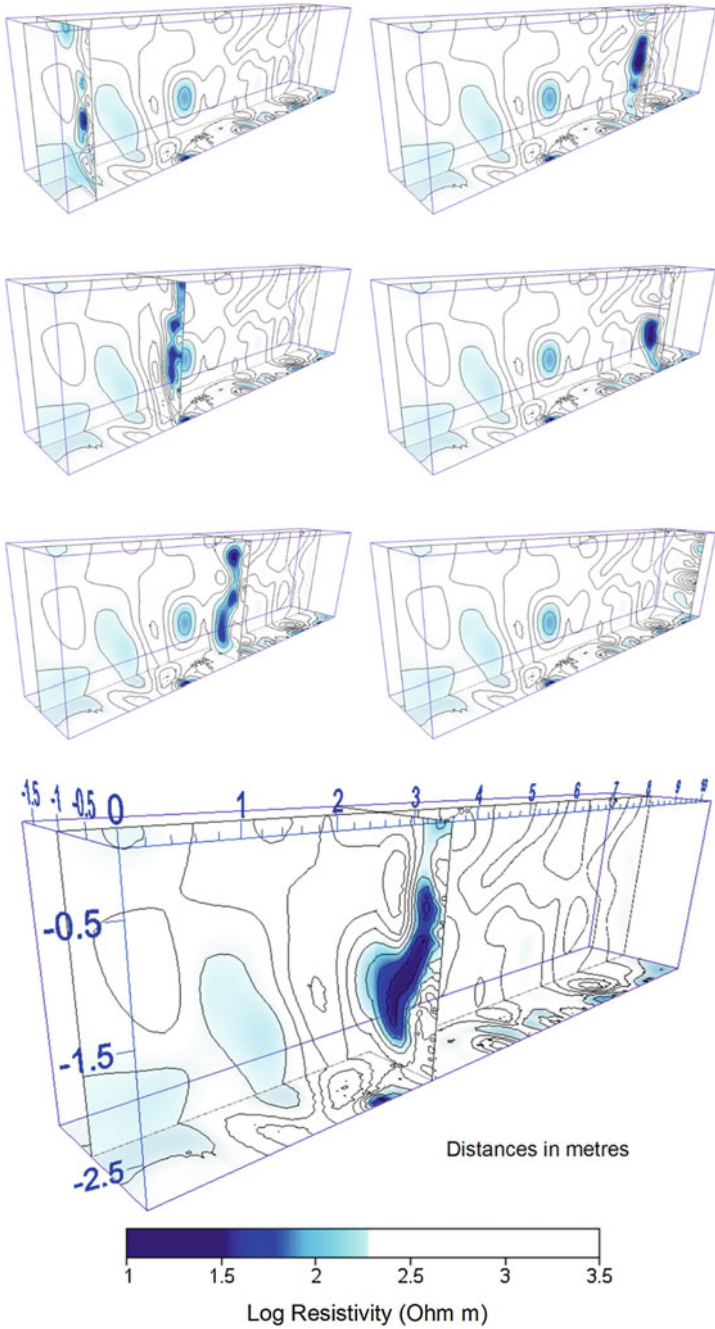
Fig. 4.7 Geoelectric tomography with a sequential view of the vertical sections at increasing offset from the origin of the y axis
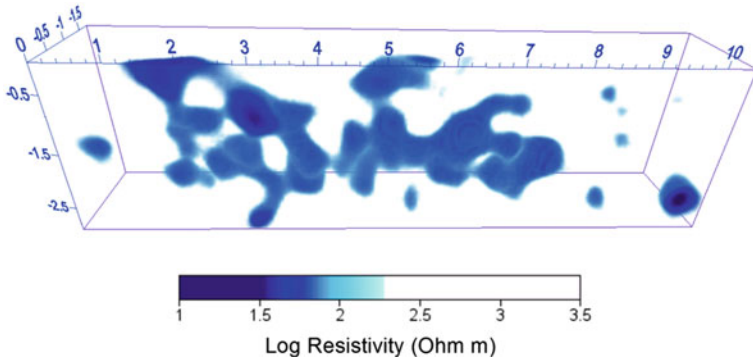
Fig. 4.8 Tridimensional tomography image limited to the nucleus including resistivity values minor to 2.25 Ω m, under a frontal point of view

Fig. 4.9 Tridimensional tomography image limited to the nucleus including resistivity values minor to 2.25 Ω m, under a lateral point of view
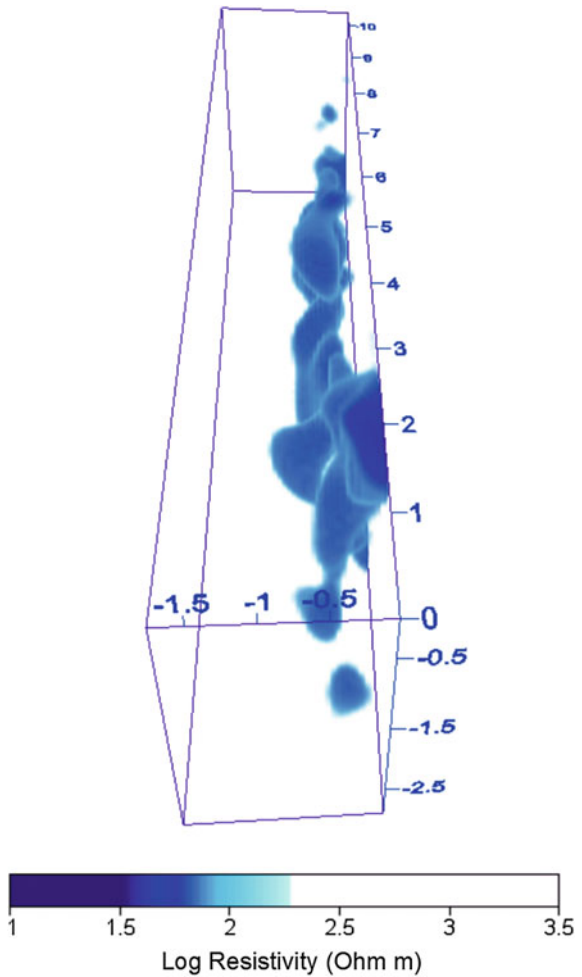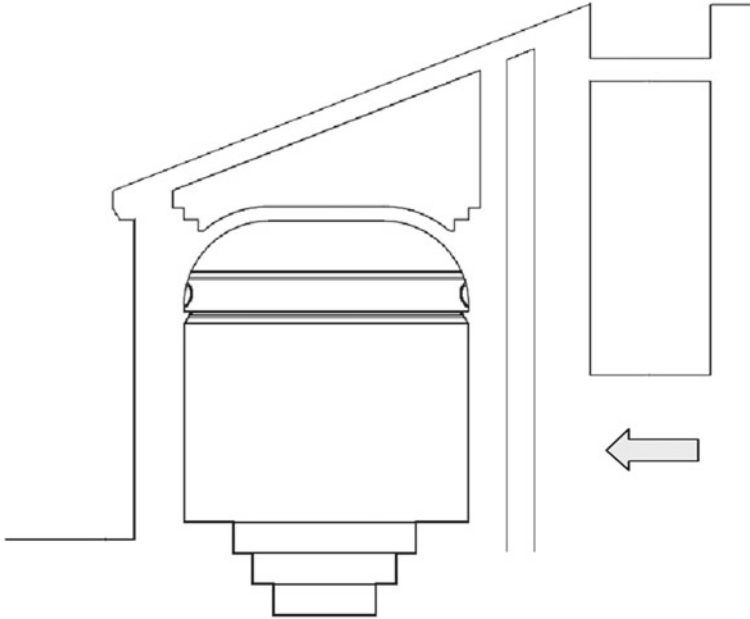
Fig. 4.10 Lateral view of the bathroom of Maria Carolina Asburgo. At the right side of the picture, the probably zone of water infiltration is signed up with an arrow

This analysis has lead to determinate the zones of greater presence of conductive elements in the wall and their exact position is simply readable from the images.

Considering the section of the air hall existing behind the wall (Fig. 4.10), the most probable hypothesis is that under it there's a consistent fluid circulation. This zone (indicated with an arrow) is spatially correlated with the conductive zone evidenced by the electrical tomographies.

4.1.2   GPR investigation at the Royal Palace of Naples (Italy)

The Royal Palace of Naples (Italy) dates back to the early 1600s when the Spanish Viceroy decided to build a large and elegant palace that could host the court and sovereigns in the course of their journeys in the city. The project was entrusted to Domenico Fontana, which was inspired by the late-Renaissance style; successive enlargements and embellishments were made in the 1700s and 1800s. In 1837 a devastating fire damaged the building and subsequent repairs were conducted by the architect Gaetano Genovese, who also built the room for celebrations and a new facade towards the sea. From 1600 to 1946 the Royal Palace was the headquarter of

the monarchic power in Naples and Southern Italy hosting at first the Spanish and Austrian viceroys, then the Bourbons and finally the Savoy.

The survey in the Royal Palace of Naples was realized near the Roof Garden built in the late seventeenth century and restructured in the nineteenth century after the fire that had involved it. Currently, the only access to the *loggia* is the X Room (the room that housed the oratory of Maria Cristina of Savoy), but in the nineteenth century it was accessed directly from the current XX Room using a cast iron bridge, which was destroyed during the bombings of the Second World War. Only the traces of the eight cast iron pins (four on each side) of this passage remain. They were inserted in the limestone blocks and anchored at the structure of the apartments to the wall (A-Wall) and to the opposite side on which the gardens lie (B-Wall) (Figs. 4.11 and 4.12).

Fig. 4.11 Royal Palace of Naples to the left (image from Google Earth) and indication of the place in which there was the cast iron bridge to the right

Fig. 4.12 Location of the 4-iron pins on B-Wall to the left and detail of the hinge on the right

   The purpose of the application of the GPR was to verify the lengths of the iron pins in the wall below the garden (B-Wall) and to testify, on the other hand, the state of conservation of Room walls built in tuff (A-Wall). The investigations were conducted primarily on both walls in areas free of decorations, so with a smooth substrate, and covered a portion of the garden where a regular grid was acquired.

4.1.2.1   Data Acquisition

On the two walls three horizontal profiles have been performed (A-Wall: profiles 4, 5 and 6; B-Wall: profiles 7, 8 and 9), long about 1.8 m and positioned in the spaces present at the base of the pins, and three vertical profiles (A-Wall: profiles 1, 2 and 3; B-Wall: profiles 10, 11 and 12), approximately 0.4 m long with the origin at the center of the previous and perpendicular to them. For this type of analysis was used an 800 MHz antenna, especially suited because small and manageable. The location of the surveys and the results of this application are shown in Figs. 4.13 and 4.14.
   The second investigation group has concerned the paved garden portion that is located immediately above the B-Wall. The purpose of this application was to intercept the pins inside the wall and to determine their total length. The profiles perpendicular to the wall (profiles 17–18–19–20) have extensions ranging from 6 to 7 m and have been programmed with the origin in the area above the pins (Fig. 4.15). All radar reflections were recorded with an antenna of 500 MHz as 16 bit data and 512 samples per radar scan. Radar reflections on each line were recorded at 40 scan s^{-1} (1 scan approximately 0.04 m).

4.1.2.2   Data Processing and Results

Standard bi-dimensional radargrams relative to single transects were processed through the Reflexw software. Band pass filters and the Gain Control were applied in order to remove high and low frequency anomalies that occurred during the data acquisition, normalize the amplification and remove reflections generated by noise due to the different signal attenuation.
   Radargrams reports in the x-axis the distance covered by the antenna on the surface and in the z-axis the time scale (expressed in ns): the two way time was not converted in depth scale (in m) as the speed propagation of materials involved by all the surveys was unknown. An analysis of the time slice reveals some interesting anomalies:

– A-Wall (Fig. 4.13): all profiles (with the exception of the profile 5) show a surface of discontinuity, in the range between −27 and −30 ns on the time axis, which may indicate the transition between two different materials. In profile 5, this surface follows an anomalous trend since it is localized in the range between −20 and −23 ns, below the segment which goes from the origin up to 0.5 m on the x-axis and only after falls in the range between −27 and −30 ns. The
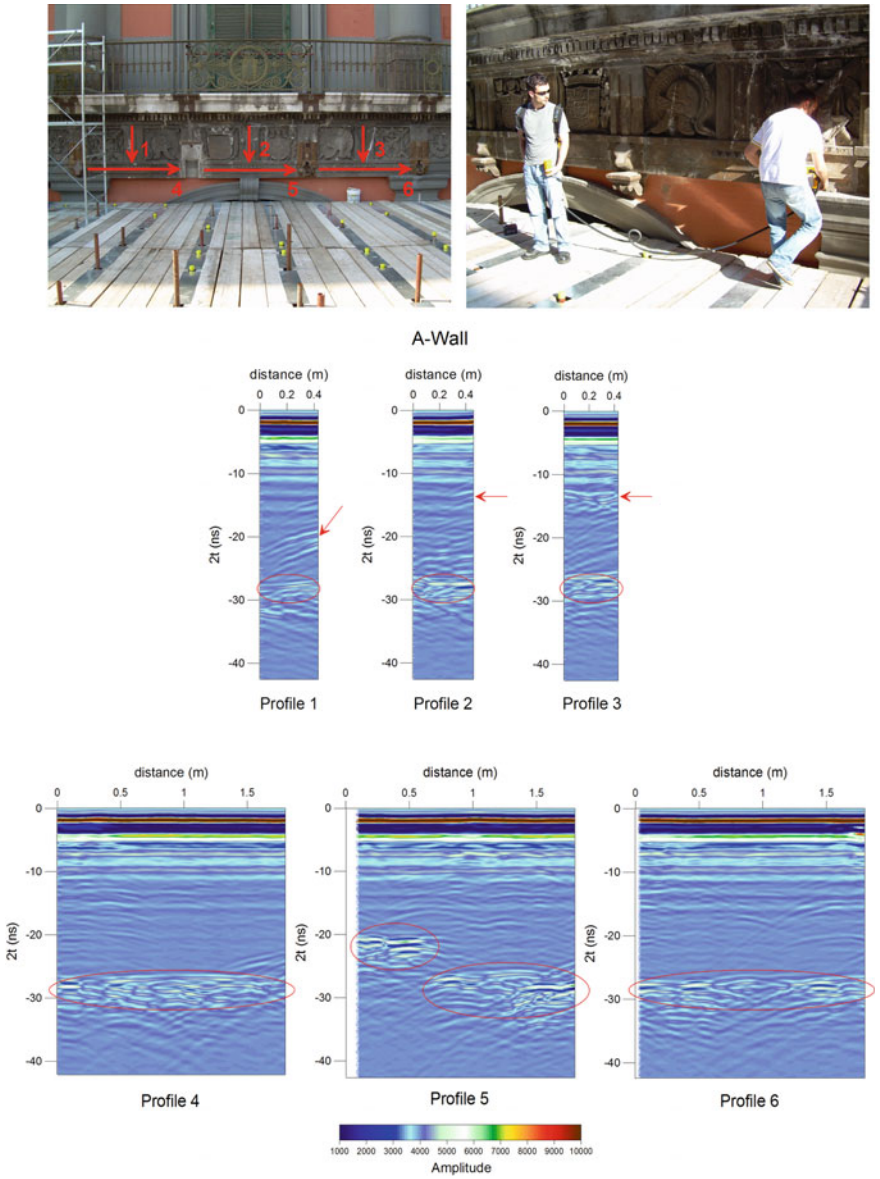
Fig. 4.13   A-Wall: location of profiles and sections using a 800 MHz antenna

semi-hyperbolic anomaly at −20 ns at the end of the profile 1 and the two similar discontinuities at about −13 ns in the right end of the profiles 2 and 3 are also worthy of note.
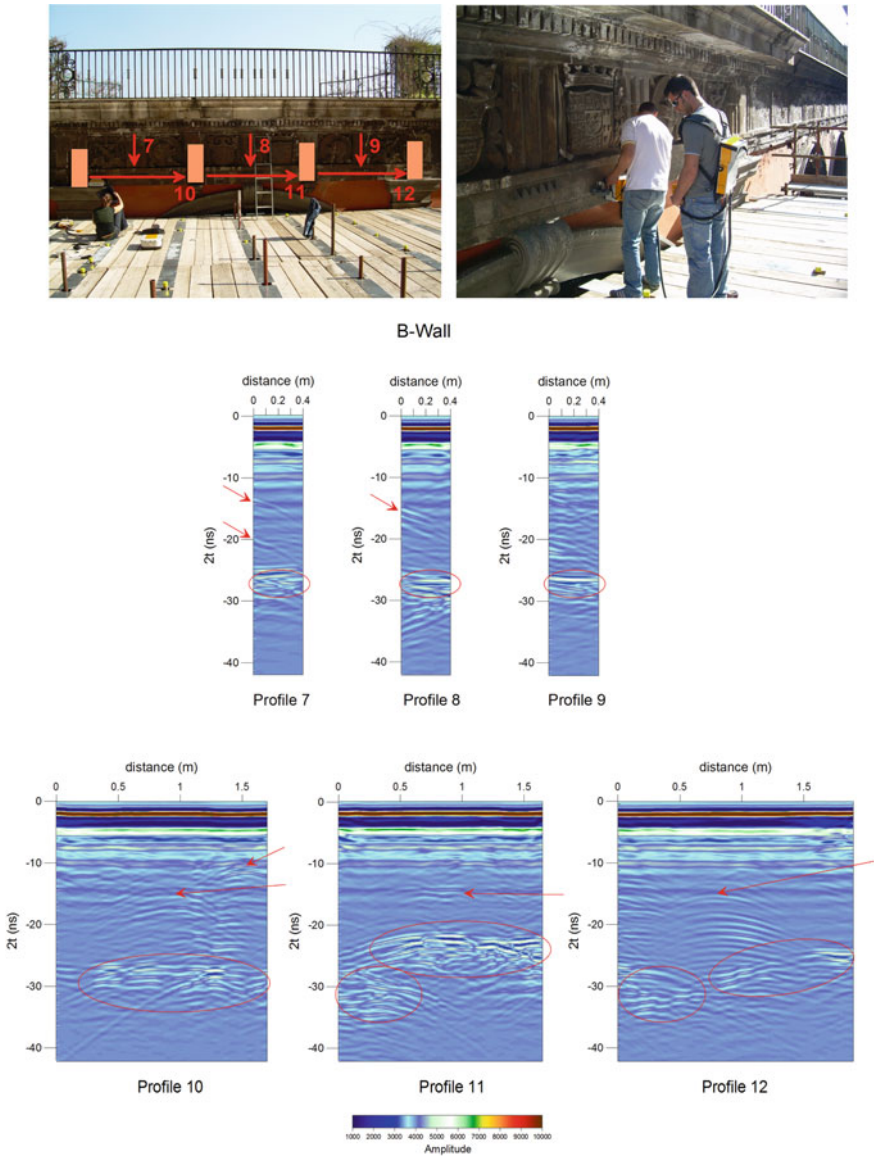
Fig. 4.14 B-Wall: location of profiles and sections using a 800 MHz antenna

– B-Wall (Fig. 4.14): in the profiles 7, 8, 9 a homogeneous surface localized in the
   interval between −25 and −29 ns on the time axis is visible. Moreover, in both
   profiles 7 and 8 a diagonal anomaly which develops below the 0–0.2 m segment
   along the x-axis, between −13 and −15 ns, is shown. A similar gap is visible in
   the profile 7 and even among −20 and −23 ns under the same portion of the
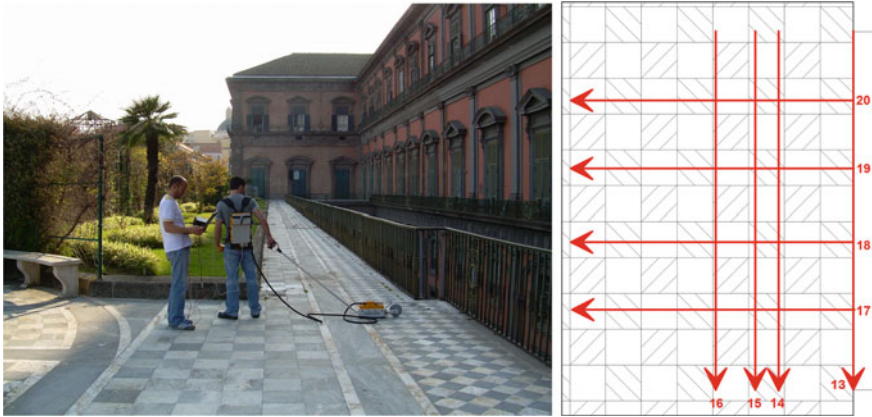
Fig. 4.15 Acquisition in the garden using a 500 MHz antenna

surface. The profile 10 shows an anomalous zone, between −27 and −30 ns, which expands almost throughout the section and inside it is very interesting the point with greater amplitude (below x = 1.3 m) from which a kind of hyperbola develops. In the profile 10 the well defined hyperbole, the apex of which is at 1.5 m along the x-axis and about −12 ns on the time axis, and the less clear hyperbolic shape that starts from the position x = 1 m to about 15 ns are also notable. The latter is also visible in sections 11 and 12. In the profile 11 an extended irregular surface is highlighted at about −23 ns on the time scale and below the segment between 0.3 and 1.7 m on the x-axis. Further down, at about −30 ns, another anomaly that affects the initial portion of the section (between x = 0 m and x = 0.5 m) is shown. In the end, a discontinuity appears in profile 12, consisting of two main bodies, which develops in diagonal direction and descends from the right (at about −25 ns) to the left (approx. −32 ns) in the section.

– Terrace (Fig. 4.16): Profile 13, parallel to the wall and realized at its margin, shows a fairly disturbed section in which there are two significant horizontal discontinuity at about −10 ns on the time scale and whose centers are located below the x = 2 m and x = 6 m, respectively. In profile 14 (realized at 1 m from the edge of the terrace) the four iron pins were intercepted at about −22 ns evidenced by four hyperboles shown in Fig. 4.16 with the numbers 1, 2, 3 and 5. A further hyperbola of reflection (indicated with number 4 in Fig. 4.16) also appears. At the base of the section, about −40 ns, a horizontal discontinuity surface is visible that interesting the entire x-axis, albeit with varying intensity. In profile 15, made at a distance of about 0.25 m from the profile 14, there are not reflections that evidence the presence of the pins: therefore with certainty they have a length of about 1 m and however not greater than 1.25 m. However, Profile 15 denoted an abnormal horizontal zone that involves the whole section at about −10 ns. The profile 16 shows a situation of general uniformity. Profiles

17, 18 and 19 probably have cut the cast iron pins, within the first meter of the
sections, at about −22 ns: this is manifested by a semi-hyperbolic discontinuity.
In the same area in the profile 20, there were no anomalies. All profiles per-
pendicular to the wall (profiles 17, 18, 19 and 20) show a discontinuity, between
x = 2 m e x = 3.5 m, which develops in diagonal direction and descends from
the right (at about − 8 ns) to the left (at about −10 ns) in sections.
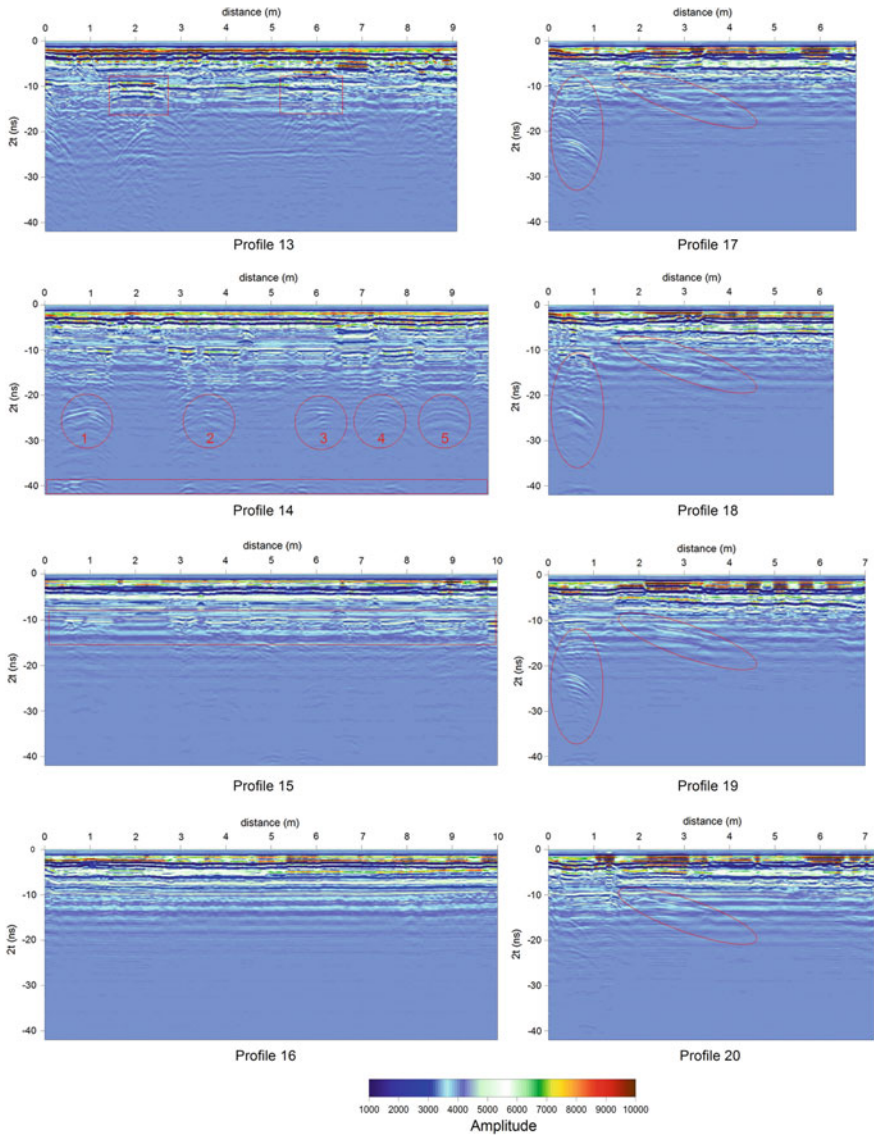
Fig. 4.16 Sections in the garden with 500 MHz antenna

Figures 4.17 and 4.18 show the sections that better make visible geophysical anomalies integrated to photo images.

4.2   Historical Buildings

4.2.1   ERT surveys at the Castle of Zena (Carpeneto Piacentino, Piacenza, Italy)

The castle of Zena (Fig. 4.19) is located in the territory of Carpaneto Piacentino, in the lowland between Fiorenzuola and Piacenza (Emilia Romagna, Italy). It is an abridgment of six historical buildings covering a general surface of around 4000 m^2.

The foundation date of the Castle of Zena are still unknown, though the first document attesting its presence dates back to 1216. The whole complex, despite the several repairs which it has been subject to in past ages, still preserves the ancient character of a fortress of square plan, as documented in the drawing of Fig. 4.20, dating back to 1701 and based on a land map of 1591. The southern wing of the
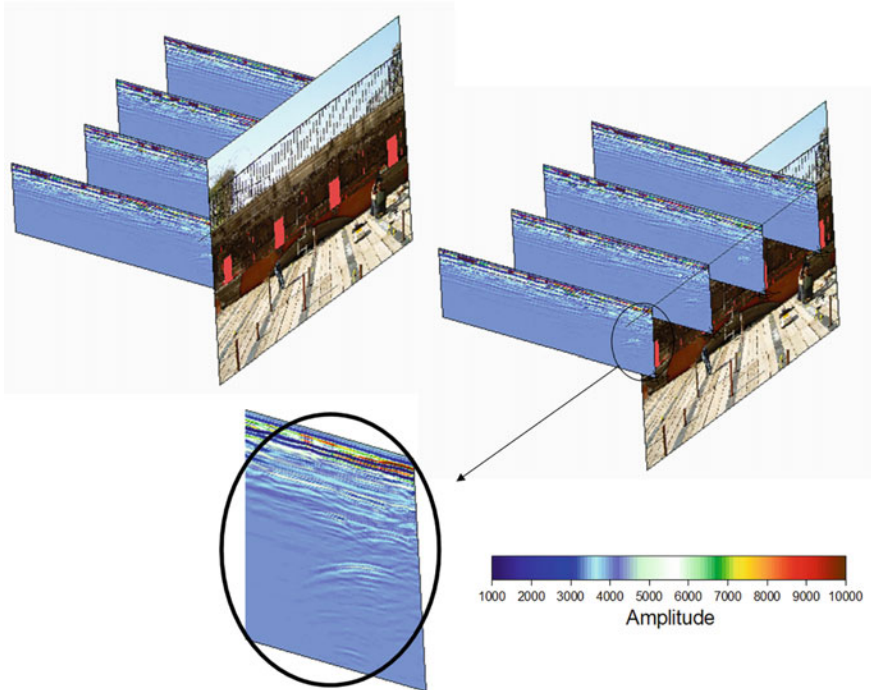
Fig. 4.17 3D visualization of the perpendicular profiles that intercepted the cast iron pins
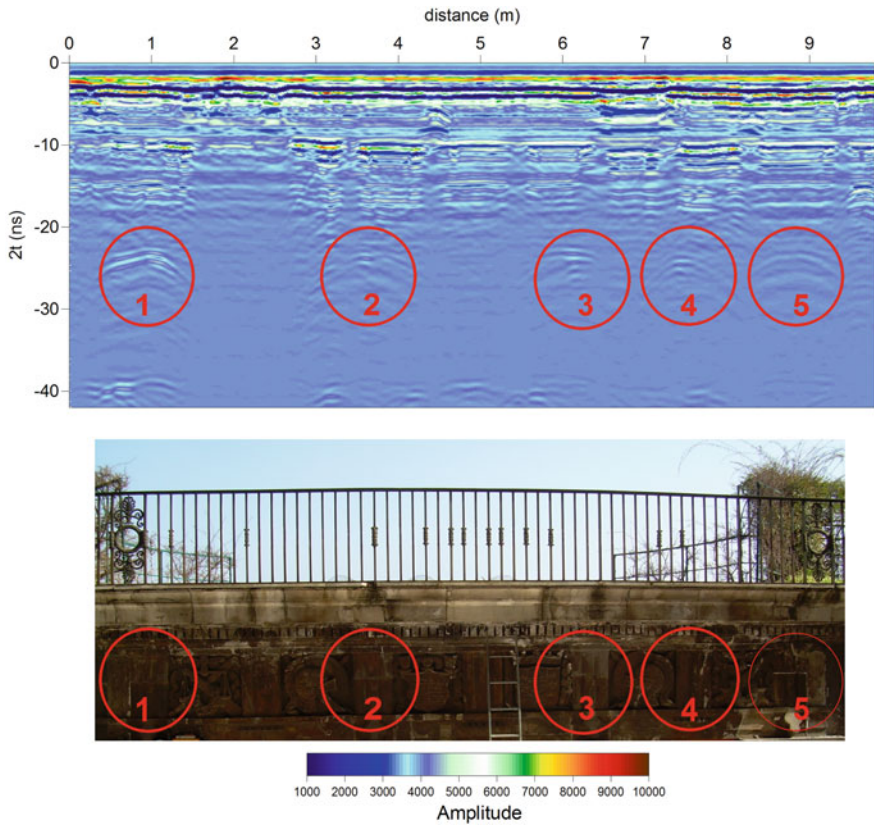
Fig. 4.18 Comparison of the photographic image of the B-Wall and the Profile 14 that intercepted the cast iron pins

building is attested to have been demolished in the 18th century, thus leaving the courtyard of the castle partially exposed. On the western front, where the entry is situated, the traces of a drawbridge, replaced afterwards by a bridge in masonry, and the ditch that surrounds the castle are visible.

The work was developed within the project S.O.C.R.A.T.E.S. whose priority is the study of the castle and the surrounding areas together with the construction of models and methodologies of general interest directed to the recovery and the exploitation of the buildings of historical and architectural interest. The activity related to the geophysical prospections was assembled in three different areas that, according to the project of restoration and renewal of the castle, will have to change the original destination of use. The investigation was conducted using the geoelectrical method and the data were elaborated according to a program of three-dimensional elaboration (Compare et al. 2009). The nature of the geophysical anomalies, probably connected to remains of archaeological interest, was then verified through mechanical surveys and subsequently through a direct activity of archaeological excavation.

Fig. 4.19 The Castle of Zena, Carpaneto Piacentino (Emilia Romagna, Italy)

4.2.1.1 Survey Planning

The ERT survey was carried out by a direct current multielectrode resistivity meter (A300E, www.mae-srl.it). The DD electrode device was adopted using 1 m long dipoles displaced at a step of 1 m along each profile with k in (1) reaching the maximum value of 10. The following three different zones (Fig. 4.21) were investigated.

– Zone A: it is an area of 1674 m^2, located close to the northern side of the fortress, where a car park underground had been planned. 37 parallel profiles, 31 m long and spaced 1.5 m apart, were realised. Each profile consisted of 235 measurements, thus totalling 8695 data points. In this zone, a *giacciara* is indicated with a circle in the old drawing of the fortress, close to its northern wing. The probable presence of the round structure, likely a brickwork room used in the past for the maintenance of food, is also suggested by the cropmarks easily visible on the ground (Fig. 4.22), nearly where it is indicated in the map of Fig. 4.20
– Zone B: it covers an area of 620 m^2, located south of the castle, where the construction of a swimming pool had been planned. 21 parallel profiles, 31 m long and spaced 1 m apart, were investigated. Each profile consisted of 185 measurements, thus totalling 3885 data points.
– Zone C: it covers an area of about 600 m^2, located inside the southwestern portion of the ditch that surrounds the fortress, where part of the destroyed
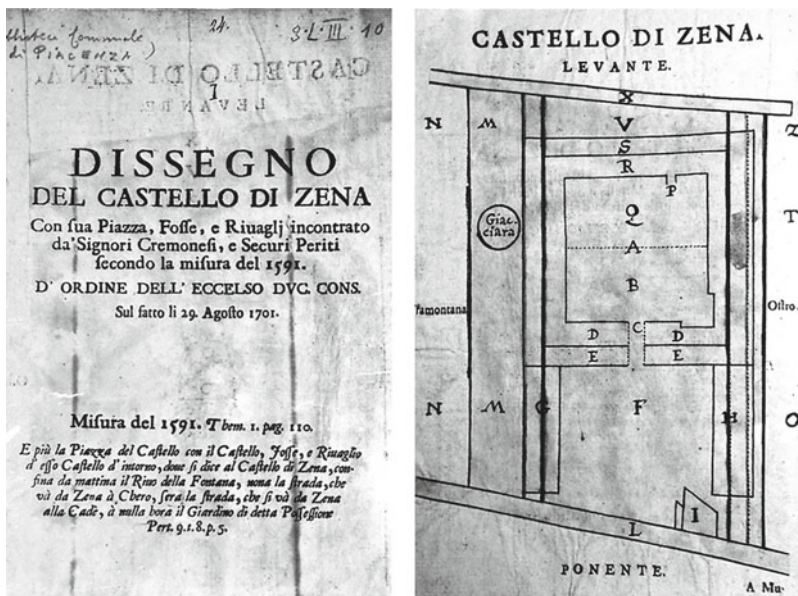
Fig. 4.20 An archive document from Piacenza dating back to 1701, showing a drawing of the Castle of Zena based on land measurements of 1591

southern wing of the castle was founded. Due to logistic difficulties, 18 profiles spaced 1 m apart, but with different lengths ranging between 15 and 31 m, were measured. The total number of data points was 3560.

Table 4.1 reports the minimum, maximum, and mean ρ_a values in Ω m obtained in each of the surveyed zones. The mean value in each zone was calculated taking the average of the logarithms of the corresponding ρ_a values.

For the sake of brevity, we show in Fig. 4.23 only three apparent resistivity pseudosections, one for each zone, in order to give an idea of the nature of the input data.

4.2.1.2 Data Processing and Results

Figure 4.24 shows the results of the 3D probability-based ERT imaging applied to the {ρa} datasets collected in the three zones marked in Fig. 4.21. In each zone, the number of the model cells used for the 3D ERT imaging is exactly the same as that of the data points. The 3D ERT image consists of a sequence of horizontal slices at increasing depth from 1 m down to 5 m beneath the ground level (b.g.l.). A rather complex pattern of resistivity anomaly sources can readily be observed. The group of sources, deserving to be analysed from the archaeo-architectural point of view, can reasonably be associated with the highs occurring within the first 3 m of depth. These highs, that is, source nuclei characterised by a positive occurrence

Fig. 4.21 A sketched map of the Castle of Zena (C-shaped central light blue area) and the three ERT A, B, and C survey zones (grey areas). The red lines A20, B9, and C10 are the profiles selected to show examples of the nature of the input data in the form of 2D pseudosections

Fig. 4.22 A-zone: cropmarks in correspondence with the *giacciara* indicated in the map of Fig. 4.20

Table 4.1 The minimum maximum, and mean apparent resistivity values in Ω m obtained in the surveyed zones A, B, and C

Zone	$\rho_{a,\,min}$	$\rho_{a,\,max}$	$\rho_{a,\,medium}$
A	0.67	52367.28	29.92
B	2.94	218.31	24.76
C	3.27	2055.32	87.05

probability, would indicate the presence of structures with true resistivity higher than the reference uniform resistivity in each zone. The large positive and negative nuclei, centred at a depth not less than 4 m b.g.l. in the B-zone and the C-zone, respectively, and within which the maximum absolute occurrence probabilities have been obtained, may reasonably indicate, instead, the presence of a vertical discontinuity. This discontinuity is assumed to separate two geological media with resistivity on a side higher and on the other side lower than the reference resistivity. The reference resistivity was taken equal to the average apparent resistivity of 29.92 Ω m in the A-zone, 22.80 Ω m in the Bzone, and 87.04 Ω m in the C-zone.

More compact 3D views of the highs of probable archaeoarchitectural interest under the surveyed zones are reported separately in Fig. 4.25. In all of these and following 3D views the resistivity anomaly occurrence probability scale has been modified, by compressing the light-to-dark colour sequence entirely within the positive half-scale and leaving colour less the negative half-scale.

Moreover, to help focus the discussion, we consider as a reference map the horizontal slice at 1 m of depth, extracted from Fig. 4.24 and depicted in Fig. 4.23. All of the relative maxima of the highs of probable archaeoarchitectural interest are located in this slice, where the sites of 10 holes, bored after the ERT prospecting for groundtruthing, are also indicated. The results of this activity are reported separately for each zone.

A-Zone. Worthy of note appears the isolated rounded sequence of nuclei visible in Fig. 4.26 at the centre of the A-zone, close to its right-hand borderline. The location of this source exactly corresponds with the cropmarks visible in Fig. 4.22. The subsequent archaeological excavation allowed a circular structure with radius and height of 3.3 m to be discovered (Fig. 4.27), immediately under the humus (Bondi et al. 2006).

It was found made of pebbles and bricks tied up with a mortar rich in sand in the top portion, made of disjointed bricks and slightly flared at the bottom, and externally surrounded by eight small buttresses, set at a regular distance of about 2.6 m. This regular and well-preserved masonry structure was readily ascribed to the circular plot indicated as *giacciara* in the ancient drawing reported in Fig. 4.20 (Bondi et al. 2006).

For a better appreciation of the resolving power of the exposed probability tomography method, Fig. 4.28 shows a zoom of the 3D image in Fig. 4.25a, under two different angles of view, limited only to the central round sequence of nuclei. A sketch of the *giacciara* is also plotted at the correct place as from the digging. In
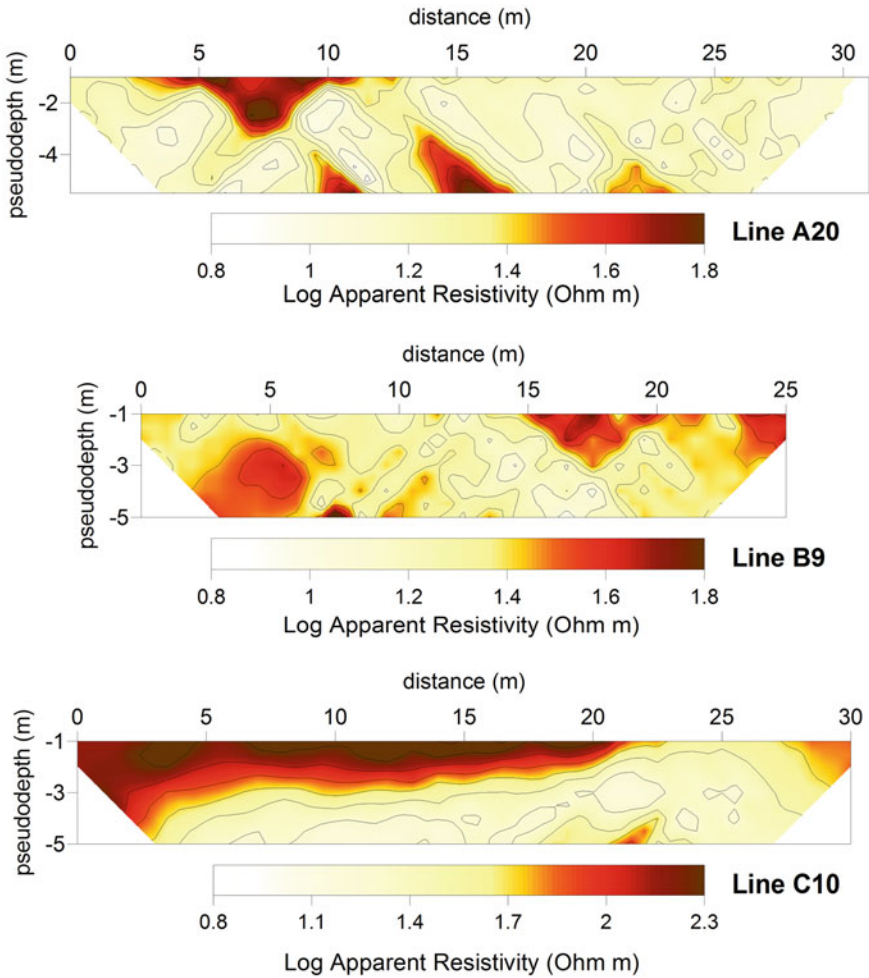
Fig. 4.23 The apparent resistivity pseudosection across the line A20 in the A-zone, the line B9 in the B-zone and the line C10 in the C-zone (their position is signed as red lines in Fig. 4.21)

both images, the round sequence of nuclei appears to correspond exactly with the trace of the *giacciara* on the horizontal plane through its centre. Furthermore, in the lateral view in Fig. 4.28a, the full bowl-shaped set of source nuclei appears to smoothly conform to the very regular nest-shaped structure of the *giacciara*.

In the A-zone 4 holes (S1–S4) located as in Fig. 4.26 were also bored. The results from the S2 hole, bored down to 5 m of depth in correspondence with the top right alignment of small positive nuclei, showed the only significant anomalies.

In S2, a layer with significant signs of human activity was in fact detected at about 1.65 m of depth. A slimysandy-clayey layer, rich of bricks and carbonaceous frustules, was found (Boschi 2006). This fertile layer has, however, not yet been
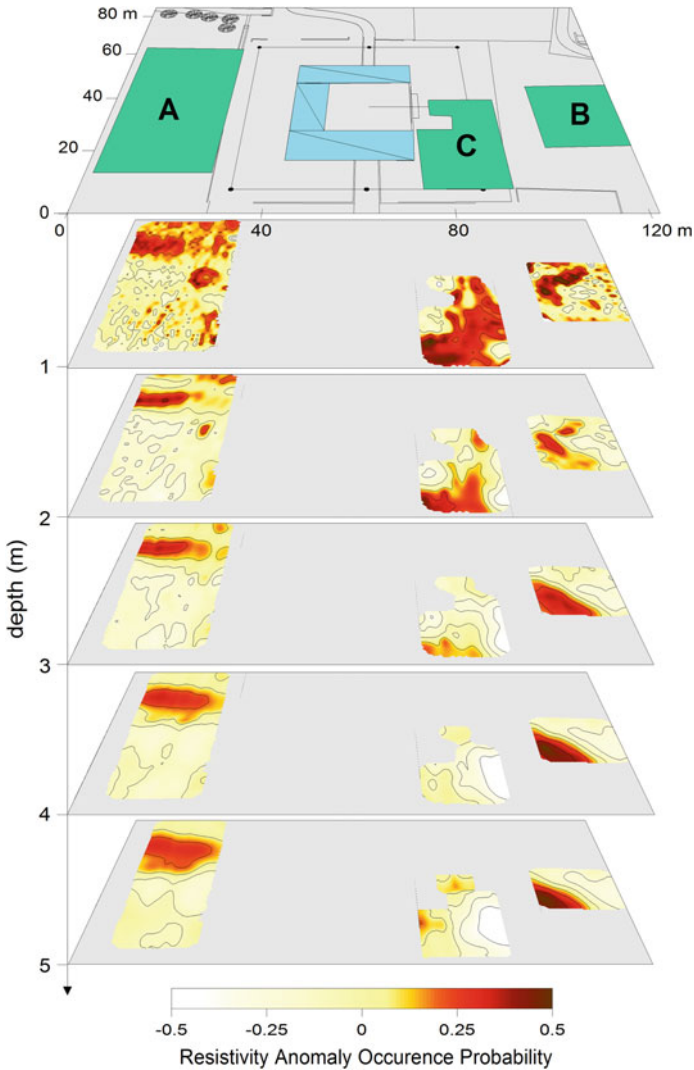
Fig. 4.24 The 3D probability tomography in the three surveyed A, B, and C zones of Fig. 4.21, represented with sequences of horizontal slices at increasing depth below the ground surface. The top slice is the reference land map with the three survey zones and the sketched plan of the castle

confirmed by direct archaeological excavations. It may reasonably extend over the whole top third of the A-zone, likely as patches separated by sterile zones. A support to this interpretation derives from the discontinuous nature of the dark nuclei and the circumstance that the hole S1, located a little outside the large horizontal sequence of nuclei in the top left-hand side of the area, did not meet any remnants.
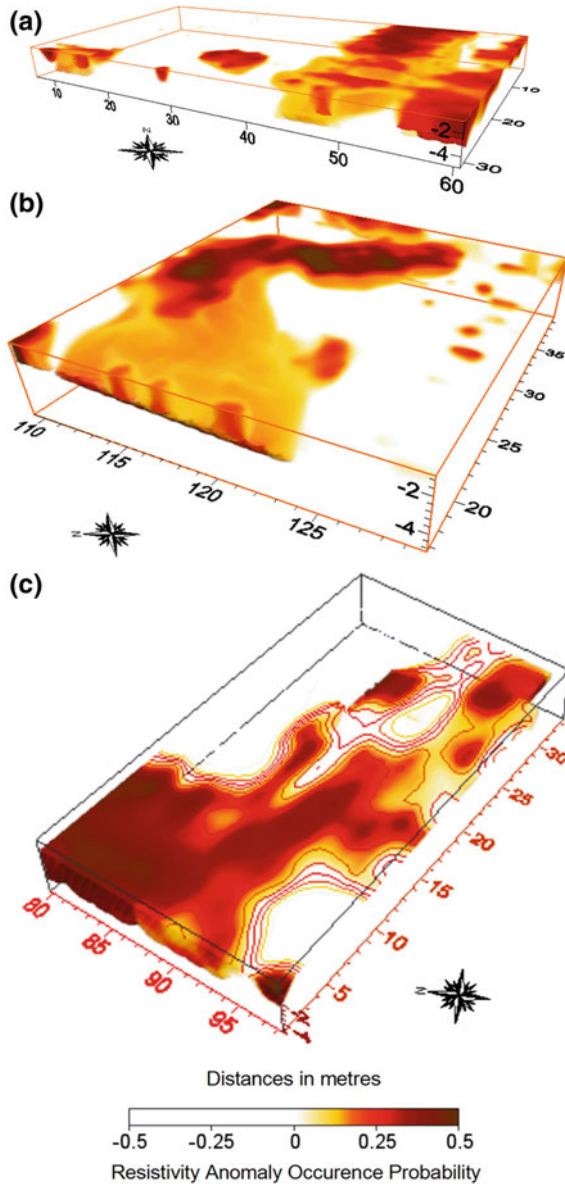
Fig. 4.25 3D views of the probability-based ERT representation in the A-zone (**a**), B-zone (**b**), and C-zone (**c**)

No interesting archaeological data came also out of the S3 and the S4 holes, thus confirming the absence of resistivity anomaly source nuclei in those areas.

B-Zone. An inclined L-shaped sequence of positive nuclei was the only interesting feature appeared in the Bzone, as shown in Fig. 4.26. Three holes (S5-S6-S7) were bored. The S5 hole, located on the longer side of the L-shaped source sequence, revealed, from 0.65 m down to 1.7 m b.g.l., the presence of residues testifying an activity of combustion and/or heating (Boschi 2006). The first 0.45 m resulted, in fact, to belong to a brick structure, the following 0.15 m to be made of ash and coal and the last 0.45 m of burnt clay. The subsequent digging brought to the light a roofless furnace dating back to the 15th–16th century (Fig. 4.29).

The complex presents two anterooms (*prefurni*) and a room of combustion that probably contained part of the last batch of bricks employed for the construction of the castle (Bondi et al. 2006).

The hole S6 was bored down to 5 m of depth, in correspondence with the small positive nucleus located at the centre of the lower half of the zone. The most significant archaeological layer was found between 0.7 and 1.47 m of depth with abundant brick fragments. In particular, the first strata are worthy of note because remnants similar to those found in the S5 hole were detected in the same depth range, allowing for a connection between them. The S7 hole, instead, was bored down to 5 m of depth in an area where the geoelectrical tomography did not put in evidence any relevant positive nucleus. The hole confirmed such a result, since only very rare fragments were there detected (Boschi 2006).
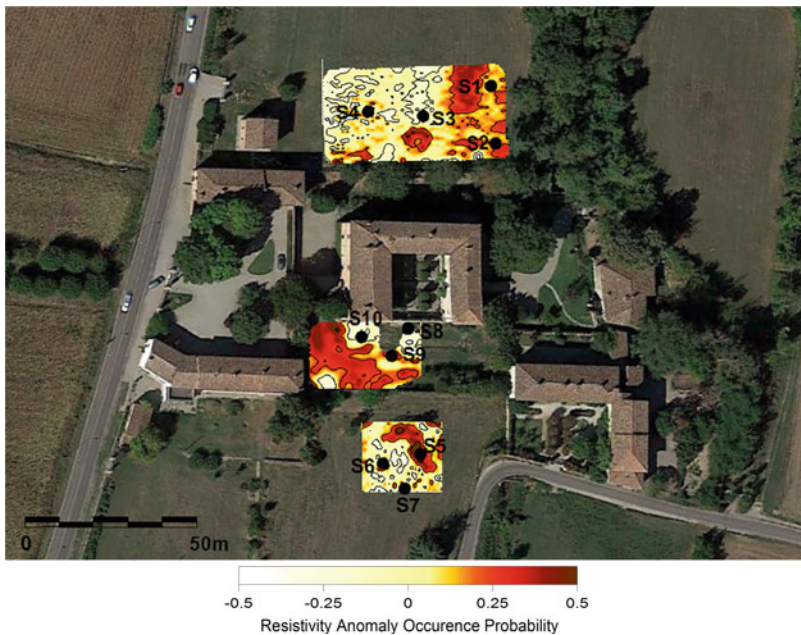
Fig. 4.26 Geoelectrical probability tomography at 1 m of depth b.g.l. and locations of the mechanical surveys S1-S10, indicated by black circlets

Fig. 4.27 A-Zone: the *giacciara* or icebox found in correspondence of the rounded sequence of nuclei in the probability tomography of Fig. 4.28

As before, a zoom of the 3D image in Fig. 4.25b, under two different angles of view, limited only to the portion of the longer side of the L-shaped sequence, where the nuclei with highest occurrence probability were found, is depicted.

A sketch of the furnace is also plotted at the correct place as inferred from the digging. In both 3D images, it can readily be observed that the selected portion of the L-shaped set of nuclei exactly corresponds with the trace of the discovered furnace on the horizontal plane through its floor. Moreover, the top view in Fig. 4.30b shows that the sequence of the small nuclei closely conforms to the disposition and shape of the discovered rooms.

C-Zone. The C-zone is almost totally dominated by a positive pattern of source occurrence probabilities, composed of a double set of parallel positive nuclei, which appear to conform at right angle to the southwestern corner of the castle. The internal sequence of nuclei may reasonably attest the presence underground of the foundations of the fourth wing, including the tower, as indicated in the drawing of Fig. 4.20, both destroyed in the 18th century. The outer sequence of positive nuclei may, instead, be associated to traces of structural elements connected to the castle, likely the base of the former embankment of the ancient ditch.

In the C-zone three holes were bored. The hole S8 was bored down to the depth of 4 m outside the area surveyed by the ERT. At 1.75 m of depth, a compacted gravel layer was found with traces of mortar, probably constituting the allurement layer of the fourth wing (Boschi 2006). The hole S9 was bored down to the depth of about 2.5 m in the area of the old ditch now turned into orchard. Bricks were found
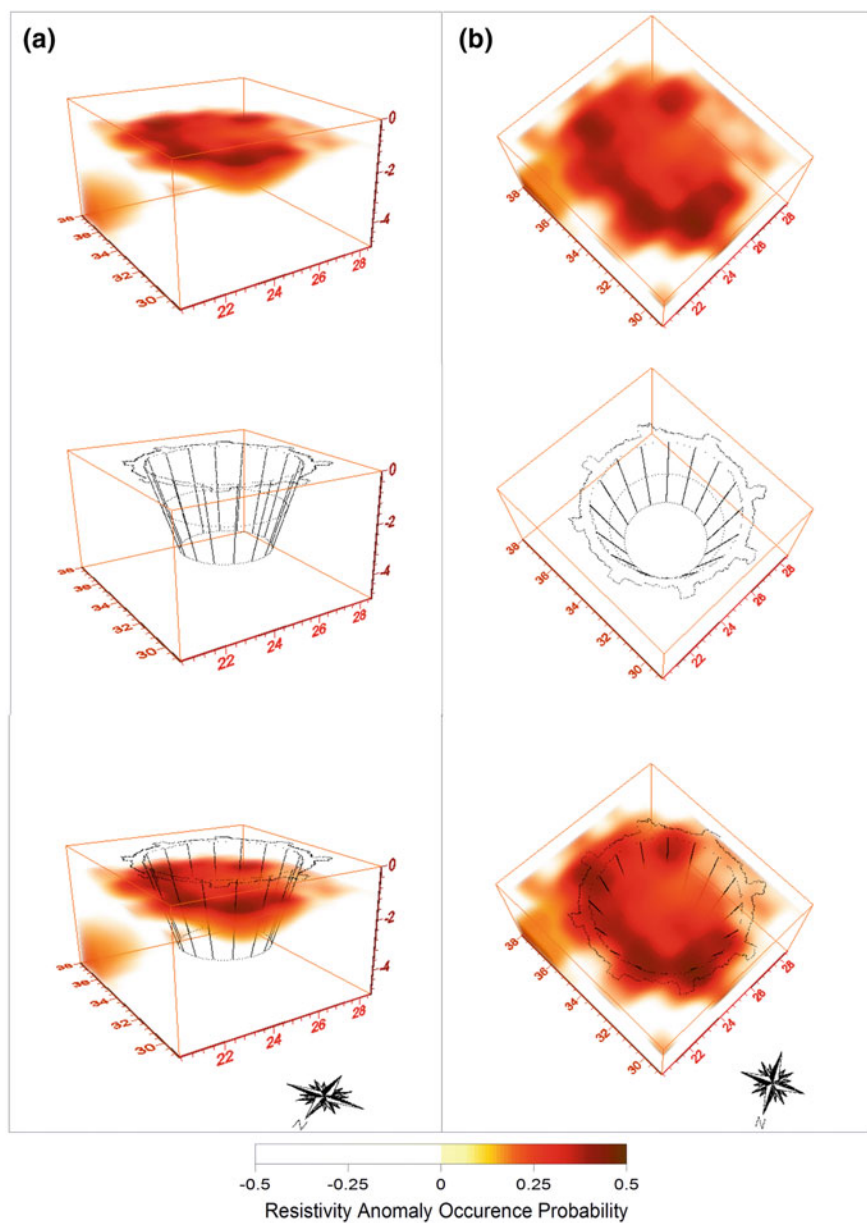
Fig. 4.28 A-Zone: a sketch of the *giacciara* compared with the particular of the round sequence of nuclei extracted from the 3D image of Fig. 4.25a, from a lateral (**a**) and a top (**b**) view

Fig. 4.29 B-zone: the furnace found in correspondence with the longer side of the L-shaped sequence of nuclei in the geoelectrical tomography of Fig. 4.26

from 0.97 m down to 1.10 m. Finally, the hole S10 of 4.5 m of depth did not reveal any elements referable to the destroyed wing, but only levels related to the depositional activity in the ditch (Boschi 2006), thus confirming the absence of positive anomaly source nuclei in the ERT of that sector of the C-zone.

The subsequent archaeological excavations (Fig. 4.31) brought to light the existence of the foundations of the collapsed southern wing of the castle and the tower at the southwestern corner (Bondi et al. 2006). Also in this case, in order to evaluate the resolving power of the 3D tomography reconstruction, the 3D
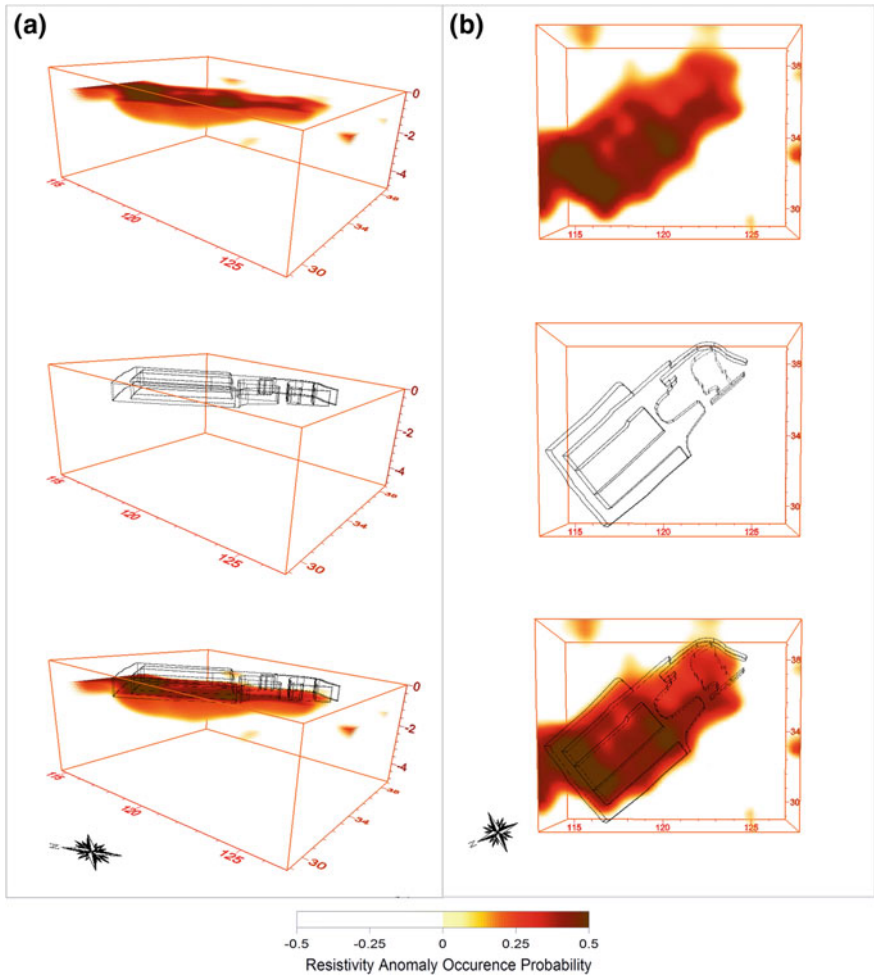
Fig. 4.30 B-Zone: a sketch of the furnace compared with the last portion of the longer side of the L-shaped sequence of nuclei extracted from the 3D image of Fig. 4.25b, from a lateral (**a**) and a top (**b**) view

tomography image in Fig. 4.25c is replicated in Fig. 4.32 for a comparison with the plotted sketch of the foundations as discovered by the digging.

Fig. 4.31 C-zone: a nearly east-westward view of the foundations of the fourth wing of the Castle of Zena found in correspondence of the inner sequence of nuclei at right angle in the geoelectrical tomography of Fig. 4.26

4.2.2 ERT surveys at the Castle of Shawbak (Jordan)

The archaeological-monumental complex of Shawbak (Valley of Petra, Southern Trans-Jordan) represents one of the best-preserved medieval settlements in the

Distances in metres

Resistivity Anomaly Occurence Probability
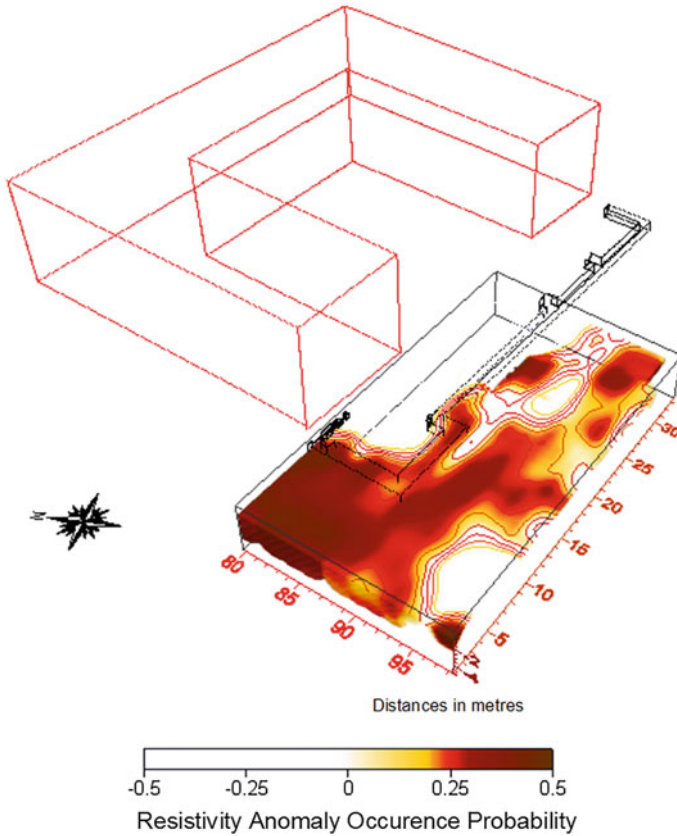
Fig. 4.32 C-Zone: a sketch of the foundations of the destroyed fourth wing and southwestern tower of the castle compared with the inner sequence of the resistivity anomaly source nuclei, replicated from Fig. 4.5c. The present outline of the castle is drawn on top

Middle East (Fig. 4.33). It occupies a strategic position in the main road system connecting the Dead Sea and Damascus to the Red Sea, Cairo and the Arabian Peninsula.

King Baldovino I built the fortification, also known as Crak de Montréal, in 1115, not far from Petra, 25 km away, on the top of a hemispheric limestone relief in a dominant position on the territory.

The crusader castle, however, had short life: in 1189 it fell into the hands of Saladin, who installed there the Ayyubide domination. Then the Mamluks, in 1260, and finally the Ottomans in 1516, came in succession. From Crusader Palace, Shawbak became a thriving city with even a tissue processing and a sugar production center. The citadel was provided with a complex and continuous defensive system, with a nearly elliptical plan, consisting of three surrounding walls (12th

century), intertwined with towers and ramparts, dating from the Crusader foundation at the time of the Mamluks (Vannini 2007; Vannini and Nucciotti 2009).

The first wall circuit of the castle defended, from the beginning, the centers of the new Transjordan Crusaded, as well as protecting the civilian quarters inhabited by the resident population at the same time.

4.2.2.1   Survey Planning

Geophysical exploration in Jordan has been carried out within the research, conservation and valorization project of Shawbak Castle in collaboration with the University of Molise (Italy), the University of Florence (Italy), the Jordanian Antiquities Department and the Institute for Technologies Applied to Cultural Heritage (ITABC, CNR of Rome).

Data acquisition was carried out using a multichannel resistive meter (A3000E, M.A.E. S.r.l) by making profiles of variable lengths inserted within regular grids. The number of electrodes involved in the individual measurements and their inter-electrode distances were determined on the base of logistical needs and the depths that were to be achieved.

Fig. 4.33   The Castle of Shawbak (Jordan)

In total, eight survey areas were performed using an axial dipole-dipole configuration, with the exception of Areas 2 and 5, where the mobile gradient configuration was used due to the current conduction difficulty:

– Area 1: located within a reversed chamber, it was affected by nine parallel survey profiles, 22 m long and at a distance of 1 m. In each survey, 23 electrodes were implicated at an inter-electrode distance of 1 m.
– Area 2: located near Area 1, outside the room, it has a triangular geometry in which the nine profiles, long 9 m, have the common origin. The distance between the electrodes was fixed at 0.5 m.
– Area 3: it is located above the so-called Ayyubide Building. Seven profiles of variable lengths between 6 and 10 m were conducted at intervals of 0.5 m with an inter-electric range of 0.75 m.
– Area 4: seventeen profiles, with variable lengths and orientations, were placed inside the Ayyubide Building. The inter-electrode distance was set at 0.75 m.
– Area 5: nine profiles, 15 m long and with a 0.75 m reciprocal distance, were placed close to the Crusader Church. The distance between the electrodes was fixed at 0.5 m.
– Area 6: seven profiles, 13 m long and 0.75 m spaced, with an inter-electrode distance of 0.75 m., were realized.
– Area 7: seven parallel profiles were gathered, with lengths between 8.5 and 14 m and spacing of 0.75 m, with an inter-electrode distance of 0.75 m.
– Area 8: nine lines, 8 m long and spaced 0.75 m, were made with a 0.5 m distance between the electrodes.

4.2.2.2 Data Processing and Results

In a preliminary analysis of the acquired data, apparent resistivity pseudo-sections and relative inversions were mapped, following the approach of probability tomography (Mauriello and Patella 1999) for each profile. Figure 4.34 shows, for example, the processed sections of some profiles.

What is most interesting is the horizontal map of approximately 1 m in depth in which the anomalies of resistivity in space are well-depicted (Fig. 4.35). Below, for each survey area, the main elements that could be attributed to buried structures are described:

– Area 1: The map shows three high resistive circular abnormalities, connected by some regular alignments (Fig. 4.36). The archaeological excavation, which is still in progress, has for now indicated the existence, at those points, of some circular structures attributable to fireplaces;
– Area 2: the presence of two linear anomalies, with high resistivity values, arranged between them so as to form a right angle, are evidenced (Fig. 4.36);
– Area 3: Two high resistive perpendicular anomalies are also shown in this area and the excavation has been confirmed to be two walls (Fig. 4.36). The anomaly
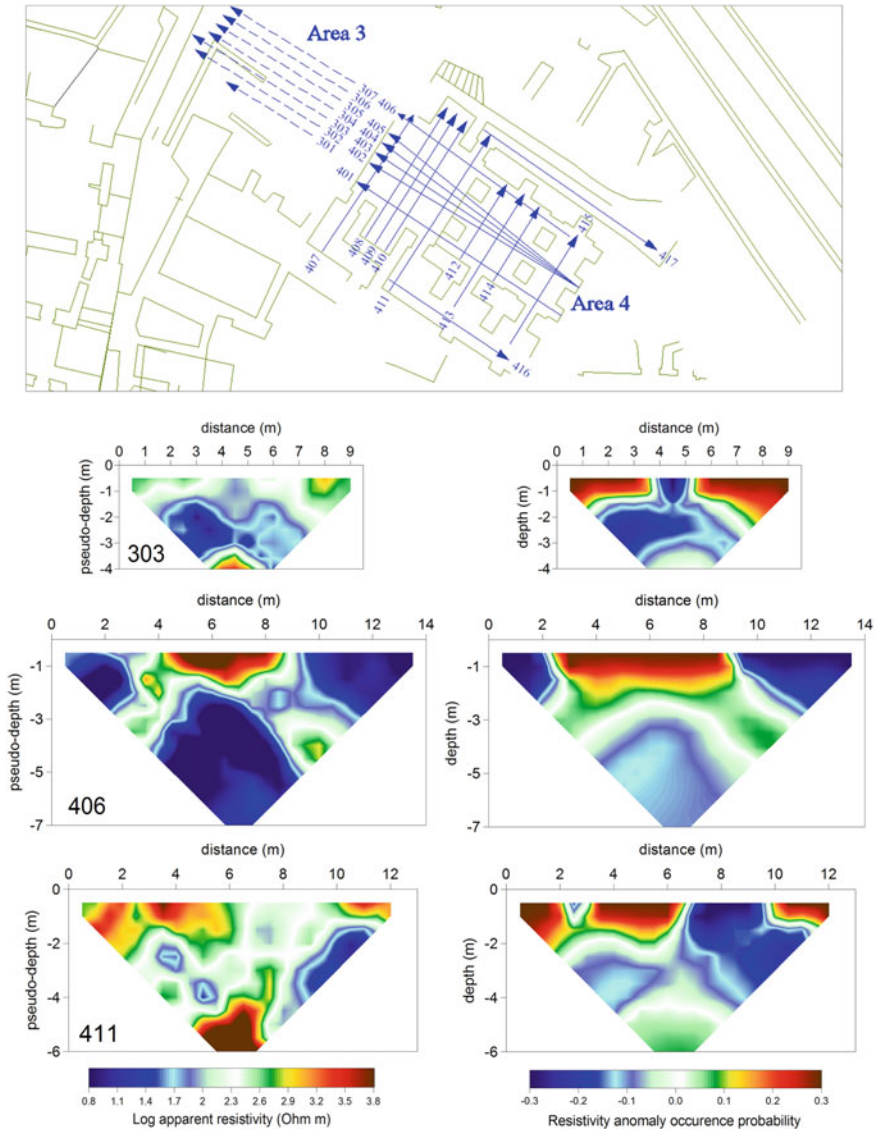
Fig. 4.34 Area 3 and 4: Pseudo-sections (left) and inversions (right) of Profiles 303, 406 and 411

marked by the circle in Fig. 4.37, instead, represents a block of stone dislocated
from its original position;

– Area 4: the tomography shows two large linear bodies perpendicular to each
  other (Fig. 4.36);
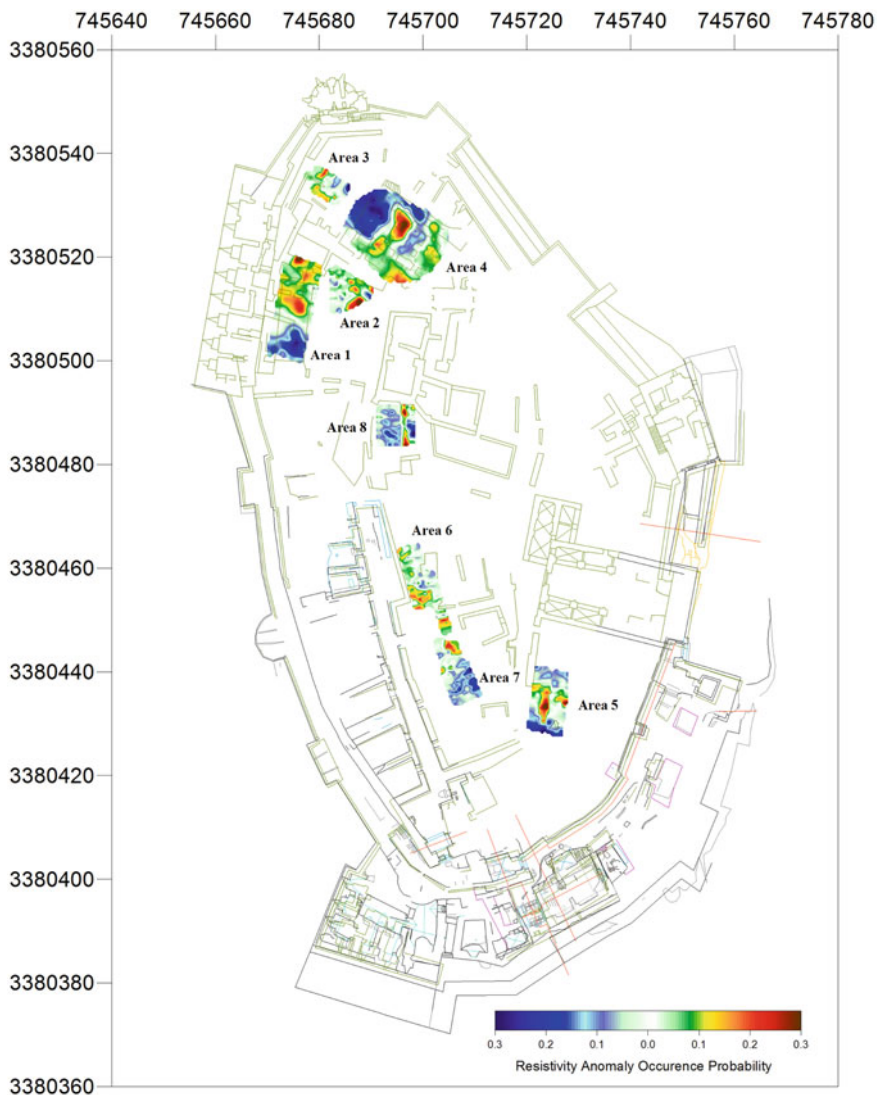
Fig. 4.35 Horizontal electrical resistivity tomography relative to 1 m in depth

- Area 5: the presence of an angled rectangular anomaly and a linear one (right in Fig. 4.37), both characterised by high resistivities, is detected. They appear to be in harmony with the walls already excavated;
- Area 6: The map enhances an abnormal nucleus, probably in connection with the corner of the existing structure (bottom and left) (Fig. 4.37). Also at the top there is a linear anomaly;

– Area 7: A straight body is visible at the top, perfectly aligned with the building on the right of the area. The rectangular anomaly located at the center of the survey area could also be connected to this structure (Fig. 4.37);
– Area 8: There is a single net anomaly, joining the visible wall below (Fig. 4.36).

The tridimensional electrical tomography allowed to work in a very dry soil and on disconnected surfaces giving a valid support in attempting analyzing the historical events that have involved the castle over the centuries. Underground traces
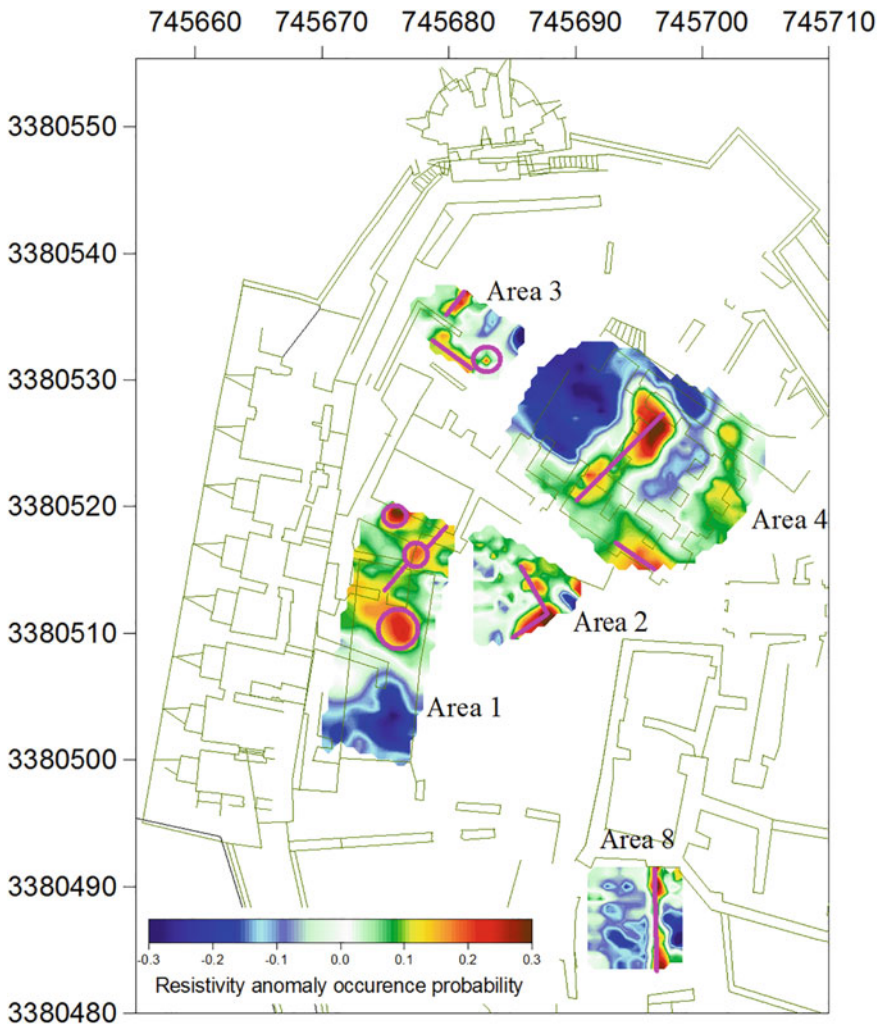
Fig. 4.36 Horizontal electrical resistivity tomography relative to 1 m in depth: data interpretation of areas 1, 2, 3, 4 and 8

of transformations, additions, demolitions, and reconstructions of various entities, have been detected.

4.2.3 GPR Investigations to Study the Area of S. Giovanni in Laterano Basilica (Rome, Italy)

With the contribution of Hynes Ian (School of History, Classics and Archaeology, Newcastle University, UK) and Liverani Paolo [Dipartimento Scienze dell'Antichità, Università di Firenze, (Firenze, Italy)] and S. Piro and D. Zamuner (ITABC-CNR).
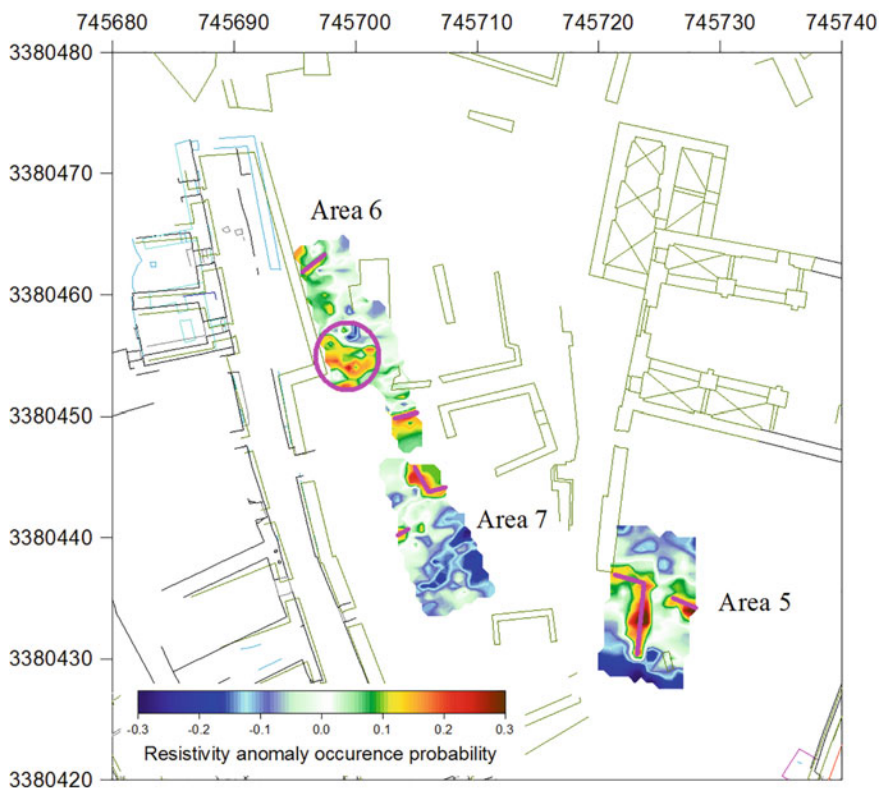
Fig. 4.37 Horizontal electrical resistivity tomography relative to 1 m in depth: data interpretation of areas 5, 6 and 7

4.2.3.1 Introduction

The Basilica of S. Giovanni in Laterano (St. John Lateran) is the Pope's Cathedral and the first public building constructed for Christian worship. Alongside it lies the first Baptistery in western Christendom. The complex has been the focus of sundry excavations since the 1730s. These have revealed traces of the earliest phases of both buildings, along with parts of the Castra Nova of the Imperial Horseguard, a bath complex and palatial housing. Interpretation of these excavations is, however, difficult; and most are either undocumented or only partially recorded.

The Lateran project is investigating the entire complex to integrate information from standing buildings, excavated structures and sub-surface features. It seeks to understand the stratigraphic, spatial and functional relationships of the different elements underlying the modern complex.

The San Giovanni In Laterano Complex is an exceptional building in its own right, the Constantinian basilica of S. Giovanni in Laterano holds the title of *caput et mater* of the churches of Catholic Christendom. The basilica is the Pope's own church, a pioneering structure and a site of remarkable archaeological importance. Extensive excavations beneath the complex have revealed not only the remains of the first powerfully influential basilica and baptistery, but also structures from still earlier periods. Chief among these are the barracks of the imperial horse guards, substantial palatial buildings, a bath house, and a street with houses. These areas are remarkably well preserved and a substantial number of frescoes and mosaics remain in situ.

Extensive research by Prof. Paolo Liverani (Florence University) has enriched our understanding of the complex, but a major collaborative project is required to interpret the remains unearthed by previous excavators. The earliest recorded excavations took place in 1730, the deepest lie 5.5 m below ground level.

This paper shows part of the results of the project, which is undertaking an intensive scientific survey of the entire structure to integrate information from standing buildings, excavated structures and sub-surface features through the collaboration of Newcastle University (UK), Florence University (Italy) and Institute for Technologies Applied to Cultural Heritage (ITABC-CNR, Italy).

The Lateran project aims to undertake a fully integrated 3D survey of the excavations under San Giovanni in Laterano.

A particular concern is to find an approach that will not only allow collaboration between researchers using a range of established and innovative methods, but also a method that allows an integrated approach to the three-levels of structural data that form the complex (Gaffney et al. 2008). There are the standing features on the modern city surface, as seen in Fig. 4.38. These can only be fully understood in relation to subsurface features and vice versa.

There are also the extensive and inter-cut structures that form the opened area of excavations. Finally, there are the unexcavated deposits that lay either beyond the immediate confines of the site or beneath the area opened to date.

4.2.3.2   Survey Planning and Data Processing

The aim of the GPR survey is to identify Roman and high-medieval age remains which could enhance understanding of the ancient topography and the urban evolution of the study area. The main goals of this survey are the following:

1. to determine the full plan of the Santa Croce oratory, built by Pope Ilaro (V century) and destroyed by Sixtus the Fifth; part of this building has been identified by Olof Brandt within the excavated area adjacent to the Baptistery.
2. to determine the full extent of the palatial housing found below the western part of the Basilica.
3. to determine the limits of *Castra Nova Equiutum Singularium*, the barracks of the imperial horse guards established by the emperor Septimius Severus.
4. to locate the remains of the buildings of the Lateran Patriarchy. These are known from renaissance plans but up until now it has not proven possible to locate them all on the ground.

Fig. 4.38 Archaeological map of the St. John Lateran Basilica (Rome). The green colour indicate the areas investigated with GPR; the numbers are related to the objectives of the survey. Courtesy of Prof. P. Liverani

For the measurements a GPR SIR3000 (GSSI), equipped with a 400 MHz (GSSI) bistatic antenna with constant offset and a 70 MHz (Subecho Radar) monostatic antenna were employed. Some signal processing and representation techniques have been used for data elaboration and interpretation. GPR surveys were performed, employing the SIR3000 (GSSI) to survey the selected areas outside the Basilica in the S. Giovanni in Laterano square and in front of the Basilica, Fig. 4.39.

The horizontal spacing between parallel profiles at the site was 0.50 m, employing the two antennas. Radar reflections along the transepts were recorded continuously, with different length, across the ground at 40 scan s^{-1}; horizontal stacking was set to 3 scans.

In the area outside the Basilica a total of 777 adjacent profiles across the site were collected alternatively in forward and reverse directions employing the GSSI cart system equipped with odometer. All radar reflections within the 90 ns for 400 MHz antenna and 195 ns for 70 MHz antenna (two-way-travel) time window were recorded digitally in the field as 16 bit data and 512 samples per radar scan.

A nominal microwave velocity of about 8 cm/ns was determined from fitting hyperbolas to the raw field data. This was used in estimating a penetration depth from the GPR survey.

Reflection profiles were analyzed for preliminary identification of the buried features and for calibration of the instrument. Reflection data, collected in profiles with 0.50 m spacing, were processed using standard techniques (Conyers 2004; Goodman et al. 2004, 2008, Goodman and Piro 2008, 2013; Neubauer et al. 2002; Leckebusch 2003, 2008; Leucci et al. 2011; Linford 2004; Piro et al. 2008; Piro and Campana 2012).

The basic radargram signal processing steps included: (i) post processing pulse regaining; (ii) DC drift removal; (iii) trace resampling along the profile (an averaged trace every 4 cm), (iv) band pass filtering, (v) migration and (vi) background filter. Reflection amplitude maps were constructed within various time (and corrected to depth) windows to show the size, shape, location and depth of subsurface
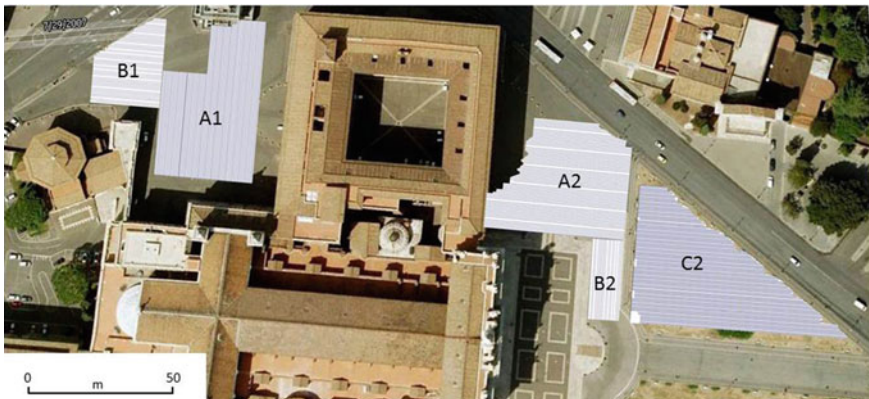
Fig. 4.39 St. John Lateran square, Rome. Location of the area investigated with GPR systems

archaeological structures (Conyers 2004; Gaffney et al. 2004; Goodman et al. 2008a b; Goodman and Piro 2013; Leckebusch 2008; Linford 2004; Neubauer et al. 2002; Piro et al. 2008). These images were created using the spatial averaged squared wave amplitudes of radar reflections in the horizontal as well as the vertical. The squared amplitudes were averaged horizontally every 0.25 m along the reflection profiles 3 ns (for 400 MHz antenna) and 6 ns (for 70 MHz antenna) time windows (with a 10% overlapping of each slice). The resampled amplitudes were gridded using the inverse distance algorithm with a search radius of 0.75 m.

All the GPR data were processed in GPR-SLICE v7.0 Ground Penetrating Radar Imaging Software (Goodman 2016).

The GPR amplitude maps, related to the profiles collected with 400 MHz antenna have been analyzed and our attention has been focused to the following time-windows: 19–22, 25–28, 30–34, 41–45, 47–50 and 58–61 ns (two-way-time), corresponding to the averaged estimated depths of 0.88, 1.10, 1.30, 1.70, 2.00 and 2.40 m respectively, without considering the first portion of the subsoil which is characterised by the presence of many surface utilities.

Few GPR time-slices, characterised by interesting anomalies, are presented and described in the following figures, firstly for the St. John Lateran square and secondly for the area in front of the Basilica.

Figure 4.40 shows the anomalies located at the estimated depth of 0.88 m (19–22 ns, two-way-time, twt), individuated in the area A1 and B1. At this depth, the area are characterised by many strong reflections due to the presence of utilities (6–7) and of portion of possible structures (1–2–3–4–5).

The size of the anomalies, indicated below, are approximate: (1) strong anomaly with linear orientation and dimension x: 13 m; y: 3.5 m, (2) anomaly with semi-circular orientation with diameter: 9 m and size 2.5 m, (3) anomaly with average dimension of x: 2 m; y: 7 m, (4) two parallel anomalies with average dimension x: 2 m; y: 7 m, (5) anomalies with different size and dimension 13 m 17 m, (6) and (7)—anomalies due to utilities with different size.

Figure 4.41 shows the anomalies located at the estimated depth of 1.75 m (41–45 ns, twt), individuated in the area A1 and B1. At this depth the anomalies are confirmed in term of location and size, but with reduced intensity. The size of the anomalies, indicated below, are approximate: (1) this anomaly is still present with dimension of x: 19.5 m; y: 3.0 m, (2) this anomaly is still present with an average dimension of 230 m^2, (5) the corresponding anomaly is present with dimension of 125 m^2, (8) two parallel anomalies, with the same dimension x: 1.7 m; y: 3 m, (9) two new anomalies with an average surface of 30 m^2.

Figure 4.42 shows the anomalies located at the estimated depth of 1.35 m (30–34 ns, two-way-time, twt), individuated in the area A2, B2 and C2. At this depth, the area are characterised by many strong reflections due to the presence of utilities (1) and of portion of structures (2–3–4–5–6–7).

The size of the anomalies, indicated below, are approximate: (1) these anomalies are due to the presence of utilities (pipes and gully-holes), (2) and (3) must be considered together, they are characterised by structures located perpendicular each other inside a total surface of 960 m^2. In correspondence of anomaly (3) a sequence

Fig. 4.40 St. John Lateran square. Area A1 and B1, GPR 400 MHz, slices at the estimated depth of 0.88 m

of squared anomalies at a distance of 1.0 m each other, are visible. (4) linear anomaly with low intensity x: 40.40 m; y: 2.0 m, (5) anomaly with a squared shape with dimension 3.7 m × 4.5 m, (6) anomaly with average dimension 2.3 m 4.20 m, (7) this zone is characterised by small anomalies.

The GPR amplitude maps, related to the profiles collected with 70 MHz antenna have been analysed and our attention has been focused to the following time-windows: 35–42,   47–53,   59–65,   71–77,   89–95   and   112–118 ns
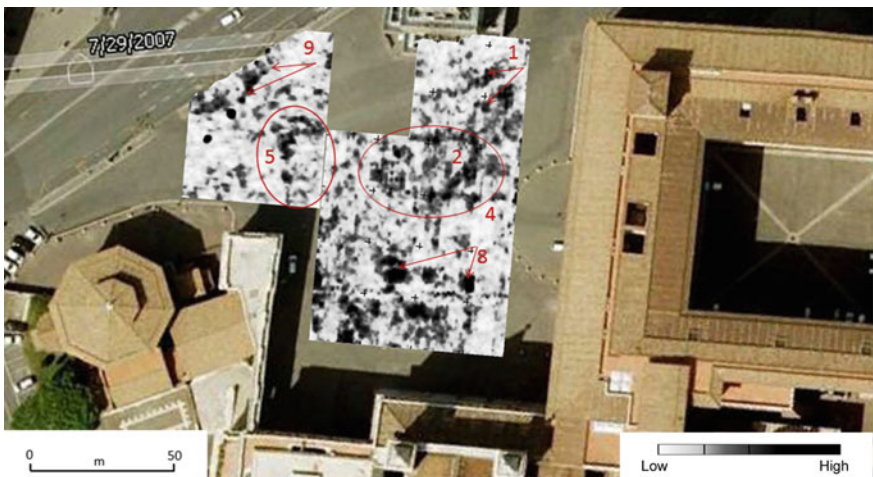
Fig. 4.41 St. John Lateran square. Area A1 and B1 GPR 400 MHz, slices at the estimated depth of 1.75 m
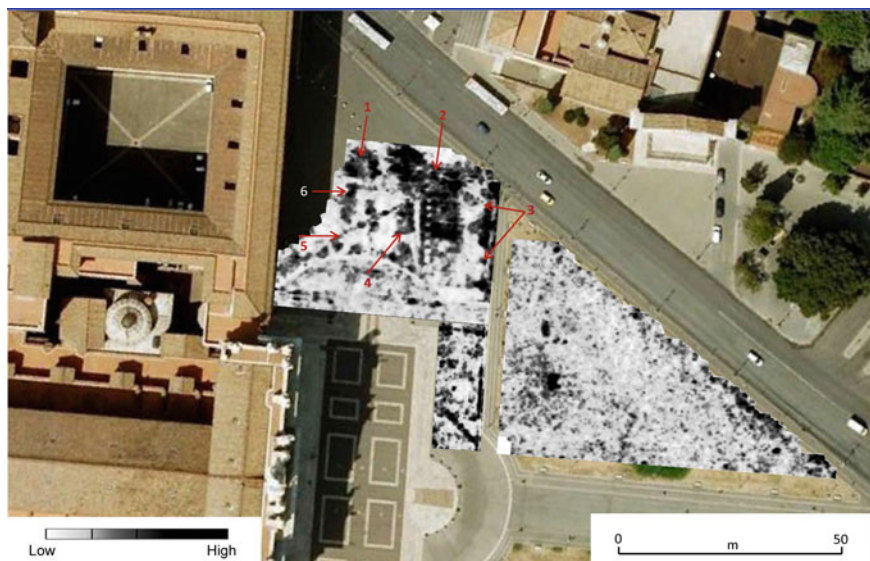
Fig. 4.42 St. John Lateran square. Area A2, B2 and C2, GPR 400 MHz, slices at the estimated depth of 1.35 m

(two-way-time), corresponding to the averaged estimated depths of 1.70, 2.10, 2.60, 3.00, 3.80 and 4.70 m respectively.

Figure 4.43 shows the anomalies located at the estimated depth of 6.00 m. At this depth, the area is characterised by anomalies contained in two sectors.

The size of the anomalies, indicated below, are approximate: (1) is characterised (portion visible) by dimension x: 1.4 m; y: 13.0 m and x: 1.4.0 m; y: 10.0 m; (2) is characterised by dimension (portion visible) x: 17.0 m; y: 3.5 m.

Ground Penetrating Radar (GPR) survey at the Lateran has produced significant and fruitful results. The use of two different antennae has enabled to reach depths of up to 6–7 m.

All the obtained results are presented in 3D animation using real time Open GL graphic displays in which isosurface rendering, 3D time slice fence diagram are mixed with the filtered radargrams.

The GPR surveys provide information on the spatial context and identification of phasing of subsurface features while the laser scanning provides a spatially accurate, detailed representation of the many materials, textures and structures of the Lateran and archaeological remains.

Acknowledgements

Fig. 4.43 St. John Lateran square. Area A1 and B1, GPR 70 MHz, slices at the estimated depth of 6.00 m

4.2.4 GPR investigations at the Cathedral of Termoli (Campobasso, Italy)

The Cathedral of *Santa Maria della Purificazione* is located in the old town of Termoli (Campobasso, Italy), protected by the castle and surrounded by walls that in antiquity had the function to defend the city from the sea attacks (Fig. 4.44).

The cathedral, which is one of the most significant Romanesque testimonies in Molise Region, was built during the period between the XII and XIII centuries on an older church of the X century attested by the presence of two apses and a floor in mosaic. On the main facade, there is an impressive portal, surmounted by an arc and preceded by a high staircase, at the sides of which there are three blind arcades for side. At the top of the facade, more recent construction than the rest of the building, a rose window is present. Over the centuries, the structure has suffered damages due to invasions and seismic events such as the 1456 earthquake that destroyed the upper part of the façade reconstructed subsequently with recovery material.

The interior of the building is the result of numerous transformations, the most radical of which were those made in the 1930s: serious injuries forced to break

down the vault, but maintaining the articulation in three aisles, which repeated the scanning of the oldest church underneath; because of this pre-existence it was necessary to overwhelm the floor; while the back area, maintaining the articulation in three apses, was moved forward with respect to the lower one. During these restorations, the crypt was found, where there was the marble sarcophagus in which the patron saints of the city were kept.

The main facade has been subjected to repeated restoration work, which can be witnessed, in particular, by the presence of blocks of different materials showing different degradation conditions.

The darker sandstone blocks, which are most altered with large pores, and those of lighter lime color, which are more compact and better preserved, since later placed, are recognizable.

4.2.4.1 Survey Planning, Data Processing and Results

Geophysical surveys were carried out in collaboration with the Superintendence for the Historical, Artistic and Ethno-Anthropological Heritage of the Molise Region with the aim to ascertain, if there were, structural damage, likely due to a masonry expansion on the portion beneath the rose window.

Fig. 4.44 Facade of the Cathedral of Termoli (Campobasso, Italy)

All radar reflections were recorded with an antenna of 1200 MHz as 16 bit data and 512 samples per radar scan. The spacing between parallel profiles at the site was 0.1 m and they were collected alternatively in opposite directions with angles of 90° in the survey grids. Standard bidimensional radargrams relative to single transects were processed through the IDSGRED software. Band pass filters and the Gain Control were applied in order to remove high and low frequency anomalies that occurred during the data acquisition, normalize the amplification and remove reflections generated by noise due to the different signal attenuation. Thus, using a sequence of parallel lines, a three-dimensional matrix of averaged square wave amplitudes of the return reflection was generated and time-slices were realized at various time windows. Data were then gridded using a moving average routine and a radius of interpolation equal to 0.2 m.

Figure 4.45 shows the slice in the time window from 5 to 10 ns (two way time). The results obtained put in evidence that the areas marked by darker shades, which tend to red, indicate greater amplitudes of reflections relative to materials characterised by pores or voids produced by erosion, such as the oldest sandstone blocks. Areas characterised by lighter shades with less amplitude of reflections, can be traced back to more integer limestone blocks, which, on the contrary, have no obvious signs of degradation. Thus it can be assumed that the masonry expansion is due to a reaction of the structure in response to the pressure exerted by the limestone blocks on sandstone, more fragile and lighter and therefore not to damage due to external causes.

4.2.5   GPR investigations at the Capua's Castle, Gambatesa (Campobasso, Italy)

Capua's Castle in Gambatesa (Campobasso, Italy) has medieval origins but since the fifteenth century it was transformed into a Renaissance residence. It is located in a strategic point for controlling the Tappino Valley and the transhumance routes, the so-called *tratturi*. The structure is still showing its two functions: on the one hand, the square shape, the basement and the two quadrangular towers at the north-east corner denounce its defensive function, on the other hand, the bugned portal, windows and balconies opened on the walls and the *loggetta* with three round arches opening on the northwest facade belong to the Renaissance stage.

In the early 16th century, the structure was enlarged with the construction on the side facing the square of a new factory, which was built on the old structure, aligning, on the left, with the angular tower of the medieval era. On the perimeter walls of the terrace, a Guelph crenellated parapet was rebuilt.

The castle develops on four levels, the most important of which is the second, the noble floor, characterised by splendid sixteenth-century frescoes of the Mannerist school commissioned by the feudalist, Vincenzo I of Capua d'Altavilla, to Donato da Copertino or Decumbertino. Of this painter that with the inscription

Fig. 4.45 Slice in the time window from 5 to 10 ns (two way time)

on an inner door "*Donatus omnia elabravit*" has signed the whole cycle of frescoes, no other works are known. Through mythological and biblical episodes, characters of ancient history, landscapes, allegories, the virtues of the family of Capua are exalted (Valente 2003, Perrella and Cavaliere 2006).

4.2.5.1 Survey Planning, Data Processing and Results

Geophysical surveys were carried out in collaboration with the Superintendence for the Historical, Artistic and Ethno-Anthropological Heritage of the Molise Region and were aimed at verifying the causes of permeable wetlands on the walls and that are endangering the precious sixteenth-century frescoes.

The georadar tests were carried out with a 1200 MHz antenna in different chambers of the castle and, in each case, a grid of vertical and horizontal measurements was made by spacing the profiles of 0.10 m. Data were processed through the IDSGRED software and band pass filters and the gain control were applied. Time-slices were realized at various time windows and data were plotted using a kriging gridding method and a radius of interpolation equal to 0.15 m. The measurement were repeated in two different periods, in autumn and in spring, in order to attest changes in the presence of water into the walls. Figures 4.46 and 4.47 show the slice in the time window from 5 to 10 ns (two way time).

In the presence of water and humidity, propagation speeds of electromagnetic waves are relatively smaller than in dry areas. From the map produced, it is possible to evaluate the distribution of wetlands (indicated by blue color) within the shallow surface of the walls. In many cases, the exact correspondence between the stains left on the surface by the water and the low amplitude abnormalities of the georadar tests are found. Between the two analyses a light difference attests a reduction of the water content in the spring season. The humidity, uniformly spread throughout the section of the castle, is probably due to water infiltration from the roof of the structure.

4.3 Urban Centres

4.3.1 ERT and GPR surveys in the historical centre of Nicosia (Cyprus)

Nicosia has been the capital of Cyprus (Fig. 4.48a) since the 10th century BC and, over the time, the city is the legacy of the island's rich cultural heritage that is reflected in its urban planning and architecture, mostly remarkable in its historic centre.

The old city, surrounded by the Venetian Walls, has a wealth of heritage of the past, among which examples of Neolithic founding, ancient Greek and Roman ruins, Byzantine churches, Medieval Gothic, Ottoman and British Colonial architectures.

In plan (Fig. 4.48b), the massive circular 16th century Venetian Wall, is characterised by its unique geometric shape, which consists of a circle with eleven heart-shaped bastions, three gates (Kyrenia gate, in the north, Famagusta gate, in
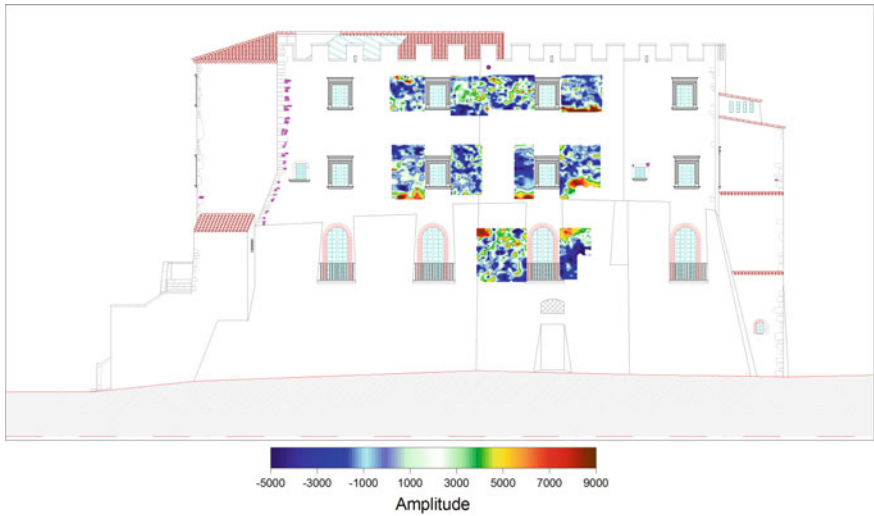
Fig. 4.46 Slice in the time window from 5 to 10 ns (two way time): data acquired in October 2011
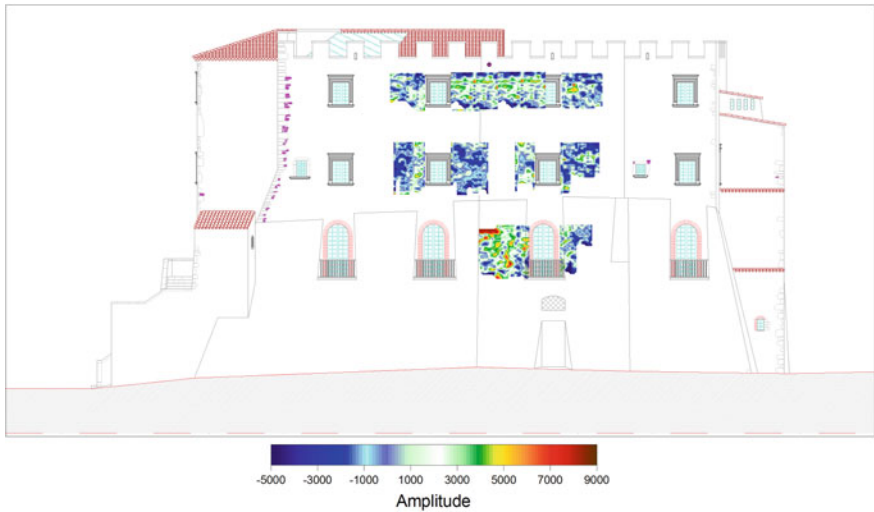
Fig. 4.47 Slice in the time window from 5 to 10 ns (two way time): data acquired in April 2012

the east, and Paphos in the west) and a ditch. It is considered as an excellent example of the bastion system of fortifications of the time.

The walled city has a diameter of about 1.6 km, which means an area of about 2 km^2.

This historical and urban centre represent both an integral part of the city's identity.

In 1974 the city was divided into two sections, the Turkish and Greek area, with a buffer zone, patrolled by United Nations peacekeeping force.

A very important aspect of the governmental policy is to preserve the historical heritage of Nicosia's buildings and the urban fabric. Conservation and valorization actions have been adopted with the aim of preserving the authenticity of the buildings and ensuring the discovery and protection of the ancient remains.

Since 2006, in the frame of the archaeological mission supported by the Ministry of Foreign Affairs and in collaboration with the Nicosia Master Plan, Italian researchers are working in the old city in order to show the application of

Fig. 4.48 a Localization of Nicosia, Cyprus; **b** City plan

(b)
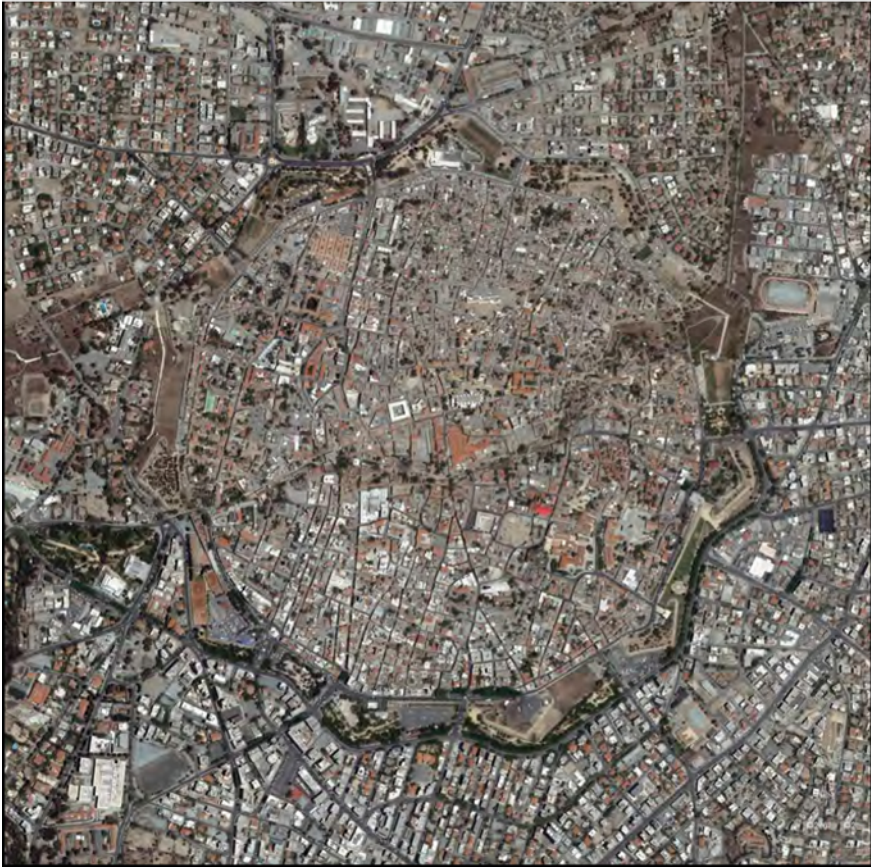
Fig. 4.48 (continued)

non-invasive geophysical surveys for the Cultural Heritage Management and Conservation of Nicosia historical centre.

4.3.1.1   Survey Planning

Some geophysical surveys were carried out on various sites using in two cases the Electrical Resistivity Tomography Method and the GPR method in the others.

The first survey was about the monumental complex of the Bedestan (Fig. 4.49a). Built in the 12th century, this Byzantine church (St. Nicholas Church) was later enlarged and altered with Gothic and Venetians annexes. During the Ottoman period, this building served as a depot and a market. Actually the shape, the size and location of the earlier church have always remained uncertain. The aim

of ERT survey was to identify the presence of the earlier basilica and recreate a stratigraphic section beneath the floor of the Bedestan complex.

The ERT survey planning was performed using a dipole–dipole array and the data acquisition was carried out using a multichannel resistive meter (A3000E, M. A.E. S.r.l). A total of 62 parallel profiles were acquired, respectively 32 longitudinal and 30 transversal, inserted within regular grids. The number of electrodes used in each profile and their inter-electrode distances were variable, due to logistical need.

The second survey was carried out on the Hospice, the historical building near the ancient Gate of Famagusta (Fig. 4.49b). The aim of this research was to assess the conservation of plaster and the presence beneath it of the previous historical building. The GPR survey was carried out using an antenna of 250 MHz frequency, 16 bit data and 512 samples per scan. The spacing between parallel profiles at the site was 0.3 m and they were collected alternatively both vertically and horizontally on the walls.

The last survey was conducted near Casteliotissa Hall (Fig. 4.49c). In this area it is possible to see ancient remains, in particular a wall, 1.9 m high and 2 m wide. The aim of this ERT prospection was to prove the existence of other parts of this structure under the surface. The three ERT profiles were carried out using a multi-channel resistivity meter (A3000E, M.A.E. S.r.l), axial dipole-dipole configuration, equally spaced at 1 m, 32 electrodes with dipolar spread of 1 m. This configuration enabled to achieve valid details in the data resolution.
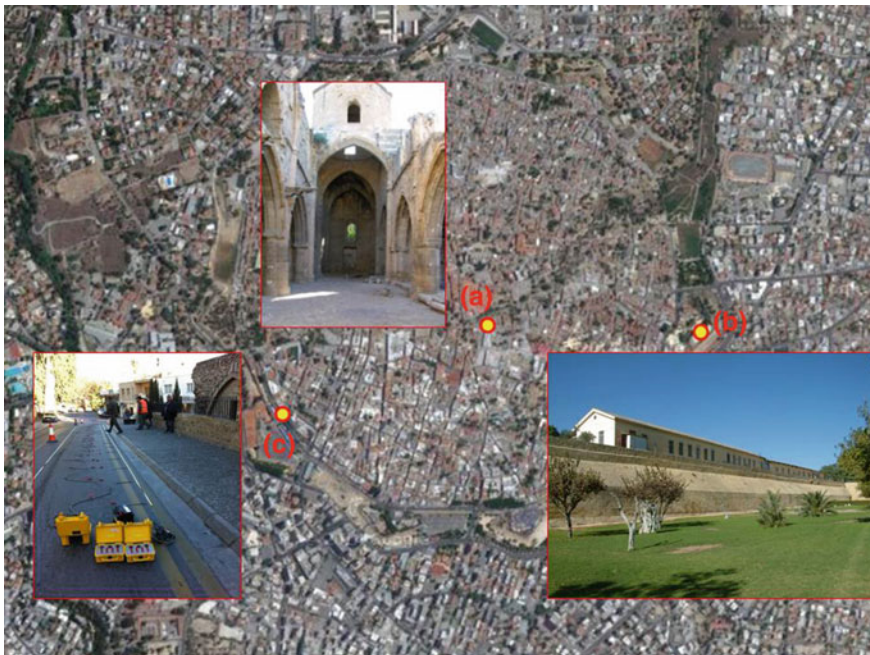
Fig. 4.49 Geophysical survey area. **a** Bedestan; **b** Hospice; **c** Area near Casteliotissa Hall

4.3.1.2   Data Processing and Results

The maps of the monumental complex of the Bedestan were obtained using the PERTI algorithm considering all the dataset. Figure 4.50 shows real modelled resistivity maps at increasing depths. The slice at 1 m points out anomalies with well-defined geometry and shape. In particular, the high resistivity anomalies, which values range from 158 to 398 Ω m, inferred the existence of a central nave with an apse and two side aisles that are the proof of the existence of remains of the earlier Byzantine basilica. The archaeological excavation, to a depth of about 0.5 m, have brought to light blocks of ancient masonry in two areas after having reported geophysical anomalies.

Standard bidimensional radargrams, referred to single profile acquired into the Hospice, were processed through the IDSGRED software. Various high-pass and low-pass frequency filters were applied (ACG, Band pass, background remove) to normalize the amplification, to remove reflections generated by noise due to the different signal attenuation, to recover the data in amplitude, to delete horizontal band visible in many GPR profile due to reflection signal. A three-dimensional matrix of average square wave amplitude of the return reflection was generated using the parallel profiles dataset. The data were processed using the moving average with a radius of interpolation of 0.2 m. The slice (Fig. 4.51) shows, at the top, greater amplitudes of reflections related to the existence of small fractures and in general to a considerable difference in the texture of the wall, visible at the bottom and the top.

The investigated area near Casteliotissa Hall is characterised by fine contrasts of resistivity values; clear anomalies with regular geometric shapes and interesting alignments revealed archaeological remains. The inversion of the apparent resistivity dataset was processed with the algorithmic probability, and specifically, the horizontal sections (Fig. 4.52) show a high resistive anomaly, ranging from 2.1 to 2.7 Ω m, to about 1 m up to 3 m in depth. This anomaly is located in correspondence of the ancient hall. In the ERT to 3 m in depth there are two more high resistive anomalies that are probably related to small parallel walls.

4.3.2   ERT surveys in the historical centre of Alife (Caserta, Italy)

Located in the Volturno valley, Alife, Caserta, Italy, is an important historical and archaeological centre (Fig. 4.53a). The fertile plain was left from a lake created by the eruptions of the Roccamonfina volcano, and lies below the Matese chain. The existing town rises on the place of the Samnite city, occupied by the Romans in the year 326 BC. Traces of the ancient settlement are still visible today, such as structures and buildings of the republican and imperial time. Alife retains the orthogonal urban structures of the Roman age (*cardi and decumani*), enclosed by
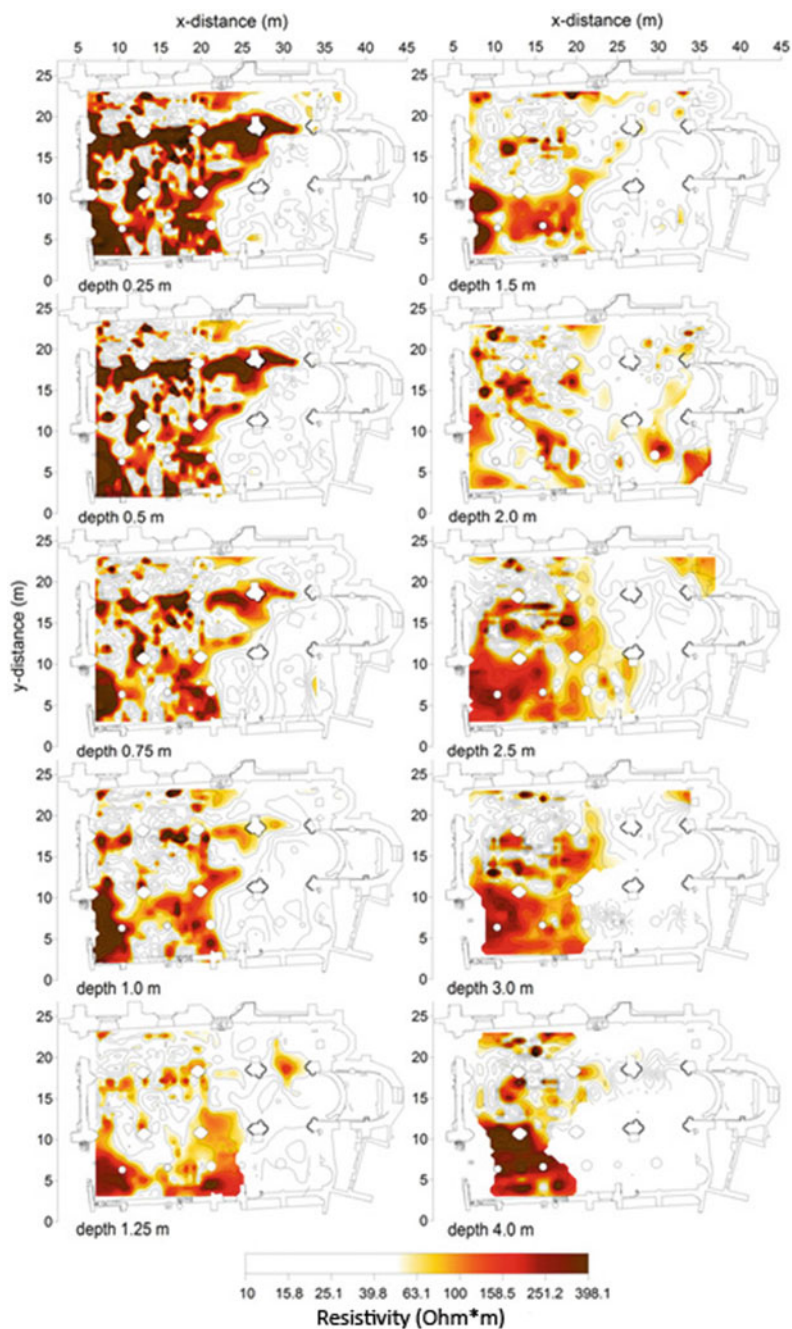
Fig. 4.50 ERT. Image map relative to different depths

Fig. 4.51 Vertical GPR slice

walls to rectangular plan (540 m * 405 m) (Fig. 4.53b). The currently visible walls
are made in *opus incertum* in the lower part and date back to the roman age, while
those in the upper part go back to the Middle Age. The height of the walls is about
7 m, with further 2 m interred. On each side of the city, there is a door and some
posterns. The historical centre retains many traces of its roman history. The *Forum*
area coincides with the current O. Michi square, where many workshops (*tabernae*)
have been discovered. Under the Cathedral, in the crypt, apart from the
Romanesque period structures, the remains of the floor of a Roman thermae with
the "*suspensurae*" have been preserved. Instead, there are not much of the remains
of the theatre, built under Silla and restored in the 2nd century BC, positioned on
the southern side of the Cathedral Square. The *cryptoportico*, a long gallery made
by two separate ambulatories, that probably supported a building, is well preserved.
Along via Latina the remains of three mausoleums are visible, the most famous of
which is that of the *Acilii Glabrioni*, dating back to the 1st century BC.

In the context of the feasibility study for the construction of a parish complex,
geophysical surveys were required. This building had to be located within the urban
perimeter of the city. The project area insists near the apse of the Alife Cathedral.
The project involved the redevelopment of an area devoted to crops with the
construction of a public building. The need to map the entire area designated for
construction originates from the particular location of the same within the historical
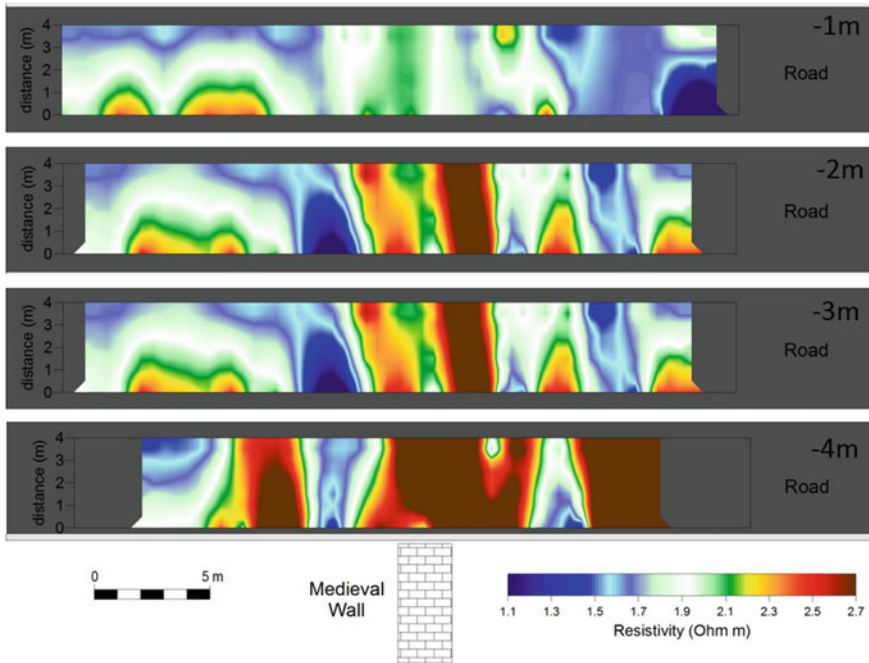
Fig. 4.52 ERT. Image map relative to different depths

centre well surrounded by the ancient city walls and from the close distance with the Cathedral (Fig. 4.54).

4.3.2.1 Survey Planning

Archaeological data suggest a complete and layered mapping of the area, as well as a sufficiently high depth of investigation. In this area, devoted to crop, it was not possible to use equipment that remains, digs up or tramples down plants. Therefore, the ERT survey, both by alternating current and direct current was realized. The first equipment enables to quickly achieve good resolution images at a depth of about 1.5 and 2 m; the second equipment, with slower data acquisition, enables to achieve higher depth levels.

To obtain a complete and multi-layered map from −0.5 to 5–6 m depth, 10 ERT profiles were collected, using the Dipole Dipole axial configuration, arrangements with 32–48 electrodes, and inter electrode distance from 0.5 at 1 m. The parallel profiles were spaced 1 m (Fig. 4.55). To allow the construction of the horizontal distribution to depth values of approximately 1.5 and 2 m, additional ERT profiles, were collected using the array in alternating current where the preceding analysis reports, on average, major anomalies. The configuration is the Dipole Dipole axial
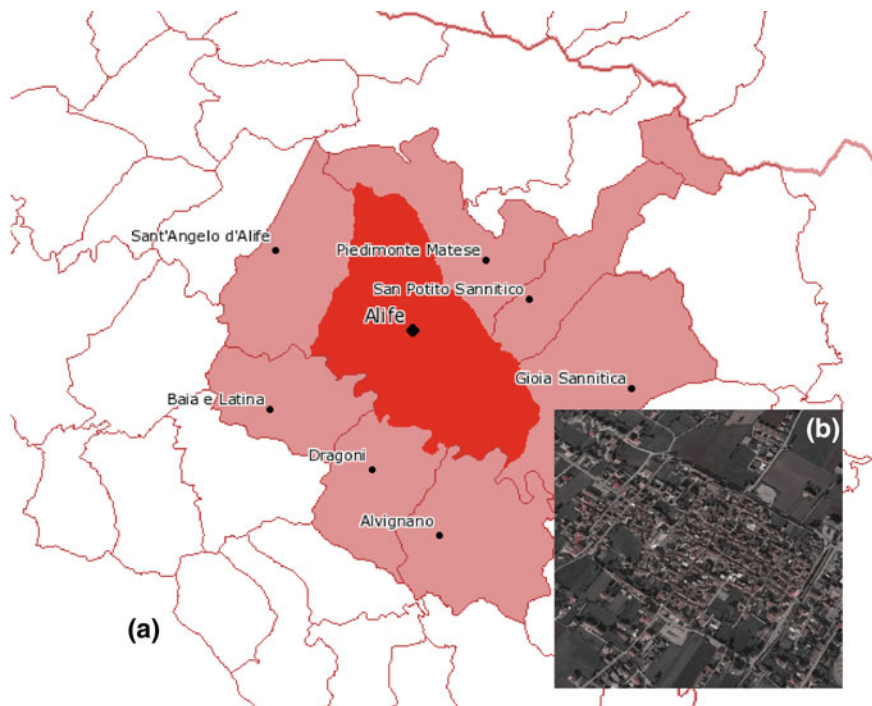
Fig. 4.53 a Localization of Alife, **b** rectangular plane of city (©DigitalGlobe Inc. di Gloogle Earth™)

configuration, inter electrode distance to 1 m and parallel profiles equally spaced at 1 m.

4.3.2.2 Data Processing and Results

For data processing, the probability-based electrical resistivity tomography inversion approach has been adopted.

Figure 4.56 shows the sequence of vertical resistivity tomography. The main evidence is the presence of a number of surface anomalies (1 m in depth) and a well-aligned system of deeper high resistivity anomalies (starting from 2 m up to about 4 m in depth), whose geometry suggests the presence of caves.

Figure 4.57 shows the ERT contour map at −1 to −2 m in depth in which a high resistivity system is present, with approximately straight trend, composed by very regular alignments. This anomaly is also evident, at the same depth, in Fig. 4.56 where the vertical tomography sequence is shown. The regular direction of this high-resistivity anomaly is particularly clear in section at 2 m depth. The regular shape and its depth, related to the presence of well-defined anomalies in the vertical

Fig. 4.54 Geophysical survey area

tomography, suggest the presence of walls and cavities (for example collector or tunnel). In the same tomography is present a low resistivity area that could be characterized by the absence of structures. It is possible the presence of an internal area, presumably filled with soil, in which it is not possible to exclude the presence of flooring.

4.3.3   High Resolution GPR Surveys in Urban Areas: The Case of Palatine Hill (Roma, Italy)

With the contribution of Clementina Panella (Sapienza University of Roma, Italy), Dean Goodman (Archaeometry Lab, CA-USA) and, Salvatore Piro, Daniela Zamuner, Daniele Verrecchia (ITABC-CNR).

4.3.3.1   Introduction

To enhance the knowledge of the subsoil between the N-E foot of Palatino Hill and Colosseum Valley (Rome) as to the location and conservation of unknown buried Roman structures, a scientific collaboration between Sapienza University at Roma (Department of Archaeology) and the Institute of Technologies Applied to Cultural Heritage (ITABC-CNR), was initiated in 2001. The study area is characterised by a sequence of complex buildings, related to the Roman period between the late

Fig. 4.55 Localization of vertical ERT
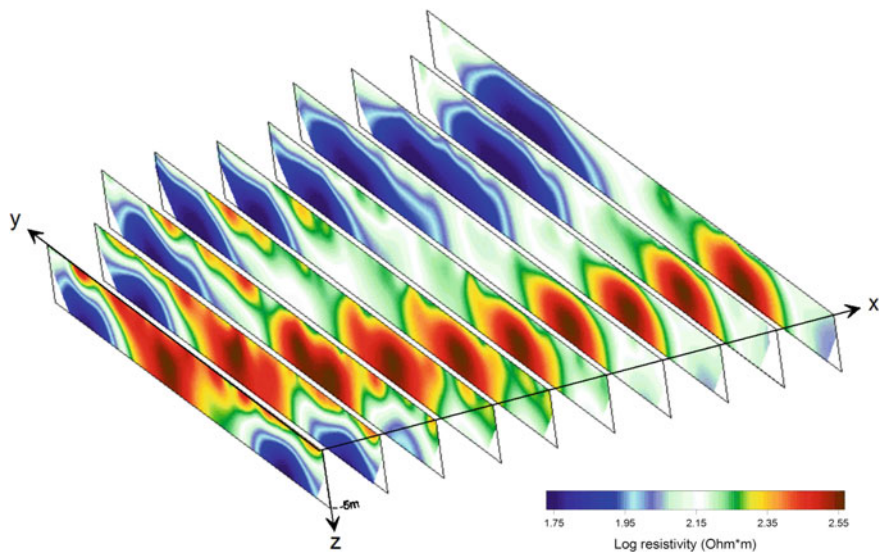
Fig. 4.56 ERT. Vertical sections
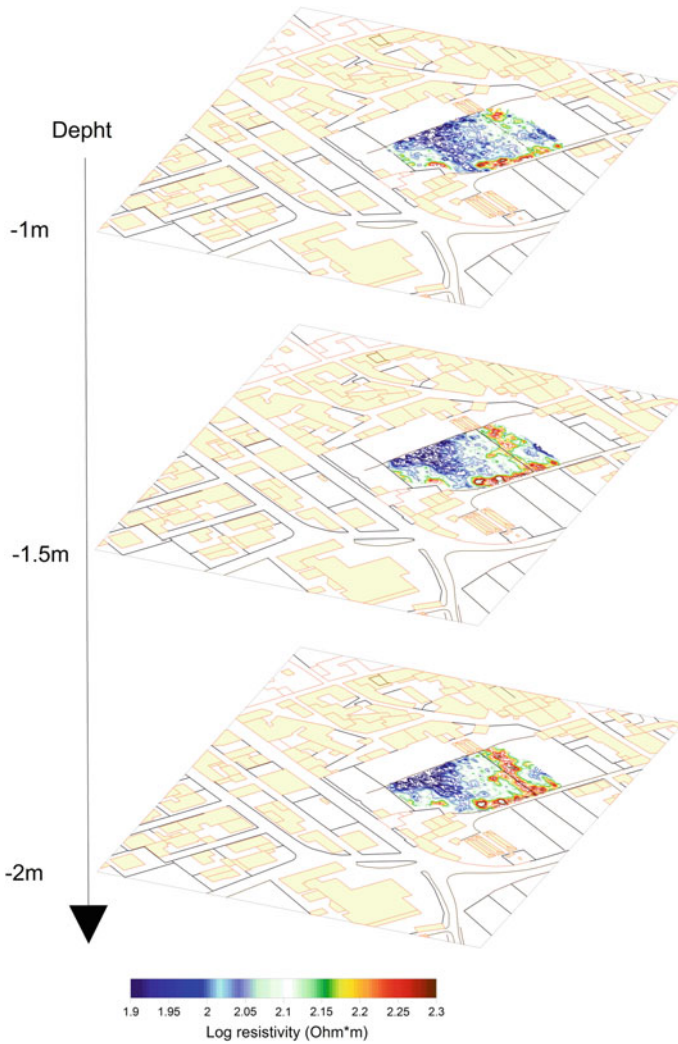
Fig. 4.57 ERT. Contour map, −1 to −2 m in depth

Republican and Severo's age (200 AD). In this complex site a series of GPR surveys employing different frequencies were carried out. For the field measurements two different GPR SIR Systems (GSSI); one equipped with a 500 MHz bistatic antenna and the other employing a 70 MHz monostatic antenna, were used. Acquisition was made using a high-resolution approach in which parallel profiles were recorded very closely across the site. Signal processing, image processing, and visualization techniques have been used in conjunction with data modelling, elaboration, and interpretation of the recorded subsurface amplitudes. Some of the recorded data were synthesized using GPRSIM simulation software to perform

forward modelling. In this process we use simulation software in an iterative approach by guessing a model, running the simulation, and then comparing the simulation with a real recorded radargram collected over the site. The beginning subsurface model is continually adjusted till we get a good match between real and synthetic radargrams. Once we have accomplished this we can then say with some confidence, that the real structure responsible for our recorded reflections are possibly given by the candidate model in the simulation program. With the aim of obtaining a planimetric image of all possible anomalous bodies, the time-slice visualization technique was applied using GPR-SLICE software. Time-slices are calculated by creating 2-D horizontal maps of the averaged squared amplitude of the radar wave in a specified time window and spatial window across parallel profiles. Filtering was used to remove the background reflections. Using these spatial averages, interpolated and solid 3D volumes of reflections amplitudes were generated.

During the archaeological investigations made, side by side to the geophysical surveys, from 2001 to 2012, between the N-E foot of Palatino Hill and the Coliseum Valley, a sequence of complex buildings, related to the roman period between the late republican and Severo's age, have been detected.

The oldest building is a *domus* of the late republican period which is located nearest a *tabernae*, in front of a line connecting the Coliseum Valley and the Roman Forum. The fire-raising of 64 a.C., signed the destruction of these buildings and the development of Neronian urbanism.

The archaeological excavations have located a portion of the foundation of a portico, which bordered the way through the Coliseum Valley and Roman Forum, a portion of a sewerage system with S-N direction and a foundation with E shape, which closed the Elagabalo's Thermae.

4.3.3.2 Survey Planning and Data Processing

GPR surveys were performed, during September 2001, November 2002, September 2003, May 2004, January 2008 and February 2011 using a 400 and 500 MHz bistatic antenna with constant offset, at selected areas on the N-E foot of Palatino Hill and in the Coliseum valley. GPR surveys were also performed during November 2002, 2003 and February 2008 with a 70 MHz monostatic antenna, to survey an area in the Coliseum valley.

The 400 and 500 MHz antenna were as a compromise between depth penetration to about 2–3 m and resolution of features on the order of 0.15–0.20 m in order to define the archaeological features of interest. The 70 MHz antenna was employed to investigate at a depth penetration more than 2–3 m and with a resolution more than 0.30 m, comparable with the dimensions of the expected archaeological foundation structures.

All profiles at the site of "N-E foot of Palatino hill" were collected alternately in reversed and un-reversed directions across the survey grids. The horizontal spacing between parallel profiles for both antenna at the site was 0.5 m. Radar reflections

along the transects were recorded in continuous acquisition mode across the ground at 80 scan s^{-1}, horizontal stacking was set to 4 scans. Along each profile markers were spaced every 1 m to provide spatial reference. All radar reflections within the 95, 105, 113 and 150 ns (two-way-travel time) time windows were recorded digitally in the field as 8 and 16 bit data and 512 samples per radar scans.

All profiles at the site "Coliseum valley" were collected alternately in reversed and un-reversed directions across the survey grids. The horizontal spacing between parallel profiles at the site was also 0.5 m and at a collection rate of 80 scan s^{-1}; horizontal stacking was set to 4 scans for both antenna. Along each profile markers were spaced every 1 m to provide spatial reference. All radar reflections within the 100 and 150 ns (two-way-travel time) time window were recorded digitally in the field as 8 and 16 bit data and 512 samples per radar scans.

The data were subsequently processed using standard two-dimensional processing techniques employing the GPR-SLICE v7.0 Ground Penetrating Radar Imaging Software (Goodman 2011, 2013). The basic radargram signal processing steps included: (i) header editing for inserting the geometrical acquisition information; (ii) DC drift removal; (iii) manual regaining to adjust the acquisition gain function and enhance the visibility of deeper anomalies; (iv) data resampling, (v) frequency analysis; (vi) band pass filtering, (vii) customized background removal filter to attenuate the horizontal banding and (viii) Kirckof migration using a constant average velocity (Goodman et al. 2007; Piro and Panella 2005).

With the aim of obtaining a planimetric vision of all possible anomalous bodies the time-slice representation technique was applied using all field profiles (Goodman and Piro 2013). Time-slices are calculated by creating 2-D horizontal contour maps of the wave energy from a specified time value across parallel profiles, employing GPR-Slice software. Time slice data sets were generated by spatially averaging the squared wave amplitudes of radar reflections in the horizontal as well as the vertical.

Background filtering was used to remove line noises that were found to exist in the raw unprocessed images. Using these spatial averages, interpolated and solid 3D volumes of reflections amplitudes were generated. The results are presented in 3D animation using real time Open GL graphic displays in which isosurface rendering, 3D time slice fence diagram are mixed with the raw filtered radargrams. Using spatially binned and interpolated volumes of radar data shows better continuity in mapping subsurface reflections, which are more useful and provide archaeologist an interpretable form of data presentation, then using simple raw or filtered radargrams as volume elements, Fig. 4.58.

One of the most useful displays of data is from overlay analysis which an option available in GPR-SLICE v7.0 Software. In this process, the user can choose a range of depths to overlay the relative- strongest-reflectors onto a single map. After the starting and ending time slice depths are chosen, the overlays can be created as an animation dataset. The overlay time slices contain reflections from within various chosen depth ranges, and plots them on a single map. In the cases when continuous archaeological features are at varying depths in the ground, the overlay analysis will accumulate reflections from these different depth ranges and help to create a useful

map containing all the relevant reflections. The results obtained on shallowly buried structures indicate that the plan of portion of buried archaeological structures can be identified and characterised from the GPR time-slices representation (Goodman and Piro 2013), Figs. 4.59, 4.60, 4.61, and 4.62.

4.3.3.3 Conclusions

The location, depth, and size and vertical overlapping of the buried buildings were effectively estimated from non-destructive ground remote sensing with a ground-penetrating radar system, together with information on the geomorphology and on the archaeology of the site.

The archaeological excavations made (by Prof. Clementina Panella—Sapienza University of Roma) during the last years, have confirmed the structures individuated with the geophysical methods. This project is still in progress and new surveys are planned to investigate the area between the Coliseum, the Costantino's Arc and the Via Sacra at Roman Forum.

The results obtained on shallowly buried structures indicate that the plan of portion of buried archaeological structures can be identified and characterised from the GPR time-slices representation. Together with information on the geomorphology and on the archaeology of the site, the location, depth, size and vertical overlapping of the buried buildings were effectively estimated from non-destructive ground remote sensing with a ground-penetrating radar system.

The archaeological excavations made (by Prof. Clementina Panella—Sapienza University of Roma) during the last few years, have confirmed the structures individuated with the geophysical methods, Fig. 4.63.

Figure 4.62 showsone time-slice, corresponding to the depth of 1.90 m, with the indication of two main walls (named USM 5008 and USM 5045), which have been found during the excavation, made after the GPR surveys. The wall named USM 5045 of Neronian period, starts from 0.60 m and has been excavated till 2.20 m in depth.

4.3.4 High Resolution GPR Surveys in the Medieval Town of Prato (Florence, Italy)

With the contribution of Chiara Marcotulli (Laboratori Archeologici San Gallo, spin-off of Florence University. Florence, Italy), Guido Vannini (Medieval Archaeological Department, Florence University. Florence, Italy), Salvatore Piro and Daniela Zamuner (ITABC-CNR).
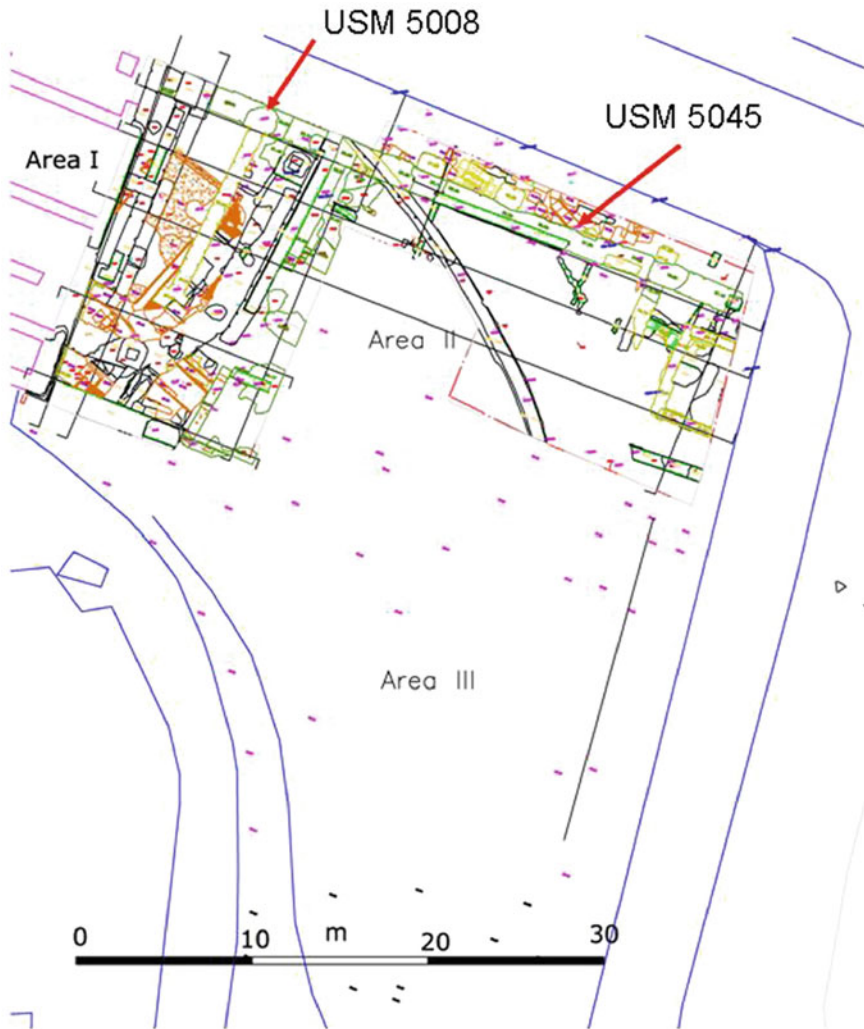
Fig. 4.58 North-east foot of Palatine hill. General plant of the investigated area; location of the sectors: Area I, Area II and Area III, which have been excavated and the USM employed to verify the GPR results

4.3.4.1   Introduction

The Chair of Medieval Archaeology from the University of Florence, in collaboration with the local *Soprintendenze* (Supervisor Authorities for Cultural Heritage) and with the Municipality of Prato, has undertaken an Urban Archaeology project, on the occasion of the restoration of Piazza (square) delle Carceri, in the town of Prato (Florence, Italy).
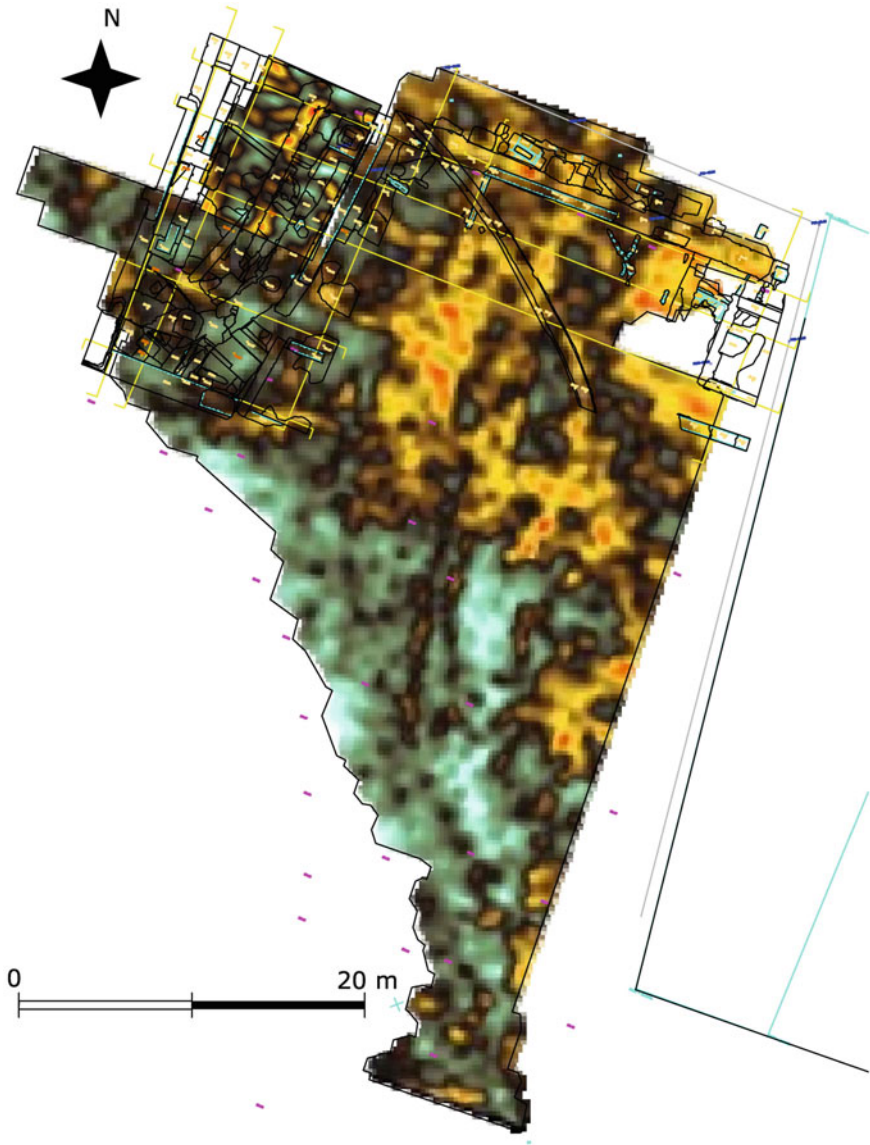
Fig. 4.59 North-east foot of Palatine hill. GPR time-slice at the time interval 5.6–10.6 ns (twt)

Piazza delle Carceri is one of the main historical places of Prato, in the middle of the three Medieval settlements which were the origin of the town. Here, according to the literatures, there were *curtis* and *palatium* of the Alberti family (Xth–XIIth centuries: Vannini 1975; Fantappié 1991), the *castellum* of Frederick II
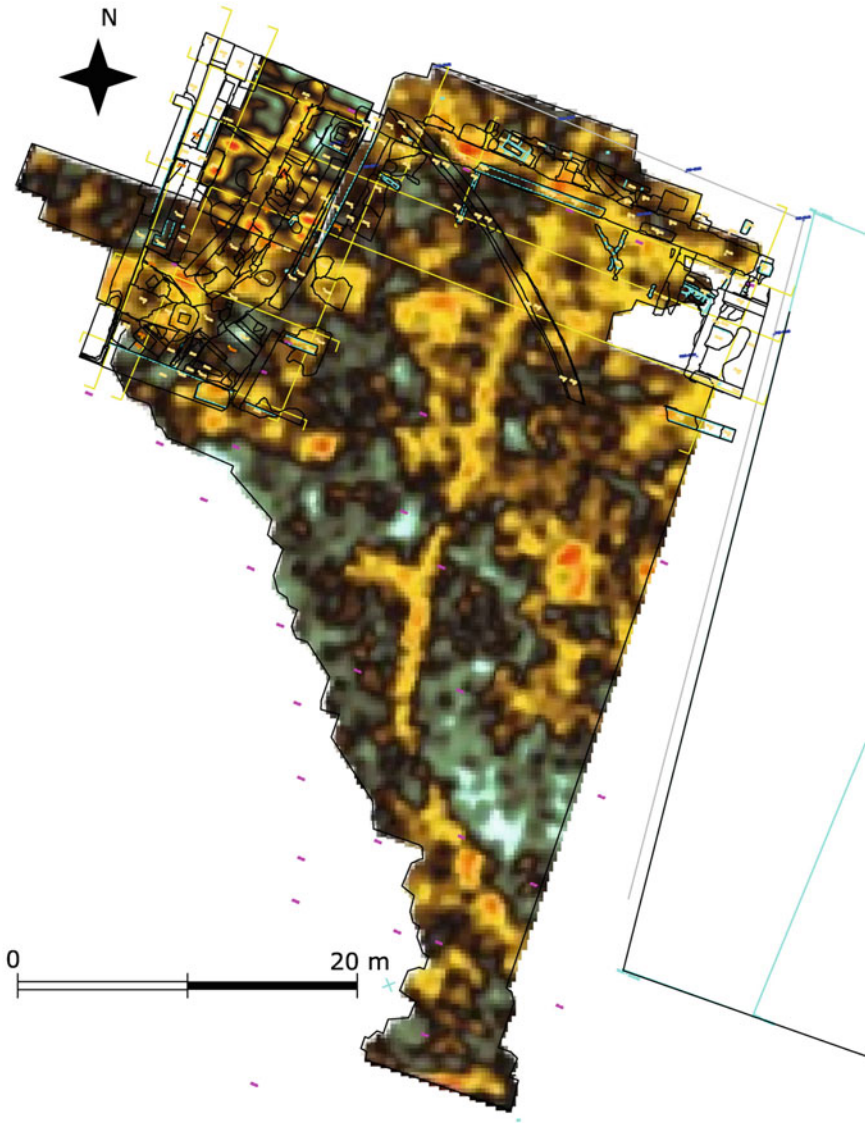
Fig. 4.60 North-east foot of Palatine hill. GPR time-slice at the time interval 11.0–16 ns (twt)

(XIIIth century) and the second urban walls (XIIth–XIIIth centuries: Fantappiè 1991).

To enhance the knowledge of the subsoil in the area of *Piazza delle Carceri*, as to the location and conservation of unknown buried medieval structures, a scientific collaboration between University of Florence (Department of Medieval Archaeology) and the Institute of Technologies Applied to Cultural Heritage
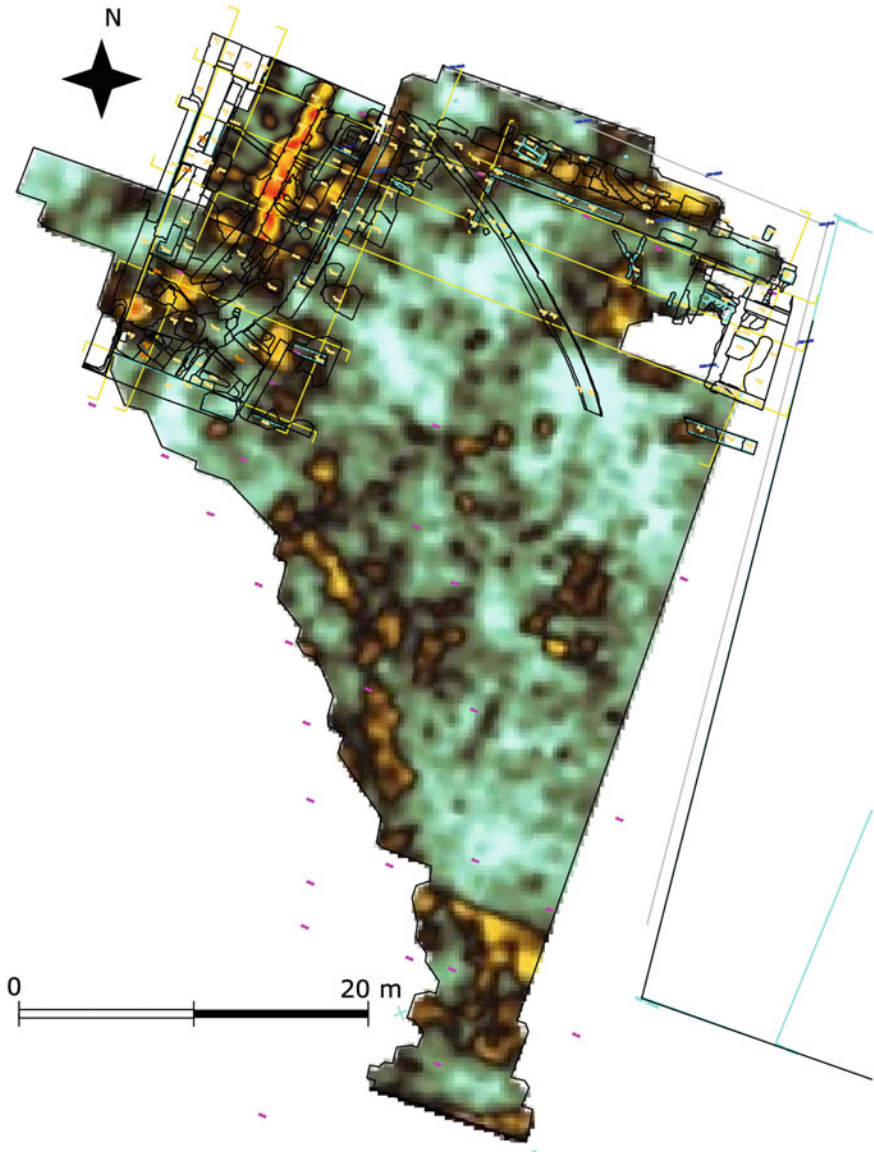
Fig. 4.61 North-east foot of Palatine hill. GPR time-slice at the time interval 33.0–38 ns (twt)

(ITABC-CNR), started in 2012 and it is still in progress. The investigated area has been hypothesized to be characterised by a sequence of complex buildings, related to the medieval period. In this complex site a series of GPR surveys employing different frequencies were carried out.
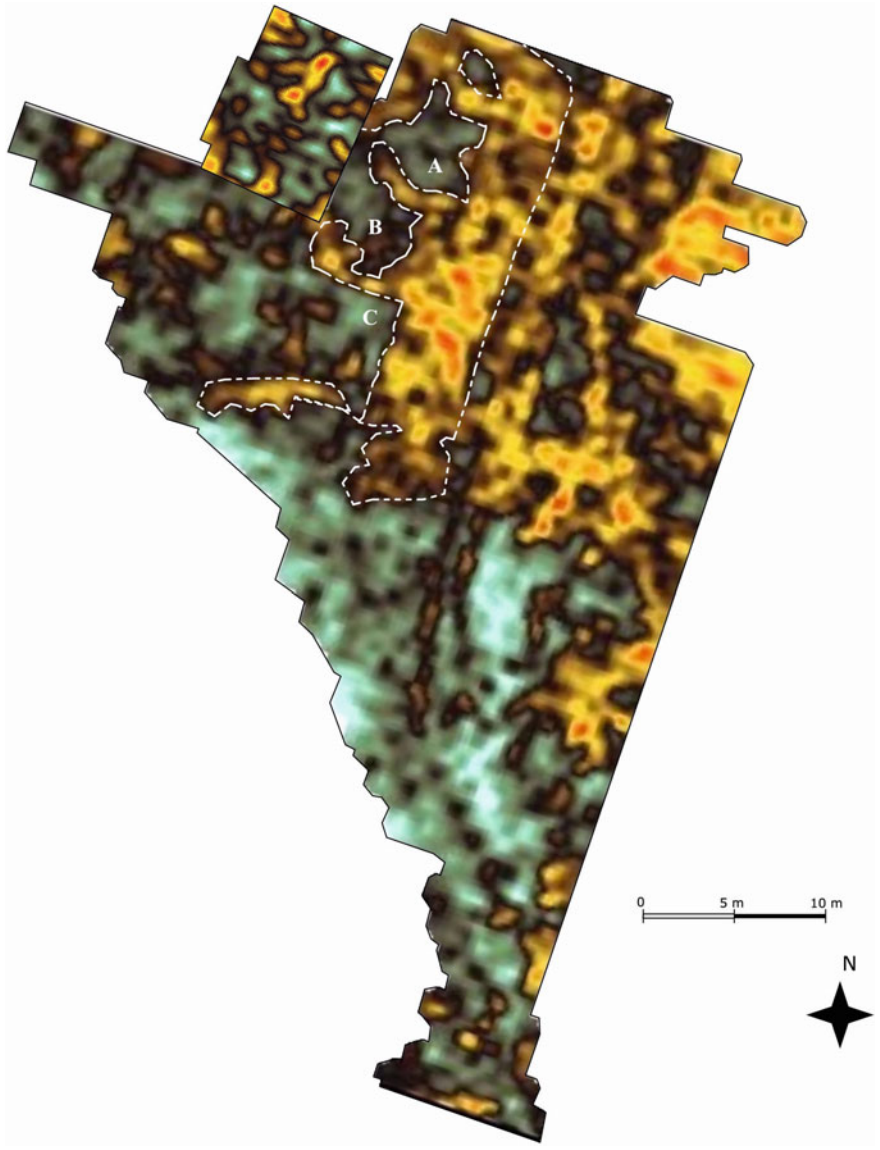
Fig. 4.62 North-east foot of Palatine hill. Location of the structure n.4 overlapped to the time-slice corresponding to the estimated depth of 0.50 m

The archaeological surveys, from September 2012 until July 2013, was organized through four different phases characterized by an increasing degree of investigations. The first diagnostic phase based on geophysical survey was followed by the opening of three stratigraphic excavations, to check the results of the GPR
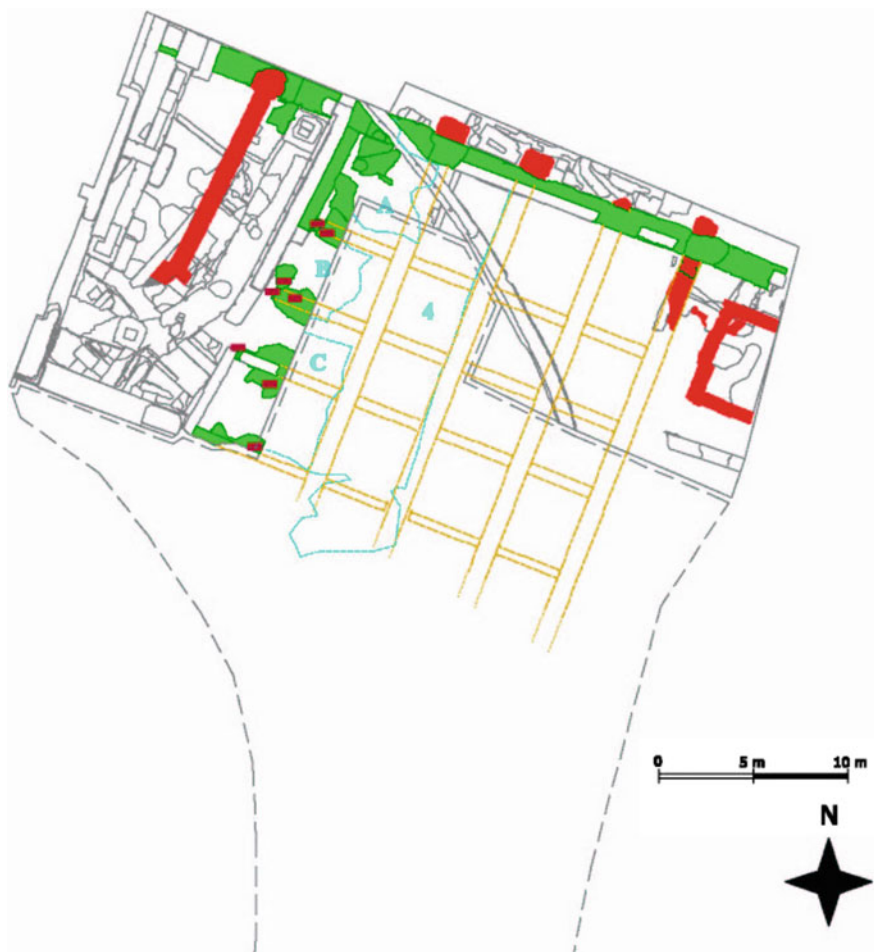
Fig. 4.63 North-east foot of Palatine hill. Correlation between the structure no. 4 and the results after the excavation. With green the structures of Nero's period are indicated; with red, the structures of Flavio's period

prospection (Surveys C, D, E, phase II). Subsequently, the three surveys were expanded and new trenches were opened (phases III–IV), to fully document the archaeological potential of the entire square (Vannini et al. 2012–2013).

4.3.4.2   Survey Planning and Data Processing

GPR surveys were performed, employing the SIR3000 (GSSI) to investigate the selected areas in *Piazza delle Carceri*, equipped with a 400 MHz (GSSI) bistatic antenna with constant offset and a 70 MHz (Subecho Radar) monostatic antenna.
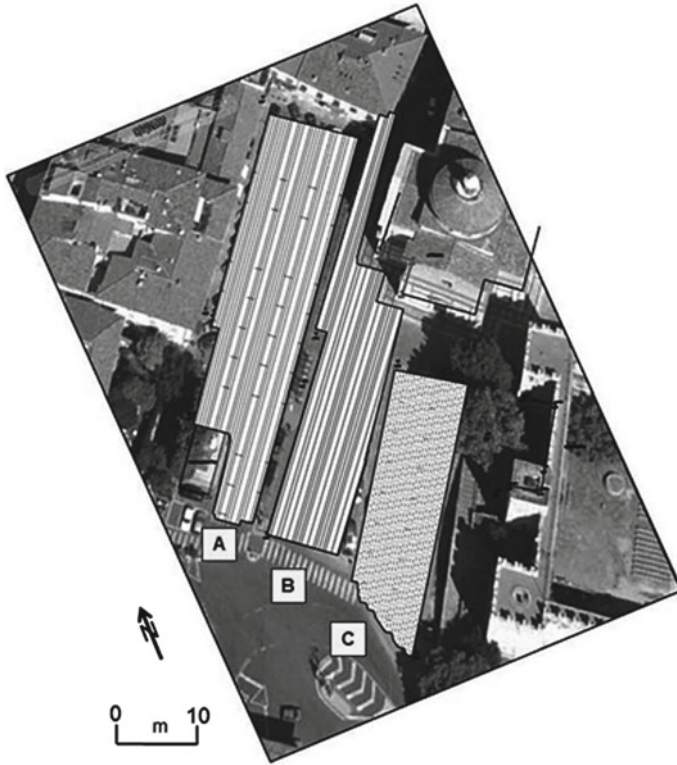
Fig. 4.64 Prato, Piazza delle Carceri. Location of the A-B-C area, investigated with the GPR system

The horizontal spacing between parallel profiles at the site was 0.50 m, employing the two antennas. Radar reflections along the transepts were recorded continuously, with different length, across the ground at 60 scan s^{-1} for 400 MHz antenna and at 30 scan s^{-1} for 70 MHz; horizontal stacking was set to 3 scans.

In the investigated area (A-B-C), Fig. 4.64, a total of 303 adjacent profiles across the site were collected alternatively in forward and reverse directions employing the GSSI cart system equipped with odometer. All radar reflections within the 105 ns for 400 MHz antenna and 185 ns for 70 MHz antenna (two-way-travel) time window were recorded digitally in the field as 16 bit data and 512 samples per radar scan. A nominal microwave velocity of about 8 cm/ns was determined from fitting hyperbolas to the raw field data. This was used in estimating a penetration depth from the GPR survey.

All the GPR data were processed in GPR-SLICE v7.0 Ground Penetrating Radar Imaging Software (Goodman 2014). The basic radargram signal processing steps included: (i) post processing pulse regaining; (ii) DC drift removal; (iii) data resampling, (iv) band pass filtering, (v) migration and (vi) background filter. With

the aim of obtaining a planimetric vision of all possible anomalous bodies the time-slice representation technique was applied using all processed profiles (Goodman and Piro 2013). The squared amplitudes were averaged horizontally every 0.25 m along the reflection profiles 4 ns (for 400 MHz antenna) and 6 ns (for 70 MHz antenna) time windows (with a 10% overlapping of each slice). The resampled amplitudes were gridded using the inverse distance algorithm with a search radius of 0.75 m.

In Fig. 4.65 the time-slices (in the depth windows from 0.40 to 0.60 m for 400 MHz antenna) for the investigated area are shown. On this map the individuated anomalies are visible and correlated with the structures located with archaeological excavations in the sectors D and E.

4.3.4.3   Archaeological Results

To summarize, archaeologists have brought three areas of particular archaeological interest to light, Fig. 4.66. In the first area (survey D) a quadrangular structure was found, well highlighted by the geophysical survey. This is identifiable as the basement of a big wooden winch, probably used for the construction of Santa Maria delle Carceri church, at the end of the XVth century.

In the second area (survey E) a stretch of paved road was found, E-W oriented, directed to Palazzo Banci; an area excavated in 2003–2006 in which another paved road and a *domus* emerged. The paved road in Piazza delle Carceri, at a depth of 1.15 m, is 3.30 m wide and is only a few centimeters thick. Near the paved road, probably abandoned in the second half of the XVth century, was a large residential building, probably a former tower transformed into a *domus* and then abandoned in the first half of the XIVth century. The archaeologists, matching the data from the geophysical survey (two walls recognized) with ones from the excavation, are able to reconstruct the original dimensions of the *domus*, that is 7.45 m × 11 m wide.

In the third area (trench 1 and survey 2-2b) a second paved road was found, N-S oriented, that, due to construction technique and size (5.30 m wide), is of great importance for the history of the Medieval town of Prato. This road, found at a depth range 1.50–2.20 m with a thickness of few centimeters, is preserved at least for a length of 38 m.

The excavations have been covered and the data processing is still in progress. The results have been extraordinary with new, fundamental archaeological evidence that have much significance in the context of the pluriannual project of Urban Archaeology dedicated to Prato. We have now a consistent and qualified documentation for projecting a new museum for the medieval town, in perspective of Public Archaeology.
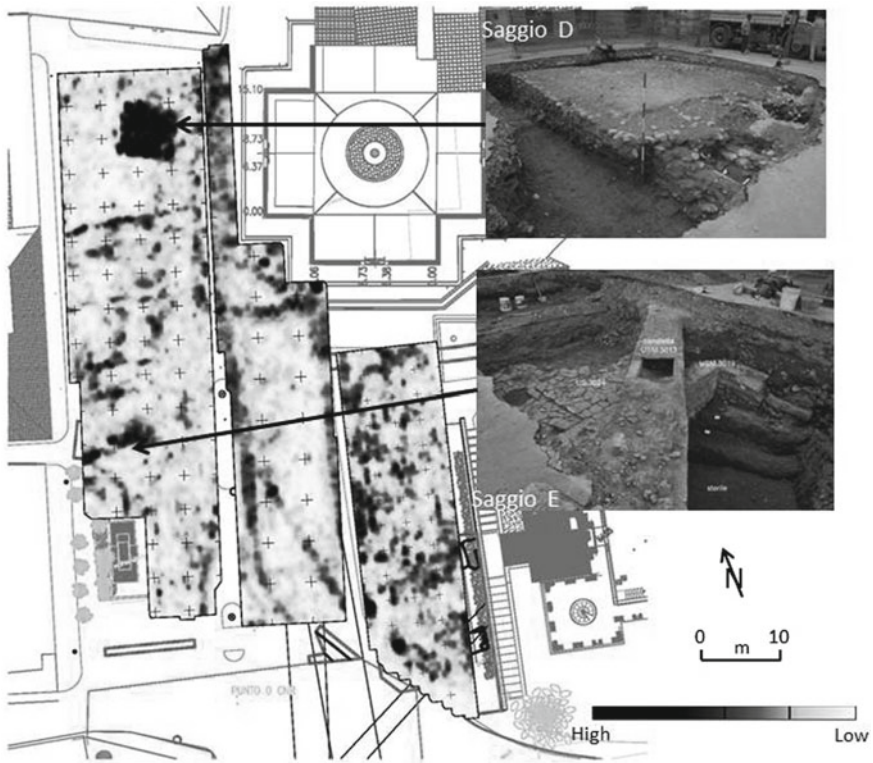
Fig. 4.65 GPR time-slices, in the depth windows from 0.40 to 0.60 m for 400 MHz antenna. On the right, two pictures during the archaeological excavations

4.4   Archaeological Parks

4.4.1   ERT surveys in the Park of Pratolino (Vaglia, Florence, Italy)

A geographical survey has been performed at the Park of Pratolino in Vaglia, Florence (Fig. 4.67), in order to research the buried remains of the Villa Medici, Pratolino, which was demolished in 1820 (Cozzolino et. al 2012). The villa and the gardens were designed by the Grand Duke of Tuscany, Francesco I de' Medici, in 1581. Following the demolition, the gardens were redesigned in an English landscape style. After the splendorous Medici period, the park was bought by the Russian Demidoff family in 1872, who occupied the secondary building of Paggerie
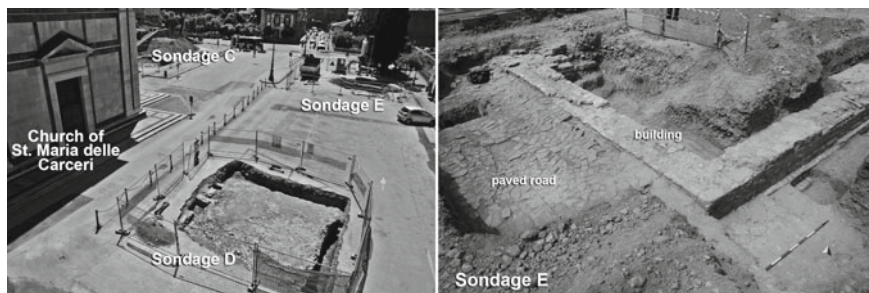
Fig. 4.66 Prato, Piazza delle Carceri. Archaeological surveys in the sectors C-D-E.

and enlarged and restored it. Since 1981, it has become a public park under the supervision of the Provincial Administration of Florence, who have modified it over the centuries. It is one of the most extensive parks of Tuscany and one of the most important in English style. Today, what we can see of the original building is the Apennine Colossus (Fig. 4.68a, left), the Paggerie (Fig. 4.68a, right) and the Buontalenti Chapel 4.68b.

4.4.1.1 Survey Planning

The investigations have been conducted in a large area—100 × 80 m—with the aim to retrace the exact site of the villa, of which there was no knowledge notwithstanding the numerous representations, both documentary and also pictorial (Fig. 4.69).

The aim of the investigations is also to establish the presence of walls, parts collapsed and conduits saved from the demolition of the villa itself.

The ERT survey was conducted adjusting to the topographic conformation and geomorphology of the area, to the probable depth of the ancient buried structures and to the resolution to be obtained during the data processing.

The geophysical survey, divided into two nearby regular grids, was carried out along 105 profiles aligned towards east–west with axial dipole-dipole array, equally spaced about 1.5 m and a dipolar spread of 1 m.

A topographic survey with a total station has been performed in order to determine the position of the measuring points.

4.4.1.2 Data Processing and Results

Figure 4.70 shows the ground floor plan (Sgrilli 1742) of Villa Medici overlaid by the probability-based ERT imaging applied to the {ρa} datasets at 1m in depth. The contour map indicated with the red colour shows the high-resistivity value, in order
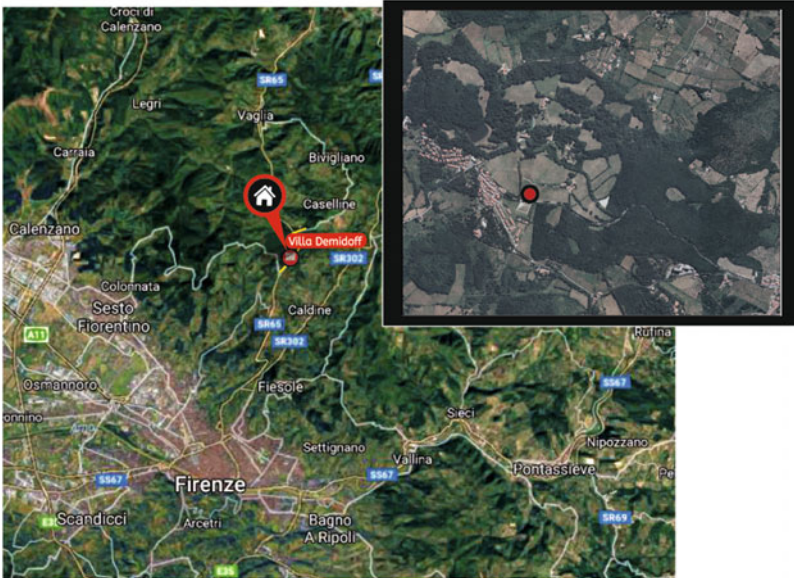
Fig. 4.67 Localization of Park Pratolino: (www.google.it; Orthophoto 2002)

to better underline the anomalies correspondent to the ruins of walls, and with the white colour to show the low-resistivity correspondent to the rooms.

The map shows numerous common elements and, in particular, it is possible to distinguish, not only the general borders of the building, but also the following environments: the principal hall, the rooms present under the stairs, the Voltone environment, the entrance hall of which are evident the four columns which support the vault; the wardrobe room, the bedrooms and the various rooms with different usage, a part of the secret kitchen, the outlines of the semi-circular staircase present to the South of the building, parts of the garden around the villa, a part of the enclosure walls to the East of the building that extends as far as the tower. The blue line indicates an anomaly, associated with the presence of a conduct that crosses the villa in the median portions: it can be located at the centre of the semi-circular staircase, through the entrance hall between the two central columns, meeting with a light curve to the West through the hall corridor and taking a normal course in proximity of the staircase. It is noted that there are also anomalies of undefined contours, located North-West on the map, leading probably to a part of the garden designated as a landfill during the demolition of the villa.

Four essays on the archaeological excavations, successive to the geophysical survey campaign, have confirmed what is showed on the ERT map.

(a)

Fig. 4.68 a The Apennine Colossus (left) and Paggerie (right). **b** Left: Sgrilli 1742; Right: historical map

4.4.2   ERT surveys in the Cuma (Naples, Italy)

The archaeological complex of Cuma, one of the most important in Campania, is part of the cultural patrimony of the metropolitan city of Naples. It is situated in the Vulcanic area of the "Campi Flegrei" in the territory of the municipalities of Bacoli and Pozzuoli (Fig. 4.71a).

The site (Fig. 4.71b) preserves the testimony of one of the most ancient Greek colonies in Italy, founded in 730 BC. The city, occupied over the centuries by various civilizations, including the Romans, was then destroyed by the Napoleonic forces in 1207. The Greek city was divided into two zones, one constructed higher above the acropolis and the lower part constructed on level land, along the coast-line, and defended by imposing walls.

Numerous buildings come to light and there is even more to look for and excavate.

Between the public buildings we find "the Forum" placed in the lower part of the city and built between the end of 2nd century BC and the beginning of 1st BC. Around the square we find numerous *tabernae* destined to commercial activities. In the centre we find the Temple of Jupiter, towards South The Capitoleum and to the North-West the Forum Baths. It is important to mention also the Terrace of the
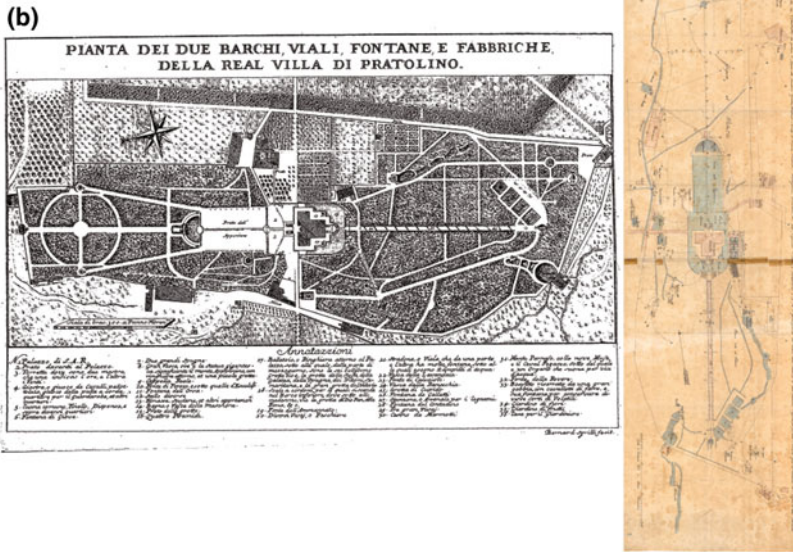
Fig. 4.68 (continued)

Fig. 4.69 Left: Catasto leopoldino; Right: Anonymous historical map1736 overlaid by the cadastral map
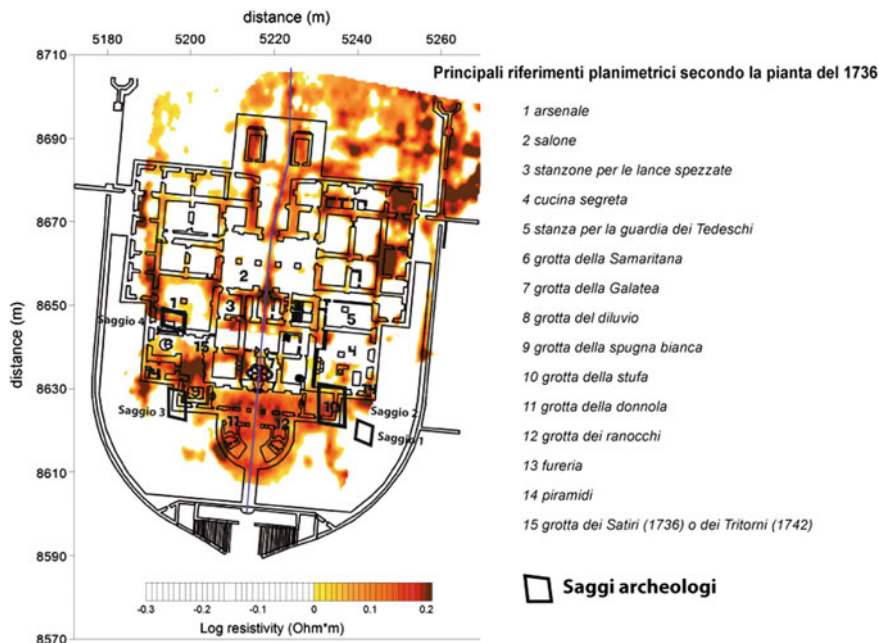
Fig. 4.70 ERT. Image map overlaid by the ground floor plan map of Villa Medici (Sgrilli 1742)

Temple of Apollo, occupied by buildings which are, up to date, of an uncertain attribution. In the vicinity of the so-called "Masseria del Gigante" we find, instead, buildings destined to the seat of the Senate and magistrates.

Between the religious buildings we find The Temple of Apollo, The Temple of Jupiter and the Capitoleum. To the South of the Forum we find the Temple with Portico built between the 1st century BC and the 1st century AD.

Between the ludic buildings we find the Forum Baths realised in the Republican Age, the Central Baths belonging to the 3rd–2nd century BC and the amphitheatre outside the enclosure walls of the city.

Since 1606 numerous teams of Italian and foreign archaeologists have taken interest and worked on this archaeological site of notable importance and splendor.

There have been numerous geophysical investigative campaigns conducted on the site since the end of the 1990s and the results have been published in a 2002 and a 2012 edition as the fruit of the scientific collaboration that shared the multidisciplinary method for the research.

4.4.2.1   Survey Planning

The investigated area is found in the Southern part of the ancient city between the Hellenistic walls and the opening, where some ERT (Mauriello 2002) were already
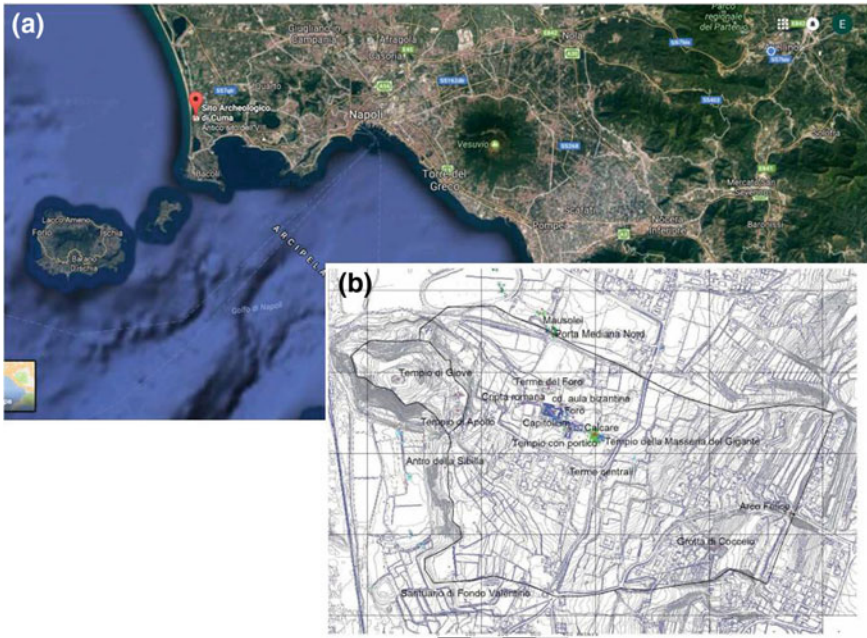
Fig. 4.71 a Localization of Cuma; **b** Map of main archaeological remains (Rescigno 2010)

realised in the past to define the stratigraphy, in a wider area, up to a relatively elevated depth. The present opera has been, instead, concentrated only in some small areas, which have been already explored, with the aim to give back information on the geometry of the structure into the first meter or a meter and a half of depth, where beforehand it was deducted the principal lateral variations of resistivity.

To speed up the proceedings of collecting data without losing information on the depth, an acquisition system has been created called a "tomographic geo-electric area" (ERT pattern area) (Fig. 4.72). Such procedure consisted in the realization of grids 20 m × 20 m in which the measures have been put into practice at cross-points at every 0.50 m. The characteristic has been to maintain an energizing electrode, fixed (A) at a remote distance, and one energizing electrode, mobile (B), that would move in the grid in correspondence with each cross-point. The electrical potential measures took place on 4 electrodes (P_1, P_2, P_3, P_4) positioned on the extension length of the two sides of the grid (those perpendicular to the orientation of the profiles) and at a minimum distance of 5 m. Therefore, for every position occupied by electrode (B) we have obtained 6 measures of electrical potential based on different combinations between the electrodes. Such procedure has allowed acquisition of data, elaboration and analysis of details in a short time without compromising the quality and therefore the reliability of the interpretation, elaborating the data with a probability-based ERT inversion method.
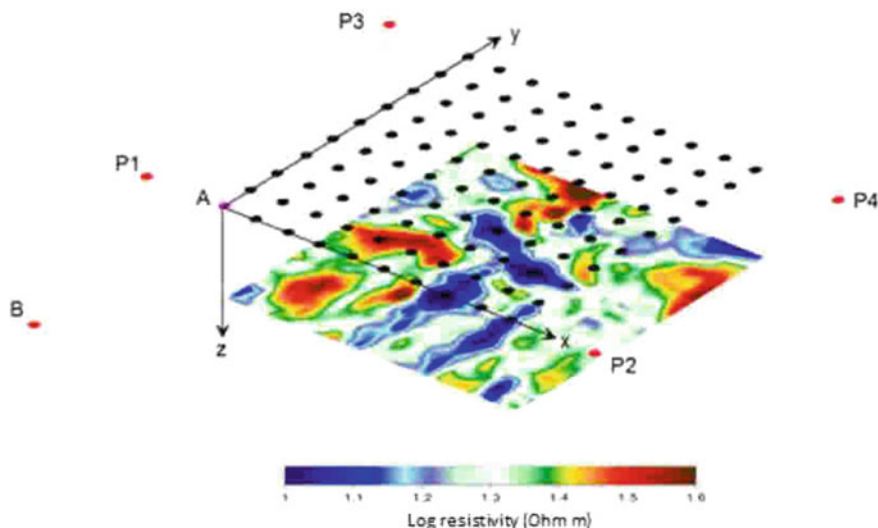
Fig. 4.72 ERT pattern area. Acquisition data

4.4.2.2 Data Processing and Results

For data processing, the probability-based electrical resistivity tomography inversion approach has been adopted.

The ERT image map, 1 m in depth, superposed to the general planimetry in the sector contained between the Forum and the North Wall (Fig. 4.73), shows the value of resistivity in a short range between 1 and 1.6 Ω m, signaling and defining, nevertheless, in a net manner, the passages between the areas more or less conductive.

The *insular* area to the East of the road individuated from the excavations shows a low-resistivity anomaly of an extending form, parallel to the supposed road network layout and nearly internally enclosed into another anomaly characterised instead by high-resistive values, referring to probable archaeological remains. In these points archaeological testings have been carried out confirming the presence of three dwellings of a late ancient epoch. The small high-resistive anomaly placed uninterruptedly and in axis with the low-resistivity anomaly, placed in the western corner of the investigative area, is to be put in relation with the presence of road-network cobble-stones. Figure 4.74 shows a comparison between the geo-physical anomalies and the plans of the excavation (Fig. 4.74).

In Fig. 4.75 details of the general map for a better reading of the anomalies are shown.

The insula to the West of the road shows a high-resistive strip, protected by the rooms of the dwelling characterised internally by fairly definite and regular perpendicular forms, so much so, to suppose the presence of other rooms in the district. In addition, it is very interesting the area towards the West of a figure characterised
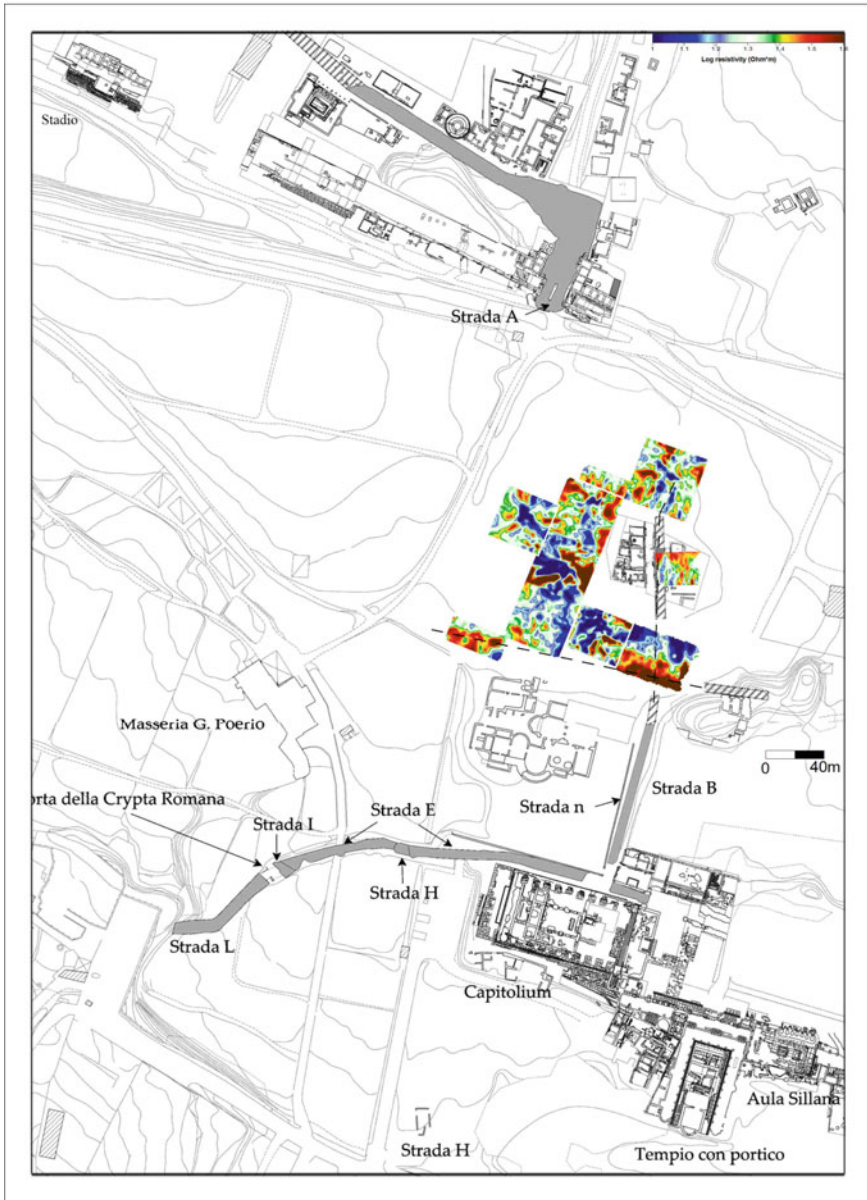
Fig. 4.73 ERT. Image map, 1 m in depth, overlaid by archaeological map (D'Agostino and D'Acunto 2009, Fig. 11, p. 496)

from a conductus zone, an extended form and surrounded by small strips with more resistive rays. This can also be associated to the probable presence of ancient houses.

Fig. 4.74 ERT. Image map. Detail of eastern area and plan of archaeological area (D'Agostino and D'Acunto 2009, Fig. 12, pp. 497)

The anomalies associated to the supposed road layout (sketched out until black broken lines) result to be characterised both by the low-resistive values, localized North on the map, and the high-resistive ones, that are positioned instead South on the map. This could depend on different lithological conditions of the earth climatic conditions or anthropological disturbances that have influenced the geophysical acquisition.

Furthermore, the supposed lay-out of the road on the part towards North seems to incline towards the East, nearly almost following the same layout similar to the road defined in B and visible in Fig. 4.73. Still, towards North we find an interesting low-resistive anomaly with a transversal orientation.

4.4.3 ERT surveys at Norba (Latina, Italy)

The archaeological area of Norba is situated in a dominant position on the Pontina plain, south of Rome, today called Norma (Fig. 4.76). The structures date back to the Latin period, with notable ruins of the city enclosure wall in polygonal plant (that encloses an area of nearly 38 ha) and with four entrance doors of access that date back to 4th century BC.

The "Porta Maggiore", of Greek origin, is nearly entirely preserved.

The city constitutes one of the best examples of urban town planning, with a regular plan, preserved in Italy dating back to an ancient age. The archaeological excavations conducted by Professor Stefania Quilici Gigli have brought to light, in the course of time, important remains of various buildings, sub-divided in irregular blocks (Decumanus). Attention is brought to two acropolis, the Major and Minor, and various temples. The Major Acropolis was home of the Temple of Diana and
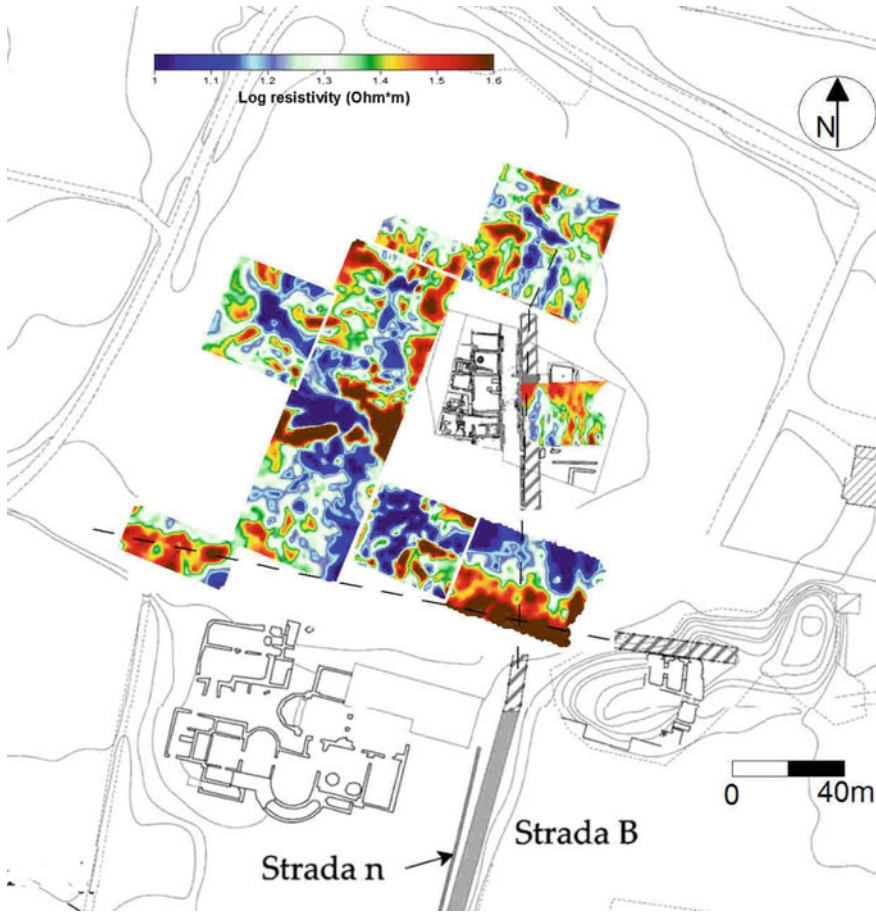
Fig. 4.75 ERT. Image map. Detail of geophysical anomalies

the government and representation offices. Downstream of these we find a very small well preserved thermal complex. The Minor Acropolis, much older, had two temples, with a rectangular plan, which were used as churches during the Middle Age.

Downstream there is a domus known as 'dei semi combusti' and the 'casa del caduceo'. Further south we find the Temple of Juno. Beyond these great structures, on the inside of the walls, it is possible to see cisterns to collect water and parts of the road paving, all preserved in an optimal condition. During the wars between 88 and 82 BC, between Mario and Silla, it was set to fire by the inhabitants so as not to yield to the enemy attack.

The hilly slopes that host the city are constituted by limited levelled terrace that make the archaeological park even more attractive (Fig. 4.76).

4.4.3.1 Survey Planning

The geophysical investigations have interested five different areas (Fig. 4.77) in order to prove the presence of archaeological structures, often laid out in proximity of roads and other dwellings.

The ERT was preferred because of the investigation depth to be reached of nearly 1 m, well known to archaeological excavations.

The ERT method, by alternating current, was carried out using axial dipole-dipole array. The acquisition grid varies in accordance to the area of measure. The survey was carried out along parallel profiles, equally spaced at 0.50/1 m, with a dipolar spread variable from 0.25 to 1 m.

4.4.3.2 Data Processing and Results

The inversion of the apparent resistivity dataset has been processing with the probability algorithm.

Figure 4.78 shows a ERT section, captured in proximity of the forum, with a perspective view, 0.5–0.75 m in depth and, to the left, a specific part of the investigation area.

There are also evident high resistive anomalies that can be associated to parts of the wall or conduits. The geometry follows a structure alignment brought to light by archaeological excavations. The 3D image with z glide coinciding with resistivity values highlights the anomalies that seem to trace dwellings and paved areas.

Figure 4.79 shows the investigations conducted inside of a domus, towards South-West of the Major Acropolis. A system of high-resistive anomalies is highlighted, with an analogue orientation to the structure with a regular and rectangular shape. The other anomalies, however, follow the perpendicular courses.

In Fig. 4.80 a further area of investigation is found, located west to the Minor acropolis, as before, on the inside of a domus. The image map describes a high-resistive anomaly, with value higher 0.35 Ω m with a quadrangle shape in line with the structures already brought to light, and two other anomalies with lower-resistivity; they follow the direction of two parts of a displayed wall. The 3D image highlights this data.

The area, indicated in Fig. 4.77 from letter D, corresponds to a complex positioned North-West of area C at the back of the road lay-out. In Fig. 4.81, the image map and 3D image are reported. Perpendicular anomalies with a high-resistive range are recorded and, on the upper part of the map, a quadrangle anomaly, positioned on the edge of the road.

The last area of investigation is positioned along the road that leads to the temple of Juno, where probably domus were located. In Fig. 4.82, both the image map and 3D image are reported. The perpendicular high-resistive anomalies describe regular shapes that can be referred to wall parts. The high-resistive anomalies describe regular shapes that can be referred to wall parts, one of which in alignment with a part, partially visible, that clearly define the rooms of the domus. The areas with
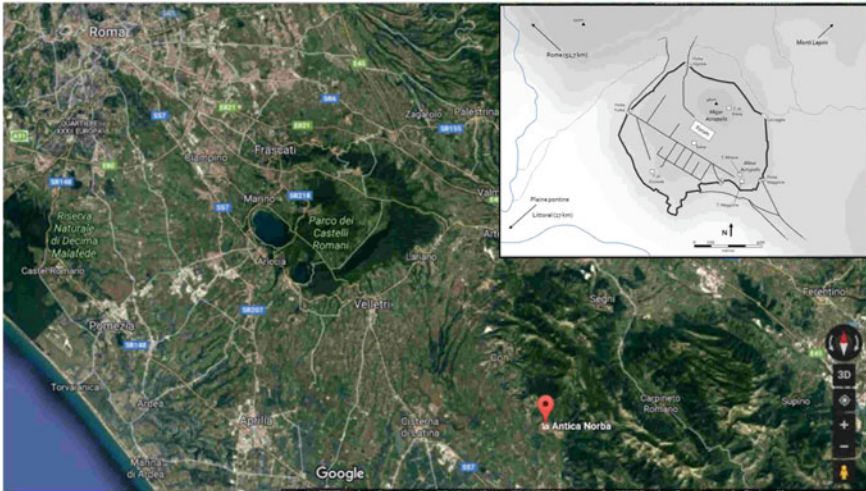
Fig. 4.76 Localization of Norba (www.google.it; Di Cassius Ahenobarbus—Opera propria, CC BY-SA 3.0, https://commons.wikimedia.org/w/index.php?curid=29763514)

major high-resistive density values leave us to suppose the presence of an accumulation of different materials or collapse.

4.4.4   Extensive Ground Remote Sensing Investigations in Aquinum Roman Site (Castrocielo, Frosinone, Italy)

With the contribution of Melda Kucukdemirci (Engineering geophysical Department, Istanbul University), Giuseppe Ceraudo (Lecce, Salento University, Italy), Salvatore Piro and Daniela Zamuner (ITABC-CNR).
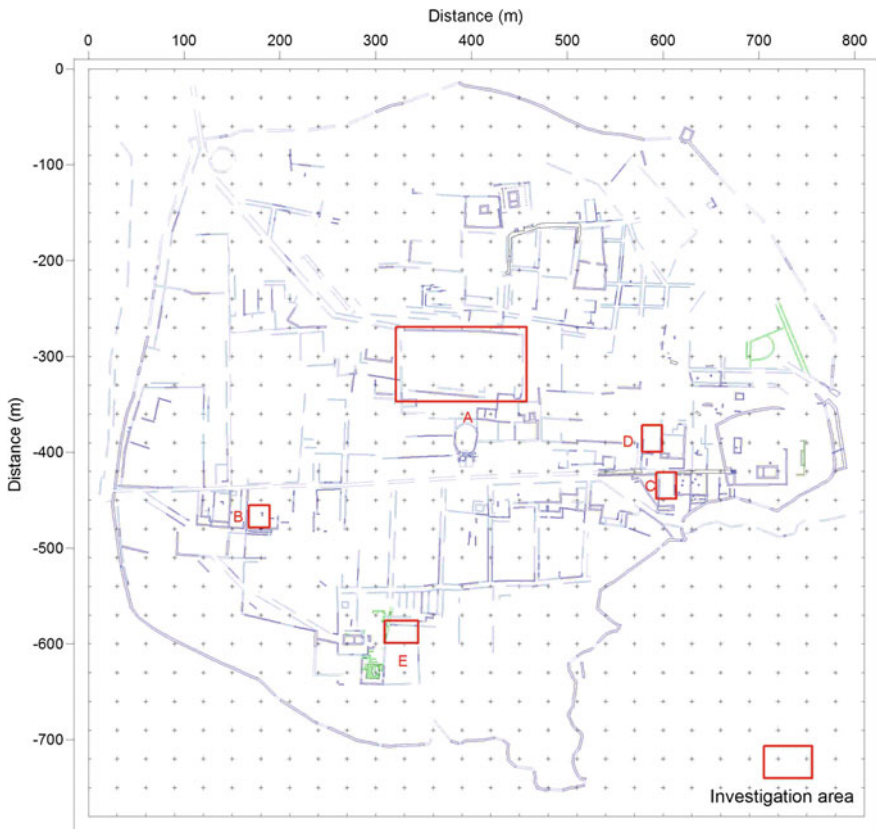
Fig. 4.77 Investigation area
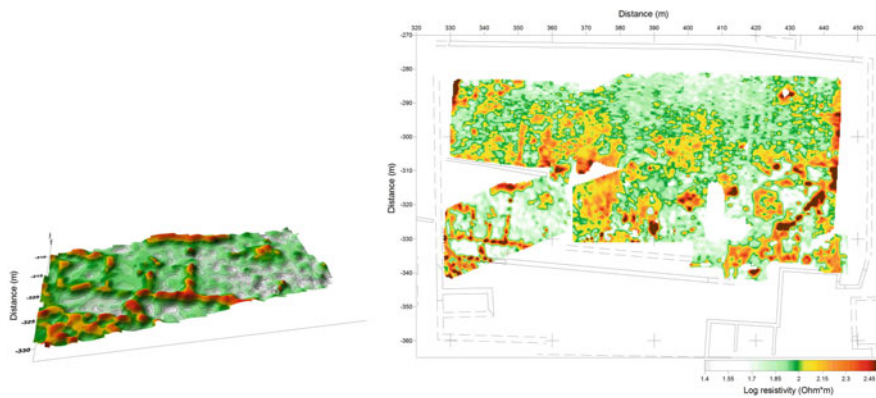
Fig. 4.78 ERT. Image and 3D map—0.5–0.75 m in depth—Area A
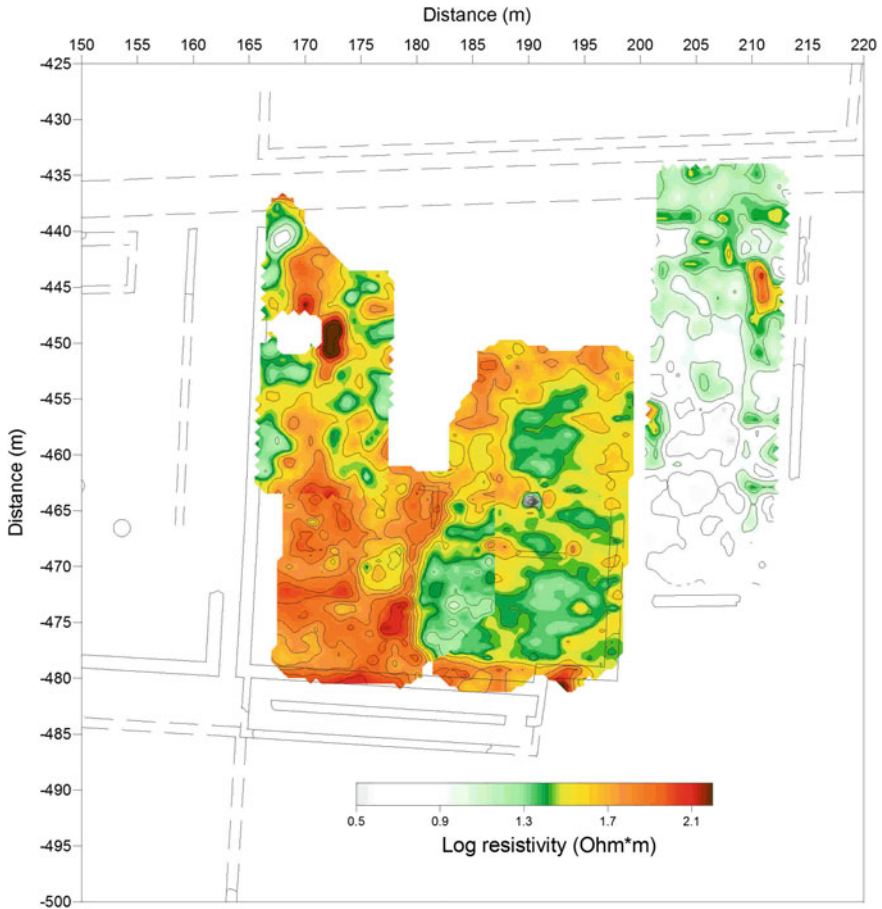
Fig. 4.79 ERT. Image map—0.5–0.75 m in depth—Area B

4.4.4.1   Introduction

This study is part of the "*Ager Aquinas* Project", jointly developed between the University of Salento (Department of Cultural Heritage—Laboratory of Ancient Topography and Photogrammetry), the Municipality of Castrocielo (Frosinone), the Province of Frosinone and the Institute of Technologies Applied to Cultural Heritage (ITABC-CNR).

The archaeological site of *Aquinum* had been identified from 1998 through the interpretation of vertical historical coverage and oblique aerial photographs showing distinctive archaeological cropmarks. Ancient *Aquinum* is characterised by two main aspects: the first depends by the presence of a very big defence-system with mighty walls and large ditch; the second characteristic is the presence of
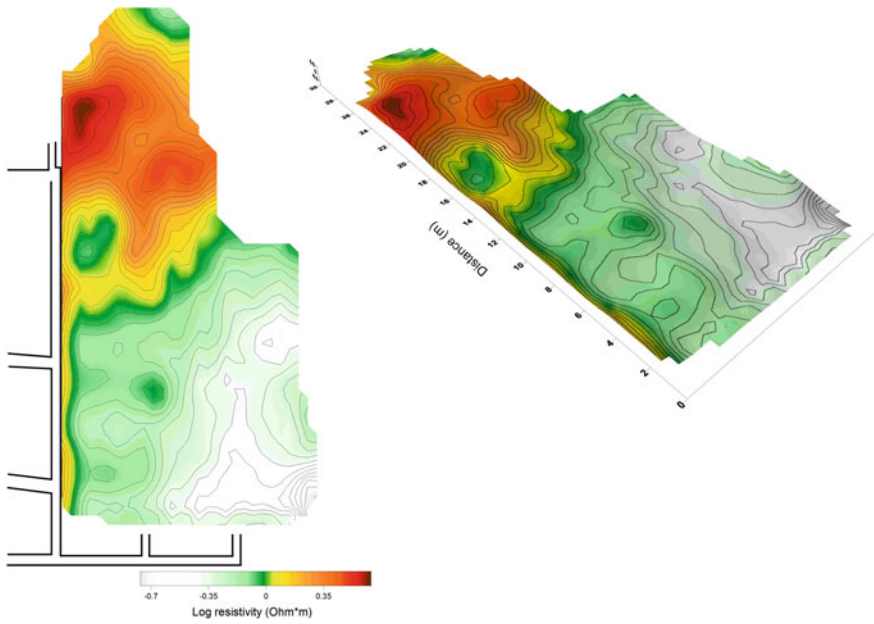
Fig. 4.80 ERT. Image and 3D map—0.5–0.75 m in depth—Area C

regular but not orthogonal road—system of the town, bordered by an unusual
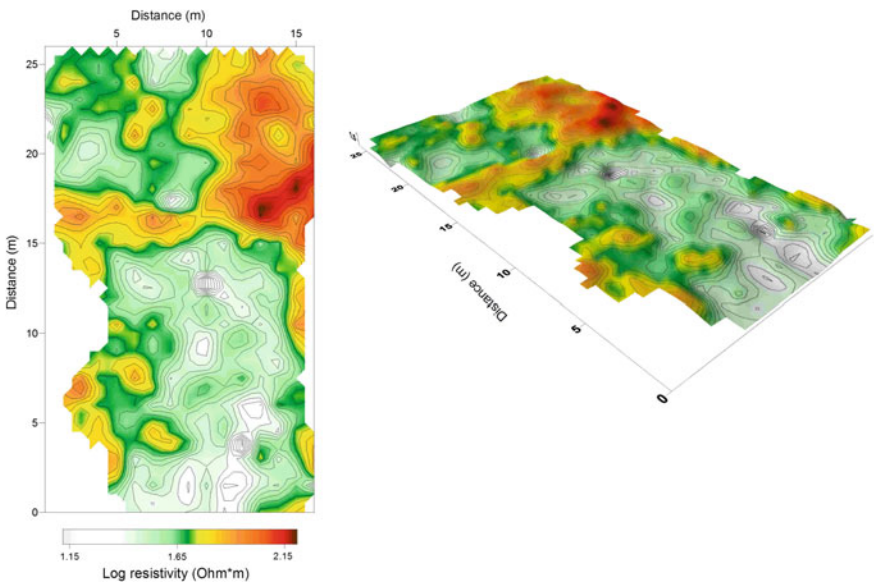
Fig. 4.81 ERT. Image and 3D map—0.5–0.75 m in depth—Area D
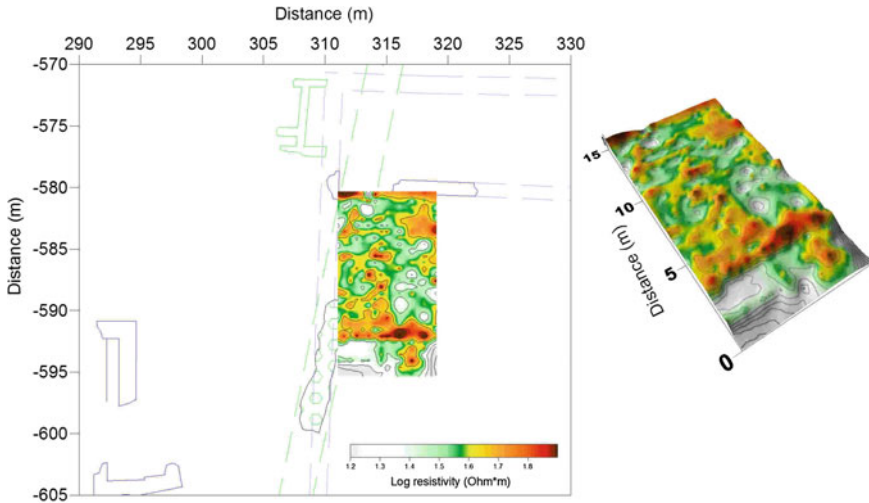
Fig. 4.82 ERT. Image and 3D map—0.5–0.75 m in depth—Area E

parallelogram shape of the blocks.

With the results obtained after the elaborations of the first aerial data sets and field-walking surveys, has been possible to map the town—planning, drawing the main road system inside and outside the town (Ceraudo 1999).

Located in different portion of the studied area, it is possible to observe the remains of some monumental ancient buildings as the *theatre*, the *capitolium*, the *amphitheatre*, the ancient walls. It was possible also to reconstruct the particular shape of the urban-planning and some blocks, Fig. 4.83. Although the analysis of the air photo evidence allowed the global interpretation of the site, it was not possible to reconstruct the archaeological evidences in the central portion of the town northern to the *theatre* (Ceraudo 2004, 2007), Fig. 4.83.

The Project, during 2008, started with new acquisition and elaboration of aerial photos, field-walking surveys and extensive geophysical surveys [Ground Penetrating Radar (GPR) and Fluxgate Differential Magnetic (FDM) surveys] with the aim to better define the urban plan of the central portion of the ancient town, Fig. 4.83.

4.4.4.2   Survey Planning and Data Processing

After the interpretation of new oblique aerial photographs and field-walking surveys, archaeologists have focused their attention on the S. Pietro Vetere area (property of Castrocielo Municipality). This area is characterised by the presence of some isolated buildings, located closely to the main road-system. With GPR method a high-resolution data acquisition technique has been adopted with the aim to reconstruct a global vision of the investigated area. GPR surveys were

performed, during October 2008 and from February till April 2009, for a total of 5 hectares as a extensive field work, employing a SIR 3000 (GSSI), equipped with a 500 MHz bistatic antenna with constant offset, to survey the selected area. Single-fold exploratory profiles were first carried out at the site with the objectives of: (1) preliminary identification of the targets; (2) calibration of the instrument; (3) analysis of the subsurface response as a function of the orientation of the profiles. Some signal processing and representation techniques have been used for data elaboration and interpretation (Piro et al. 1998, 2011; Goodman and Piro 2008).

A total of 2125 adjacent profiles across the site were collected alternately in forward and reversed directions (zigzag) across the survey grids employing the GSSI cart system equipped with odometer. The spacing between parallel profiles was 0.5 m. All radar reflections within the 65 ns (two-way-travel) time window were recorded digitally in the field as 8 bit data and 512 samples per radar scan.
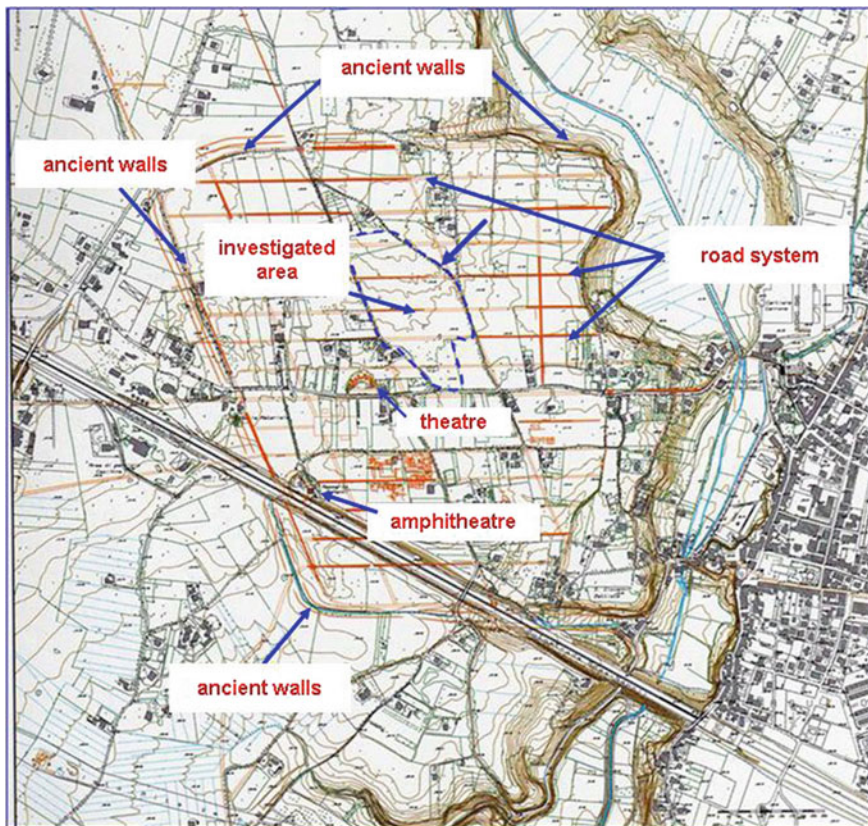
Fig. 4.83 Aquinum. Archaeological map. The arrow indicates the studied area

A nominal microwave velocity of about 7 cm/ns was determined from fitting hyperbolas to the raw field data. This was used in estimating a penetration depth from the GPR survey. All the GPR data were processed in GPR-SLICE v7.0 Ground Penetrating Radar Imaging Software (Goodman 2016). The basic radar-gram signal processing steps included: (i) post processing pulse regaining; (ii) DC drift removal; (iii) data resampling and (iv) background filter (Goodman and Piro 2013).

With the aim of obtaining a planimetric vision of all possible anomalous bodies individuated in the ground, the time-slice representation technique was applied using all field profiles (Piro et al. 2011; Goodman and Piro 2008, 2013; Goodman et al. 2008; Leckebusch 2008; Linford 2004). Time-slices are calculated by creating 2-D horizontal contour maps of the averaged absolute value of the wave amplitude from a specified time value across parallel profiles, Fig. 4.84.

Time slice data sets were generated by spatially averaging the squared wave amplitudes of radar reflections in the horizontal as well as the vertical. The squared amplitudes were averaged horizontally every 0.25 m along the reflection profiles 3 ns time windows (with a 10% overlapping of each slice). The resampled amplitudes were gridded using the inverse distance algorithm with a search radius of 0.75 m. In addition pseudo three-dimensional volumes of the reflections were generated to produce isosurface images.

All the obtained results are presented in 3D animation using real time Open GL graphic displays in which isosurface rendering, 3D time slice fence diagram are mixed with the raw filtered radargrams.

For the FDM Magnetic survey the measurements were carried out using a GEOSCAN FM 256 fluxgate gradiometer in September 2010 and March 2011. This instrument measures the vertical gradient of the Z component of the Earth magnetic field with a fixed inter-sensors spacing of 0.5 m. The measurements were collected with a sampling interval of 0.5 m along each profile. The total surveyed area was subdivided into many 20×20 m squares and all profiles were recorded parallel to each other S-N profiles spaced 0.50 m apart.

The magnetic data, after the usual pre-processing techniques such as de-spiking, filtering and rearranging, Piro et al. (1998, 2007) are represented by the gradient of the Z component for the all assembled squares (Fig. 4.85).

The magnetic measurements, in this particular portion of the site, present a good S/N ratio; to use these data sets for the development of the integrated approach, the bidimensional cross-correlation technique was applied to achieve a better estimate for the centre of prospected body.

The problem of recovering the anomalies masked by the noise is to choose and to apply suitable techniques to improve the signal-to-noise ratio. As showed in detail in the previous papers (Piro et al. 1998, 2007), that if we have at least a rough estimation of the shape, dimensions and physical properties of the expected body, the best filter (operator) is the theoretical anomaly of the structure itself, this operator is "*an absolute optimum*" in the case of Gaussian noise. In the particular case of coherent noise (autocorrelated) the best operator is still the theoretical anomaly which minimizes the prevalent frequencies of the autocorrelated noise.
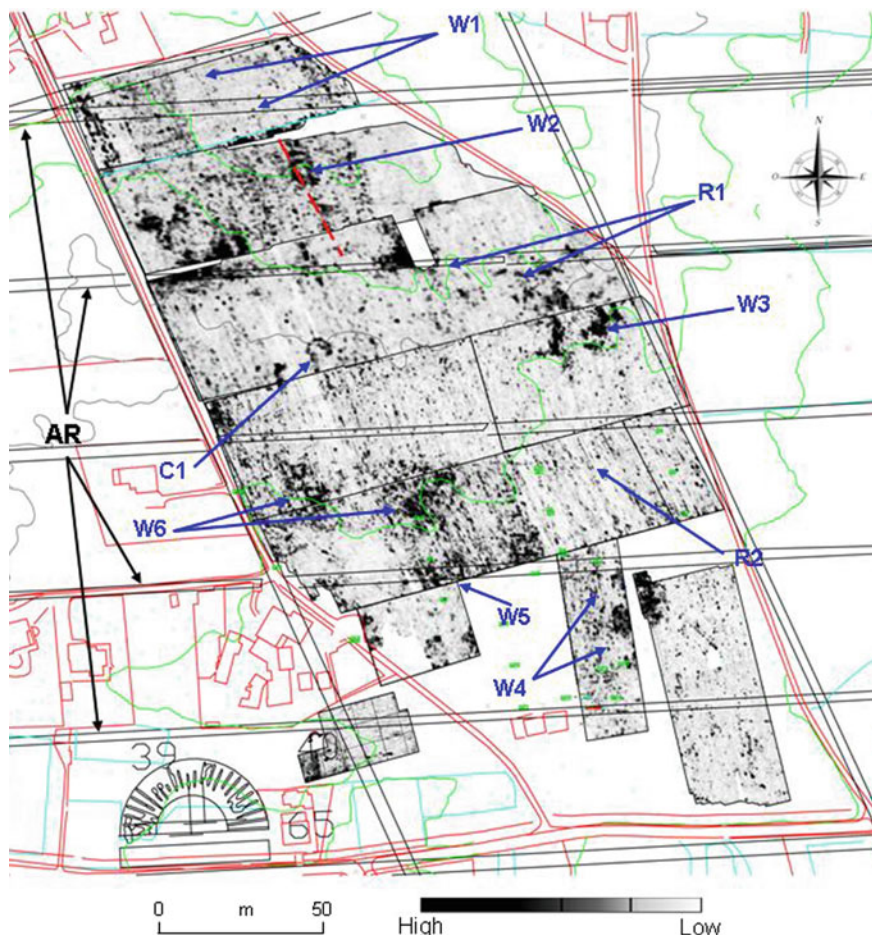
Fig. 4.84 Aquinum. GPR slices at the estimated depth of 0.65 m. The arrows indicate some clear reflections

The application of this operator, in the space domain, consist in the cross-correlation of the raw field data with the calculated theoretical anomaly resulting in a cross-correlation function that is a measure of similarity between sets of data (Piro et al. 1998, 2007). The theoretical magnetic anomalies for a body with dimensions of $1 \times 1 \times 1$ (grid units) were computed using the relations proposed in the previous paper (Piro et al. 2007). The calculations were performed with geomagnetic parameters: F = 45,000 nT, I = 55°, D = 0° and uniform magnetization M of the body. For uniform susceptibility contrast, different values were used in relation to the different archaeological site conditions.
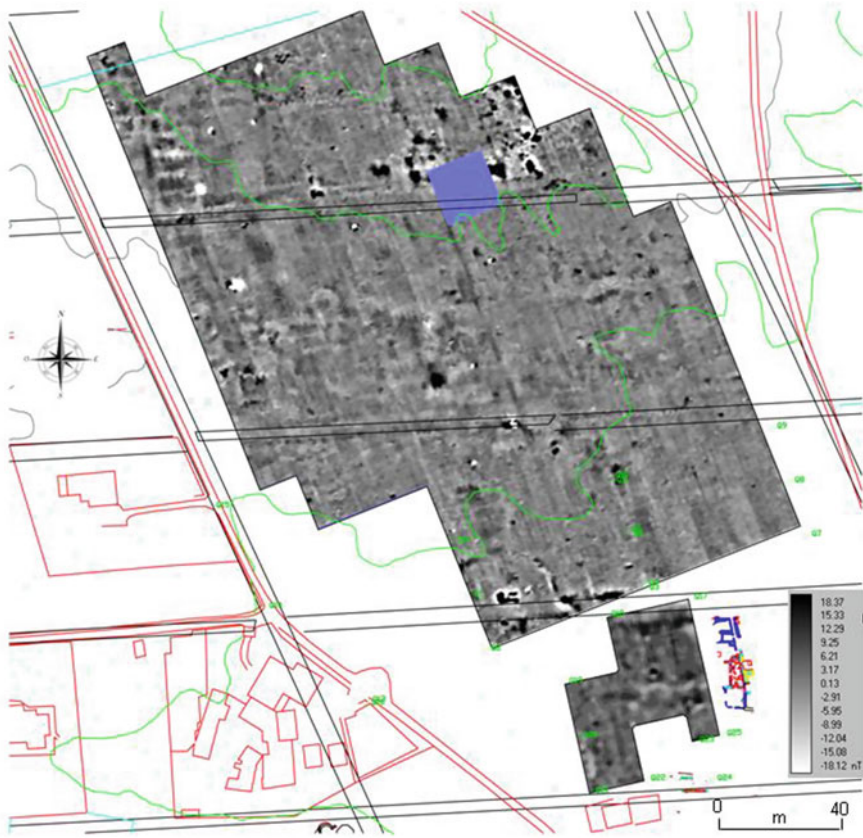
Fig. 4.85 Aquinum. Fluxgate gradiometer gridded contour map of the total surveyed area. Data range from -19 to +19 nT/m.

4.4.4.3 Geophysical Results

The corners of each surveyed sectors have been positioned on the topographical map after a differential global positioning system (DGPS) survey and then all georeferenced GPR maps have been imported into a geographic information system (GIS) to allow data visualization, estimation of the averaged dimension and interpretation.

Figure 4.84 shows an example of the GPR amplitudes map in the time window 17–19 ns (twt), corresponding to the averaged estimated depth of 0.65 m. The images represent a portion of all investigated surfaces in the selected area. Some of the most clear reflectors are indicated with the blue-arrows. It is possible to observe the different dimensions, orientation and shapes of the individuated structures that have been interpreted with the help of the archaeologists as walls of rooms and buildings still present in the ground.

Figure 4.85 shows the contour map of the gradient of Z component of the Earth Magnetic Field. The analysis of this map shows that the larger survey area is characterized by many dipolar anomalies in a range of −35, +55 nT/m. These anomalies are spatially organized as pseudo-linear or circular features and are characterized by a prevalence of the positive component of the dipole.

Figure 4.86 shows the contour map of the gradient of Z component and the results of the normalised 2D crosscorrelation for the southern investigated area. If the normalized cross-correlated values should approach unity for one output, the best synthetic operator will fit the field data. From this information and our assumptions about the other source/field parameters, it seems possible to determine the location and limit the depth-range of the investigated area (for details see Piro et al. 2007).

The analysis of these figures show that the investigated area is characterized by the presence of anomalies due to many buried bodies, forming a linear distribution perhaps interpretable as wall's remains and segments of the hypothesized ancient roads. The obtained results closely match the aerial photograph interpretation and show also that, in the southern part of the investigated area, clear unexpected archaeological structures as building's remains are still present in the subsurface.

In Fig. 4.87 a portion of GPR slice at the estimated depth of 0.70 m, corresponding to the southern part of the studied area, is shown. These slices represent unexpected results, respect to the information obtained with aerial photographs, which has induced the archaeologists to focus here their attention with an excavation test made during summer 2009–2010 on two limited portions of this area.

The first, investigated for a surface of 100 m^2, is characterised by the presence, at depth of 0.35 m, of a wall (made in '*opus reticolatum*'), east-west oriented and visible for a length of about 9 m.

The second excavated area, is located north-eastern respect the first one and has been investigated for a surface of about 400 m^2. In this area, wall's remains related to rooms previously located with GPR survey, have been found and interpreted as public thermal building. The central room (B) with trapezoidal plan with dimension of 20 m^2, north-south oriented, has been identified as a worm room heated with hot air circulating below the floor and behind the walls (*Caldarium*). Other heated rooms inside the thermal building have been found at south (E, with averaged dimension of 6 m × 6 m) and at west (D, partially excavated), while northern to this a small room (A) with a surface of about 6 m^2 has been discovered. The eastern area, investigated for a space of 11 m in length and 1.5 m in width is characterised by the presence of a tessellated paving, which has been interpreted as undressing room ('*Apodyterium*') Fig. 4.87.
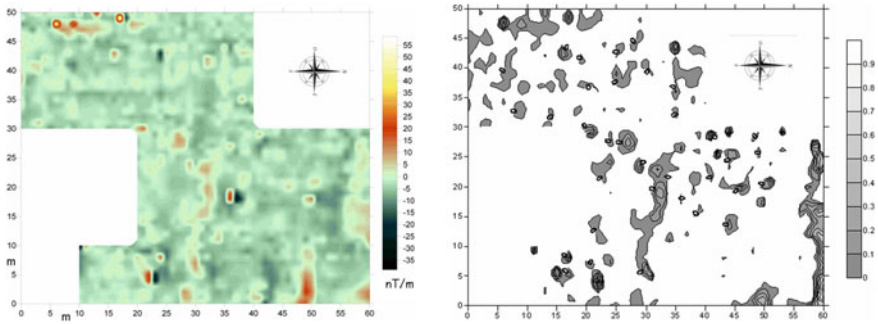
Fig. 4.86 Aquinum. Fluxgate gradiometer gridded contour map of the southern portion of the investigated area (left); contour map of 2D normalised crosscorrelation (right)

4.5 Preventive Archaeology

4.5.1 GPR Surveys in the Territory of Ancient Tarquinia (Viterbo, Central Italy)

4.5.1.1 Introduction

The paper presents the results of a study of the territory of Ancient Tarquinia (Viterbo, Central Italy). The work is part of the University of Milano's "Tarquinia Project", which studies the monumental area of this territory with particular attention to the "*Ara della Regina*" temple site.

To enhance the knowledge of this territory, finalised to the location and the conservation of the unknown buried structures, below the actual studied levels, a scientific collaboration between the University of Milano (Department of Science of Antiquity) and the Institute of Technologies Applied to Cultural Heritage (ITABC-C.N.R.) has been developed, during the time 2000–2004 based on the integration of topographical surveys, the 3D lasers scanner survey of the temple and the ground-based remote sensing surveys.

The remote sensing surveys were carried out using the Ground Penetrating Radar (GPR) method.

The researches of the University of Milano, related to the tableland of "*monumental area of Ancient Tarquinia*" (Civita plateau) Fig. 4.88, have interested and will interest the big sanctuary (temple), known till nineteenth century with the name of "*Ara della Regina*", Fig. 4.89. This monument has been interested by a systematic studies made, firstly, by Prof. Pietro Romanelli in the period 1930–1940. These studies have been enhanced by "Soprintendenza Archeologica per l'Etruria Meridionale" in the period 1957–1969 and from 1983 till now by the University of Milano (Department of Science of Antiquity).

The archaeological documentation indicate that the Civita Plateau and the Ara della Regina site have been selected in the past as location for the religious and
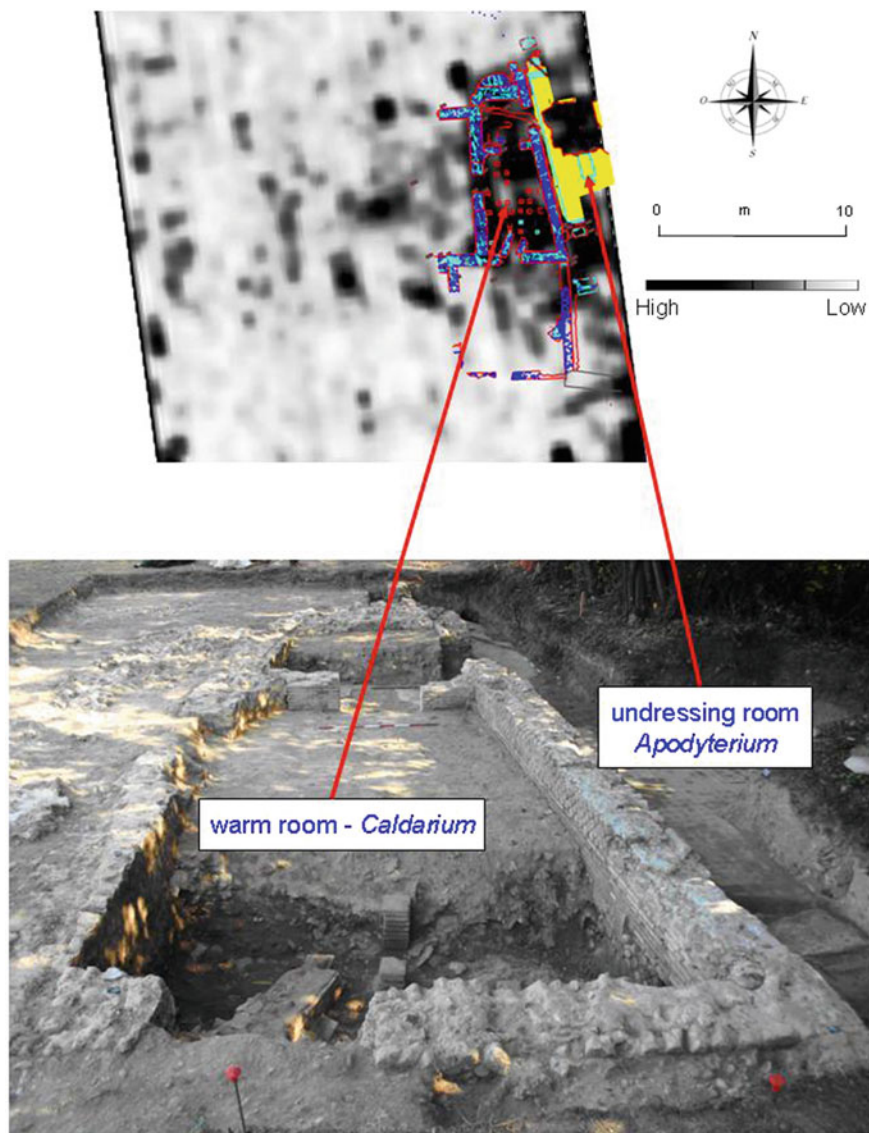
Fig. 4.87 Aquinum (Castrocielo, Frosinone). Southern portion of S. Pietro Vetere area. Details of the archaeological survey overlapped on a portion of GPR slice at the estimated depth of 0.65 m. Picture of the discovered rooms after the first excavation, summer 2009

political meetings for Etruscans leaving in that territory. The Ara della Regina Temple, built over a big basement, with East-West orientation, is lined by two roads, coming respectively from the ancient town and from the valley and converging towards the entrance of the monument. The temple, in the last phase, was

characterised by a "*pronao*" with columns, by the *cella* and by two "*alae*". Over the smaller basement of the older construction (Temple I; VI century), it has been added a second basement which represents the big terrace with, in the middle, a steps (Temple II; end of VI century). The archaeological excavations made during 1986–1993 (Prof. Bonghi Jovino 1993), have confirmed that this second building had annexed the smaller temple of the first middle of VI century.

The more recent studies are related to the re-reading of the basement of the sanctuary, new detailed archaeological excavations, new surveys of the surrounding area with the aim to understand the develop of the temple area in relation to its territory.

Since 2000 a scientific collaboration between the Department of Science of Antiquity (University of Milano) and the Geophysical team of the Institute of Technologies Applied to Cultural Heritage (ITABC-CNR) has been developed with the aim to locate the unknown buried structures, below the actual studied level.

The integrated project is based on the following items: (a) topographical survey, based on the application of integrated methodologies (D-GPS and a Total Station system), with the aim to construct topographical micro-model; (b) the survey of the "Ara della Regina Temple", based on the employment of Laser Scanner 3D, with the aim to obtain a very high density measurements to construct geometrical models of the monument; (c) high-resolution GPR investigations, with the aim to define the location, the shape, the dimensions and the depth of the unknown archaeological structures.
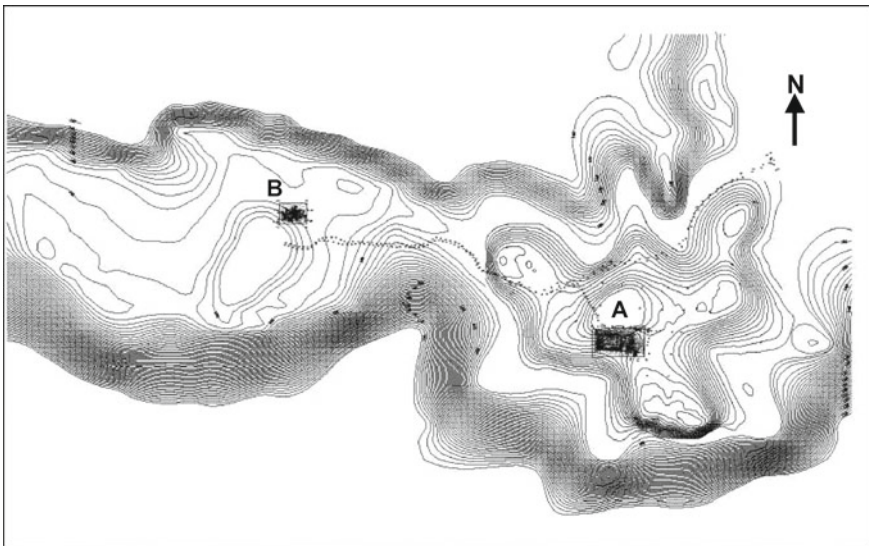

Fig. 4.88 Tarquinia (Viterbo). Topographical representation of the Ancient Tarquinia. **a** Ara della Regina temple; **b** Civita monumental area (scale 1:10,000)
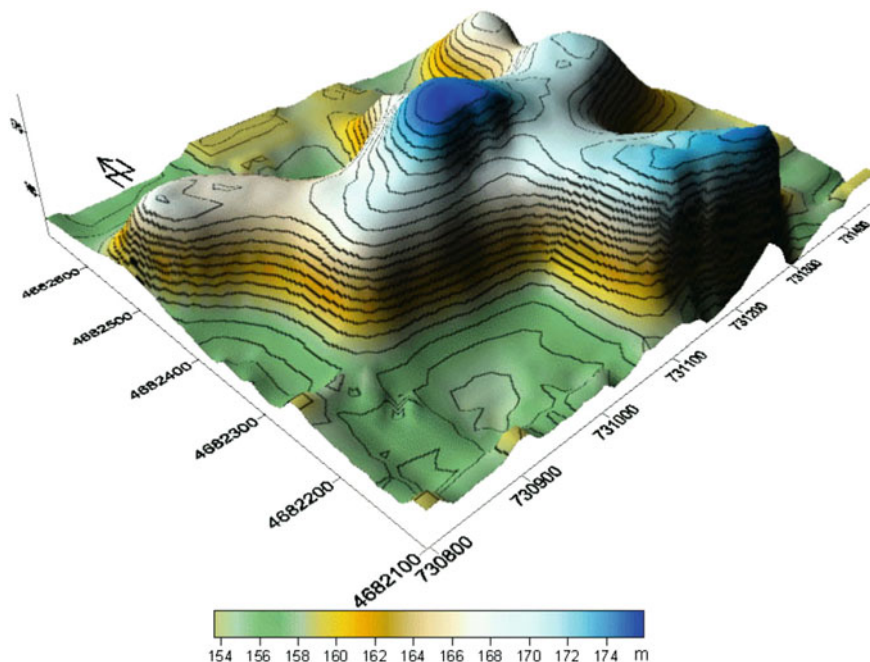
Fig. 4.89 Ara della Regina plateau. Topographical three-dimensional representation

4.5.1.2   Survey Planning and Data Processing

From 2000 to 2004, a series of topographic and high resolution GPR surveys took place at "Ara della Regina temple" site which provide a basic map of the ancient temple centre. The topographic survey permitted standing monuments and contemporary features to be located within a common grid, while remote sensing surveys allowed the identification of buried structures and features.

Taking into account the surface condition of the "Civita plateau", in particular the presence of vegetation with different height and outcrops in the surface, the selected area have been surveyed topographically employing a D-GPS (Differential Global Positioning System) model SR530 Leica, integrated with an Elettronic Total Station Trimble (model 5600).

The measurements were made to reconstruct the topography of the studied area, to insert the three dimensional image of the temple and to locate the surfaces investigated with GPR method. For the micro-morphological representation with contour map, the surveyed area has been integrated with the contours extracted from the digital Regional Topographic Map (CRT, 1:10,000) and the final contour map has been obtained with a contour interval of 1 m, Fig. 4.91. The topographical survey has been employed to construct also the three-dimensional model of the terrain, which represents the morphological aspect of the territory, Fig. 4.89.

For the high-resolution survey of the "Ara della Regina" temple a Laser Scanner Callidus CP 3200 system (Trimble) was employed. The measurements have been collected from 16 view-points with a sampling of 0.125°, for the horizontal resolution, and a sampling of 0.25° for a vertical resolution. During the survey, a digital camera has been used to collect pictures of the investigated surface of the monument. For the elaboration the 3D-Extractor software was employed, which automatically lines up the pictures made by digital camera together with a polygonal model, making a three-dimensional geometrical reconstruction. The software stores automatically the three-dimensional measurements and reconstructs only one three-dimensional object (in this case the temple), Fig. 4.90a, b. The obtained geometrical model gives us the global vision of the monument and the possibility to extract geometrical and visible information (Soucy et al. 1996a, b).

With GPR method a high-resolution data acquisition technique has been adopted with the aim to reconstruct a global vision of the investigated volume of subsoil. GPR surveys were performed, during September 2000–2002, for a total of 3 weeks as a field work, employing a SIR 10A$^+$ (GSSI) equipped with a 500 MHz bistatic antenna with constant offset and with 70 MHz monostatic antenna, to survey the area round the Ara della Regina temple; during October–November 2004, for a total of 4 weeks as a field work, employing a SIR 3000 (GSSI), equipped with a 500 MHz bistatic antenna with constant offset to survey the area outside the temple site. Single-fold exploratory profiles were first carried out at the site with the objectives of: (i) preliminary identification of the targets; (ii) calibration of the instrument; (iii) analysis of the subsurface response as a function of the orientation of the profiles. Some signal processing and representation techniques have been used for data elaboration and interpretation (Goodman et al. 1995, 2004; Malagodi et al. 1996; Piro et al. 2003, 2004).

A total of 1694 adjacent profiles at the site were collected alternately in reversed and unreversed directions across the survey grids. The horizontal spacing between parallel profiles at the site was 0.5 m. Radar reflections along the transepts were recorded continuously, with different length, across the ground at 80 scan s^{-1}; horizontal stacking was set to 4 scans. Along each profile markers were spaced every 1 m to provide spatial reference. All radar reflections within the 65–85 ns (two-way-travel time) time window were recorded digitally in the field as 8 bit data and 512 samples per radar scans.

When GPR profiles are collected on closely spaced profiles, the data can be processed to display horizontal maps of the recorded radar amplitudes. Referred to as time slice processing, these anomaly maps can be generated at various time/depth windows across the recorded radargram dataset. The time slice maps can provide information regarding the size, shape, location and depth of subsurface archaeological structures buried beneath a site (Goodman and Piro 2013; Piro et al. 2003, 2004).

Time slice data were created using the spatially averaged square wave amplitudes of the return reflection. The squared amplitude, which is essentially the energy in the waveform, was averaged horizontally every 0.25 m along the radargram profile, and in 4 ns time windows to create a time slice parameter. These
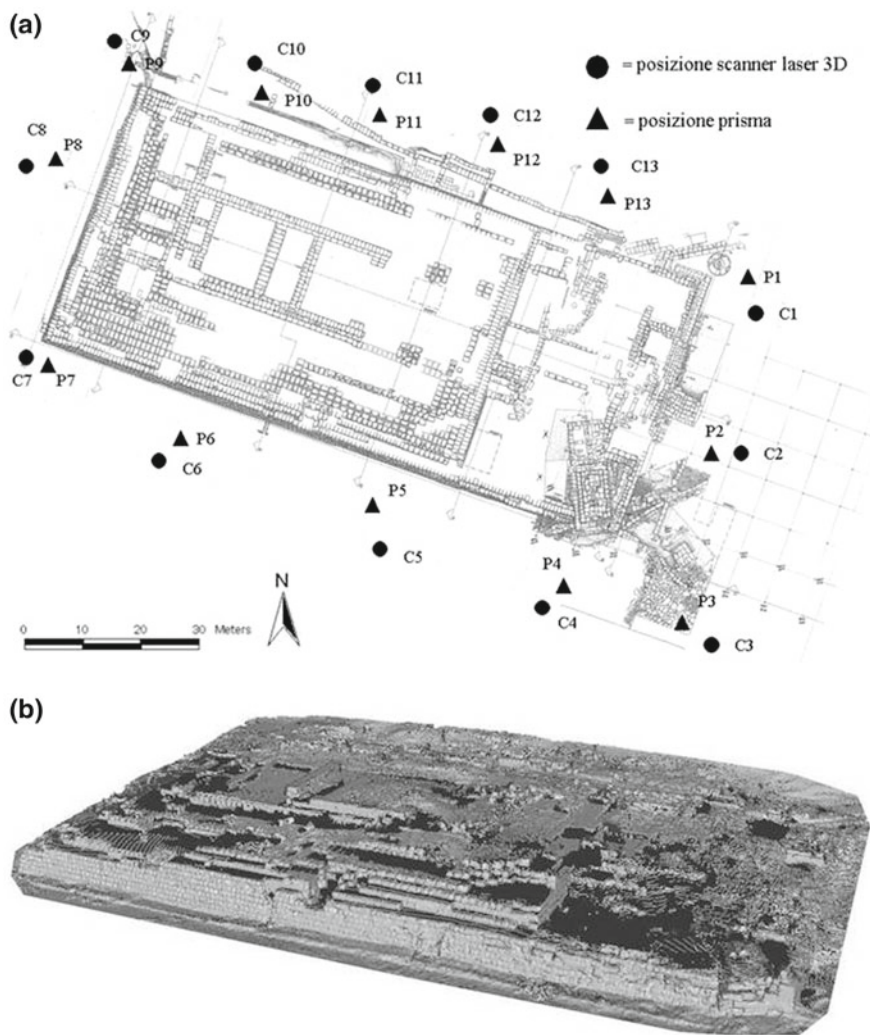
Fig. 4.90 a Ara della Regina temple. First digital reconstruction and geometrical three-dimensional model of the southern side of the monument. **b** Ara della Regina temple. Corner S-W, view from the station P7 of the laser scanner

averaged square amplitudes were then gridded using a Kriging routine that included a search of all data within a 1.0 m radius of the desired point to be interpolated on the grid (Goodman and Piro 2013).

Filter was used to remove the background reflections. Other line noises, parallel to the profile direction, were removed using a moving filter with customised threshold settings. Filter thresholds were set to signal levels just below the average reflections from buried Roman walls.
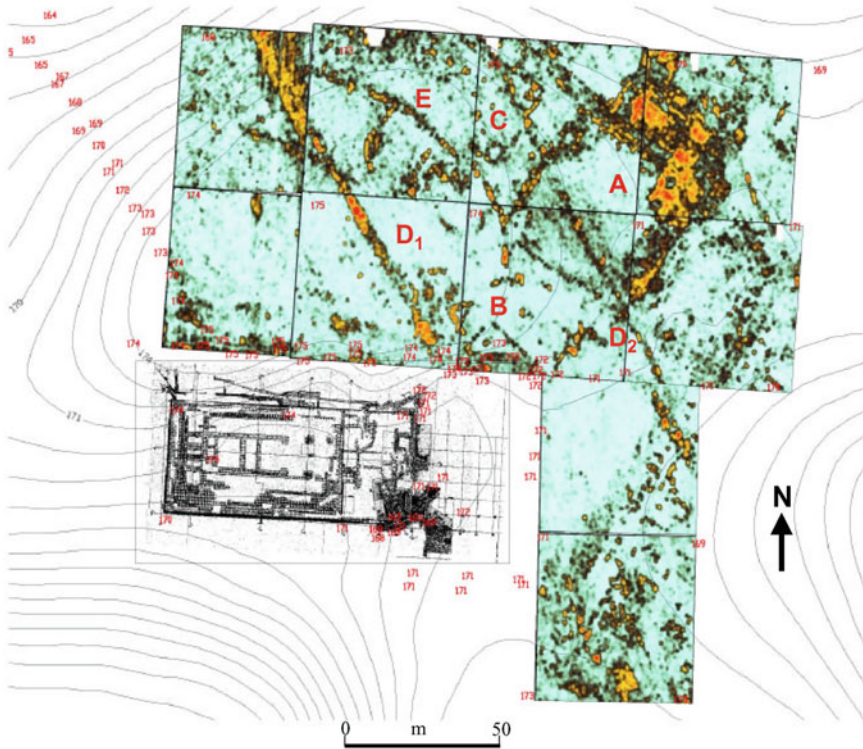
Fig. 4.91 Area outside the Ara della Regina temple. GPR time slices at the estimated depth of 0.50 m

A high-to-low amplitude scale is normally presented as part of the legend of each map, but without specific units because, in GPR, absolute reflected wave amplitudes are usually arbitrary.

4.5.1.3 Results

Figure 4.91 shows the GPR time slices at the estimated depth of 0.50 m (171.50 m sea-level) in the area outside the temple site. The investigate area is characterised by the presence of many anomalies due to wall's remains with different direction and dimension. It is possible to see the remains of a building with dimension 59 m in width and 70 m in length (anomaly **A**); a small building with dimension 13 m in width and 21 m in length (anomaly **B**) and other short rooms with average dimension of 11 m × 7 m and 11 m × 6 m (anomalies **C**). The area is charac- terised by other linear structures **D1** and **D2**, parallel each other, with a length of about 150 m, which go through the area with direction N-W and S-E. These anomalies have been correlated to medieval subdivision of the ground.

The anomalies individuated at this depth are visible also in the Fig. 4.92 at the estimated depth of 0.80 m (171.20 m sea-level) and 1.10 m (170.90 m sea-level).

The results obtained in the Ancient Tarquinia's territory indicate that the plan of portion of previous building can be identified and characterised from the ground based remote sensing surveys.

As known topographical surveys made employing high-resolution acquisition techniques give us the possibility to reconstruct a micro-model of the ground; the use of 3D laser scanner technology permits to collect a high number of measurements with which it is possible to reconstruct the accurate three dimensional image of the temple, giving us the global vision of the monument and the possibility to extract geometrical and visible information. Finally, the location, depth, size and general structure of the buried buildings were effectively estimated from non-destructive remote sensing with a ground-penetrating radar system.

4.5.2   ERT surveys in the territory of Petroio (Valdarno Inferiore, Florence, Italy)

Petroio is a hamlet belonging to the municipality of Vinci, which is situated in Arno valley, called Valdano Inferiore, on the slopes north-west of Montalbano, 30 km from Florence (Italy).

Archaeologically its history is linked to an Etruscan occupation, becoming later on in time a Roman camp.

The castle that today is the Leonardian museum dates back to Medioeval times and it was dominated by the Tuscan Family of Count Guidi (1164). Isolated from the main part of the town with an ellipse plant, it is partially surrounded by a wall.

The geophysical investigations have been conducted on a small hillock and its morphology leaves us to suppose not a natural origin but an anthropic one (Fig. 4.93). This part of Tuscany is in fact well-known for the presence of material evidence which refers to Etruscan period. Not far from the small hillock remains an ancient church is found, resulting in the plans relative to the eighteen hundreds (1800s) conserved in the Leopoldino Land Registry Office.

4.5.2.1   Survey Planning

The area has been investigated with ERT method using instruments with a continuous current.

The choice has been made, both by considering the depth of investigation to reach (over 5 m) and also for the morphology of the site that is presented as a hillock with quite sloping versants (Fig. 4.94a).

Profiles have been acquired both of the four sides of the rise and also of the central area that represented the part topographically elevated. It has been used a
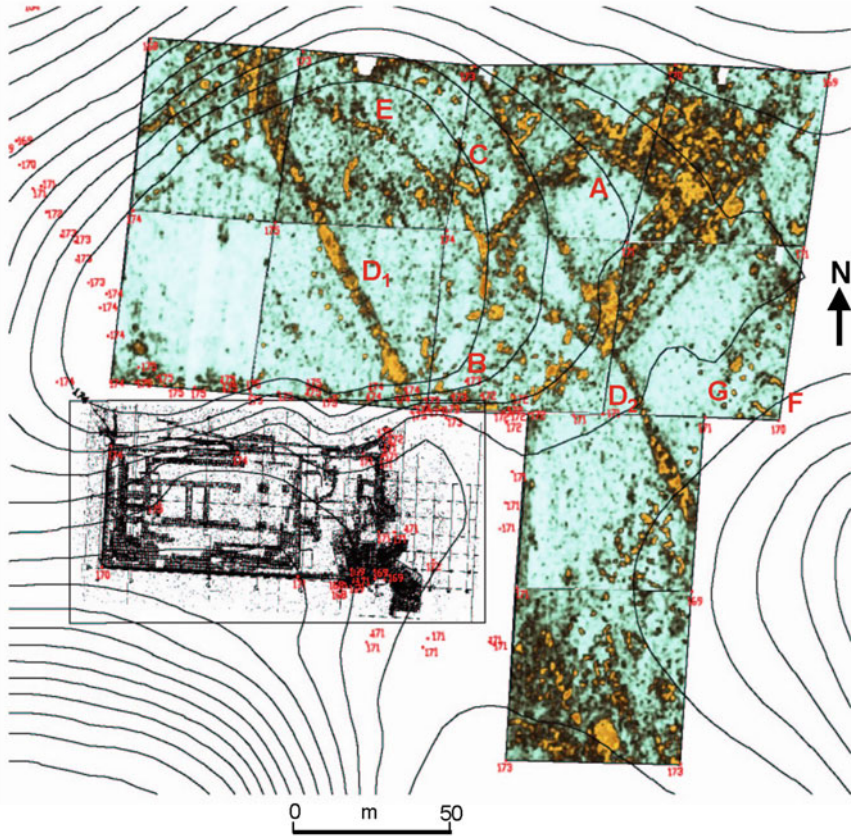
Fig. 4.92 Area outside the Ara della Regina temple. GPR time slices at the estimated depth of 0.80 m

dipolar array with 32 electrodes, dipolar spread of 1.2 m. The grid presents regular parallel profiles equally spaced about 1.5 m.

A topographic survey has also been conducted out with a total station to determine precisely measure points (Fig. 4.94c).

4.5.2.2   Data Processing and Results

Figure 4.95 shows a horizontal section obtained through the application of the probability-based ERT inversion applied to the $\{\rho a\}$ datasets from the depth of 1–2 m up to 4.2 m from the spatial planning. Figure 4.96 shows a 3D image at the depth of 2.4 m in which many anomalies are very evident. The first is a high-resistivity system with ovoid alignments, constituted by two rings approximately concentric.

Fig. 4.93 Localization of Petroio, Vinci-Firenze (www.vinci.ldpgis.it; www.google.it)

The very regular form and continuity of these anomalies leave us to suppose the presence of wall structure. This system seems to interrupt only in two points, probably because there is the presence of two accesses if the structure results to be a tumulus.

A strong resistive anomaly is present externally to this double oval, highlighted in the centre by a more conductive one and positioned on the borders of the investigated area. It could be supposed it refers to an area of land with a backfill of earth.

In the centre of the map, on the inside of the above-mentioned anomalies are highlighted a new high resistive system and a low resistive one with a nearly regular course. The first is better shown in Fig. 4.96 at the depth of 1.8 m and it could be reported to an empty cavity on a wall structure. The opposite values taken in a range from −0.02 to −0.012 Ω m, can be linked to the absence of a structure or a cavity backfilled with earth. Some essays on excavations made at the summit of the hillock confirm the presence of ancient walls in the same direction with what has been identified by the geophysical survey.

Fig. 4.94   a Investigated area; **b** acquisition data; **c** topographic survey

4.6   Ancient Viability

4.6.1   Remote sensing, EMI and ERT surveys for studying the Road Network of Egnazia site (Fasano (Brindisi), Italy)

Egnazia is located in southern Italy, in Puglia Region (Fig. 4.97). It was an important center of the Messapia and an example of a multi-stratified city, *municipium* after the social war and episcopal location since the second half of the IV century A.D. (Cassano et al. 2007). Thanks to the absence of modern overlays, it allows to verify forms and dynamics of living within a long period between the age of Romanization and the High Middle Age.

   The first urban settlement appeared between the end of the IV and III century. BC receiving a more organized organization, even with regard to the viability, in the following centuries. Between the ages of Augustus and the I century A.D., spaces and structures typical of a Roman city were realized and, at the beginning of the II century A.D., they were remodeled, especially in the area crossed by the Via *Traiana,* the main road. After the middle of the IV century A.D., there was a sharp change in the urban and rural landscape with a strong vitality until the end of the

Fig. 4.95 ERT. Image map,
1–4.2 m in depth
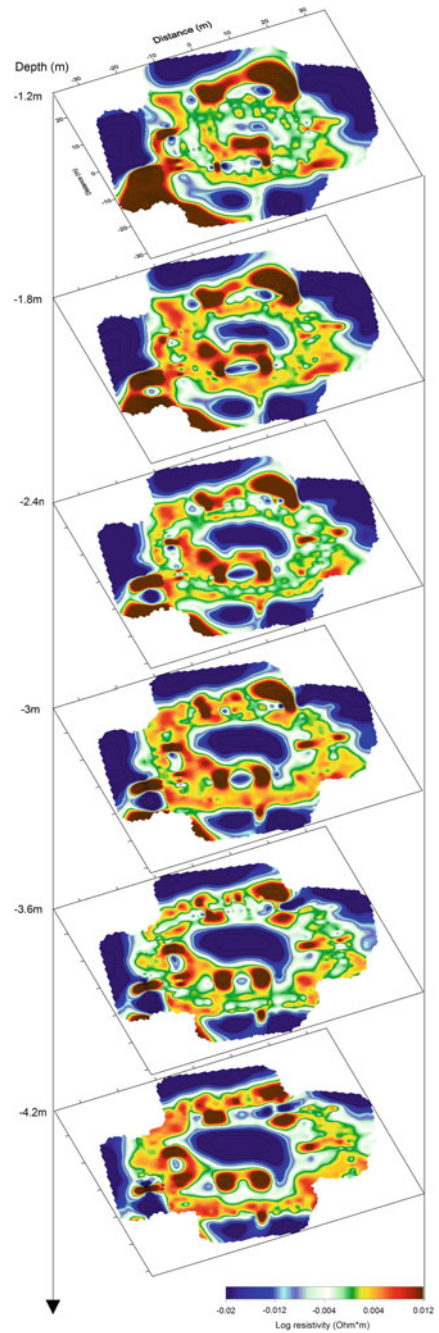
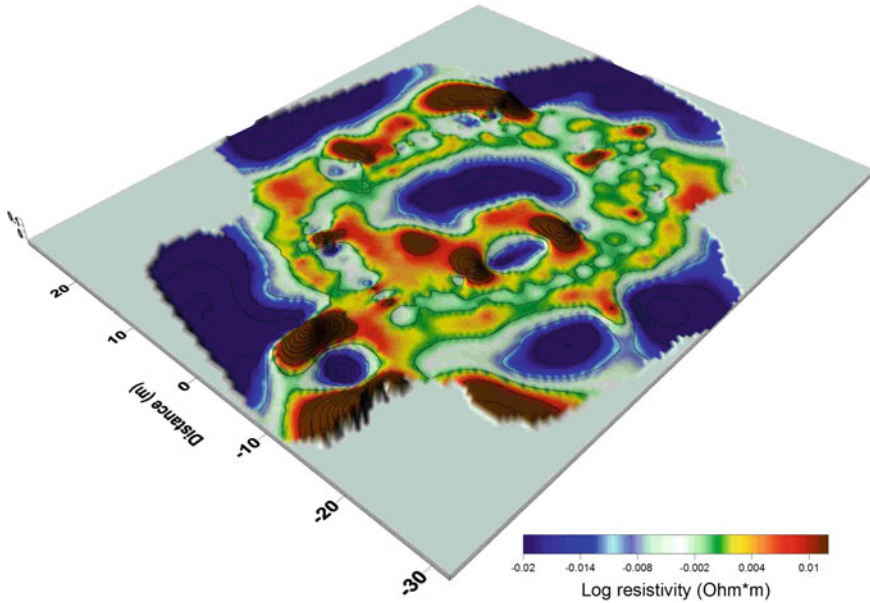sixth century. Subsequently, the inhabitant returned to rest within the ancient

Fig. 4.96 ERT. 3D map, 2.4 m in depth

acropolis and continues until the XIII century A.D.

In the area already under investigation, the Via *Traiana* plays a priority role: it passes through the city in the direction of NO-SE, separates the public areas, concentrated between the road and the acropolis, from the residential and production areas, and continues towards Brindisi, in the sothern part of Puglia Region. To the east of the street, monumental buildings are placed side by side in a single public sector without the use of secondary arteries. To the west of the main road, instead, the homes and the crafty areas are located within isolated blocks defined by secondary roads that start right from the path of the Via *Traiana*. These roads, oriented in the NE-SO direction, are placed at a regular distance ranging from 30.39 to 30.94 m. The trend is regular, though not orthogonal: it is particularly evident they are diverted to the SW in the southern part of the excavated area.

Multi-methodological researches were realized for a wider reading of Egnazia urban viability through the GIS study of historical and modern cartography, the analysis of multispectral, multitemporal and multi-scalar aerial and satellite imagery (MIVIS, QuickBird, Google Earth™), integration and verification of remote data through geophysical data and archaeological surveys. The research was carried out in the frame of the Project "Landscape Archeology of Adriatic Puglia in roman age: innovative technologies for sustainable planning and knowledge of cultural identity", by the Italian Universities of Molise and Bari and the Politecnico di Bari.

Fig. 4.97 The archaeological site of Egnazia (BR), Italy

4.6.1.1   Survey Planning and Data Processing

The surface layer of the soil covering archaeological remains can differ from the surrounding matrix for compactness, fertility, water content, chemical and physical characteristics. These factors generally result in anomalies in growth, distribution, health status and density of vegetation or in color and tone of the soil, producing variations in spectral and thermal response, resulting in a different visibility of the same trace on remote sensing images (Piccarreta and Ceraudo 2000). The archaeological park of Egnazia is an area dedicated to seasonal farming activities, which in fact make the alternation for the same field of bare ground and vegetation. Taking into account these considerations, remote images have been elaborated to emphasize even the slightest spectral variations with different processing techniques such as the Principal Components Analysis (PCA) transformation, the Normalized

Difference Vegetation Index (NDVI) calculation, the Supervised Spectral Angle Mapper classification (SAM) and the Thermal Capacity calculation (CT).

For this study, an important image dataset was acquired by aerial and satellite platforms:

- 1 panchromatic aerial photography of 1967;
- 1 color digital ortophoto at 1:10,000 nominal scale (IT2000 flight of the Italian Ministry of the Environment) with resolution of 1 m/pixel;
- 2 orthophoto © 2004–2016 Blom Terra Italy, years 2005 and 2008, with a resolution of 0.50 m/pixel;
- 6 satellite imagery © 2013 DigitalGlobe Inc. of Gloogle Earth™ of (May 9, 2005; July 1, 2009; October 16, 2009; October 30, 2009; March 26, 2012; May 18, 2013);
- 1 color orthophoto of October 19, 2006 (457091) at a nominal scale of 1:10,000 (Ministry of Environment flight) with resolution of 1 m/pixel;
- 2 QuickBird images captured on February 14, 2008 and March 3, 2008 with a pixel resolution of 2.80 m/ pixel(multispectral) and 0.70 m/pixel (panchromatic);
- 1 MIVIS image owned by the *Carabinieri* Army acquired on September 20, 2011 at a relative flight altitude of 1500 m with a resolution of 3 m/pixel.

All elements of the dataset refer to the UTM-WGS84 (33N) cartographic coordinate system and a Geographic Information System (GIS) was built. The images resulting from the elaborations were interpreted from the archaeological and topographical point of view, trying to attribute a precise meaning to each single trace, comparing it with the assumed hypotheses and the results obtained by geophysical surveys and excavation activities.

Moreover non-invasive geophysical surveys were carried out within the archaeological park for a priori knowledge of the studied area verifying the presence of archaeological structures and road sections still buried into the subsoil.

During the early stages of the project, a sampling area of 23 × 54 m, near the *thermae* (Fig. 4.98), was identified where various survey methods were applied varying for each one setup and configuration parameters during data acquisition, mode and order of application of the techniques, data processing and correlation between different abnormalities, data reversal routines and representation of results. The objective of the preliminary test was to establish the best strategy for a quickly and accurately mapping of a vast area of the city taking into account the characteristics of the archaeological site (type of structures, dimensions and depth), the geological nature of the terrain, the logistic conditions of the area and the presence of anthropic disturbances.

Verified that the depth of the structures is included in the first 1.5 m of the subsoil and checked the response of the various systems to the ground conditions, it was decided to proceed with the integration of the electromagnetic induction survey and the tridimensional electrical tomography (Fig. 4.98). The first method was used to achieve a large-scale reconnaissance of the site, the second method was applied

to obtain a greater resolution in the discrimination of structures in the southern sector of the thermal system.

In the electromagnetic prospection, the GSSI Profiler EMP-400 (www.geophysical.com) was used. Data acquisition was carried out along lines filled in regular grids and spaced maximum 0.5 m. Data were collected in continuous modality (thanks to the integrated GPS in the instrument that allowed to acquire the geographical position of each measurement), using frequencies of 2000, 8000 and 15,000 Hz with a vertical orientation of the dipoles. During data processing, the conductivity values were converted into electrical resistivity values and they were represented with a contouring software for the realization of a two-dimensional map.

The three-dimensional geoelectrical tomography was realized through the combined use of a multichannel resistivimeter (A3000E, www.mae-srl.it) and a portable resistivimeter (ELMES ADD-01). The geometry of the electrodes used in data acquisition is the dipole-dipole axial configuration, particularly sensitive to the lateral variations of resistivity. During field operations, the device was moved along survey lines, spaced approximately 0.5 m, roughly parallel and georeferenced by a topographic station. The obtained data were then processed using the probability-based ERT inversion (PERTI) proposed by Mauriello and Patella (2009).
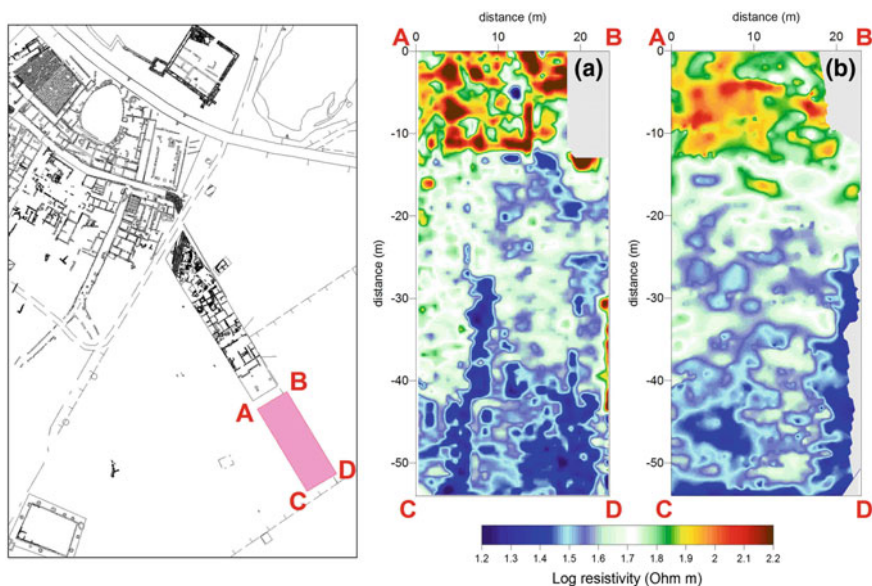

Fig. 4.98 The sampling area where the tridimensional electrical tomography (**a**) and the electromagnetic induction survey (**b**) have been applied during the preliminary test

4.6.1.2 Results

The photointerpretation of remote images have allowed detecting the presence of different linear light-colored traces, attributable to possible ancient paths, which arise both within urban and suburban areas. Figures 4.99, 4.100, 4.101 and 4.102 show some examples of remote sensing, showing the identified archaeological traces.

Anomaly no. 1 is visible above all on historical aerial photographs (Figs. 4.99 and 4.101b). It is found in the southern part of the city, from the South Gate continuing to north through the residential district, the thermal system and the public buildings area. Taking into account the topographic information and the different colors and shades of the trace compared to the surrounding terrain, it is possible to identify it as pertaining to the ancient route of Via *Traiana*. In the northern sector, next the public buildings, documentation from the various excavation campaigns carried out after 1967 confirmed that identification (Fig. 4.103).

Another important trace (no. 2), located on aerial photography of the 1967 (Fig. 4.99), is located in the southern part of the city, near the eastern side. The anomaly is visible on the aerial photos as a linear dark-colored path bordered on both sides by a light-colored trace. By type, color and shape it has been identified as pertinent to an ancient road. This artery starts from Via *Traiana* in the point where the *decumanus* describes the curve between the civil *basilica* and the *thermae*. The recent excavations have highlighted the first segment of this road: it is only pedestrian, as it should be probably in the whole part that across the square of the *forum*. After passing this area, the road seems to divert to get out of the town and continue on the coastal path of which a section was recently discovered in the rocky bank (Palazzo 2009).

Two distinct anomalies (no. 3–4, Figs. 4.99 and 4.101b) have been identified in the eastern side of the Via *Traiana*: they are parallel and curve in the direction of
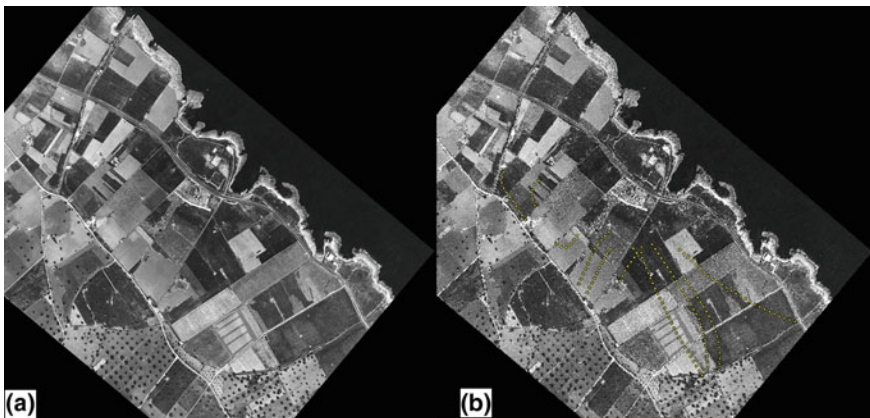

Fig. 4.99 Aerial photograph (1967) showing the identified archaeological traces
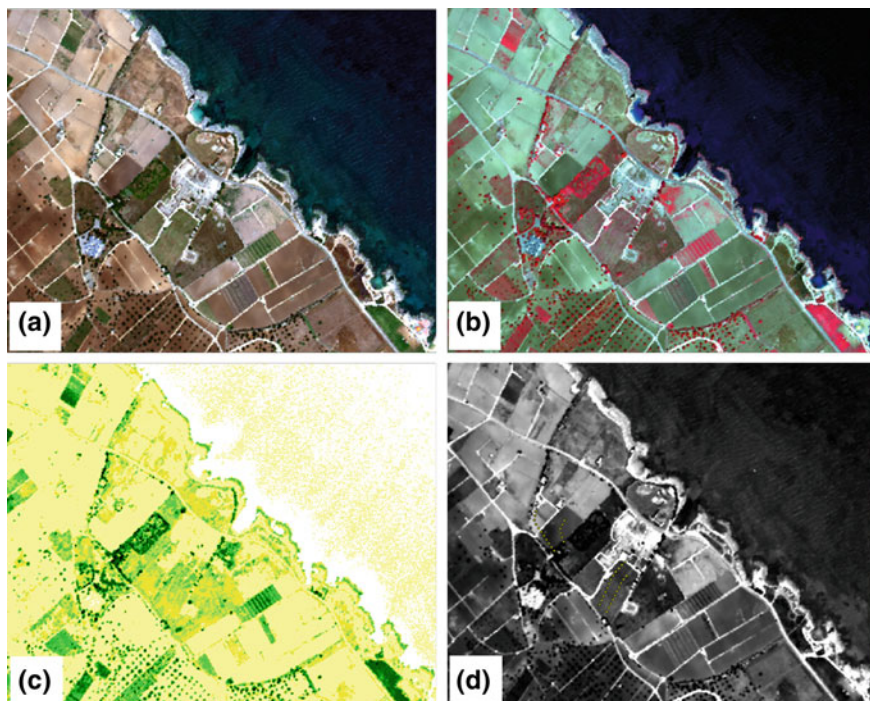
Fig. 4.100 Immagine MIVIS acquisita il 20 settembre del 2011: **a** RGB; **b** false color representation; **c** Normalized Difference Vegetation Index (NDVI); **d** Adaptive LEE filter showing the identified archaeological traces

the South Gate. The traces of light color and orientation NE-SO, may be relevant to ancient urban viability.

The trace no. 5 links the cryptoportic to the isolates of the northern sector of the city.

The traces no. 6 and no. 7 (Figs. 4.99, 4.100 and 4.101b) have been located inside the city wall, to the western side of the public area. The anomalies, parallel to each other, are visible on the remote image for the light color with linear EO direction. By type and form, they could be interpreted as traits of the internal viability jointed to the Via *Traiana*. The trace no. 7 in particular is the continuation of the secondary road that dates back to the II century BC, persists at the time of the construction of Via *Traiana* and is obliterated by the episcopal basilica.

The trace no. 8 follows the road already investigated during digging activities of previous years in the first section and then diverts to the north where it appears to be linked to the trace no. 9 which should represent its natural continuation.

The curve trace no. 10 (Figs. 4.99, 4.100 and 4.101b) has been identified and interpreted as a sign of the western end of the wall (Ceraudo 2003).

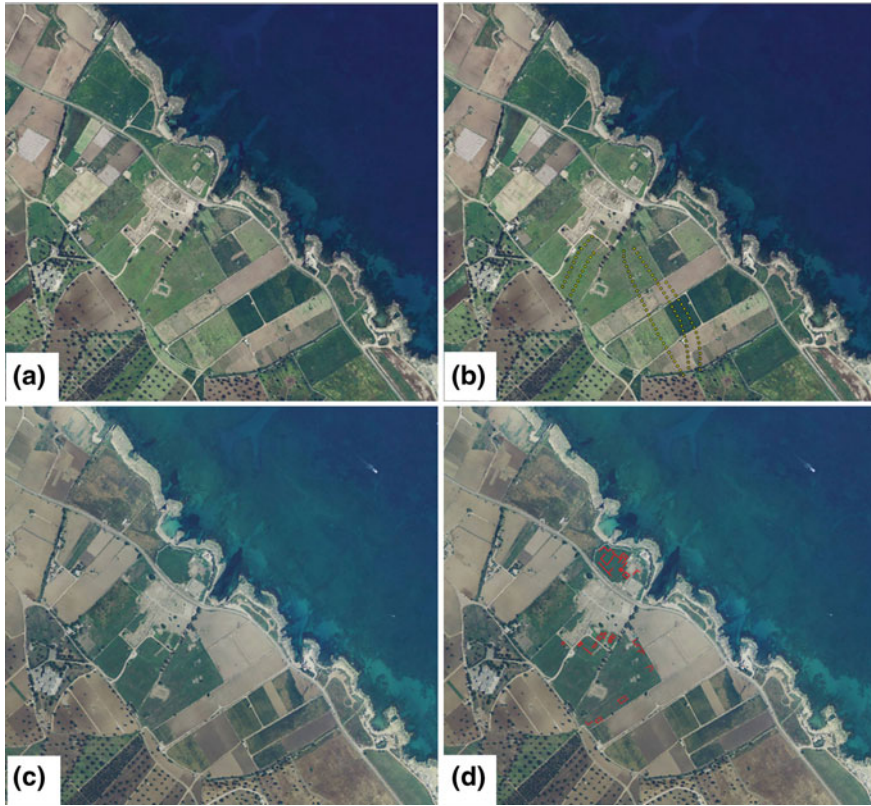In the different areas of the city, there are traces that can be traced back to the urban area.

Fig. 4.101 Orthophoto © 2004–2016 Blom Terra Italy: **a** RGB (2005); **b** RGB with traces of viability (2005); **c** RGB (2008); **d** RGB with traces of structures (2008)

In the SE sector of the urban system there are many anomalies that, taking into account their shape and typology, can be pertinent to buried structures located along the urban road. In the area of the acropolis, anomalies documents the presence of buried human structures (Fig. 4.101d).

In the tomographic maps resulting from the geophysical surveys, a chromatic scale was developed to emphasize the characterization of high resistive materials correlated with the presence of buried archaeological structures by uniformly coloring all values minor to 1.8 Ω m in green. Regarding the map obtained by the electromagnetic induction survey, the map obtained using a frequency of 15000 Hz is the most significant as it provided detailed information about the distribution of anomalies in the shallow subsoil (Fig. 4.104).

The map of resistivity shows with a discrete resolution several anomalies attributable to the traces of road axes connected with the structures brought to light by recent excavations (indicated by magenta in Fig. 4.104b, c) and allowed to trace the
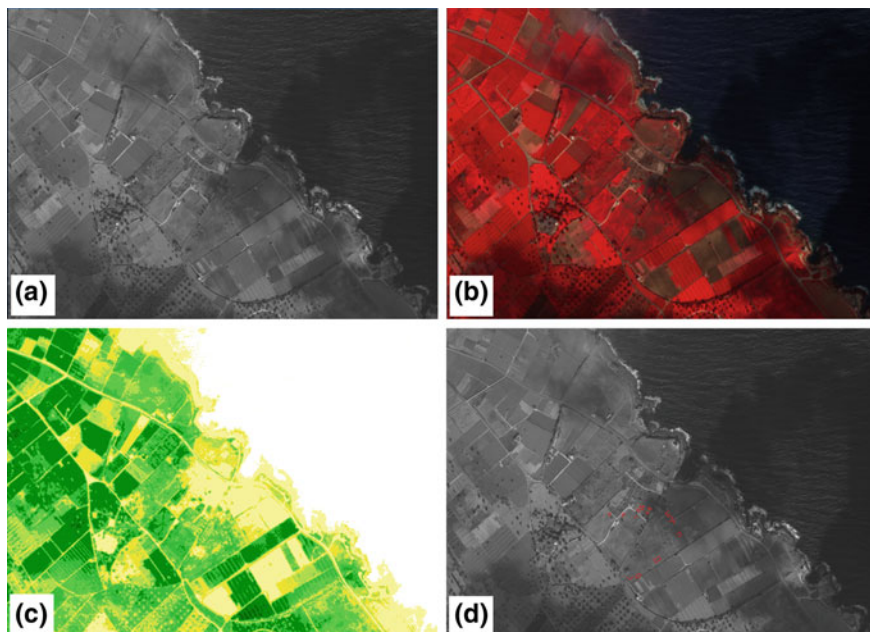
Fig. 4.102 QuickBird images captured on February 14, 2008: **a** panchromatic image; **b** false clor representation; **c** Normalized Difference Vegetation Index (NDVI); **d** panchromatic image showing the identified archaeological traces
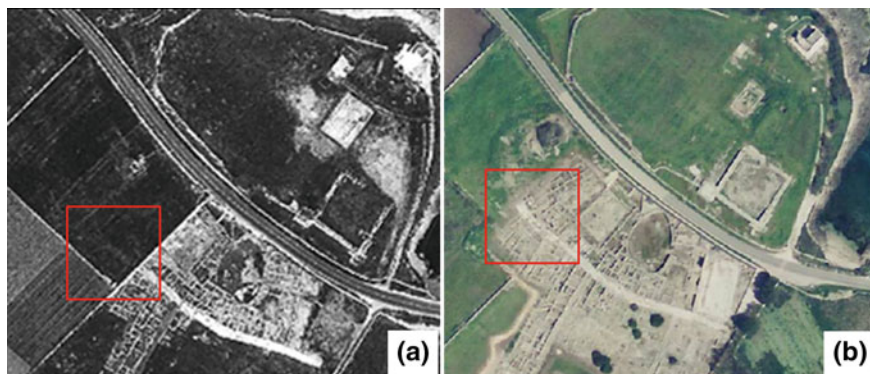

Fig. 4.103 Aerial photograph (1967) showing the identified archaeological traces (**a**) and the confirmation of the trace by archaeological exavation of the *Via Traiana* (**b**)

path of the Via *Traiana* in the southern sector of the *thermae* (marked with the purple color in Fig. 4.104b, c).

The survey also outlined large-scale areas where there are significant abnormal areas attributable to probable buried archaeological structures; in particular, a low resistivity anomaly of remarkable size and rectangular shape (attributable to the forensic square around which there is, on the western side, the civil *basilica*) has been identified.

The most relevant map resulting from the application of the three-dimensional geoelectrical tomography is relative to 0.5 m in depth (Fig. 4.105). For the SO sector of the *forum*, the results show the presence of a dense mesh of structures (blue traces in Fig. 4.105b, c) served by three road paths: the Via Traiana (no. 1 in Fig. 4.105c) and two secondary axes (nos. 2–3 in Fig. 4.105c) of which the most western (no. 3 in Fig. 4.105c) has the function of connecting the cryptoportic with the North sector of the city.

Among the wide blocks defined by the arteries that follow the Via *Traiana* orientation, in the one closest to the southwest side of the *forum*, the excavations carried out over the last two years have highlighted a dense residential sector since the 2nd century BC In the area close to the *thermae*, just beyond the current excavation limit, the buildings are located in a continuous way directly on the road (no. 2 in Fig. 4.105c) that crosses with the Via *Traiana*. With the change of the urban landscape at the end of the IV century, the track remains fully active at the service of the deeply transformed isolation. In the southwest side, whose curved margin is marked by the Via *Traiana*, substantial anomalies appear to be the result of another highly articulated sector, in which future stratigraphic surveys can clarify the characteristics and modalities of the urban fabric articulation.

The multi-methodological and multi-scale integrated approach adopted in the city of Egnazia has allowed acquiring objective, complementary and high quality information through a comprehensive assessment of the convergence of multiple physical parameters that describe the same situation. The agreement of geophysical anomalies and remote sensing traces is well visible in Fig. 4.106 that summarizes the whole results.

The collaboration and the continuous flow of information among different disciplinary researchers has been a key point for a constant exchange of ideas and

Fig. 4.104 The electromagnetic induction survey: **a** map of electrical resistivity; **b** map of electrical resistivity with indication of anomalies; **c** map of anomalies
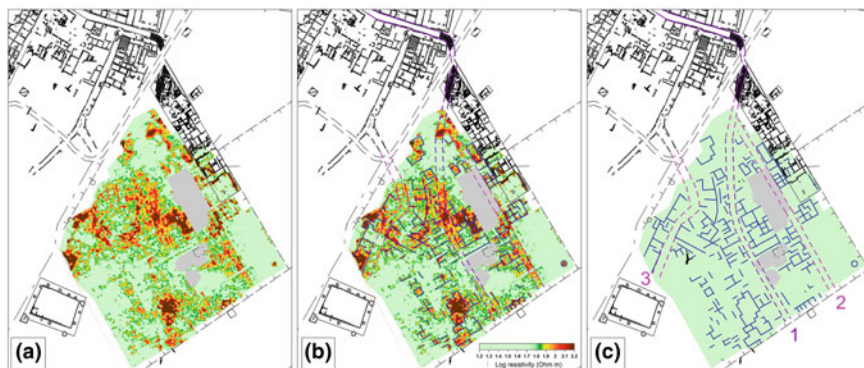
Fig. 4.105 Three-dimensional geoelectrical tomography: **a** map of electrical resistivity; **b** map of electrical resistivity with indication of anomalies; **c** map of anomalies

results. The results achieved add new elements that enrich the state of knowledge on urban road organization and provide useful information for the reconstruction of the urban system. Finally, archaeological investigations have provided very important data and their overlapping with the results of geophysical and remote surveys can be considered as a confirmation of the validity of the proposed methodology in the location of the buried targets and the resolution power of this approach. An example is the result reached at the southern end of the *thermae*: here, where the aerial photo analysis and electrical tomography highlighted clear and significant anomalies, the archaeological excavation, still underway, confirmed the presence of a three-nave religious building that obliterates partly the *domus* at the *atrium* (Fig. 4.107).

4.7   Integration of 3D Metric Survey and Geophysical Prospection

4.7.1   Photogrammetric survey and ERT at the Treasury Tomb, Archaeological Park of Petra, Jordan

In 1985, the monumental area of Petra became one of the sites on the UNESCO World Heritage List in recognition of its unique cultural and natural heritage. It is located on the left margin of the Rift Valley in central-southern Jordan. Overall valley there is an uninterrupted presence of anthropic traces from the X–VIII millennium BC. (Early prehistoric settlements), the Edomite settlement period (VIII–VII century BC), the Nabatean period of monumental tombs (VI BC–II AD) until the Roman period (II century AD: conquest of Petra in 106 under the Emperor Traiano), Byzantine, Arab and Medieval. The most known part of the site is a series

Fig. 4.106 Resulting map with indication of traces identified by remote sensing and geophysical anomalies

of tombs and temples dating back to the Nabatean era, whose architectural structures have been realized by sculpting directly the rock walls, made up of sandstones that can easily be modeled in ancient but subject to continuous erosion over the centuries. Walking through the narrow Siq gorge, behind a turn, the majestic Tomb

Fig. 4.107 **a** aerial photography acquired in 2010 in the southern sector of the *thermae* (image given by Gianluca Mastrocinque, University of Bari); **b** geophysical results (in pink and blue) and archaeological results (in black)

of the Treasury (al-Khaznah) appears (Fig. 4.108). The facade of the building is about 40 m high and 28 m wide with a very elaborate double Corinthian order. The lower part consists of a six-column pronaos surmounted by a triangular pediment; in the two lateral blind inter-columns, some unreadable reliefs are placed. The upper part, on the other hand, has a central circular temple with a conical cover flanked by two lateral wings that echo the lower blind inter-columns and are closed with a semi-fronton.

Since 2012, a multidisciplinary Italian Team is working to improve the Heritage Management and Conservation of Petra. Each research group applied different innovative technologies to make a complete tridimensional survey over and under the place of the Treasury Tomb.

4.7.1.1 Survey Planning, Data Processing and Results

Some geophysical surveys were carried out using the Electrical Resistivity Tomography Method.

The instrument used for data acquisition at Petra was the ELMES ADD-01 (Fig. 4.109, left), which consists of two separated light portable boxes, the measuring control unit and the current generator, respectively, interconnected via a wireless radio frequency device. A total of 35 dipole-dipole parallel profiles placed in the space in front of the tomb, equally spaced about 1 m, in a few cases 1.5 m, were measured in order to cover an area of approximately 35×50 m^2 (Fig. 4.109, right). Along each profile, the dipoles were displaced and spaced at steps of 1 m, up to the maximum pseudo-depth of 9 m. Figure 4.110 shows a sample pseudosection across a profile close to the tomb.

Figure 4.111 shows a sequence of horizontal slices, where the modelled real resistivity maps are drawn at increasing depths below ground level. The maps have
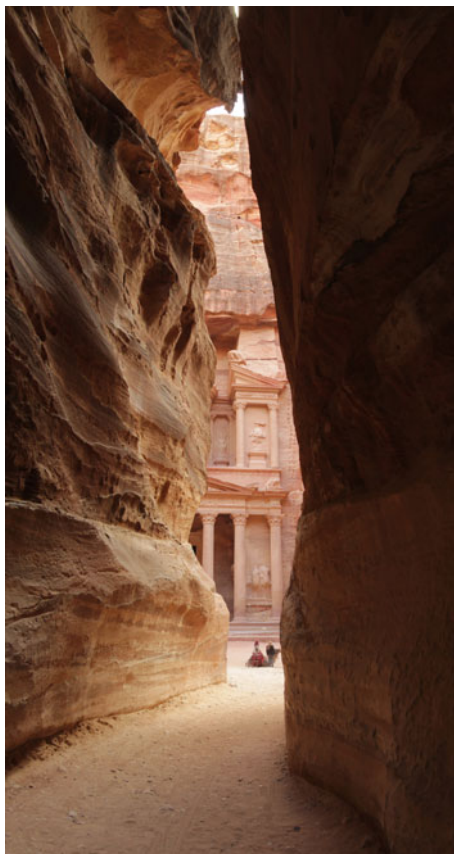
been obtained using the PERTI algorithm (Mauriello and Patella 2009) and including all of the profiles distributed in the survey area. The color scale adopted in those visualizations was realized in order to empathize only values major to 2 Ω m (the average resistivity). Overall, the investigated area is characterized by good contrasts of resistivity values that outline abnormal geometry with defined geometric shapes and interesting alignments consistent with archaeological evidence. Specifically, the horizontal section of 6 m in depth shows resistive abnormalities (in red tones) of regular shape that, starting from the base of the Treasure Tomb, develop perpendicularly in the front square enclosing a low resistivity zone (blank) (Fig. 4.112). This figure could be interpreted as the presence of further structures on the sides and in front of the monument and of an internal clearing to them.

Furthermore, tridimensional reconstructions of "Invisible Heritage" obtained by geophysical surveys have been integrated with 3D models of "Visible Heritage". A strip of photogrammetric images over the excavation area outside the Tomb have been and processed them by means of the Structure from Motion (SfM) methodology (d'Annibale and Fangi 2009; d'Annibale 2011). The input
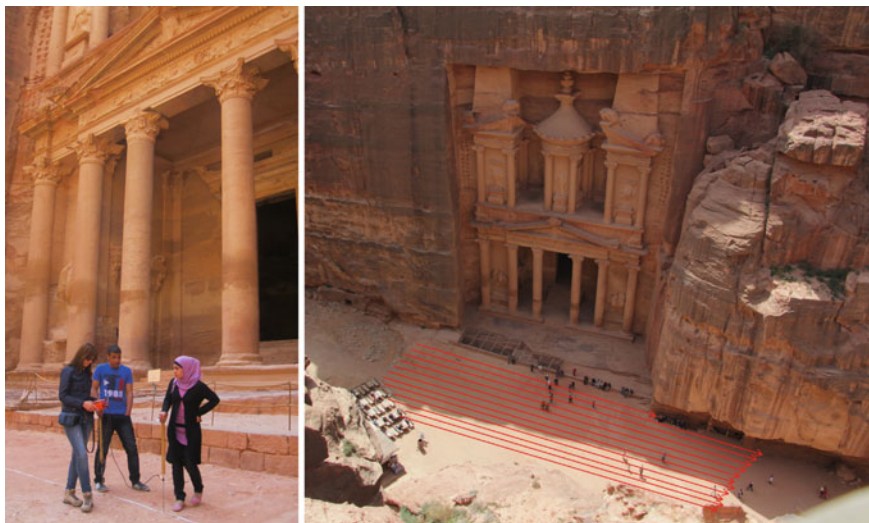
Fig. 4.109 Electrical Resistivity Tomography acquisition (left) and grid data location (right)

images have been taken from the same points of view to form the set of panoramic photos with equirectangular projection. The SfM approach allowed to recover a good 3D reconstruction of subjects visible in more images by means of automated operations: image matching, camera calibration and dense point cloud creation. In Fig. 4.113 the 3D model of the Treasury Tomb is joined with the 3D geophysical reconstruction of buried structures.

4.7.2 Laser scanning, photogrammetric survey and GPR investigations at the Abbey of Santa Maria a Mare, San Nicola Island, Tremiti (Foggia, Italy)

The Abbey of Santa Maria a Mare, San Nicola Island, Tremiti (Foggia, Italy) was built in 1045 AD by the Benedictines. It retains the original plant with a rectangular plan with three aisles that extend longitudinally from the entrance to the main altar (Fig. 4.114a, b). The elaborate middle mosaic floor (XI–XII century), in polychrome tiles and the painted wooden ceiling made in the 18th century to replace the dome are particularly important. The monument has some obvious signs of degradation that materialize in substantial detachments of plaster, water infiltration, surface damage on the walls and column fractures (Fig. 4.114c–e). Given the important need to preserve the artefacts, to continue to make good use and to safeguard public safety, a high detail estimate of the state of conservation of the Church has been achieved through the realization of 3D metric surveys
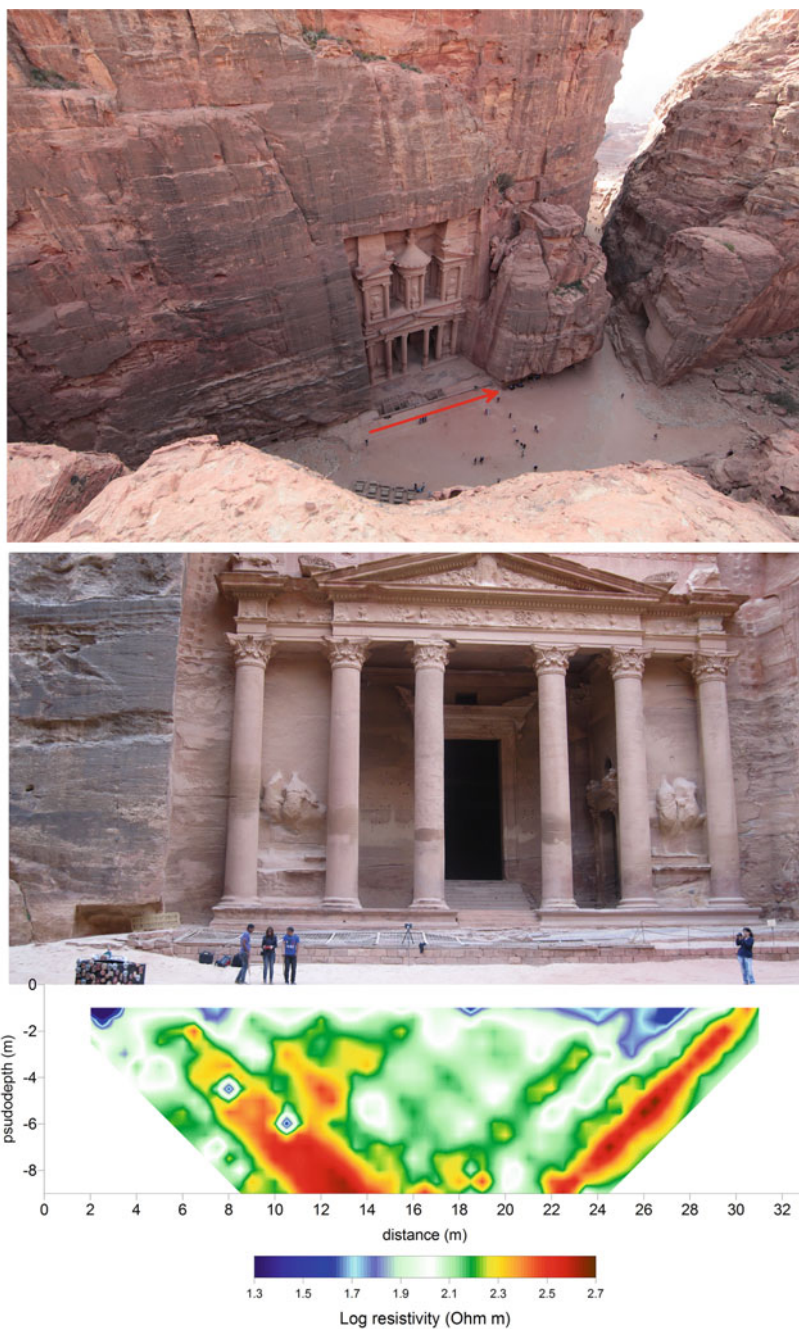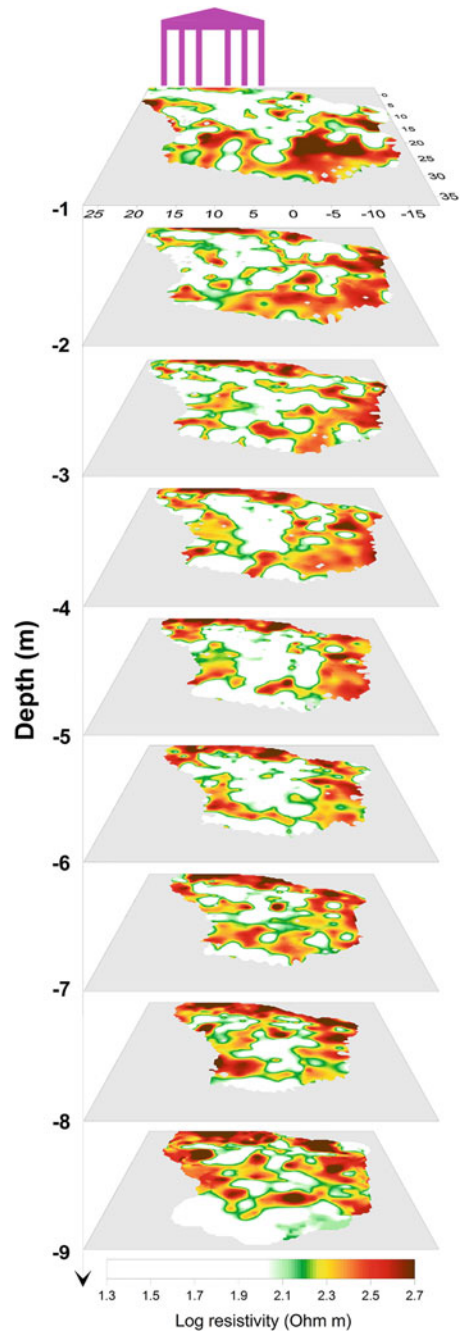
Fig. 4.110 A sample pseudosection across a profile close to the tomb

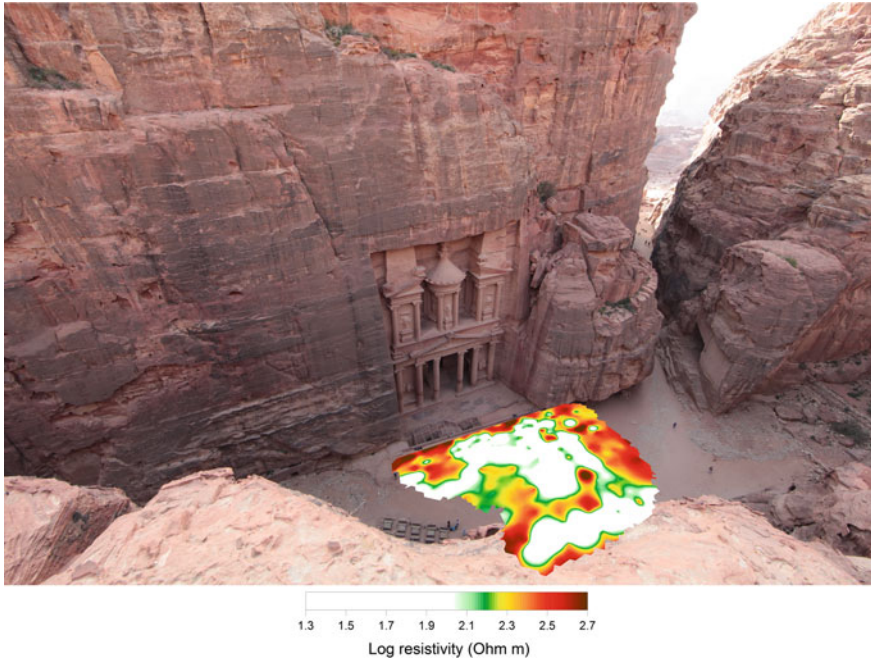Fig. 4.111 Resistivity tomographies relative to different depths

Fig. 4.112 Integration between a panorama photo and the resistivity tomography relative to 6 m in depth

(photogrammetry and laser scanner) and non-invasive geophysical surveys (Ground Penetrating Radar Technique). The use of non-destructive testing techniques at different scales can integrate direct tests to provide assessment tools for building characteristics, state of conservation and building safety. The work was done in collaboration with the Superintendence of Archeology, Arts and Landscape for the provinces of Foggia and Barletta-Andria-Trani and with the support of the Banca del Monte Foundation.

4.7.2.1 Survey Planning and Data Processing

The three-dimensional laser scanner is able to detect, in a small time interval and with a millimeter accuracy, the spatial position of hundreds of thousands of points by elaborating point clouds. In the work, a FARO Focus 3D MS120 laser scanner (Fig. 4.115a) has been used with an optimal range of about 50 m and has a precision of 2.5 mm. The density of points chosen for the single scan secured about 1 point every 5 mm–10 m of distance (space separating the hypothetical surface from the laser emitter). After carefully analyzing the monument, the correct laser scanner positions have been determined to make the relief minimizing the shadow parts to obtain correct spatial spacing of the point clouds and hence their correct recording.
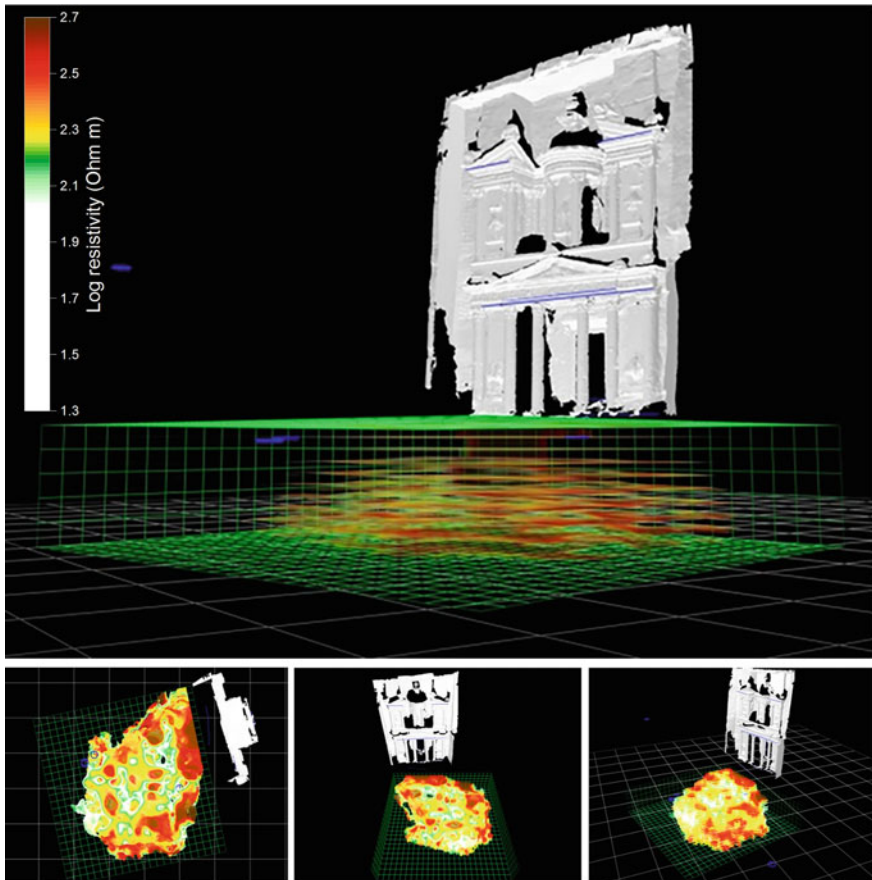
Fig. 4.113 Integration between tridimensional reconstructions and geophysical results (image processed by E. d'Annibale)

In total, 55 stations (3 exteriors and 51 inside the building) were made to ensure that at least three homologous points existed for each point cloud.

Data processing has provided several steps:

– The georeferencing of individual clouds.
– The colorimetric overlays.
– The construction of the overall model and extraction of all the products required for the design of the works (DXF Plants, Sections and Sections for Vector Data, JPG for Photographic Data and PLY and OBJ for Surface).
– The surface editing operation.
– The production of orthophotos and high resolution textures by perfecting the model with photogrammetric shooting. In total, about 4200 high-resolution photos were acquired. The elaboration has provided in detail:

1. Frame alignment through the Structure From Motion (SFM) technique. Three data sets have been generated: a discrete dot cloud (consisting of few thousands of points that will describe the object's geometry), camera positions at frame capture and internal calibration parameters of the camera (focal length, three coefficients of radial distortion and two tangential to a main point).
2. Construction of the geometry through dense cloud and mesh production (the point cloud has been transformed into a surface consisting of an x triangulated dot number).
3. Construction of the texture through the application of the photographic images to the template (exportable in .dxf, .obj, .txt, .pdf, etc. format) and creating ortophoto in TIFF, JPEG, PNG, etc. formats.

Three-dimensional laser scanning has enabled the creation of a 3D model of the interior of the building and the external facade made up of approximately 18 million points (1 point every 5 mm–10 m between surfaces and emitter). Figure 4.115 shows a three-dimensional view of the product of the point cloud conversion in meshes and some images obtained from the colorimetric overlay operation (RGB). The dot cloud was used to extract plants and sections in DXF format for vector data and TIFF for photographic data. Figure 4.116 shows the location of 11 cross sections and 8 longitudinal sections with respect to the main body of the building.
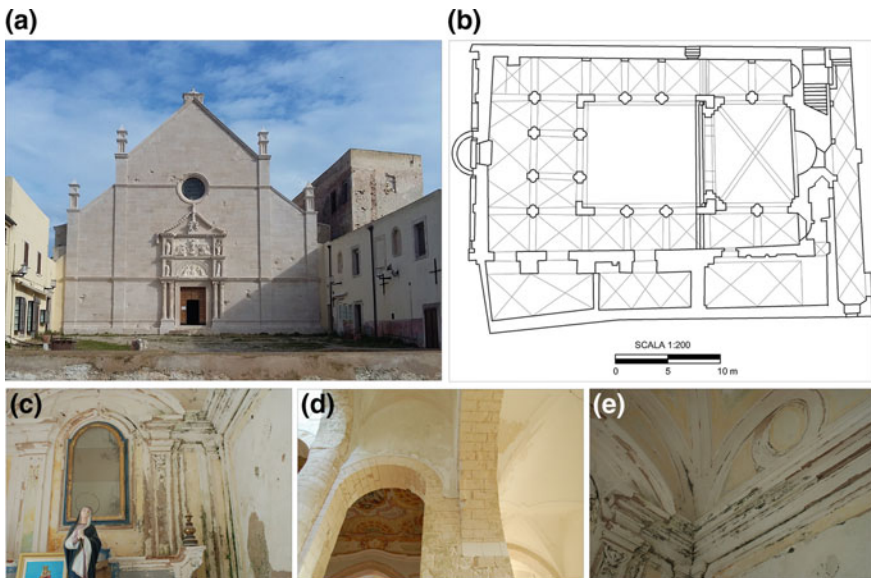

Fig. 4.114 The Abbey of Santa Maria a Mare, San Nicola Island, Tremiti (Foggia, Italy): the facade (**a**), the plan (**b**) and some critical examples of degradation (**c**, **d**, **e**)
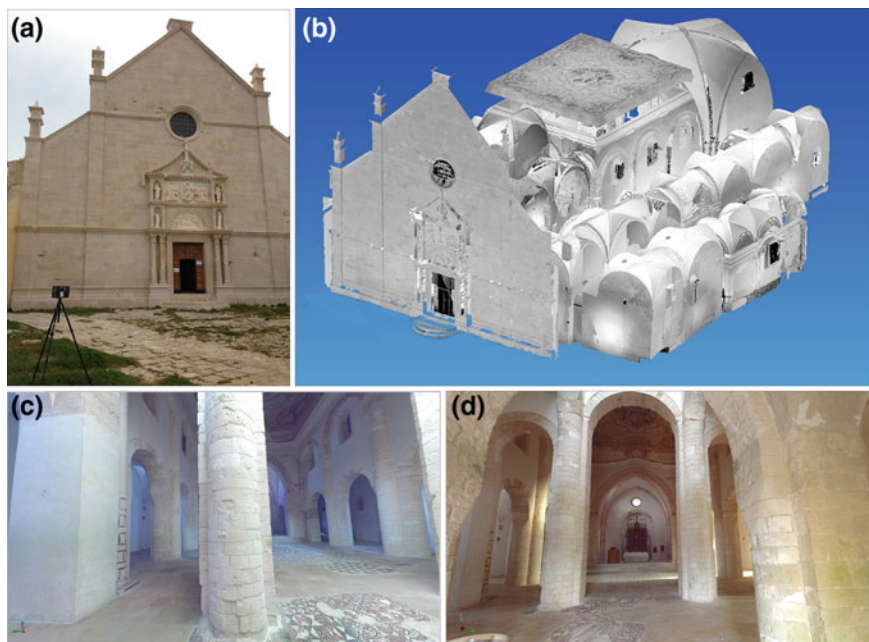
Fig. 4.115 Laser scanner Focus 3D MS120 (FARO) (**a**), mesh visualization of the model (**b**), RGB visualization of the cloud points (**c**, **d**)

In Fig. 4.117, the reflection section extrapolated from the 3D model with the application of orthophotos of the visible surfaces and the characterization of fractures, traces of moisture, detachment of the surface, plaster and modern interventions on the foreground surfaces are reported for LA-LA^I, LH-LH^I e TI-TI^I sections.

Figure 4.118 depicts an orthophoto of the painted ceiling, its characterization and a surface elevation model located on the section of the three-dimensional model.

Non-invasive diagnostics represent a photograph of a physical state of the work at that precise time and can represent a valuable tool for the restorative action of a single good. The instrumentation used in this work is the IDS georadar RIS-K2 with a TRMF (200–600 MHz) antenna and a 1200 MHz high-resolution antenna. Data were processed using the GPR-SLICE 7.0 software. Technically, data acquisition took place on lines where instrumental readings were executed in continuous mode. The standard profiles have been processed band pass filters, noise reduction filters and gain procedure. In this case, for each surveyed area, several parallel profiles have been acquired forming a grid pattern to verify the extent and size of the buried targets. Thus, a 3D matrix data matrix was obtained underneath the investigated surface from which the horizontal sections (time slice) were extracted at different depths in which the various hidden structural features are displayed in different colors.
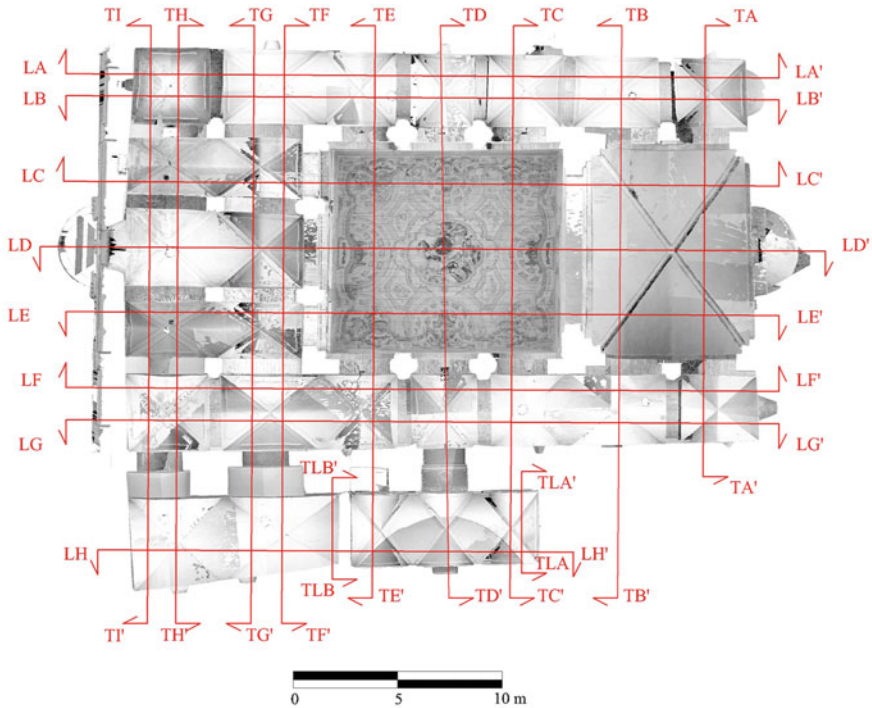
Fig. 4.116 Location of the sections extrapolated by the point cloud

Five areas were investigated on the floor using a multi-frequency antenna (200–600 MHz). In total, 37 survey profiles were made for a total length of 445.7 m. Figure 4.119 shows the horizontal slice relative to 0.5 m in depth positioned on the floor plan of the building. Finally, using a 1200 MHz antenna, a high resolution survey was carried out on the left wall of the building and on the inner wall of the entrance to verify the presence of moisture inside the masonry. Figure 4.120 shows the slice of 0.20 m deep on LA-LA^I and TI-TI^I sections.

4.7.2.2   Results

The analysis of the results clearly shows a level of advanced degradation of the interior of the building perceived by the presence, on each analyzed wall, of substantial moisture traces often associated with considerable separations of plasterwork, swelling, mold appearance and blasting of paintings. In particular, a detail evaluation of any sign of deterioration of the building has been achieved, whose nature, extension and location can simply be drawn graphically from the elaborate images.
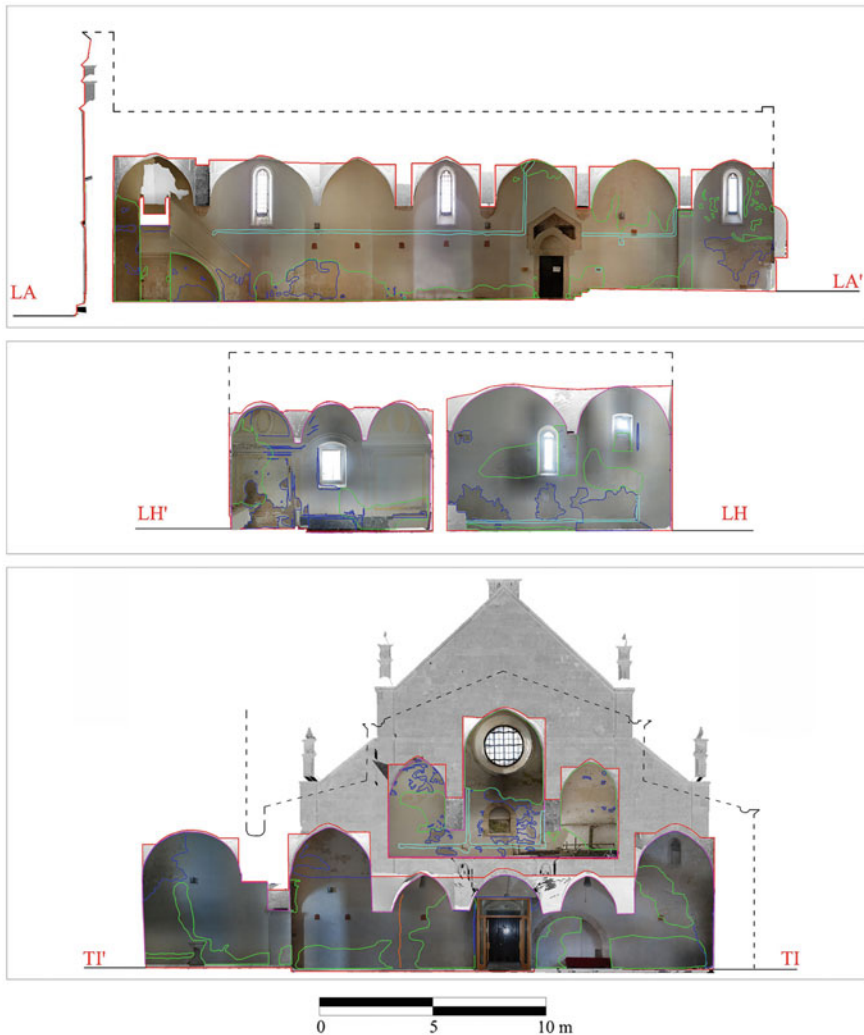
Fig. 4.117 LA-LA^I, LH-LH^I and TI-TI^I sections: reflection section extrapolated by the 3D model with application of the orthophotos of the visible surfaces and indication of anomalies (cutting plane in pink, detachments of plaster in dark blue, modern intervention in light blue, traces of humidity in green, fractures in orange, the section line in red)

The most critical conditions were found in sections near the outer walls[2] (Fig. 4.117) where the decay phenomena are more pronounced. The georadar surveys carried out on the inner wall of the entrance (ground floor and loggia) and on the left wall of the building confirm the presence of water within the analyzed

---

[2]Sections: LA-LA^I, left side; LH-LH^I, right side; TI-TI^I, wall of the entrance.
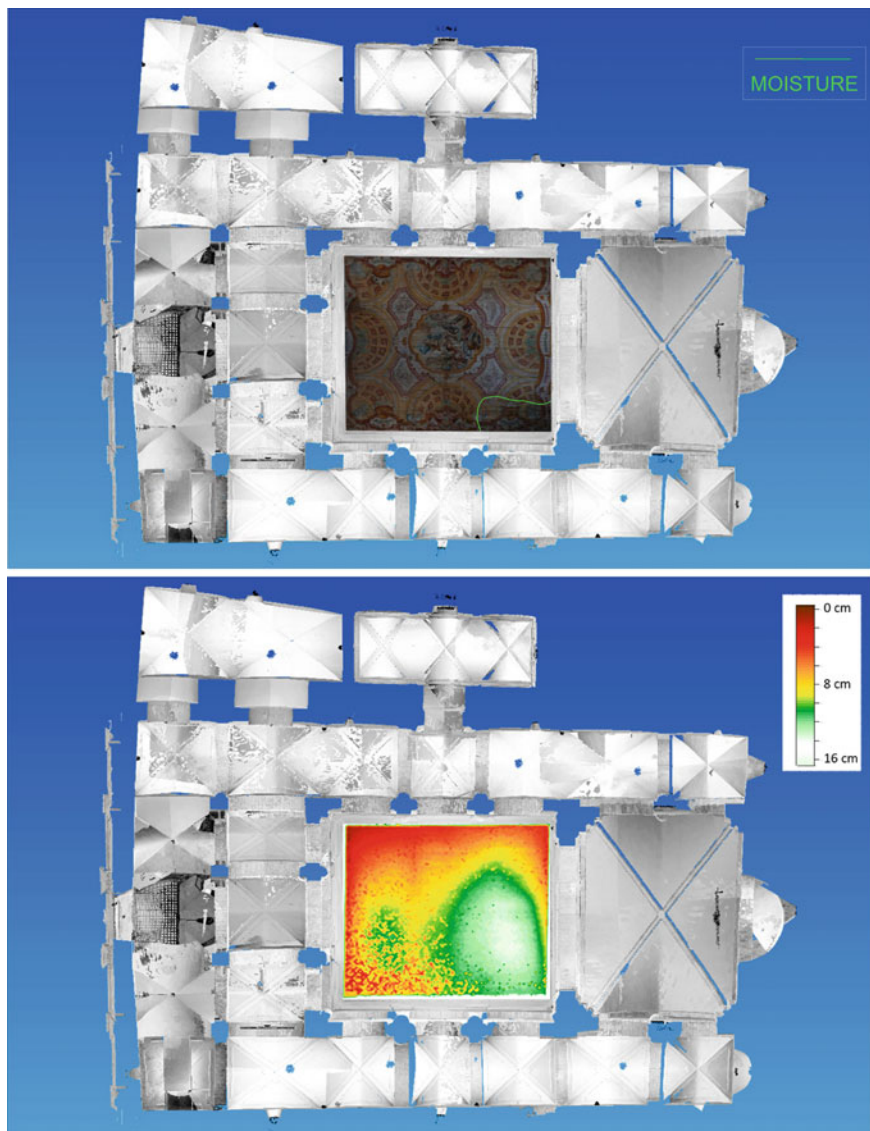
Fig. 4.118 Orthophoto of the wooden ceiling located on a section of the 3D model with indication of anomalies (top) and model of elevation (bottom)

surfaces. This is evidenced by the total absorption of electromagnetic signals found in radargrams and in the slice parallel to the walls (Fig. 4.120). In the latter, in the spots indicated by the green-white color, low signal amplitudes have been detected coinciding with obvious traces of moisture on the surface.
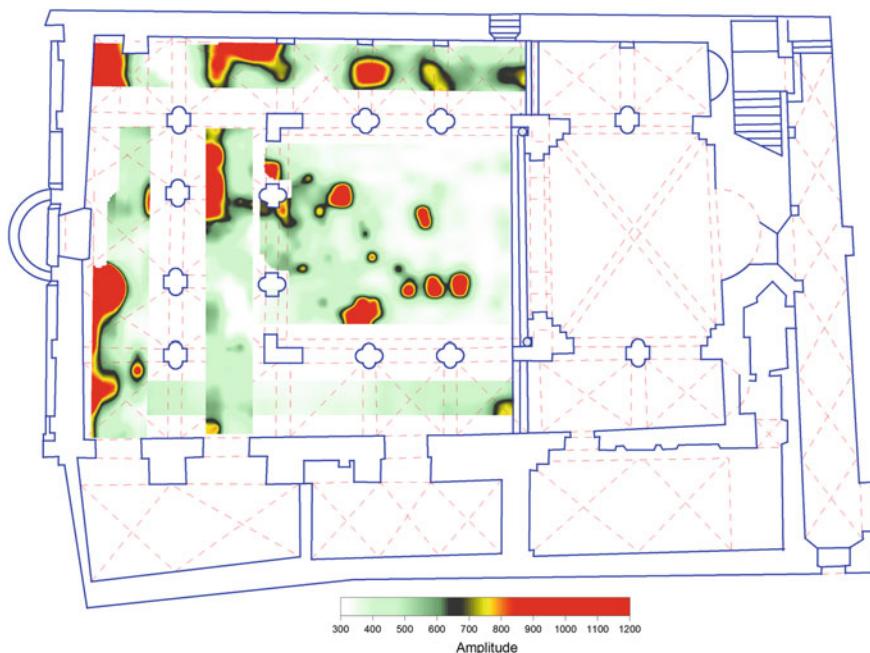
Fig. 4.119 Horizontal slice relative to 0.5 m in depth

Given the extent of degradation events, it can be assumed that water infiltration can be mainly due to the absorption and diffusion of rainwater through external surfaces constructed of non-water-repellent porous limestone stones. Probable penetration through non-tightened openings and non-watertight or deteriorated covers should be added to these phenomena.

With regard to the cracking framework of the monument, it was possible to document vertical lesions concerning the two columns of the entrance[3] and a column of the left nave[4] (some of these fractures are already known and monitored), the frames at the base of the decorated wooden ceiling[5] and some walls.[6] In order to evaluate the evolution of deformations, active movements and rotations, it would be desirable to continuously monitor lesions and to program interventions that increase the resistance of the structure, especially in view of possible external actions and strains such as seismic ones.

The laser scanner survey finally enabled a precise geometric determination and an accurate morphological knowledge of the building. In detail, some elements that

---

[3]Sections: TE-TE^I and TF-TF^I.

[4]LB-LB^I section.

[5]Sections: LC-LC^I, and TE-TE^I.

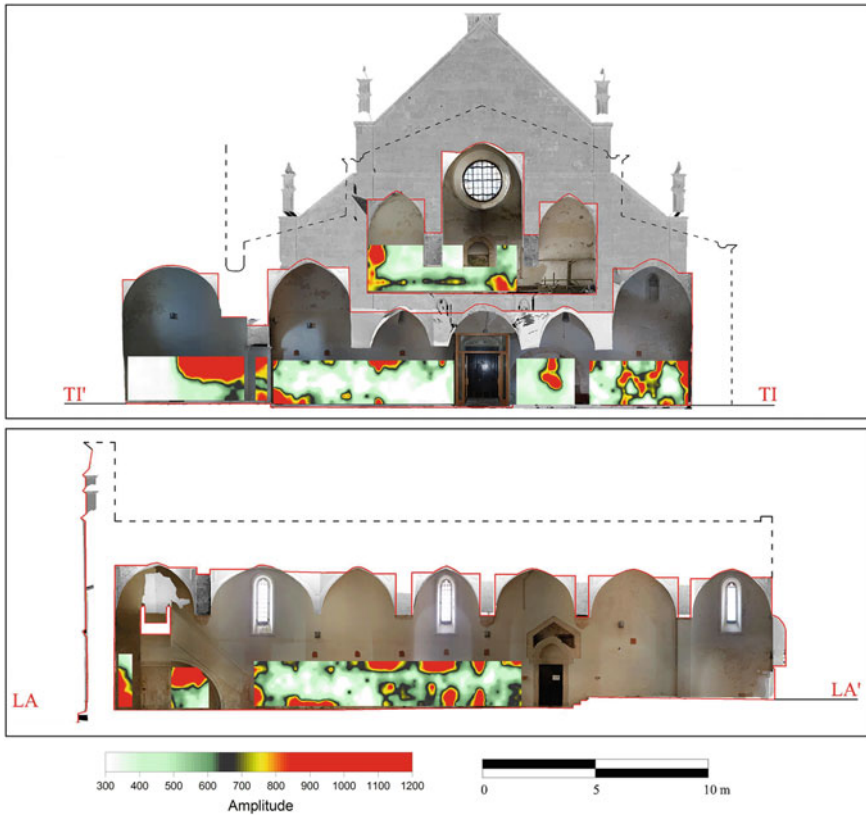[6]Sections: LD-LD^I, LF-LF^I, TA-TA^I, TE-TE^I and TI-TI^I.

Fig. 4.120 Vertical slice relative to 0.20 m in depth

could be attributed to constructive defects and/or structural interventions carried out in recent times and/or to deformations caused by natural events (seismic movements and substrate settlements) may have emerged. Some sections[7] show a non-verticality of the walls of the chapel located to the right of the church (deviation from the vertical axis between 0.1 and 0.24 m) and the outer wall of the left nave (deviation from the vertical axis between 0.1 and 0.14 m) (Fig. 4.121). In particular, due to the presence of major fractures in the masonry of the rooms above the right aisle, such irregularities could favor, in case of seismic stresses, the right-tipping mechanisms of the right body.

As regards the wooden ceiling, some sections[8] indicate a deviation from the horizontal axis between 0 and 0.16 m, concentrated above all on the left side. The

---

[7]Sections: TB-TB^I, TC-TC^I, TF-TF^I, TG-TG^I, TH-TH^I and TI-TI^I.
[8]Sections: LB-LB^I, LC-LC^I, LD-LD^I, LE-LE^I, LF-LF^I, TC-TC^I, TD-TD^I, TE-TE^I, T5-T5^I and T6-T6^I.
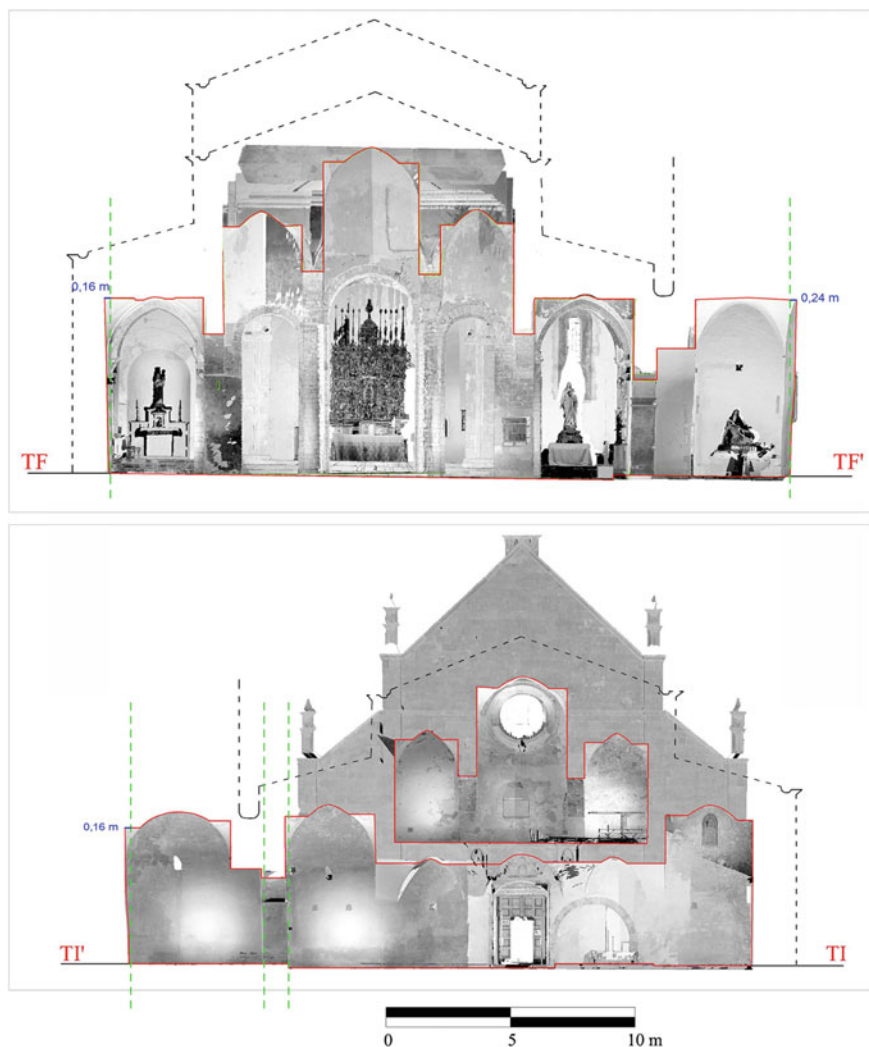
Fig. 4.121 Deviation from the vertical axis of the lateral walls (TF-TF^I and TI-TI^I sections)

digital elevation model extrapolated from the dot cloud (Fig. 4.118) shows variations in detected altitudes, differences partially coinciding with a visible moisture trace on the surface. For this anomaly, deform metric monitoring of active movements would be desirable in order to assess the evolution of the phenomenon.

Finally, numerous irregularities and depressions emerged in the paved floor (especially near the mosaic), a slope from the left to the right side of the building

(0.24–0.26 m) and from the central square to the entrance (0–0.09 m).[9] Georadar prospecting has not shown any anomalies that can be attributed to cavities or voids but only the presence of some elements probably attributable to structural elements prior to the present construction. In the central nave area, the bonding materials used in the restoration of the mosaic heavily disturbed the investigations.

The results of the investigations carried out at the Abbey of Santa Maria a Mare have provided good elements to stimulate and promote the systematic planning of diagnostic, consolidation and restoration projects.

4.8 Geographical Information System Implemented with Geophysical Prospections the case of Molise Region (Italy)

The Molise Region (Italy) has a rich natural, archaeological, architectonical, librarian and cultural heritage that testifies the complex history of its territory from the prehistory until present (De Benedittis 1979).

The most ancient proof of the human presence in Molise is attested by the Upper Paleolithic settlement of Isernia La Pineta, dated back about 700,000 years BP (Coltorti et al. 1982; Esu 1983). The site represents a unique example in the history of the human frequentation in Europe for the presence of a great number of paleontological finds associated to lithic artifacts and for the complexity of the site. More recent prehistoric evidences are indicated at Rio Verde (Pescopennataro, IS), Piana S. Mauro (Carovilli, IS), Fonte Curello (Carovilli, IS), Grotta Reali (Rocchetta and Volturno, IS), Morricone del Pesco (Civitanova del Sannio, IS), Monte S. Croce (Cerro al Volturno, IS), Biferno Valley (Barker 1975; Grimaldi 2005; Minelli and Peretto 2006).

Between the IV and the I century BC the panorama of the territory is characterized by the presence on the major mountains of about thirty Samnites fortifications, built with the technique of *opera poligonalis* and in communication between them through transhumance routes, the so called *tratturi* (AA. VV. 1980). Example of the Samnites culture are the remains of Pietrabbondante (Capini and De Benedittis 2000), the small temples of Vastogirardi (Morel 1984) and S. Giovanni in Galdo (Stek 2010), the fortifications of Terravecchia di Sepino (Matteini Chiari et al. 1984) and Monte Vairano (De Benedittis 1974, 1988) are examples of the Samnites culture.

The city of *Saepinum* is the symbol of the history of Roman civilization, whose events are identified with the development of the *tratturo*: in the VI century BC it was a commercial Samnitic *forum* and a service center, then it became a Roman city of taxation and in recent times it was transformed into a medieval and modern rural village (Gaggiotti and Matteini Chiari 1979; De Benedittis 1981).

---

[9]Sections: L1-L1[I] and L2-L2.

The monastery of San Vincenzo al Volturno (Marazzi and Delogu 1996) and the necropolis of Campochiaro (Ceglia 1988) attest the early medieval phase.

The cathedrals of Trivento, Guardialfiera, Termoli and Larino and the castles of Civitacampomarano, Roccamandolfi, Cerro al Volturno, Termoli, Venafro, Gambatesa and Campobasso are also noteworthy testifying the Middle Ages through their stories and their transformations, representing important pages of the history.

The Baroque period is significantly represented for example by the churches of Ripalimosani and Campodipietra.

The neo-Gothic stile is symbolized by the sanctuary of Castelpetroso while a manifestation of the Florentine Gothic is the building of the municipal museum of Baranello, container of the most beautiful nineteenth-century museum of the south-central Italy.

The short and certainly not exhaustive overview of the historical and cultural reality of Molise provides guidance to understand how much hidden heritage there is still in this area, to explore and exploit, but on the other hand, how much known heritage exist to protect and monitor preventing the destruction and loss. In this context, the use of non-destructive geophysical methods becomes a valuable tool of cognitive investigation immediately in the bud of any archaeological verification projects, restoration and architectural restoration, safeguard through preventive archeology operations, exploration of large areas within archaeological parks and redevelopment of city centers. From 2000 until present, a fruitful collaboration between the University of Molise and the Regional Directorate of Cultural Heritage of Molise has led to undertake significant actions of intervention for the knowledge and the preservation of the ancient landscape.

The project involved a reconnaissance activity oriented to a definition of a geo-referenced archaeological map, a critical analysis of the archaeological literature and a multi-scale and multi-methodological analysis through non-invasive diagnostics. The focus of the research has been placed on both the most important archaeological sites than on the recent findings following the surveys carried out in the frame of important public works (pipelines) or during the preliminary survey for photovoltaic and wind systems (in application of the regulations relative to preventive archeology according to the articles. 95–96, d.Lgs 163/2006). All data were stored in a Geographic Information System that allowed drawing up a new archaeological map that gives an updated view of the rich archaeological heritage of Molise.

117 sites have been investigated in the territory of Molise Region and their localization is showed in Fig. 4.122. Taking into account the features of the sites and the problem to solve, the method of prospection has been chosen for each site in order to obtain the better result:

– ERT was implemented in 76 surveys. Even if the time of data acquisition is higher than in other methods, it is very advantageous because it gives easily interpretable results, is very versatile and is ideal for the individuation of deep structures.

– The EMI prospections were realized in 28 sites in order to have, in a very fast way, extensive information at a wide scale of the analysed territory.
– The GPR surveys were realized in 13 cases. It was unsuited to being applied on uneven soils but it was very useful for the study of historical building and for the analysis of paved surfaces: in these cases it was the less invasive prospection.

Geophysical prospection were realized with the following purposes:

– Acquiring information about structures still buried into the soil of 60 well-known archaeological sites.
Geoelectric surveys were carried out, for example, at Fonte Romita, Capracotta (IS) (site no. 21 in Fig. 4.122). It is the place where in 1847 an important Osco inscription (the so-called Tavola of Agnone) was discovered, currently preserved at the British Museum. The tomographic map relative to 1 m in depth has been linked to the structures (shown in blue), currently buried, found in the excavations in 1980 (Rainini 1996) (Fig. 4.123). Clear resistive alignments are evident with a trend and orientation similar to that of the already known constructions. The series of environments almost certainly belongs to a Sannitic farm.
The three-dimensional electrical tomography was also applied at the site of Grotta Reali at Rocchetta a Volturno (IS) (site no. 89 in Fig. 4.122), one of the most important prehistoric contexts in the region where numerous fossils and artifacts related to Neanderthals were found (Minelli and Peretto 2006). The investigation, realized with the aim of understanding the succession of the Musterian site located on the walls of a travertine bench, allowed to outline the geometry of an occluded portion of the prehistoric cavity and to represent three-dimensionally a high resistivity vertical body (identified by excavations and corresponding to a travertine column) (Fig. 4.124) (Compare et al. 2009). Another example is site no. 53. It is located in Piazza Celestino V in Isernia where excavations brought to light a section of the walls of the Roman colony (Terzani 2005). The purpose was to verify the existence of other archaeological structures still buried beneath the pavement of the modern square. Two GPR survey areas were realized: the first one was arranged within the eastern portion of the excavation trench, parallel to the ancient wall, through the realization of 8 profiles, spaced 0.5 m and with a length of 20 m; the second one, composed by 18 lines, spaced 0.5 m and ca. 22 m long, was placed in the north-western sector of the excavation trench. Figure 4.125 shows the resulting slice of site G1 expressed in the time window from 9 to 24 ns (two way time). On the east side of the trench excavation, the presence of small straight anomalies have led to hypothesize the continuation of some medieval walls leaning on the blocks in polygonal technique. In the northern part of the wall, high amplitude spots seem to attest the presence of the continuation of the wall circuit within the subsoil. On the west side of the slice two segments forming an angle of 90° are observable and could correspond to the corner of a buried structure (Amato et al. 2016).
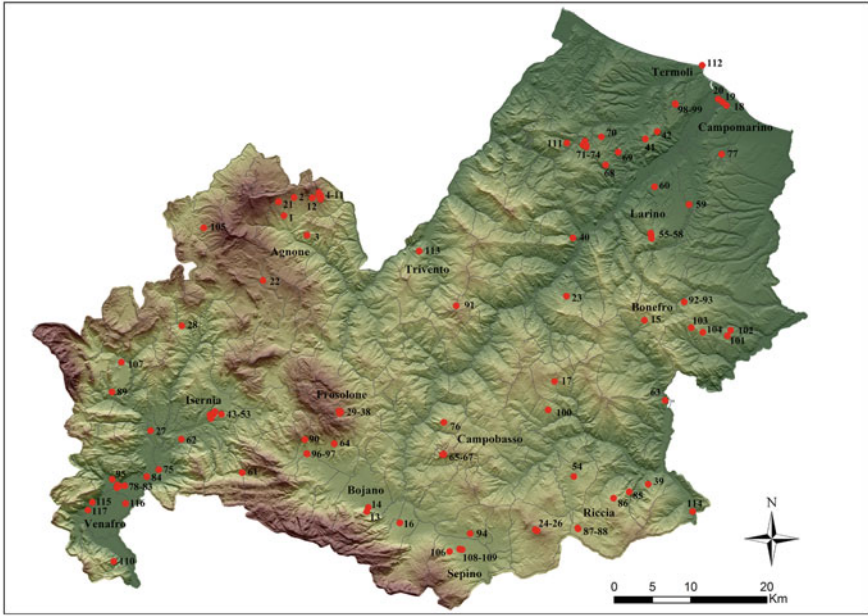
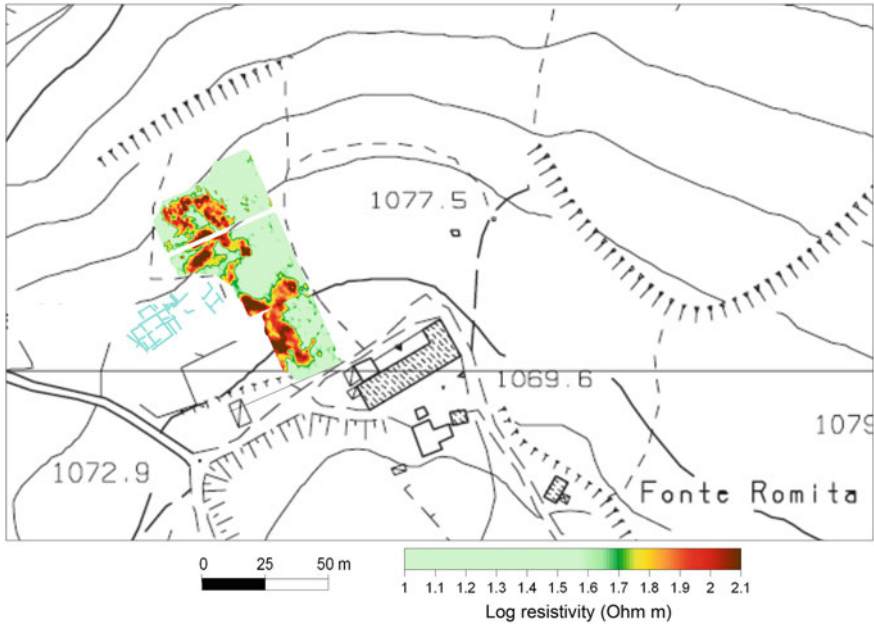Fig. 4.122 Localization of the 117 surveyed areas

Fig. 4.123 Fonte Romita (Capracotta): electrical resistivity tomography relative to 1 m in depth
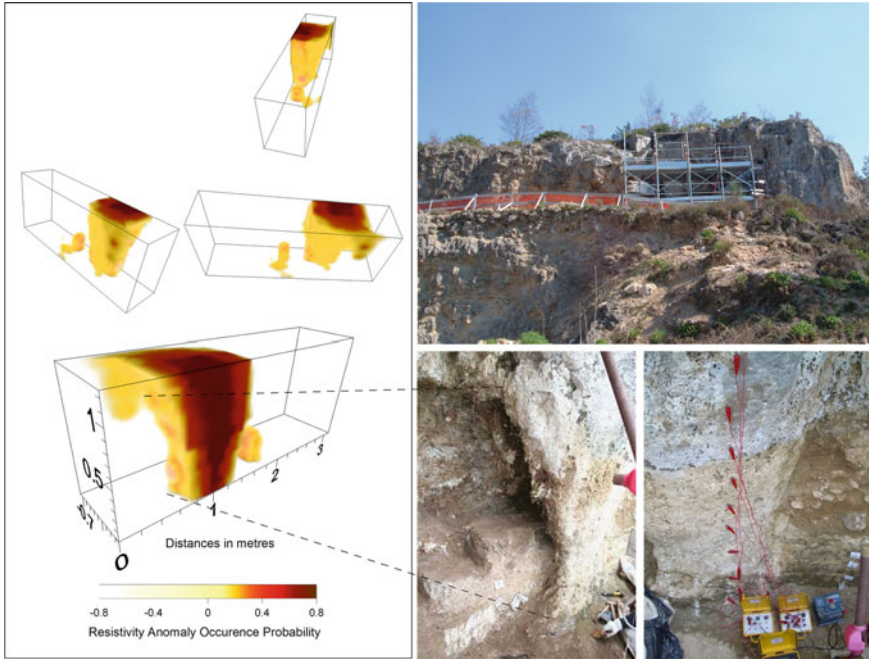
Fig. 4.124   Grotta Reali (Rocchetta and Volturno): electrical resistivity tomography

Figures 4.126 and 4.127 show the results of the geoelectric surveys carried out at the Roman villas of S. Maria Vecchia (site no. 62 in Fig. 4.122) (Pagano et al. 2005) and Valle Porcina (Colli a Volturno) (site no. 27 in Fig. 4.122). The results show clear evidences of buried structures.

– Identifying the three-dimensional features of buried structures whose presence is supposed to high concentrations of finding detected by pedestrian surveys in 26 sites.

An example is the site site no. 77 located in the south-eastern part of the Portocannone (CB) (Fig. 4.128), where the archaeological survey conducted (Prof. C. Ebanista, University of Molise) highlighted the presence of abundant archaeological material such as to hypothesize the presence of a complex structure. Geoelectrical prospecting was carried out in order to clarify the geometry and extension of the presumed archaeological constructions buried on a surface of 100 × 40 m. From the study of the resistivity map, it was possible to detect several anomalies with respect to the median values measured in the survey area. The main element, indicated by a magenta-colored arrow, is represented by a probable archeological structure of rectangular shape whose major side develops in NE-SO direction. Within it, it is even possible to perceive a division in smaller elements. Interestingly, there are also straight-line heterogeneities, marked with blue arrows, located northwest of the investigated area
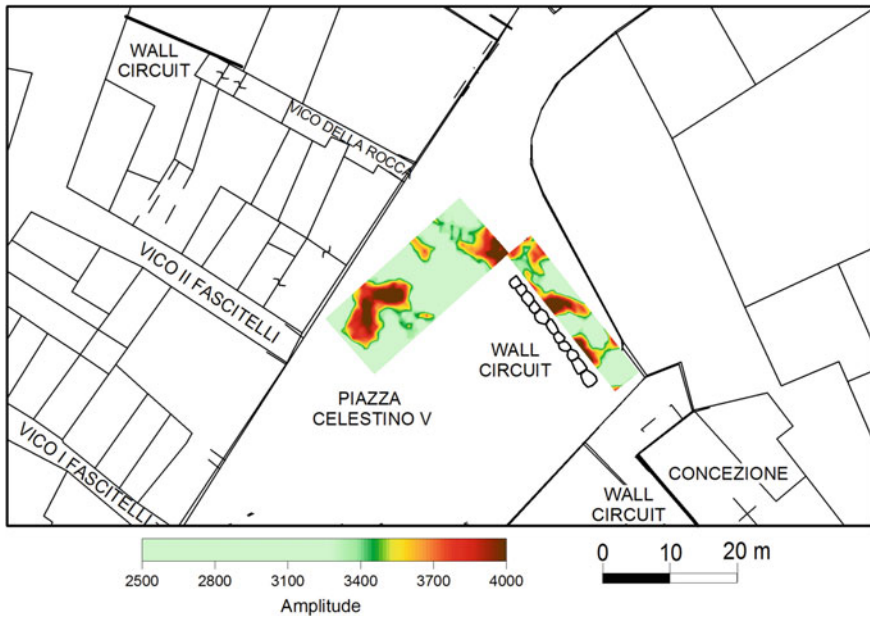
Fig. 4.125 Isernia: time slice in the time window from 9 to 24 ns

and linked to the previous anomaly: they are perpendicular to each other and
appear to be confined by delimiting a likely outer courtyard.

– Verifying the presence of archaeological evidences in 23 areas in the frame of
actions of preventive archaeology for public or private works (building
restorations and installation of pipelines, photovoltaic and wind systems).
An articulated study was carried out near the Industrial Area in the Pozzilli plain
(IS). The area has a high archaeological potential as evidenced by the many
findings that have occurred during the construction works of industrial buildings
and the creation of roads. In particular, traces of the Augustus aqueduct
(Scaroina 2004) and an archaic necropolis dating back to the VI and V centuries
BC. (Capini 1989) were found. Electromagnetic and geoelectric surveys have
been carried out on a large area covered by private works. An example of a
result is shown in Fig. 4.129 (site no. 78 in Fig. 4.122): in correspondence of an
abnormal light-color trace visible on the satellite image of Gloogle Earth of
October 15, 2005, geophysical surveys have identified a rectangular structure
with East-West orientation. The archaeological digging, conducted by the
Superintendence of Archeology of Molise, has verified the existence of a small
Roman building precisely in the point signed by the geophysical anomaly.
Another example is the prospection carried out in the territory of S. Giacomo
degli Schiavoni (site no. 98 in Fig. 4.122). In this case the results of EMI
surveys clearly show some very high resistive anomaies probably attributable to
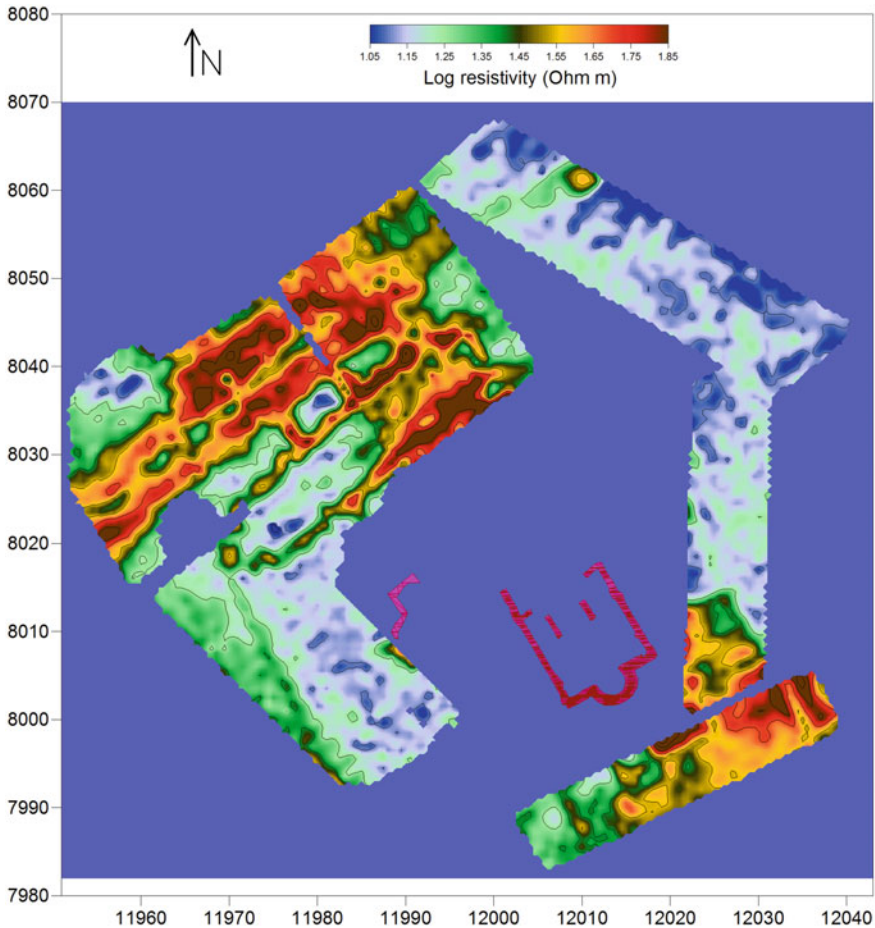buried archaeological structures (Fig. 4.130).

Fig. 4.126 Roman villas of S. Maria Vecchia (Macchia d'Isernia): electrical tomography relative to 1 m in depth

– Providing a proper representation of the conservation status of 8 historical buildings (churches and castles) for the display of potential structural anomalies, the location and extent of hidden structures inside the walls and the individuation of wet points into the walls. The results of the surveys in the Castle of Gambatesa (Site 39) and the Cathedral of Termoli (Site 112) are showed in Paragraph 4.2.

All the data was finally implemented in a Geographic Information System (GIS) that allowed an updated view of the rich archaeological heritage of Molise through the production of a computerized map of submerged and "invisible" heritage. This product, constantly updating, perfectly integrates with the existing information systems relating to "visible" archaeological sites and represents an operational tool for the bodies present in the territory for the definition of guidelines for knowledge, study, protection and promoting the Molise Cultural Heritage.
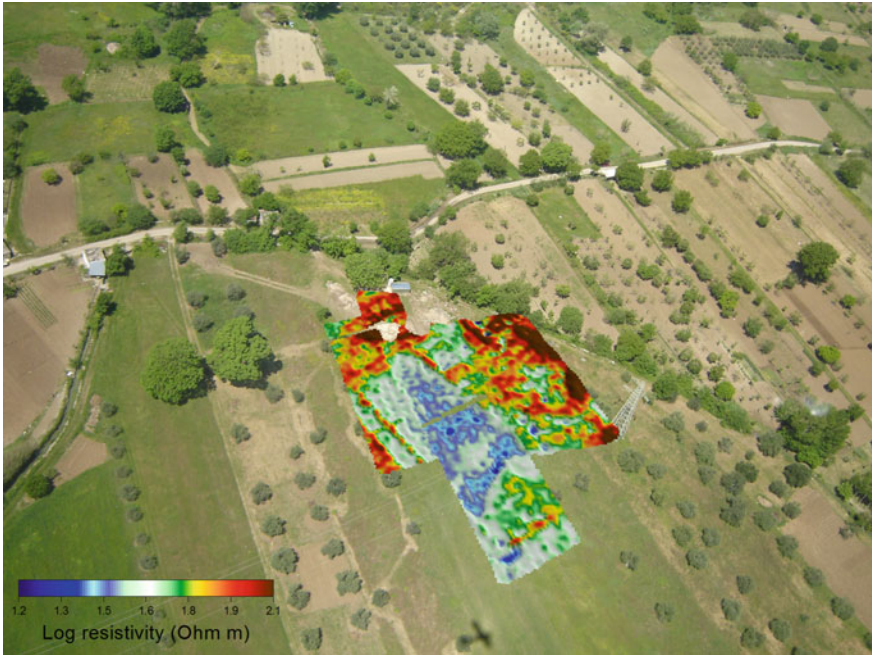
Fig. 4.127 Roman villas of Valle Porcina (Colli a Volturno): electrical tomography relative to 1 m in depth
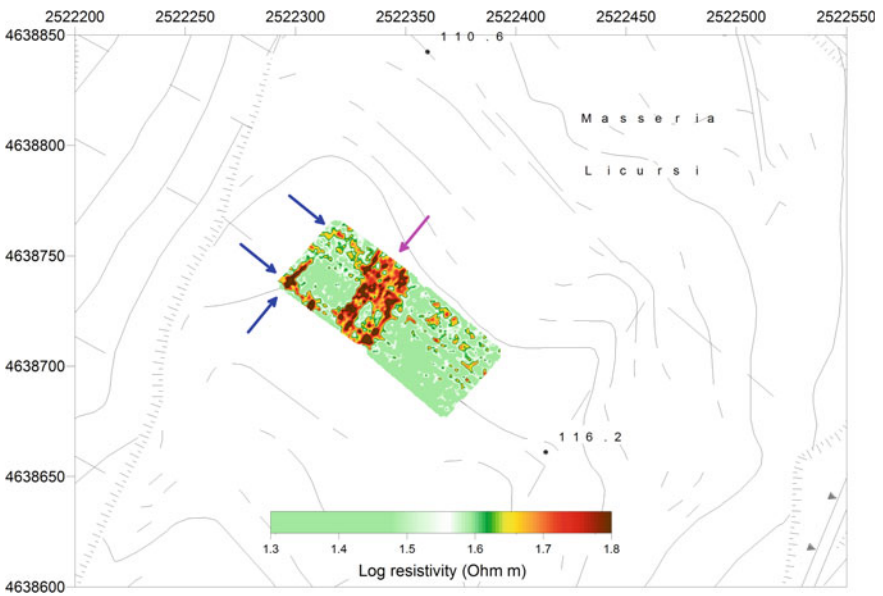

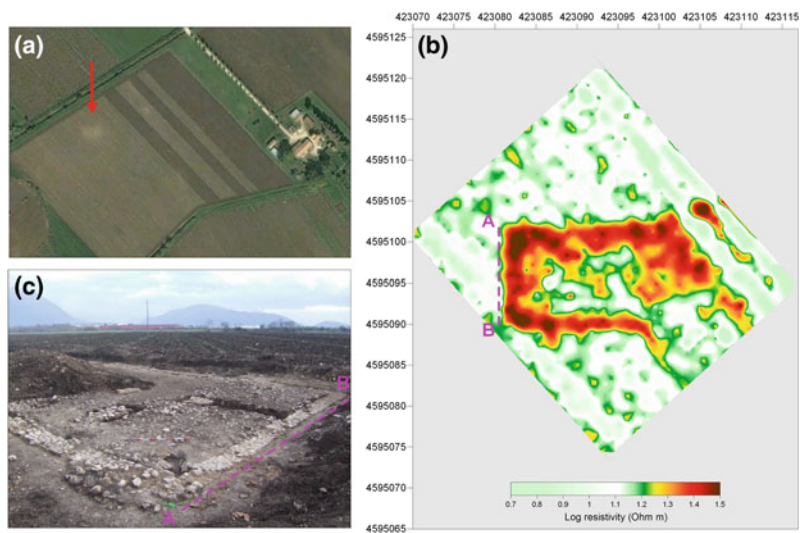**Fig. 4.128** Portocannone: electrical tomography relative to 1 m in depth

Fig. 4.129 Industrial Area of Pozzilli. **a** light-color trace visible on the satellite image © 2013 DigitalGlobe Inc. di Gloogle Earth™, October 15, 2005; **b** geophysical anomaly; **c** picture of the escavated structure
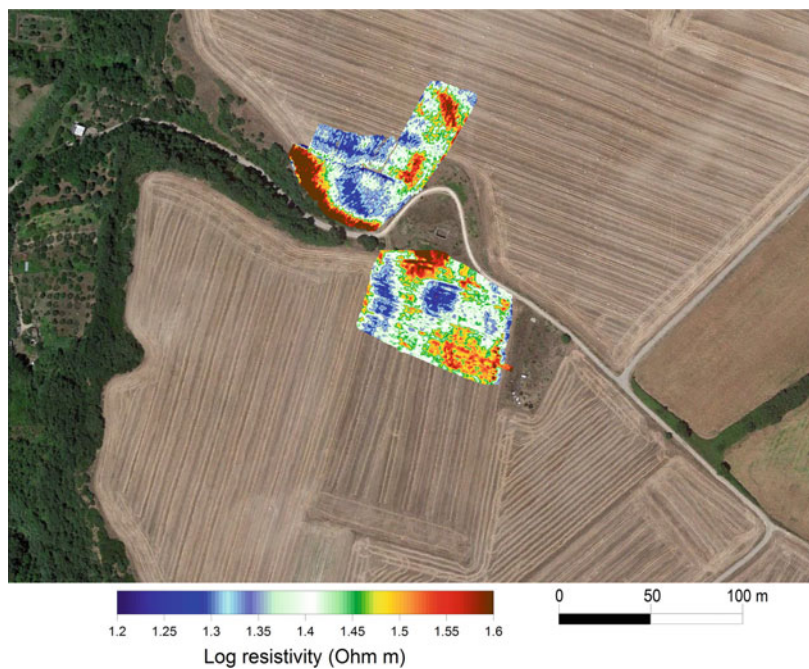

Fig. 4.130 San Giacomo degli Schiavoni: EMI results

References

A. Minelli, C. Peretto (a cura di). *Preistoria in Molise. Gli insediamenti del territorio di Isernia*. A. Minelli, C. Peretto (a cura di), Aracne editrice, Roma, 2006.

AA. VV. 1980. *Sannio: Pentri e Frentani dal VI al I sec. a.C., Catalogo della mostra*, Isernia, Museo Nazionale, ottobre-dicembre 1980, Roma 1980.

AF. Valente, *Il castello di Gambatesa: storia, arte, architettura*, Ed. Enne, Ferrazzano, 2003.

Bajaj C.L., Bernardini F., E Xu G. 1995, Automatic reconstruction of surfaces and scalar fields from 3D scans, in *Siggraph '95 proceedings*, 109–118.

Baribeau R., Rioux M., Godin G. 1992, Recent Advances in the use of a Laser Scanner in the Examination of Paintings, *Restoration' 92*, Amsterdam, 69–73.

Bondi, M., Cavallazzi,M., Musina, G., 2006. Progetto di recupero e valorizzazione del Castello di Zena e delle sue pertinenze. Campagna di scavo 2006. www.castellodizena.it.

Bonghi Jovino M., 1993. A proposito dei rapporti tra Sicilia, Magna Grecia e Etruria: la testimonianza archeologica dell'Ara della Regina di Tarquinia. In "Magna Grecia, Etruschi, Fenici". Proceedings of the *30th Conference on "Studi sulla Magna Grecia"*. Arte Tipografica Napoli, pp. 449–485.

Boschi, F., 2006. Progetto di recupero e valorizzazione del Castello di Zena e delle sue pertinenze. Campagna di sondaggi meccanici 24–28 Luglio 2006. www.castellodizena.it.

Terzani C., 2005. *Scavo archeologico della cinta muraria di Aesernia*, in Fasti on Line Documents & Research.

Cappella C., La cattedrale di Termoli, Materdomini, 1973.

Ceraudo G., 1999. Il contributo dell'aerofotogrammetria per la ricostruzione dell'impianto urbano di Aquinum. In "Terra dei Volsci", *Annali*, 2, 1999, pp. 161–168.

Ceraudo G., 2004. "Ager Aquinas". Aerofotografia archeologica lungo la Valle dell'antico Liris. Caramanica Editore, Marina di Minturno (LT). ISBN 88-7425-041-X.

Ceraudo G., 2007.Progetto Ager Aquinas. 10 anni di ricerche: risultati e prospettive. In "Spigolature Aquinati. Studi storico-archeologici su Aquino e il suo territorio". Atti della giornata di studio – Aquino. 19 Maggio 2007. Aquino, (FR), pp. 39–48.

Compare, V., Cozzolino, M., Mauriello, P., Patella, D. 2009. Resistivity probability tomography at the Castle of Zena (Italy). *Journal of Image and Video Processing*, Eurasip, vol. ID 693274, ISSN: 1687-5176, https://doi.org/10.1155/2009/693274 .

Compare V., Cozzolino M., Di Giovanni E., Mauriello P., 2010. "Examples of diagnostic for cultural heritage". *Diagnosis for the conservation and valorization of cultural heritage*. Naples, 9–10 December 2010: 141–149.

Conyers, L.B. and Goodman, D. 1997. Ground-penetrating radar. An introduction for archaeologists. *AltaMira Press. Division of Sage Publications*, Inc.

Cozzolino M., Mauriello P., Patella D., 2013. "Resistivity Tomography Imaging of the substratum of the Bedestan Monumental Complex at Nicosia, Cyprus". *Archaeometry*. (www.interscience.wiley.com), https://doi.org/10.1111/arp.12018 .

Cozzolino M., Di Giovanni E., Mauriello P., Geophysical prospection applied to historical centres, Proceedings of the 19th International Conference on Cultural Heritage and New Technologies 2014 (CHNT 19, 2014), Vienna 2015, http://www.chnt.at/proceedings-chnt-19/, ISBN 978-3-200-0416-7.

Cozzolino M., Di Giovanni E., Mauriello P., 2010, *Il tumulo di Petroio: un caso di applicazione delle metodologie geofisiche per l'archeologia preventiva.* In Notiziario della Soprintendenza per i Beni Archeologici della Toscana, vol. 6, pag. 233–236, ISSN:2035-5297.

Cundari, C., 2005. *Il Palazzo Reale di Caserta. Testi Immagini Rilievi*. Vol. I: Saggi e Contributi, Ed. Kappa Napoli, 79–86.

Esu D., 1983. "*Malacofaune continentali della serie '"La Pineta'" Isernia*". In: Isernia La Pineta. Un accampamento più antico di 700.000 anni. M. Coltorti (Ed.), Calderini, Bologna, pp. 5–39.

d'Annibale E., Fangi G., 2009, *Interactive Modeling by projection of oriented spherical panorama, Ad Deir, Petra, Jordan*, Proceedings of 3° International Workshop 3D ARCH, 3D Virtual Reconstruction and Visualization of Complex Architecture (ISPRS Archives - Vol XXXVIII-5/W1: 1682–1777 on cd) – Trento (Italy).

d'Annibale E., 2011, *Image Based Modeling from Spherical Photogrammetry and Structure For Motion. The case of the Treasury, Nabatean Architecture in Petra*, Proceedings of XXIIIrd International CIPA Symposium, Prague (Czech Republic), 2011.

De Caro S., Miele F., 2001, *L'occupazione romana della Campania settentrionale nella dinamica insediativa di lungo periodo,* in Modalità insediative e strutture agrarie nell'Italia meridionale in età romana, a cura di E. Lo Cascio, A. Storchi Marin, Bari 2001, 501–581.

Piccarreta, F., Ceraudo, G., 2000. *Manuale di aerofotografia archeologica. Metodologia, tecniche e applicazioni*, Bari, Edipuglia.

Marazzi, F., Delogu, P., 1996. *San Vincenzo al Volturno: cultura, istituzioni, economia*, Montecassino Vulturense 3.

Ceraudo G., 2003. *Insediamenti italici* in M. Guaitoli (a cura di) *Lo sguardo di Icaro. Le collezioni dell'Aerofototeca Nazionale per la conoscenza del territorio*, Campisano Editore, p. 306.

Barker G., 1975. *The archaeology of Early Man in Molise: the Report of the '74 Survey of the Biferno Valley.* Campobasso.

De Benedittis G., 1974. Il centro sannitico di Monte Vairano presso Campobasso. *Volume 5 di Documenti di antichità italiche e romane*. Soprintendenza ai monumenti alle antichità e alle belle arti del Molise.

De Benedittis G., 1979. *Abruzzo Molise. Guide d'Italia*, Milano, Ed. Touring Club d'Italia.

De Benedittis G., 1981. *Saepinum: città e territorio tra tardo Impero e basso Medioevo*, Archivio Storico per le Province Napoletane, 20.

De Benedittis G., 1988, *Monte Vairano, la casa di "LN"*, Soprindentenza di B.A.A.A.S. del Molise, I.R.R.S.A.E. del Molise, Campobasso.

Gaffney V., Piro S., Haynes I., Watters M., Wilkes S., Lobb M., Zamuner D., 2008. Three-Tier Visualization of San Giovanni in Laterano, Rome, Italy. *12th International Conference on Ground Penetrating Radar, June 16–19, 2008, Birmingham, UK*. Proceedings Extanded Abstract Volume.

Godin G., Cournoyer L., Domey J., Taylor J. 2000, Three-dimensional recording of objects and sites using laser range imaging. Centro di Ricerche Informatiche per I Beni Culturali, *Quaderni 10,* Scuola Normale Superiore, Pisa, p.139–150.

Goodman D., Piro S., 2008a. Ground Penetrating Radar (GPR) surveys at Aiali (Grosseto). In "*Seeing the Unseen. Geophysics and Landscape Archaeology*". Edited by Campana and Piro. CRC Press, Taylor & Francis Group. Oxon UK, (ISBN 978-0-415-44721-8), pp. 297–302.

Goodman D., Piro S., Nishimura Y., Schneider K., Hongo H., Higashi N., Steinberg J., Damiata B., 2008b. GPR Archeometry. In "*Ground Penetrating Radar Theory and Applications*", Edited by: Harry M. Jol. Elsevier (Ed.), pp. 479 – 508.

Goodman D., 2016. GPR-Slice 7.0, Manual. (http://www.gpr-survey.com, January/2016.)

Goodman D., Piro S., 2013. GPR Remote sensing in Archaeology. Springer (Ed), ISBN 978-3-642-31856-6, ISBN 978-3-642-31857-3 (eBook), https://doi.org/10.1007/978-3-642-31857-3. Springer, Berlin, (Germany).

Goodman D., Piro S., 2008c. Ground Penetrating Radar (GPR) surveys at Aiali (Grosseto). In "Seeing the Unseen. Geophysics and Landscape Archaeology". Edited by Campana and Piro. CRC Press, Taylor & Francis Group. Oxon UK, (ISBN 978-0-415-44721-8), pp. 297–302.

Goodman D., Nishimura Y., Rogers J.D., 1995. GPR time-slice in archaeological prospection. *Archaeological Prospection* 2: 85–89.

Goodman D., Piro S., Nishimura Y., Patterson H., Gaffney V., 2004. Discovery of a 1st century AD Roman amphitheatre and other structures at Forum Novum by GPR. *Journal of Environmental & Engineering Geophysics*, Vol. 9, issue 1: 35–41.

Rainini I., 1996. *Capracotta. Campagne di scavo alla Fonte del Romito.* In Del Tutto Palma L. (a cura di) 1996, *La tavola di agnone nel contesto contesto italico*, Agnone 13–15 aprile 1994, Firenze, pp. 129–145.

Morel J.P., 1984. *Il santuario sannitico di Vastogirardi. Resoconto degli scavi archeologici degli anni 1971, 1973 e 1974.* In: Sannio, Pentri e frentani dal VI al I secolo a. C., Atti del convegno, 10 e 11 Novembre 1980. Edizioni Enne 1984.

Scaroina L., 2004. *Il complesso termale dell'Acqua Solfa di Pozzilli*. In Conoscenze 1–2 2004, pp. 27–36.

Leckebusch, J. 2000. Two- and Three-dimensional Ground-penetrating Radar Survey across a medieval chair: a case study in Archaeology. *Archaeological Prospection*, 7 (4): 189–200.

Leckebusch J., 2008. Semi-automatic feature extraction from GPR data for archaeology. *Near Surface Geophysics*, Vol. 6, N.2, 75–84.

Linford N., 2004. From Hypocaust to Hyperbola: Ground-penetrating Radar surveys over mainly Roman Remains in the UK. *Archaeological Prospection,* 11, 237–246.

Coltorti M., M. Cremaschi, M.C. Delitala, D. Esu, M. Fornaseri, A. McPherron., M. Nicoletti, R. Van Otterloo, C. Peretto, P. Sala, V. Schmidt, J. Sevink, 1982. "*Reversed magnetic polarity at Isernia La Pineta, a new lower Paleolithic site in Central Italy*". Nature, 1982, vol. 300, pp. 173–176.

Gaggiotti M., M. Matteini Chiari, 1979. *Sepino. Archeologia e continuità,*Campobasso .

Matteini Chiari M., M. Gaggiotti, G. De Benedetti, 1984. *Saepinum-Sepino*, Campobasso, 1984.

Pagan M., M. Raddi, A. Pannucci 2005. *La Villa Romana e la Chiesa paleocristiana di S. Maria Vecchia (Macchia d'Isernia) 1-2/2005*, pp. 100–112.

Malagodi S., Orlando L., Piro S., Rosso F., 1996. Location of archaeological structures using the GPR method: three-dimensional acquisition and radar signal processing. *Archaeological Prospection* 3: 13–23.

Marazzi F, Stanco EA , 2010*, Alife. Dalla Colonia romana al gastaldato longobardo. Un progetto di lettura interdisciplinare delle emergenze storico-archeologiche*, in Paesaggi e insediamenti urbani in Italia Meridionale fra tardoantico e altomedioevo, a cura di Volpe G., Giuliani R., Bari, Edipuglia, 329–348.

Martucci, E., Romano, A. M., Jacobitti, G. M., 1993. *La città reale: Caserta*. Guida Editori, Caserta, 153–162.

Mauriello, P., and Patella, D., 2009. A data-adaptive probability-based fast ERT inversion method, *Progress In Electromagnetics Research*, 97, 275–90. https://doi.org/10.2528/pier09092307

Neubauer W., Eder-Hinterleitner A., Seren S., Melichar P., 2002. Georadar in the Roman Civil Town Carnuntum, Austria: an approach for archaeological interpretation of GPR data. *Archaeological Prospection*, 9, 135–156.

Perrella O., G. Cavaliere, 2006. *Molise Castelli*, Palladino Ed., Campobasso.

Mauriello P., D. Patella, 1999a. *Resistivity anomaly imaging by probability tomography*, in *Geophysical Prospecting*, 47, pp. 411–429.

Palazzo P., 2009. *Savelletri di Fasano. Località Masciola,* www.fastionline.org/docs/FOLDER-it-2009-161.pdf   .

Mauriello P. and D. Patella, 1999b. *Resistivity anomaly imaging by probability tomography*, Geophysical Prospecting, vol. 47, no. 3, pp. 411–429.

Piro S., Goodman D., 2008. Integrated GPR data processing for archaeological surveys in urban area. The case of Forum (Roma, Italy). *12th International Conference on Ground Penetrating Radar, June 16–19, 2008, Birmingham, UK*. Proceedings Extanded Abstract Volume.

Piro S., Campana S., 2012. GPR investigation in different archaeological sites in Tuscany (Italy). Analysis and comparison of the obtained results. **Near Surface Geophysics, 2012**, **10, pp. 47–56,** https://doi.org/10.3997/1873-0604.2011047.

Piro S., Ceraudo G., Zamuner D., 2011. Integrated geophysical and archaeological investigations of Aquinum in Frosinone, Italy. *Archaeological Prospection*, 18: 127–138. https://doi.org/10.1002/arp409.

Piro S., Samir A., Versino L., 1998. Position and spatial orientation of magnetic bodies from archaeological magnetic surveys. *Annali di Geofisica*, Vol. 41, n.3, 343–358.

Piro S., Sambuelli L., Godio A., Taormina R., 2007. Beyond image analysis in processing archaeomagnetic geophysical data: examples on chamber tombs with dromos. *Near Surface Geophysics* Journal *(EAGE)*, Vol. 6, 405–414.

Piro S., Goodman D., Nishimura Y., 2003. The study and characterisation of Emperor Traiano's Villa (Altopiani di Arcinazzo, Roma) using high-resolution integrated geophysical surveys. *Archaeological Prospection* 10: 1–25.

Cassano R., C.S. Fioriello, A. Mangiatordi, G. Mastrocinque, 2007. *Ricerche archeologiche nella città di Egnazia. Scavi 2004-2006. Relazione preliminare*, in M. Pani (a cura di) *Epigrafia e territorio. Politica e società. Temi di antichità romane*, VIII, 2007, pp. 7–136.

Ragni L., Il duomo di Termoli, Napoli, 1907.

Capini S., 1989. *L'area del Nucleo Industriale nella pianura di Pozzilli (IS),* in *V Settimana Beni Culturali, Tutela,* pp. 31–40.

Capini S., G. De Benedittis 2000. *Pietrabbondante: guida agli scavi.* Tipolitografia Fotolampo.

Grimaldi S., 2005. *Nuove ricerche sul paleolitico del Molise. Materie prime, industrie litiche, insediamenti.* Centro Europeo di Ricerche Preistoriche, Collana Ricerche, 2, Isernia.

Soucy M., Godin G., Baribeau R., Blais F., Rioux M. 1996a, Sensors and algorithms for the construction of digital 3-D colour models of real objects, *Proc. of the IEEE ICIP*, Lausanne, Suisse, Vol. II. 409–412.

Soucy M., Godin G., Rioux M. 1996b, A texture-mapping approach for the compression of colored 3D triangulations, *The Visual Computer*, 12, 503–514.

T.D. Stek, *Cult Places and Cultural Change in Republican Italy*, Amsterdam 2010.

Utsi E., 2006. Improving definition: GPR investigations at Westminster Abbey. Proceedings of 11th International Conference on GPR. Columbus Ohio, USA.

Amato V., M. Cozzolino, G. De Benedittis, G. Di Paola, V. Gentile, C. Giordano, P. Marino, C.M. Rosskopf, E. Valente 2016. *An integrated quantitative approach to assess the archaeological heritage in highly anthropized areas: the case study of Aesernia (southern Italy),* in ACTA IMECO, Vol. 5 (2), pp. 33–43.

Ceglia V., 1988. Lo scavo della necropoli di Vicenne, in Conoscenze, 4, Matrice 1988, pp. 31–48.

Compare V., M. Cozzolino, P. Mauriello, D. Patella, 2009b. "3D Resistivity probability tomography at the prehistoric site of Grotta Reali (Molise, Italy)", Archaeological Prospection, 2009b. vol. 16, n.1; pp. 53–63, ISSN: 1099-0763, https://doi.org/10.1002/arp.347 .

Vannini G. 2007, *Insediarsi in Oriente: l'incastellamento del XII secolo nella Trangiordania meridionale. Una lettura archeologica,* in Archeologia dell'insediamento crociato-ayyubide in Transgiordania: il Progetto Shawbak, a cura di G. Vannini, Firenze 2007, pp 1'–21.

Vannini G. & Nucciotti M. 2009, *Da Petra a Shawbak, Archeologia di una Frontiera,* Giunti Editore.